Switched Reluctance Generator Drive in the Low and Medium Speed Operation: Modelling and Analysis

A thesis presented in partial fulfilment of the requirements for the degree of

Doctor of Philosophy

In

Electrical Engineering

at Massey University, Manawatu,

New Zealand.

AMISSA MOHD SHAIDI ARIFIN

2013

ABSTRACT

Wind is a natural source of energy related to the low and medium speed range. Electricity can be generated from the wind by using a variable speed machine. Among the common types of machines available are: double fed induction generator (DFIG), induction generator and also synchronous generator. However, the latest addition to the group is the Switched Reluctance Generator (SRG), which has attractive features such as simple in construction, inexpensive, robust and reliable. Current research on the SRG has been focusing on optimizing its performance individually in terms of structure, control and also reducing the components of power electronic devices. Despite the extensive research on the individual component of the machine, the comprehensive performance of the SRG has not yet been published. The main contribution of this thesis is the proposed modelling framework of the SRG. Based on the framework, extensive and in depth comparative analysis can be conducted.

Firstly, the design of the existing machine including the winding configuration and rotor structure using finite element method is investigated. Secondly, based on the principle of electromagnetism, a simulation framework that adopts a heuristic method to perform comparative analysis between different types of SRG has been proposed. This framework serves as a platform to the development of the SRG in the low and medium speed operation. It can be used to predict the performance of the machine before it can be implemented on a prototype, thus, saving time and costs.

Thirdly, the procedure to determine the optimal control variables is proposed. Basically, the controller plays an important role to determine the placement of the firing angles along the inductance profile. The most influential parameter that affects the percentage of power generated which are the firing angles and voltage level has been identified. A polynomial function relating the percentage of power generated in terms of the optimal control variables has also been developed.

Lastly, a novel control method is proposed to operate the machine in single pulse mode as opposed to the current chopping mode during the low speed range. The proposed control

scheme provides the highest percentage of power generated during the low speed range. Overall, the research will aid in the development of the SRG by allowing user to choose the best generating operation within any speed range.

ACKNOWLEDGEMENT

Praise to the Almighty the most gracious and the most merciful for His blessings and guidance, and for giving me the best of health and strength to enable me to successfully complete this study.

I am deeply grateful to my supervisor, Dr. Ibrahim Al-Bahadly for his endless support and supervision throughout my PhD journey. Through his invaluable advice, constructive criticism and opinions during this period has helped me to complete this research. Also, his boundless optimism throughout this journey has always been inspirational and illuminated the way forward, even when things seemed grim.

My sincere appreciation is also extended to my co-supervisor Professor Dr. Subhas Chandra Mukhopadhyay for providing me with guidance and support during my research.

Thank you to Mike Lusby for his time to set up the experiment test bed and help in taking measurements of the Switched Reluctance Machine. Special appreciation also goes to my friends in the School of Engineering and Advanced Technology in particular Linda Chua, Pramila Gamage, Raziyeh Zarre, Ayesha Hakeem and Le Thu Nguyen for their moral support, motivation and friendship along this journey. Also, thank you to Michele Wagner for all the administrative support given. Special thank is dedicated to my best friend Fariza, who has been providing me with the necessary advice and guidance from a far.

I am also grateful to Majlis Amanah Rakyat (MARA) for giving me the opportunity to pursue my study overseas and providing me with financial support throughout my studies.

Last, but not least, special thanks to my beloved husband Ezanee and my wonderful daughters, Aisya Sofea and Aimi Syazwani for their love, encouragement, support and care in this memorable journey of life. Thanks also to my parents and families for their good wishes, understanding, assistance and patience during the years of this study.

Table of Contents

List of Figures

List of Tables

CHAPTER 1

INTRODUCTION

1.1 Background

The widely used energy source to generate electricity includes coal, fuel, oil and also natural gas. These main suppliers of electricity take millions of years to form, and is reaching the peak of their production. Hence, their prices are expected to increase due to the high demand and low supply of these resources. Apart from that, these energy sources contribute to the build-up of the on-going human related greenhouse gasses. The smoke stacks produced during the generation process of these conventional energies are released into the atmosphere forming part of the greenhouse gasses. These emissions have come under increasing scrutiny by the regulatory bodies in their quest to curb them and their impact on the environment. For this reason, industries and electric utilities have to comply with the regulations imposed. Therefore, a lot of initiatives and drives were set to mitigate the concern which leads to the green technology. Figures released by the International Energy Outlook 2011 (IEA2011) [1] have shown that there will be an increase in the production of electricity using the renewable energy by the year 2035. These factors have prompted the study and development of various types of new generators, which are energy-efficient, affordable and durable.

The switched reluctance machine is making good progress in the motoring industries due to its attractive features such as robust, simple in construction, fault tolerant and the ability to operate over a wide speed range. Also, having no brushes and permanent magnets on the rotor makes it a highly competitive machine alongside the existing machines in the current market. The application of the machine as a generator concentrates more on high speed applications where it was used as starter generators for the aircraft industries. The potential of the machine operating as a generator in the low and medium speed range for wind energy application is actively being explored.

1.2 Requirements of Electric Power Generation

The International Energy Outlook 2011 (IEA2011) [1] report forecasted that the electricity consumption is expected to increase from 573 quadrillion British thermal unit (Btu) in 2015 to 770 quadrillion Btu in 2035 as shown in Figure 1-1. The increase is proportional to the expected growth in population from 7 to 9 billion in the year 2040. The residential sector will consume a large portion of the energy demand due to the rise in population. In this day and age, energy is essential to enhance our lifestyle, keep us safe and healthy. This urges from the desire to sustain and improve the well-being of one self, family and also the community. Furthermore, the advance in technology and the competitive innovation in electronic gadgets also contribute to the consumer demand.

The development of other competing resources such as the alternative energy is influenced by the increase in energy demand, depleting conventional energy resources and not to mention the rising price of these resources. Industries are turning to alternative energy in an attempt to meet with the world's energy demand whilst preserving the fossil fuels and keeping to the regulatory requirements to reduce the emission of carbon dioxide. This is projected in the report issued by the International Energy Agency (IEA) which projects the medium and long term energy consumption through to the year 2035 as illustrated in Figure 1-2. As compared to the year 2010, there will be a decrease in the consumption of oil and coal. This is in contrast to the renewable and liquid biofuel, which shows an increase by 3%. The role of nuclear power is projected to stay constant as a

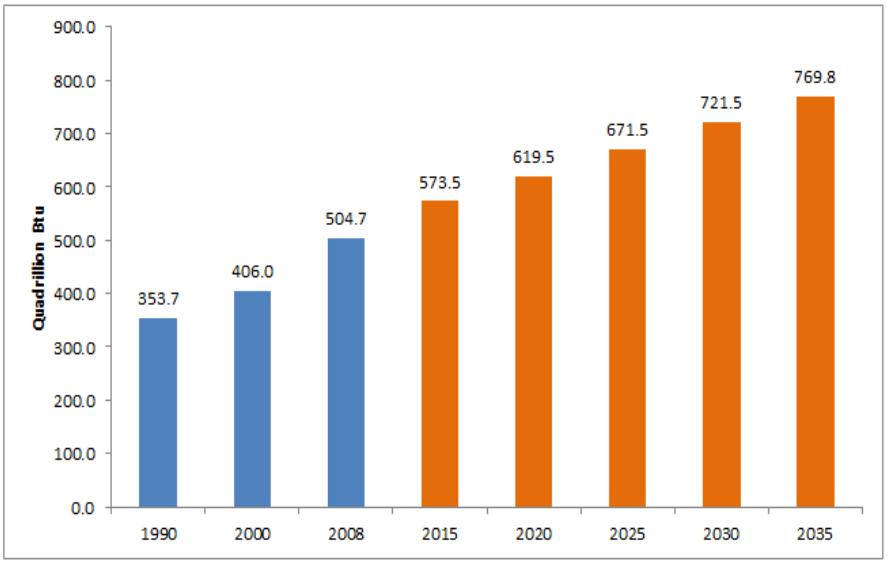

Figure 1-1: World net energy consumption 1990-2035

result of the recent earthquake and tsunami in Japan. Its safety has been revised due to the dangers associated by the release of its atomic power[2]. Furthermore, the nuclear plant needs to be located near the water resources for cooling purposes. While climate change is affecting the water supply, so does the development of the plant [3].

Therefore, the responsibility to contribute to the rising demand of electricity is placed on other renewable energies such as the sun, hydro and wind. These are clean energies which do not produce any form of emissions detrimental to the environment and are constantly available. Although the use of water hydro plants has started way earlier, the availability of water resources are restricted depending on the area. Amongst the growing potential of renewable energy nowadays is the wind energy which would account for 6% of the world's electricity demand by the year 2020 [4]. It can be categorized into two groups: large wind turbine (LWT) and small wind turbine (SWT). The former provides generation of electricity from large grid connected wind farms whereas the latter has been applied for off grid supply in various fields such as road lighting, mobile communication base tower and also for individual housing consumer. In developed countries such as the USA, the SWT is employed to supply electricity to remote regions. However, there is great potential to use the SWT in a fully developed area where there is limited space for the expansion of power supply as it can be placed in areas such as roof top. Although the industrial scale is far behind as compared to the LWT, its contribution to the power generation is equally important. The report by the World Wind Energy Association 2012 (WWEA) [5] forecasted a promising increase of growth pattern in the installed capacity

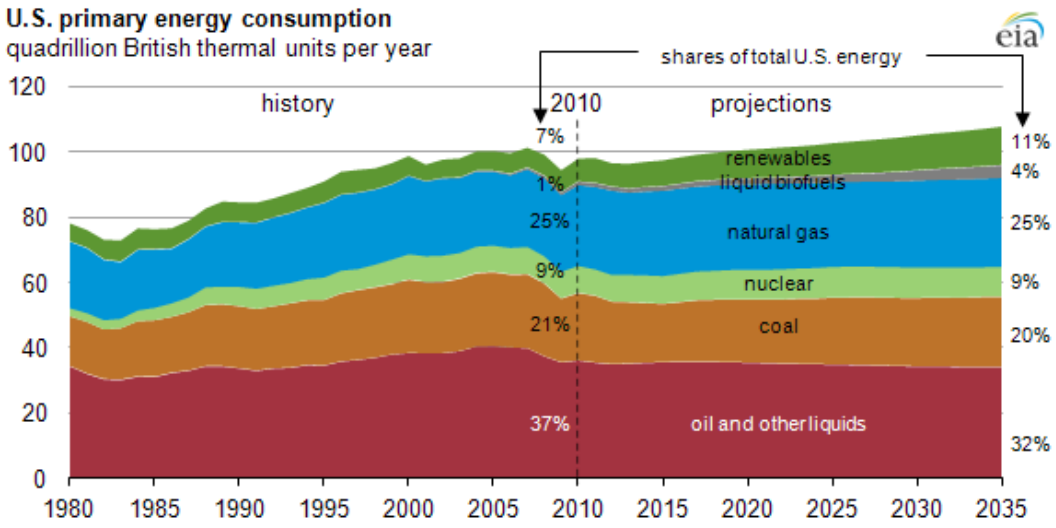

Figure 1-2: Projection of the energy consumption issued by the IEA

of power using SWT as depicted in Figure 1-3. It contributes to the total global installed wind capacity of 239GW [4]. The driving factors that will promote the future growth of the SWT industries have been identified as the constant increase in fossil fuel price, global warming and the growing demand of electricity. One of the main challenges with the development of renewable energies is the requirements of special equipment and infrastructure to capture and convert the energy into electricity.

As mentioned earlier, the wind energy has been identified as one of the main contributors of electricity generation amongst the available renewable energies. The existing technologies such as the permanent magnet (PM) generators, doubly fed induction generator (DFIG), synchronous generators and also the squirrel cage induction generator has been widely used in the wind energy application [6]. However, the existing generators have their shortcomings such as the squirrel cage induction generator operates at constant speed as well as having large values of capacitor to attain the power factor close to one. The issues with using permanent magnet are the high cost and the demagnetization of the material [7]. Also it operates on high torque which is a disadvantage at lower speed [8]. The induction machine though is robust and requires less maintenance produces low efficiency. Furthermore, there are concerns over the safety system for the DFIG during fault conditions due to the limited converter rating on the rotor side as compared to the DC link converter [9].

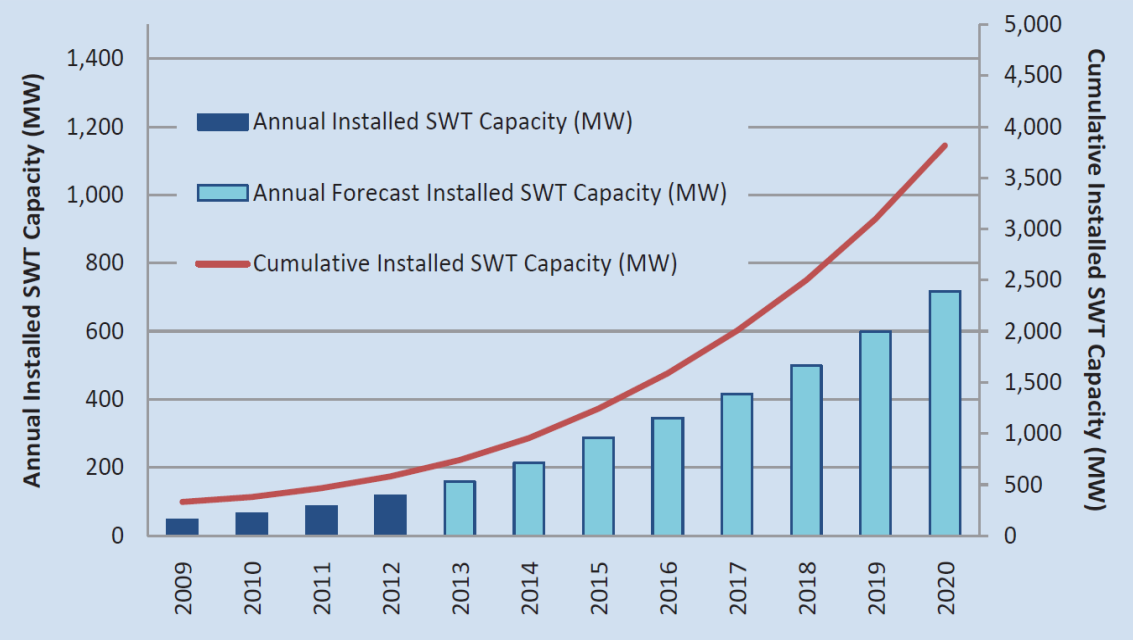

Figure 1-3: The Small Wind Turbine (SWT) installed capacity world market forecast 2020

This has encouraged researchers to explore other generators, which are efficient, reliable, and able to work under variable speed condition and also to maximize the power generation [10]. One of the electric drives that is receiving much attention is the switched reluctance generator (SRG). Although the SRG has several disadvantages such as high acoustic noise and torque ripple, other factors listed below which are required of a generator outweigh the disadvantages. It has taken years of research before the existing generators penetrates the market, the same will be for the new generations of machine. Further research is required to close the commercial gap. The general requirements for electric generators are as listed:

- low maintenance
- fault tolerant
- efficient
- low in cost
- variable speed operation

The following section outlines the structure, development and progress of the SRG system in the wind energy application.

1.3 The Advantages and Challenges of the SRG drive

The Switched Reluctance Generator drive system consists of the machine itself, the converter and also the controller as depicted in Figure 1-4. The machine has a structure

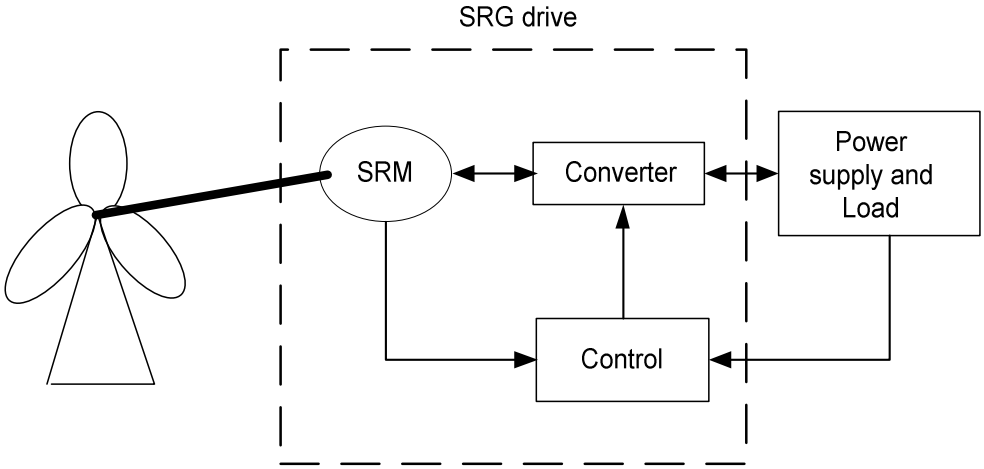

Figure 1-4: A simplified diagram showing the main components which form the SRG system

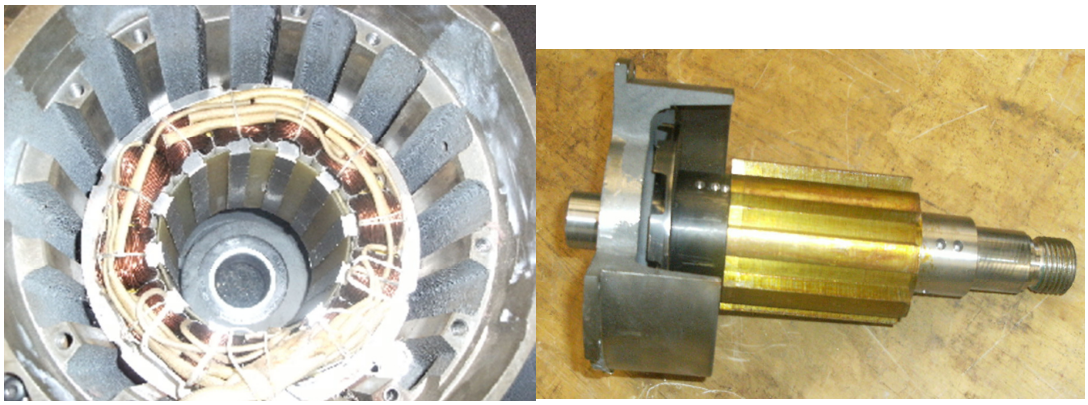

(a) (b)

Figure 1-5: Structure of the SRG with twelve stator poles and eight rotor poles (a) stator poles (b) rotor poles

whereby both its stator and rotor poles protrude into the air gap. There are several combinations of the machine depending on the number of its stator and rotor poles. An example of the structure which will be used in this study is a 12/8 machine having 12 number of stator poles and 8 number of rotor poles as illustrated in Figure 1-5.

The rotor and the stator are made of steel laminations, and only the stator poles have windings concentrated around them [11, 12]. Since the machine does not have any windings or permanent magnets on the rotor as in Figure 1-5(b), it is very robust and is able to operate at a very high speed. The rotor can also cool the copper windings on the stator pole during operation. Due to the machine not having a permanent magnet, the magnetic field within the machine has to be created using an external supply. Because of this, the SRG drive requires a separate excitation circuit which is connected directly to the windings on the stator poles. The machine therefore relies on a single excitation source; a battery, a magnet or a charged capacitor with an initial voltage connected in series with the load [13].

One end of the winding of each phase is connected to a set of switching devices from a converter. The series connection of the switching device and the winding avoids a shoot through fault. Furthermore, the phase winding operates independently of each other making it a fault tolerant machine [14]. A fault in any one of the phases does not affect the operation of the other phases although the total efficiency of the machine will reduce [15].

The continuous rotation of the magnetic field is achieved by energizing and de-energizing the set of windings. The position of the rotor is determined by a sensor placed on the shaft. Nevertheless, a large number of publications have been proposed for sensorless rotor position estimation [16, 17]. The scheme does not require additional hardware equipment but depends strongly on the machine characteristics such as mutual inductance, back EMF and phase resistance calculation [18]. The result of exciting the phase winding in sequence produces a continuous pulsed current. Generally the characteristics of the machine are highly nonlinear due to the salient pole structure and saturation of the iron along the flux path. This nonlinearity of the phase current is one of the factors causing torque ripple and acoustic noise, which may not be acceptable for some applications. Hence, a special controller or specific design of the machine is required as compared to the other machines.

The operation of the machine in generating mode requires the phase winding to be excited when the rotor is moving away from the stator pole, creating a braking torque. Because the excitation is during the maximum inductance value, the initial phase current will be small. The current will increase as the inductance decreases. As this occurs, the back electromagnetic force (EMF) of the machine may be larger than the terminal voltage which further increases the phase current. Thus, the increase of phase current after the switches are turned off cannot be predicted and controlled. A high current can harm the electronic switches as well as increases the volt-ampere (VA) rating of the semiconductor devices resulting in a larger machine size. The situation can be controlled by selecting the optimal values of firing angles. The task to determine the optimal angles is not straight forward due to the nonlinearity of the machine being very dependent on both the current and the rotor position [19]. Researchers have identified the optimal angles based on the application of the machine (i.e. –optimal angles in terms of minimum RMS current and minimize losses). These firing angles are not unique and changes according to its performance criteria [20].

Despite the disadvantages of the machine such as high torque ripple, high acoustic noise and highly nonlinear, the attractive characteristics of the machine make it a potential candidate as a variable speed drive machine. The main attractive features of the machine can be summarized as follows:

- The machine can be manufactured in bulk since the rotor is free from the permanent magnet and winding. It will be cheaper as compared to the conventional induction machines (IM)[21].
- High reliability
- More robust
- It does not have a cogging torque, which normally exists in a permanent magnet (PM) machine and hence is able to operate at a much lower wind speed [22].
- Concentrated coils that reduce costs.
- The unequal number of stator and rotor poles allows the starting and operation of the machine without pole clamping in both rotation directions.
- The high torque at low speed is suitable for direct drive applications [23].

Nevertheless, the on-going researches on the switched reluctance generator (SRG) are rapidly evolving.

1.4 Recent Progress in the Development of the Switched Reluctance Generator

The simple construction of the machine that leads to a low manufacturing cost has widened the acceptance of the machine. The application of the machine as a motor has been commercialized and can be seen in domestic appliances such as the washing machines and vacuum cleaners. The features of the machine such as having the ability to operate under faulted condition, robust to harsh operational conditions and having a high power density has extended its motoring operation in the traction applications [24, 25] and automotive industries for hybrid vehicles [26-29]. Currently, the application of the machine as a generator concentrates more on high speed applications such as for the aircraft industries [30-35]. To date, the machine has yet to be commercialized in the wind energy application.

Due to the attractive features of the machine as mentioned above, the operation has been extended to the low and medium speed applications. The structure of the machine and its inherent capability to start with low inertia has made researchers realize the potential of the machine for wind energy applications. The study on SRG includes the feasibility of

the machine for wind energy applications [7, 8, 36-39]. The selection of the machine is based on criteria such as control simplicity, able to be integrated with the grid and also the ability to operate at variable speed for higher wind extraction. Based on the application of the machine, the operation of the SRG can be categorised into low, medium and high speed operation. The operation of the machine at high speed can exceed the speed of 20,000rpm for the aerospace applications, which is beyond the speed encountered in wind energy system that could be as low as 200rpm. On the whole, the acceptance of the machine for variable speed application has initiated an in-depth research into areas such as the control strategies, optimization method, machine structure and also on converter topology which, will be covered in the following sub-sections.

1.4.1 Control Strategies for SRG

The generating operation on the machine is said to mirror the operation of the motoring mode [40]. For this reason, similar control strategies can be adopted. However, the control objectives and control implementation of the motoring operation differs for the generating mode [20]. In motoring mode, the excitation of the phase windings is made during the minimum inductance profile. During this time, a high rise of current is expected hence at low speed, current chopping mode is employed for overcurrent protection. In contrast to the generating operation, the excitation is made during maximum or increasing inductance profile. Initially, the phase current will be low and will slowly increase as the rotor moves away from the stator pole, during the decreasing inductance profile. Once the signal reaches the turn off angle, the increase in phase current can no longer be controlled. Its value is dependent on the back EMF [41]. As the back EMF increases, the current chopping mode (CCM) fails and thus the machine operates in single pulse mode (SPM).

Existing control strategies for SRG provide a constant output voltage or power over a wide operating speed range by controlling the firing angles [42]. Several studies investigating the single pulse mode (SPM) operation show that the firing angles such as the turn on (T_{on}) and turn off (T_{off}) angles are the key elements to improve the performance of the machine in terms of efficiency [43]. Various control strategies can be employed to determine the turn on and turn off angles such as fuzzy logic, magnetization curve (MPPT), flux linkage and also curve fitting. The implementation of these firing angles can be grouped into:

• Fixing both turn on and turn off angles
• One of the angles may be varied whilst keeping the other constant
• Vary both turn on and turn off angles

The turn off angle can be characterized as a function of power and speed [44]. An analytical curve is used to determine optimal turn off angle whereas turn on angle is adjusted to regulate the power. It is assumed that the machine gives optimal efficiency once optimal turn off angle has been determined. Mese et. al. [45] uses a mapping strategy to determine turn on and turn off angles that produce maximum power based on a minimum rms phase current. Heuristic selection algorithm is used to identify the optimal angles hence the method is rather time consuming. Furthermore, it did not include any development of a function relating the optimized parameters with machine performance. Similarity between the two methods involves the use of phase current as a state variable. A simple formula to compromise the performance between high efficiency and low torque ripple has been proposed using flux linkage control. It can be used for both the single pulse [42] and current chopping mode [46]. The method assumes excitation period equals generation period at constant speed and relies heavily on the flux, current and inductance profile to determine the intersection angles of the maximum flux and peak current. Also, the output power generated is catered for a specific load requirement. A capacitive output filter is designed to reduce the voltage ripple using a voltage feedback control method [47]. A new control method using multi-objective optimization function was proposed to accomplish three criteria including high torque, high operating efficiency and also low torque ripple for an electric vehicle application [48]. For those reported methods, in summary, the proposed techniques are targeted for high speed applications whereby the objectives were confined to maximize torque production, minimize losses and also to minimize torque ripple.

There are not many literatures, which focus on the low and medium speed operation. The current chopping mode control method in generating operation is normally used at low speed for wind energy conversion system (WECS) application [49]. A power control strategy was used to maintain the required load demand. Another method to control the output power is achieved by using a fuzzy logic controller to regulate the turn on angle whilst the turn off angle is kept constant [50]. The resources on the application of the machine for the control strategies in wind energy are still limited. The method based on

constant output power requires the machine to follow the set of reference power. This limits the potential of the machine to extract energy according to the wind velocity.

1.4.2 Power Converter Circuit for SRG

The same converter topology can be employed for both the motoring and generating operation. The end windings of each phase are connected to the converter circuit which controls the phase current through the windings. It provides a path through the switches during excitation and diodes during the generating operation. Therefore, the operation of the machine during one cycle can be categorised into two stages: excitation and generation. Thus, the switching strategy has an impact on the efficiency of the SRG [51].

The commonly described converter circuit for the SRG is the Asymmetric Half Bridge Converter (AHBC) consisting of two switching devices and two power diodes per phase. The implication of using a higher number of switching devices per phase limits the number of phases for a machine in terms of space constraint and cost. Various studies have emerged on the alternative converters for SRG using a reduced number of devices. In [52], a converter topology having one number of switch and diode per phase allows the load to be supplied from the grid even when the SRG is not running. Unlike the conventional AHBC converter, the supply voltage will be in series with the back EMF during the generation process supplying load continuously. It is only suitable for constant speed applications. Another converter topology with a reduced number of devices was proposed in [53]. The operating characteristic of the new proposed suppression resistor converter topology is similar to a conventional AHBC; however, it is only suitable for a single pulse mode operation. Aside from generating DC power, the SR generator can also be used to regenerate AC power using a sparse converter [54]. This opens a new research area in terms of generating AC voltage using SR generator.

On the whole, the research on converter topology focuses on ways to reduce the number of semiconductor devices with the aims to minimize costs and size of the overall device. However, with a reduced number of switching devices, the converter is not flexible in terms of control. This might be one of the reasons that although new topologies have been suggested, researchers still choose the conventional AHBC converter. Other types of converter which have been proposed to be used with the machine are tabulated in Table

Table 1-1: Comparison of voltage level across the phase winding for various converter topologies

Type of Converter	Excitation	Generation	Freewheeling
AHBC	$V = 2v_{sw} + L\frac{di}{dt}$	$-V = 2v_D + L\frac{di}{dt}$	$0 = v_D + L\frac{di}{dt}$
Bifilar	$V = v_{sw} + L\frac{di}{dt}$	$-V = v_D + L\frac{di}{dt}$	-
Reduced count switch (one switch per phase)	$V = v_{sw} + L\frac{di}{dt}$	$V + v_{emf} = v_D + L\frac{di}{dt}$	-
Suppression resistor Converter	$V = v_{sw} + L\frac{di}{dt}$	$0 = v_D + L\frac{di}{dt}$	-

V = voltage across phase winding
v_{sw} = voltage across switching semiconductor device
di/dt = change of instantaneous phase current with time
v_D = voltage across diode
L = Phase inductance
v_{emf} = back EMF voltage

1-1. It shows the voltage across the phase winding for various converter topologies under study for the generating operation. The generating cycle determines the type of converter to be used for a particular application. At the moment, there is no special preference of converter topology for either the low, medium and high speed operation.

1.4.3 Machine Structure

There is no specific design or structure which has been associated for either the generating or the motoring operation. However, various researches on parameters relating to the structure of the machine have been established and can be grouped as in Figure 1-6. It also shows that the performance of the machine is affected by the overall structure of the machine.

1.4.3.1 Stator and Rotor Pole Combination

The numbers of the stator and rotor poles are designed to avoid the zero torque regions. This leads to the design of the machine having a symmetrical and equally spaced number of stator and rotor poles [55]. The switched reluctance generator has been used in various applications as previously mentioned in Section 1.4. Therefore, using the available

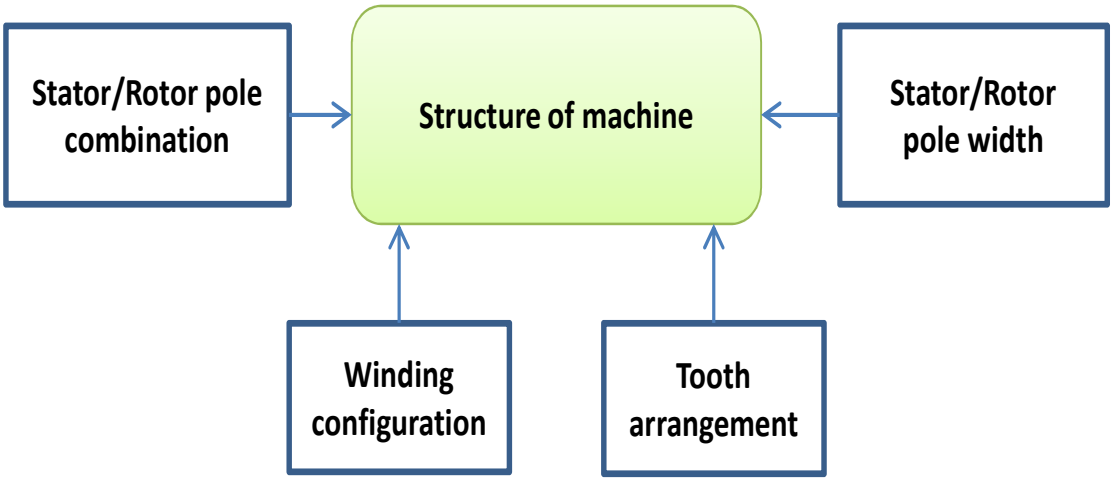

Figure 1-6: Parameters relating to structure of machine

literatures, the combination of the stator and rotor poles can be categorized based on the application of the SRG according to the low, medium and high speed applications as illustrated in Table 1-2. It is apparent from Table 1-2 that there is no specific configuration for the low, medium and high speed operation. Based on the structure of the machine, the lower number of poles have bigger dwell angle which is determined by the difference between the turn off and turn on angles. The number of rotor poles relates to the periodic cycle of one rotor position which decreases as the number of rotor poles increase shown below where N_r is the number of rotor poles.

$$1 \text{ cycle of rotor position} = \frac{2\pi}{N_r}$$

The lower number of poles machine have been suggested for a high speed application whereas the high number of poles is for a low speed application [56, 57]. The reason being, lower number of poles has larger dwell angles thus allowing the flux to reach its desired level at high speed. At a lower speed, the magnetic flux requires longer time to build up as compared to the higher speed [58]. Therefore, a high number of poles at low speed avoid saturation in the machine. In addition, with a higher number of poles, the aligned and unaligned inductance ratio is also reduced. The low inductance leads to a high peak current resulting in higher converter VA requirement [59].

The findings by Mueller [59] and Lovatt et. al [60] states that the relative performance such as current density and co-energy will not be affected by increasing the number of poles per phase. This is true since an increase on the number of poles per phase will

Table 1-2: Stator and rotor poles configuration for switched reluctance machine

Applications	Configuration of poles						
	6/4	**8/8**	**8/6**	**12/8**	**16/12**	**12/16**	**18/12**
Low and medium speed	[36]	[38]	[8, 39, 49]	[50, 61]		[62, 63]	
High speed	[31, 33, 34, 64]		[24, 28, 48, 65]	[32, 66]	[44, 67, 68]		[29, 35]
One periodic cycle of rotor position (degree)	90	45	60	45	30	22.5	30

reduce the number of machine phases. For example, a conventional three phase 12/8 machine is subjected to having four poles per phase. If this number is increased to six, the machine is subjected to a two phase 12/8 machine. Nevertheless, the machines are able to produce the required output power at a given rating. The selection of machine depends onthe type of application. Although the 12/8 machine provides the best power factor and excitation penalty, a 12/16 was preferred by Mueller based on its torque density performance. A new family of the SR machine with a higher number of rotor poles than stator poles can be achieved using a pole design (PD) formula [69, 70]. A significant improvement in torque per unit volume characteristics with lower ripple as compared to the conventional machine structure which has a higher number of stator poles has been shown previously [69, 70] .

At this stage of research, there is no right combination of stator and rotor poles which gives an optimum output performance. In terms of maintenance and reliability, large number of poles with a large number of phases has the advantage in terms of fault tolerance. A fault caused on one of the phases may be isolated leaving the others working with less interruption. Apart from that, the current per phase may be reduced by splitting across phases, which can lower the rating of the semiconductor devices per phase [71]. Nevertheless, having a higher number of poles and phases increases the control requirement. This dissertation involves analysis of different number of rotor poles whilst maintaining the same geometrical stator structure of the three phase 12/8 machine.

1.4.3.2 Winding Configuration

The winding configuration depicts how the coils are placed around the stator poles. It determines the flow of magnetic flux within the machine structure, producing either a short or long flux path. The short flux path produces symmetrical pattern and can be realized in a machine with an odd number of phases [72]. The long flux path is avoided to reduce losses in the iron core. The winding arrangement can influence the torque angle characteristics of the machine [73].

Another method to increase the torque per unit volume of the machine is through the winding arrangement of coils on the stator poles. The conventional design has concentric windings around the salient poles termed half pitch winding. The fully pitched winding places the coils in between the stator poles resulting in a larger excitation area [74]. The implication of a larger excitation area increases the field density thus torque will be increased [75]. Generally, the objective of the existing literatures on the winding arrangements focuses on improving torque, which relates more to the motoring operation.

1.4.3.3 Tooth Arrangement

Previous studies on the SR machine mostly cover the conventional design of one tooth per slot machine. Various studies on the effect of tooth width on torque production [76, 77] and acoustic noise [78] have been made to optimise the machine design. Examination on multi tooth per slot on the stator poles also shows improvement in the mass to torque ratio, which is an essential feature for wind turbine generator [79]. Although the various tooth design offer advantages over the conventional structure, the research was limited and it is not available commercially. This may be due to the complicated design of the teeth which have structure such as 26/16, thus reducing the space available for the winding. Furthermore, there are other methods available to improve torque and acoustic noise without performing major changes on the machine structure.

1.4.3.4 Stator and Rotor Pole Width

Any changes on the structure of the machine will affect its magnetic characteristic including the structure of the stator and rotor pole width. The changes in the widths of the

poles affect the inductance profile. The conventional design has a wide stator pole width as compared to the width of the rotor pole, producing a larger inductance profile. The surface area for the rotor pole to pass through is longer if the stator pole is wide. The rotor pole forms part of the flux path to complete the magnetic loop, thus having a small rotor pole width will result in higher pole saturation. An SR machine with a higher number of rotor poles has a limit on the value of the rotor width [70]. A double stator pole design of SR machine was proposed to generate motional forces to increase the energy conversion of the machine [80].

1.5 Statement of the Research Problem

Overall, the previous studies have acknowledged the potential of the SRG as one of the candidates for variable speed applications. Various researches have been performed as described in Section 1.4. Most of the available literatures were focused on the operation of the machine as a motor. The generating operation mainly covers the high speed application and studies are done on the specific individual element of the SRG drive such as the control, converter and also the machine geometry. For such specific study, an experimental set up is feasible since it does not involve many changes on the machine parameters. However, to analyse the machine thoroughly, various changes on the parameters have to be made. This would incur high cost and would be time consuming if the changes were to be performed during the experimental stage. The development of the SRG lacks a platform which enables researchers to perform analysis on the overall system before developing the machine prototype. To aid in the development of the SRG and to close the commercial gap between the existing machines, a simulation platform of the overall system is required. While a number of papers on simulation model of switched reluctance machine for motor [48] operation have been published, there is no model for SRG to determine the optimum design in terms of efficiency and performance during the low and medium speed operation to the best of our knowledge.

1.6 Research Methodology

This study will concentrate on the operation of the machine during the low and medium speed range. To meet the requirement for an optimal performance of the machine, the

dynamic operation together with its other elements such as converter and controller needs to be incorporated together. Therefore, this thesis is aimed at developing an integrated simulation platform of SRG to aid in the development of the machine. The development of the simulation platform is conducted using MATLAB/SIMULINK whereas COMSOL is used for machine study. The simulation platform will be used to find solutions to maximize the generating operation of an existing machine.

The first objective of this research is to perform a detailed analysis and investigation of the SRG conversion behaviour from mechanical to magnetic and to electrical energy. As a result of this investigation, a mathematical model of the SRG is produced. The second objective is to identify the design parameters and control parameters that affect the generated output power. Then, a simulation platform of the complete SRG system is produced and subjected to wide testing conditions for different sets of machine and different range of related control parameters.

1.7 Thesis Contributions

The main outcomes of this analysis are:

- Firstly, the design and development of an integrated simulation platform for SRG has been made.
- Secondly, a comparative analysis between different sets of machine and various ranges of control variables is performed. The restrictions and limitation in selecting the optimal control variables has been identified. The relationship between the optimal control parameters has also been proposed.
- Finally a simple controller to implement the proposed polynomial function is developed. The simulation model of the SRG serves as a platform to analyse various machine parameters to achieve optimal performance.

1.8 Thesis Organization

The dissertation is organized into eight chapters. It starts with the introduction and background which covers the current status of the electrical power generation and the requirement of electric generators. The choice of SRG and its recent development has

also been highlighted. The fundamental principles of the SRG drive are discussed in Chapter 2. It will cover the operational characteristics of the machine during generating operation and the energy conversion process. Basically, it will cover the fundamentals of the SRG drive which will be referred to in the following chapters. Chapter 3 describes the design of the machines considered in this research. It also outlines the methods to model the non-linear electromagnetic characteristics of the Switched Reluctance Machine (SRM). These characteristics embody the behaviour of the machine to be used for modelling and design of the controller. It forms the basis to the development of the simulation platform. Chapter 4 introduces the mathematical description and various modelling techniques which can be applied to develop the SR generator system. It also highlights the modelling technique and simulation package chosen based on the research objectives. Chapter 5 identifies the factors that affect the magnetic characteristics of the machine which influence the shape of its magnetization curve. This is achieved using different winding polarity and different number of rotor poles. Using the developed platform and the machines considered in Chapter 2 and 5, various control variables affecting the generated power is identified in Chapter 6. Chapter 7 describes the limitations in selecting the control variables and highlights the development of functions relating the optimal control variables with the generated power. Based on the findings, a novel control scheme is proposed. Lastly, the current work and future work is summarized and proposed in Chapter 8.

1.9 Conclusions

This chapter has briefly discussed the current status of the requirement for the electric power generation and also electric generator. The requirement for a generator which has the advantages to maximize the power generated at variable speed has been highlighted. In addition, the choice of a switched reluctance generator has been presented. The recent developments based on each of the components which form the SRG system have also been discussed. The next chapter will cover the fundamentals of the SRG drive and its characteristics operating as a generator. Based on this characteristic, the performance of the machine in terms of percentages of power generated will be highlighted.

CHAPTER 2

FUNDAMENTALS OF THE SWITCHED RELUCTANCE GENERATOR (SRG) DRIVE

The main SRG drive consists of the generator machine, the controller and the converter. The machine can be connected directly to the shaft of the prime mover. The shaft is then coupled directly to the rotor of the generator. Thus, any changes in the speed of the prime mover will directly affect the rotor of the generator, which is free from magnets and windings. The end of the concentrated windings on the stator pole is connected to the power converter, which receives signals from the controller. The controller is the heart of the system, which stabilizes the generated power through closed loop control of the voltage or current. It sends signals to the switches on the converter circuit. Upon receiving the signals, the converter performs excitation and demagnetization to build the flux up then bring it down to zero during each cycle of operation.

This chapter will describe in detail each component of the drive and investigate the energy conversion behaviour of the generator from mechanical to magnetic and to electrical energy.

2.1 History of SRG

The term switched reluctance, variable reluctance and electronically commutated reluctance motor refers to the same machine. Tremendous efforts have been made to distinguish the machine with other electrical machines. The term switched reluctance was first used by Nasar in his paper in 1969 and the widespread use of the term was influenced by Lawrenson [81].

The machine started way back in the early 1830s based on the concept of electromagnet. It was first used as a traction drive for an electric locomotive in the early days. Its development was hindered due to requirement of complicated control circuits and the high cost of power electronic devices. Furthermore, the emergence of the commutator motor in the 1870s and the introduction of the magnetic circuit law in the 1880s, results in

motors that outweigh the performance and requirement of the reluctance motor [81]. The Switched Reluctance Machine (SRM) made its come back in the 1960s due to the rapid development of the power electronic devices and also the availability of high speed computers coupled with the advanced programming languages [81]. It was first used as a motor drive in the 1980s and has made good progress since.

2.2 Structure of the Switched Reluctance Generator

In general, the SRG is a double salient machine where both its stator and rotor poles protrude into the air gap [82]. The rotor and the stator are made of steel laminations and only the stator poles have windings concentrated around them [56]. This leaves the rotor free from windings, magnets and brushes. The windings of one stator pole are connected in series with the opposite stator to form one phase. The windings are arranged in such a way that more than two opposite stator poles form one phase. The typical configurations of the machine include a three phase 6 stator and 4 rotor poles (6/4) machine, a three phase 12/8 machine, a four phase 8/6 and also a four phase 16/12 machine. Figure 2-1(a) shows an example of the 4 phase SR machine with 8/6 poles configuration while Figure 2-1(b) depicts a 3 phase machine with 12/8 poles configuration.

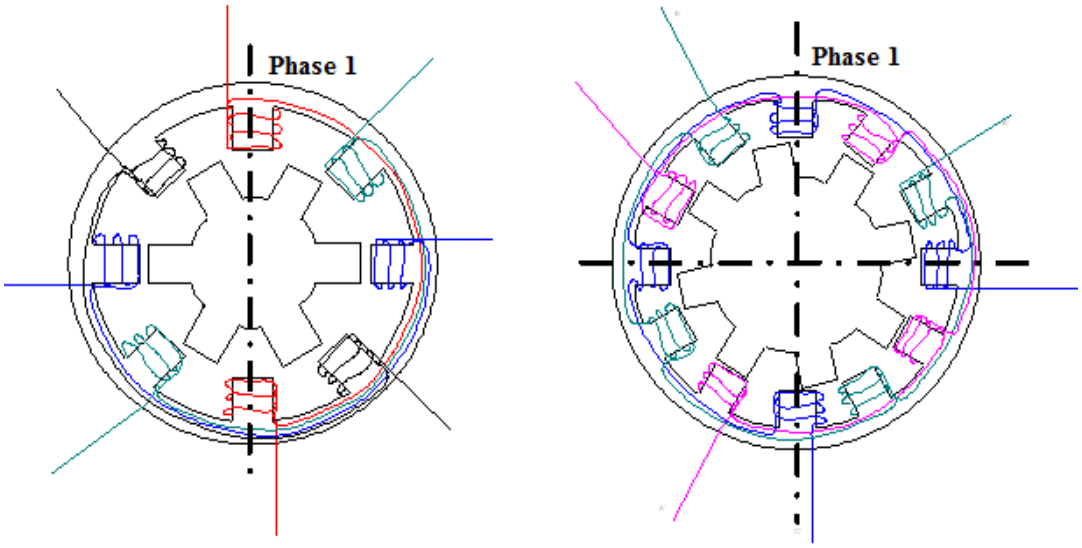

(a) (b)

Figure 2-1: Configuration of Switched Reluctance Machine: (a) 4 phase 8/6 and (b) 3 phase 12/8

2.2.1 Operation of Switched Reluctance Generator

The machine operates in such a way that the rotor will move to the position of minimum reluctance. The rotation of the rotor is achieved by energizing and de-energizing the phase windings on the stator poles. When the windings are energized, the stator pole behaves as an electromagnet pulling the rotor towards the excited phase. The stator phase has to be energized in synchronism with the rotor position to ensure continuous rotation. When the rotor moves towards the stator pole, there will be a change in the distance of the air gap, resulting in a change of the reluctance of the magnetic path. When the rotor is aligned with the stator pole, reluctance is minimum, whilst inductance is maximum. As the rotor moves away from the stator pole, the air gap increases and the inductance starts to decrease. During the unaligned position, inductance will be at its minimum value. By proper excitation of the phase winding, the machine can operate as a motor during the increasing inductance region, and as a generator during the decreasing inductance region. To operate the machine as a generator, the windings are excited as the rotor is moving away from the stator poles.

The excitation of the machine during the generating operation is illustrated in Figure 2-2a(ii) and Figure 2-2b(ii) whereas for motoring, the excitation is on the increasing inductance region. When the stator phase is excited as the rotor is moving pass the stator pole as in Figure 2-2a(ii) there will be a braking torque trying to realign the poles back together creating a negative torque, extracting energy from the prime mover. The torque T is produced by the tendency of the rotor moving towards the excited stator phase winding. It is independent of the direction of current, i shown by the equation below:

$$T = i^2 \frac{dL(i,\theta)}{d\theta} \tag{2.1}$$

where L is the phase inductance which varies as a function of both the current, i and rotor position, θ. From equation 2.1, the value of torque is dependent on the slope of the inductance profile, positive for motoring and negative for generating. As soon as the poles start to overlap, the torque starts to develop and when the poles are not overlapping, the torque will be zero and no energy is converted.

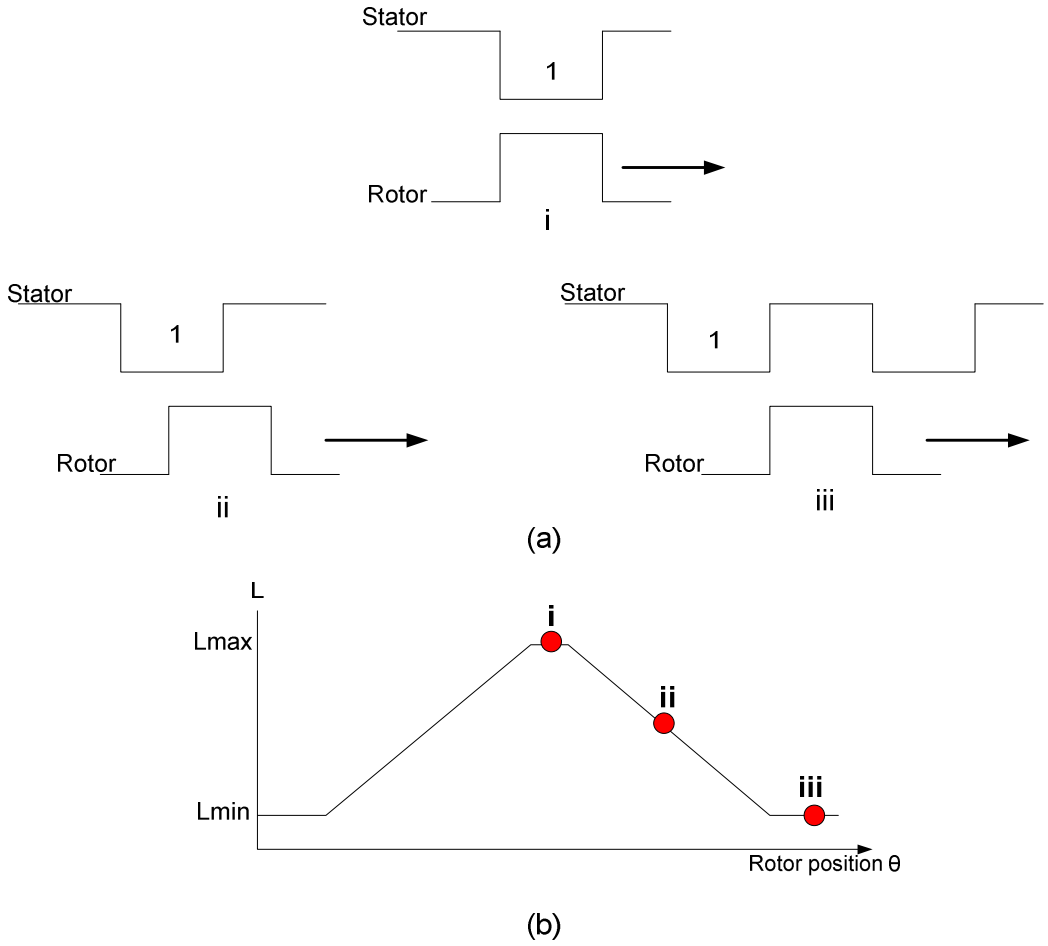

Figure 2-2: Variation of inductance with respect to movement of rotor. (a) rotor movement with respect to stator pole i) Maximum inductance, minimum reluctance (full alignment) ii) Inductance decreasing linearly iii) Minimum inductance (mis-alignment) (b) Complete inductance profile

2.3 Characteristics of the SRG

The magnetic characteristics of the machine can be determined from the flow of flux within the magnetic material. The flux is established when the current flows through the phase windings during excitation. The intensity of the magnetic field is represented by the flow of flux in the magnetic material. It changes with both the current density and rotor position. The flux intensity is high during the aligned position since the flux flows directly from the stator pole to the rotor pole. As the rotor moves, the air gap will increase and less flux is able to link to the rotor pole. The change of flux with the phase current at different rotor position is also known as the magnetization curve shown in Figure 2-3. The phase inductance can be determined from the magnetization curve by the following relationship:

$$\lambda(i,\theta) = L(i,\theta)i \tag{2.2}$$

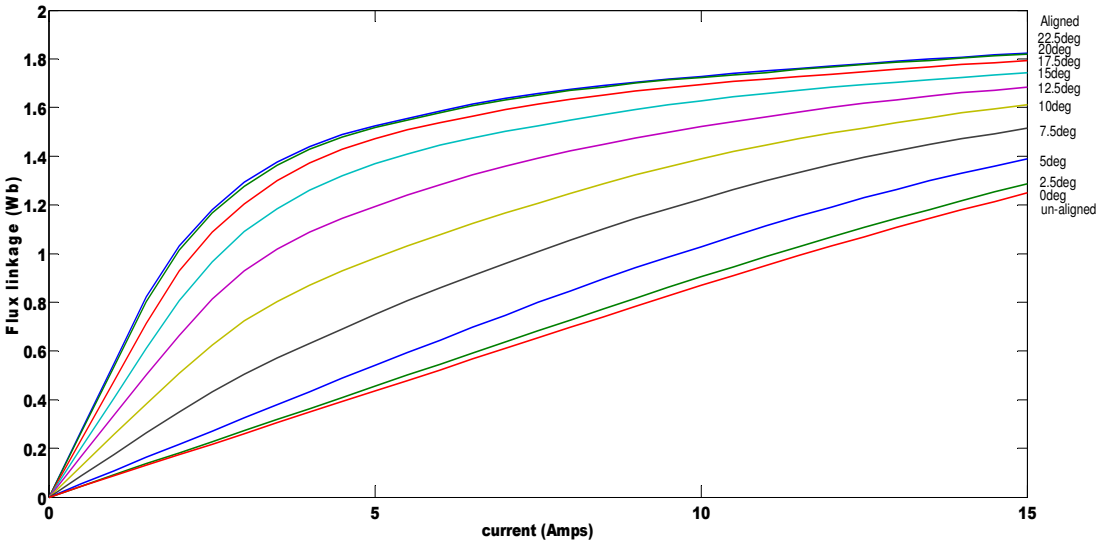

Figure 2-3: The flux linkage curve versus current at different rotor position from aligned to unaligned for the 12/8 machine

where λ is the flux linkage, L is the phase inductance, i the phase current and θ rotor position. The curve of the inductance as a function of current and rotor position determined using equation (2.2) is illustrated in Figure 2-4.

Therefore, the SRG can be represented by using the flux linkage or inductance profile. The details on the representation of the characteristic of the machine are explained in Chapter 3, which focus on the nonlinear electromagnetic characteristics of the machine.

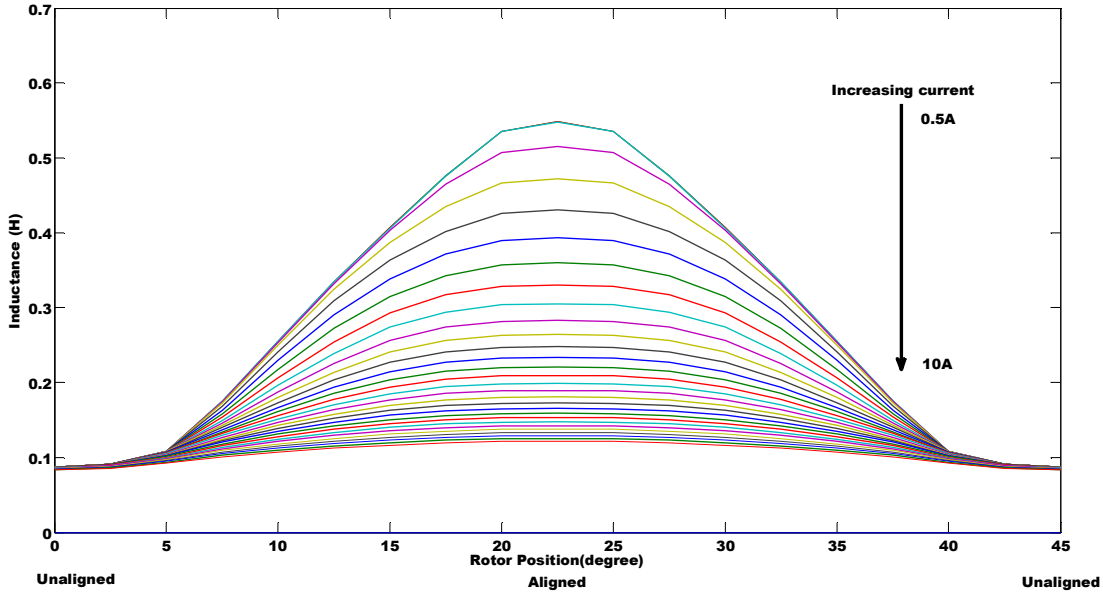

Figure 2-4: Variation of the phase inductance with rotor position at different phase current for the 12/8 machine

2.4 Electromagnetic Energy Conversion of SRG

The principle of energy conversion for the SRG is best explained by using the conventional asymmetric half bridge converter (AHBC) and the magnetization curve. The battery is connected directly across the phase winding through the switches and diodes. As mentioned earlier, the excitation is made as the rotor is moving away from the stator poles by closing the switches on the converter. When the switches T1 and T2 are closed as in Figure 2-5(a), the current will flow from the battery to the windings through the switches. The full terminal voltage will be across the phase winding; hence current will slowly build up and the energy is stored in the magnetic path of the coil. The energy is developed by the opposing torque on the prime mover. Both the switches will open when it receives signal from the controller upon reaching the turn off angle as depicted in Figure 2-5(b). The flow of current in the winding is maintained, however instead of storing energy, the stored energy is released through the diodes going into the battery or load. The output generated by the SRG using the AHBC is in DC form. Therefore,

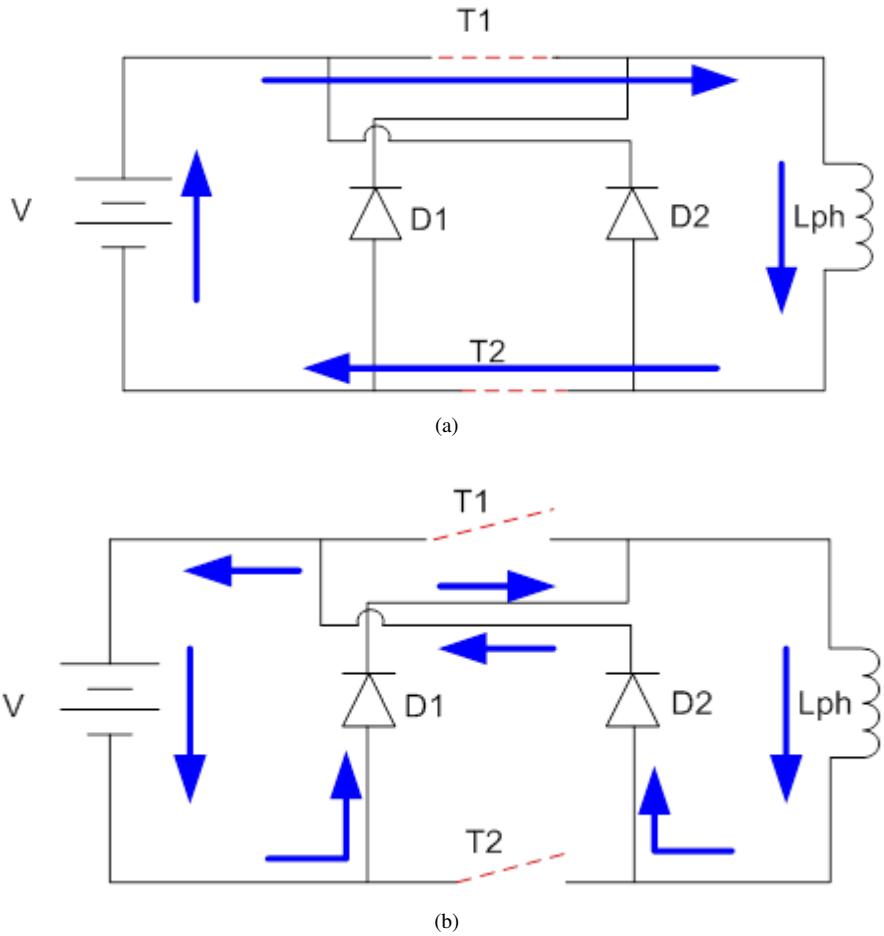

Figure 2-5: The flow of current in the phase winding for one phase using asymmetric half bridge converter (AHBC) during (a) excitation stage and (b) generation stage

another converter is required to convert it to an AC output if required.

2.4.1 Calculation of Magnetic Energy

The magnetic energy can be calculated from the magnetization curve of the flux linkage versus current at a particular rotor position as shown in Figure 2-3. However, for ease of understanding, the explanation is made by assuming a linear magnetic flux linkage region as illustrated in Figure 2-6. Since the excitation is performed during the maximum inductance profile, the phase current, i slowly increase from O to A as in Figure 2-6(a) and the magnetic stored energy, W_1 can be written as:

$$W_1 = \int_0^{i_m} i.d\lambda = \frac{1}{2} i_m^2 L_a \tag{2.3}$$

where i_m and λ are the current level and flux linkage. The slope of OA represents the phase self-inductance at the aligned position, L_a whereas the slope OC represents the

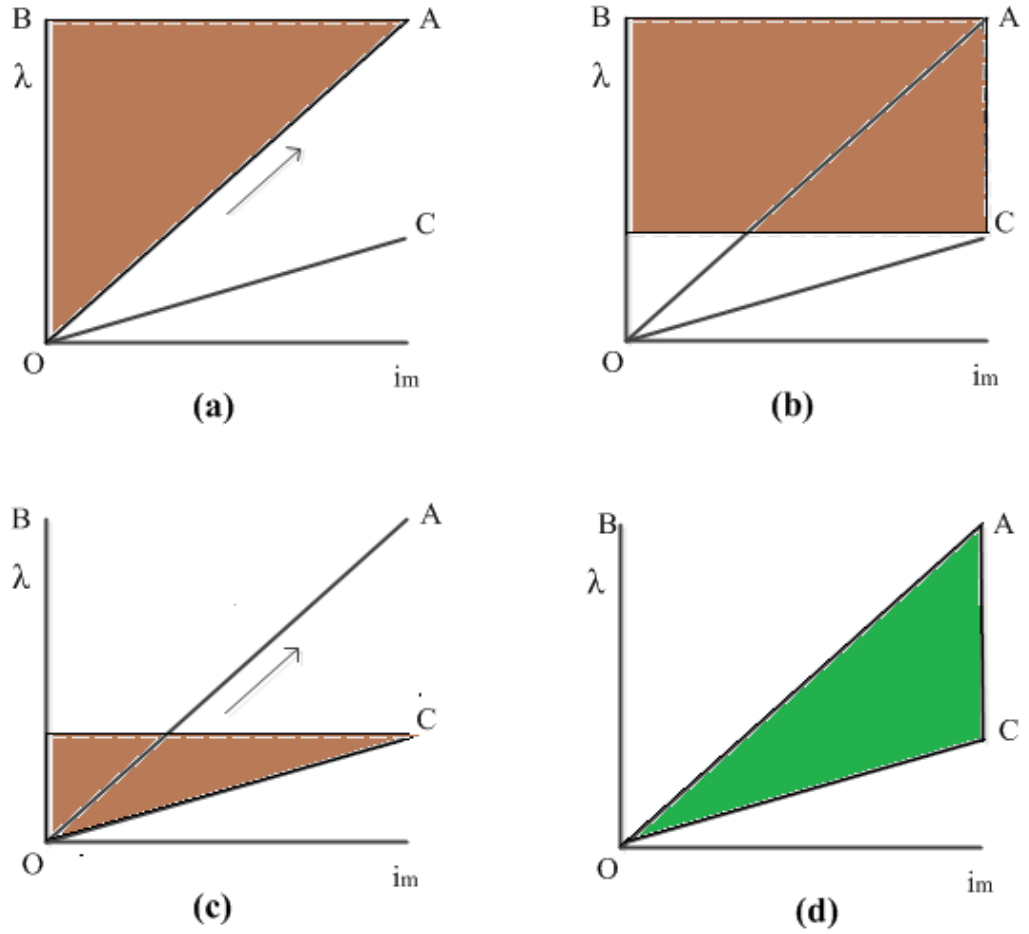

Figure 2-6: Linear energy conversion process for the SRG using the flux linkage versus current curve (a) magnetic stored energy, W_1 (b) energy returned to the supply, W_2 (c) remaining stored energy returned to the supply, W_3 and (d) co-energy, W_{total}

phase self-inductance at the unaligned position, L_{un}. As the rotor moves away from the stator pole and reaches the turn off position, no energy is extracted from the prime mover. At that moment, the energy W_2 is returned to the supply.

$$W_2 = i_m^2 (L_{un} - L_a) \tag{2.4}$$

During the unaligned position, the torque is zero. Hence, the remaining stored energy W_3 is also returned to the supply.

$$W_3 = \int_{i_m}^{0} i.d\lambda = -\frac{1}{2} i_m^2 L_{un} \tag{2.5}$$

The total energy generated W_{total} is the sum of the areas, which is the addition of the magnetic stored energy and energy being returned to the supply at the end of each stroke.

$$W_{total} = W_1 + W_2 + W_3 = \frac{1}{2} i_m^2 (L_u - L_a) \tag{2.6}$$

The same concept of energy calculation can be applied when the saturation is taken into account. There are two types of energy within the magnetization curve; the stored magnetic energy, W_m and the co-energy, W_c represented graphically as in Figure 2-7. The average output power generated by the SRG is proportional to the area between the aligned and unaligned curve. When the saturation is taken into consideration, the calculation of the magnetic co-energy is determined by integrating the area under the magnetization curve as defined by the following equation:

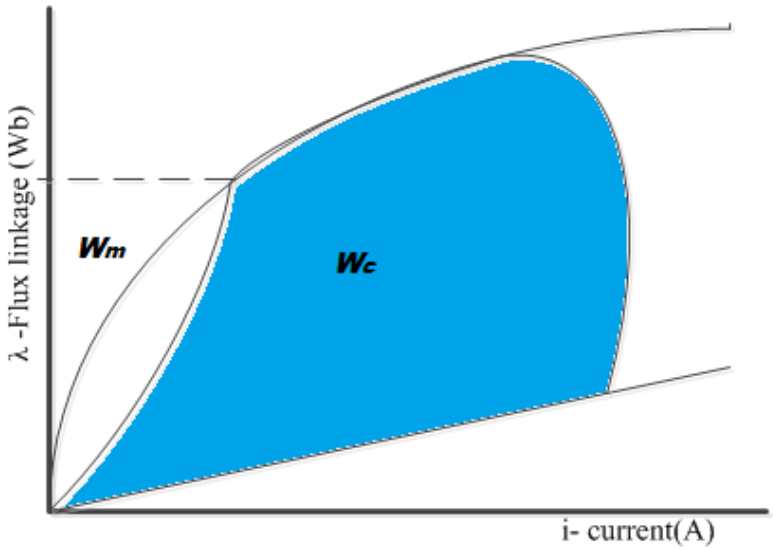

Figure 2-7: The non-linear conversion of magnetic energy in the switched reluctance generator

$$W_c = \int_0^i \lambda . di \tag{2.7}$$

The details of the calculation will be described in Chapter 3.

2.5 Mathematical Model of SRG

The mathematical model of the SRG is represented by the voltage equation across the phase winding. It consists of a resistance being in series with an inductance. Each phase of the SRG is considered to be independent of each other since the current and flux rises and returns to zero during each operating cycle. Thus, the phase voltage V across the winding is expressed as:

$$V_j = Ri_j + \frac{d\lambda_j}{dt} \tag{2.8}$$

Where R is the phase resistance, λ_j is the flux linkage of phase j, as a result of current, i flowing in the excited phase at time, t. Since the flux linkage varies as a function of the current and rotor position, equation (2.8) can further be expanded as follows:

$$V_j = Ri_j + \left(L_j + i_j \frac{\partial L_j}{\partial i_j} \right) \frac{di_j}{dt} + i_j \frac{\partial L_j}{\partial \theta} \omega \tag{2.9}$$

Where L_j , θ, ω are the inductance of phase j, rotor position and speed respectively. The last term in equation (2.9) is the motional back EMF, which can either be positive or negative depending on the slope of the inductance profile. The equivalent circuit for the SRG can thus be illustrated as in Figure 2-8. Since the back EMF is negative during the decreasing inductance slope, it will add on to the terminal voltage and aid in increasing the phase current during the generating operation. The flow of current in the phase winding remains the same; however the terminal voltage changes polarity. Therefore, equation (2.9) becomes negative and the current will be extinguished to zero at the end of the cycle, when the inductance reaches the minimum value.

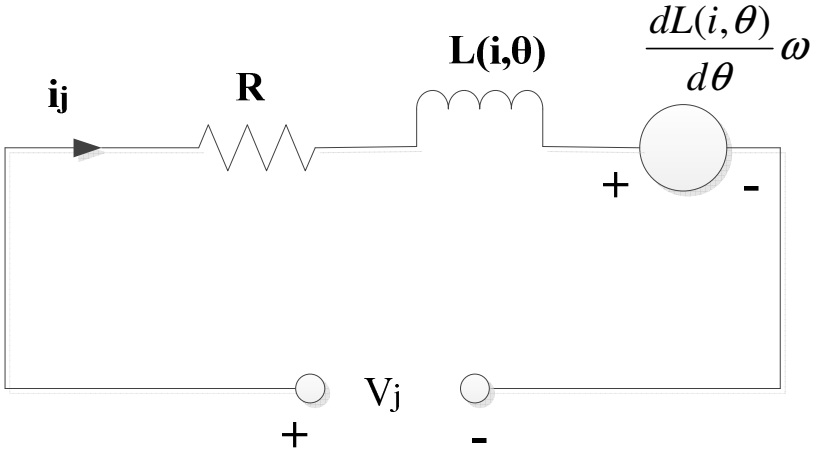

Figure 2-8: Representation of an equivalent circuit for one phase of the SRG

2.6 SRG Drive Converter

The function of the drive converter for the SRG is to perform excitation to build up the flux in the winding and demagnetization to bring the flux to zero before the excitation of the next phase [20]. Therefore, it must consist of a switch to allow the current to flow to the winding and a diode to allow the magnetic energy to freewheel back to the supply or load. The performance of the switching strategy gives an impact on the efficiency of the SRG [51]. The current can be controlled by the timing of the current pulses made in synchronism with the rotor position. At the moment there is no special preference of converter topology for either the low, medium or high speed operation.

Although there are various topologies which can be employed, the commonly described converter circuit is the Asymmetric Half Bridge Converter (AHBC). It consists of two switching devices and two power diodes per phase. There are several other types of circuits that use lesser components as compared to AHBC such as C-dump power converter, R-dump converter, bifilar type converter and also the split DC converter [83, 84].

However, due to the availability of the drive in the market and its control flexibility, the AHBC is selected. It has the ability to shape the phase current using three switching sequence as in Figure 2-9(a) positive voltage, (b) zero voltage and (c) negative voltage. This form of switching is suitable during the low and medium speed range, which

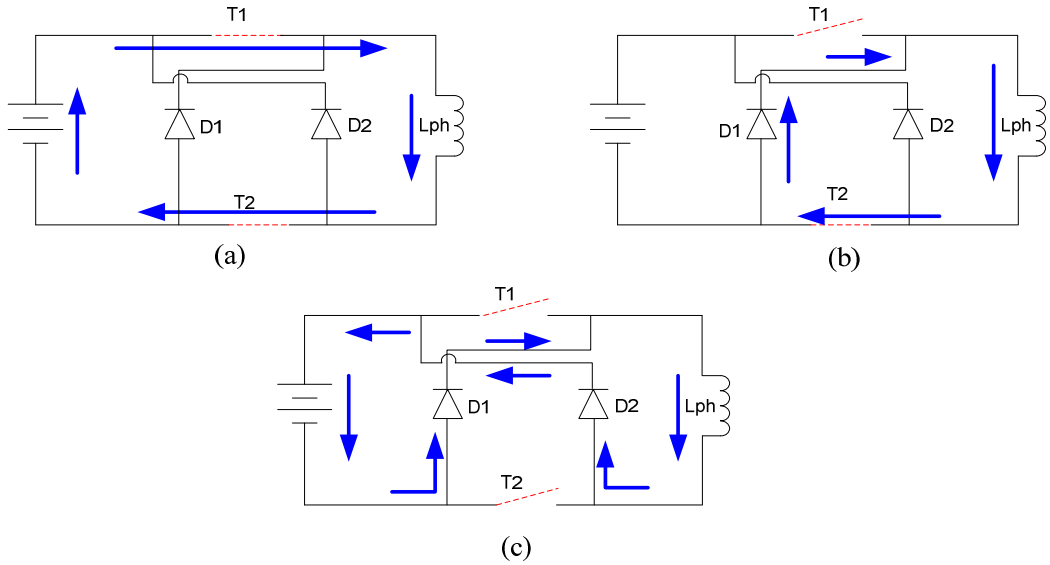

Figure 2-9: Switching sequence for the AHBC converter at (a) positive voltage (b) zero voltage and (c) negative voltage

employs the current chopping mode [51]. When the two switches T1 and T2 are turned on, the terminal voltage V will be across the phase winding given by the following equation:

$$V - \omega i \frac{dL}{d\theta} = Ri + L\frac{di}{dt} \tag{2.10}$$

where ω, i, R, L, θ are the speed, phase current, phase resistance, phase inductance and rotor position respectively. When T1 is open and T2 is closed as in Figure 2-9(b), the current will freewheel through the diodes and the winding. Hence, no energy is returned to the source. During this time, depending on the speed, the back EMF of the coil will aid in increasing or maintaining the current in the winding as shown in the following equation.

$$-\omega i \frac{dL}{d\theta} = Ri + L\frac{di}{dt} \tag{2.11}$$

When both the switches are open as in Figure 2-9(c), the current will freewheel through the diodes and the energy is fed back to either the load or to recharge the supply. Since the current returns to the source, the phase winding is subjected to a negative dc bus voltage. At this point, the shape of the current depends on the back EMF voltage. The relationship between the back EMF and terminal voltage determines the behaviour of the phase current [46]. Three conditions may occur:

- Back EMF voltage > terminal voltage - the current will increase after turn off angle before reducing to zero.

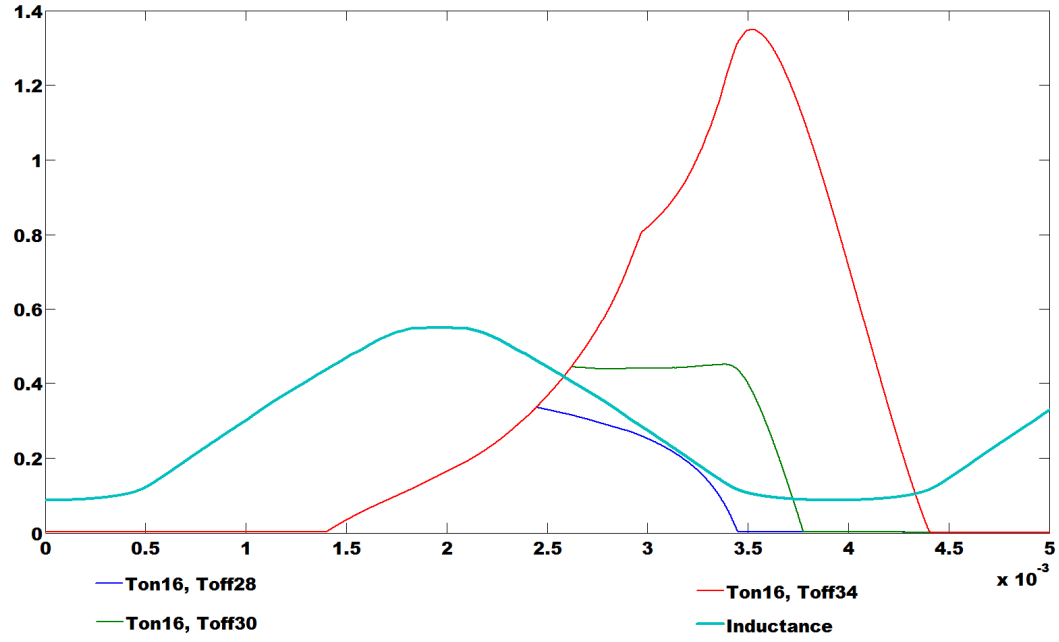

Figure 2-10: Graph of phase current (A) and inductance (H) against time(s) showing the effect of back EMF on the phase current at voltage of 150V and speed of 200rad/s. The turn on angle is constant at 16deg whereas the turn off angle is varied.

- Back EMF = terminal voltage – the current will stay constant and reduce to zero as the rotor approaches the minimum inductance region
- Back EMF < terminal voltage – the current will drop to zero after turn off angle due to the negative voltage.

The effect of the back EMF and terminal voltage after the switches are closed is depicted in Figure 2-10. It can be seen that the phase current can be regulated by the switches on the converter circuit. The AHBC converter is widely used in the low, medium and high speed application such as for the aircraft starter/generator and for the wind energy application. Although it has been reported to have voltage instability under the open loop control [40], it can be overcome by employing a closed loop control circuit. The operating modes of the converter will be explained in the following section.

2.7 Operating Modes of the SRG Drive

Based on section 2.6, the shape of the phase current are dependent upon the terminal voltage, back EMF, firing angles and also the speed. Therefore, the operating modes of the SRG can be categorized as current chopping mode and single pulse mode.

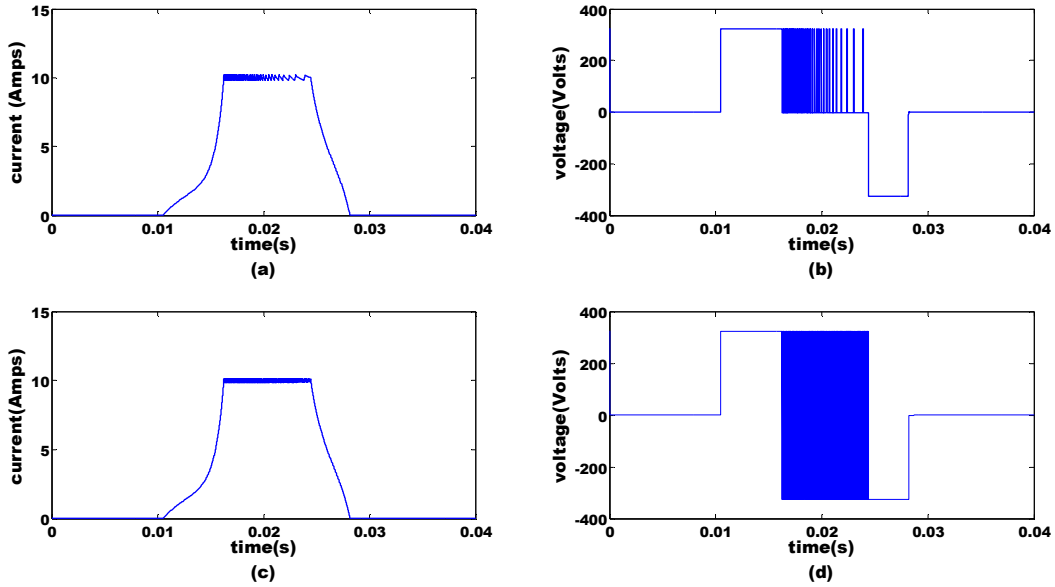

Figure 2-11: The phase current and voltage profile at turn on angle of 15deg and turn off angle of 35deg. Voltage=325V and speed=25rad/s (a) soft chopping current (b) soft chopping voltage (c) hard chopping current and (d) hard chopping voltage

2.7.1 Current Chopping Mode

The current chopping mode is commonly employed during the low speed range. For motoring operation, the excitation is performed during the minimum inductance profile whereas for generating operation, the excitation is made along the increasing inductance slope. The phase current can be controlled according to the reference limit as depicted in Figure 2-11. Figure 2-11(a) and (b) displays the soft chopping mode where one of the switches are on whilst the other are switched on and off depending on the reference limit. Figure 2-11(c) and (d) illustrates the hard chopping mode operation where both the switches operate simultaneously. The current chopping mode operates when the value of back EMF is lower than the terminal voltage [46]. During this time, the phase current is directly proportional to the terminal voltage.

Unlike the motoring operation, the initial rise of current during the generating operation is slow due to the high inductance value. Therefore, to aid in the fast increase of phase current towards reaching the reference limit, a boosting circuit is required [61]. The excitation can also be made along the decreasing inductance profile.

2.7.2 Single Pulse Mode

During high speed, the back EMF is more than the terminal voltage and the current no longer depends on the voltage. Hence, the machine operates in single pulse mode. The shape of the current depends on the placement of both the turn on and turn off angles along the inductance profile [85]. Depending on the amount of energy stored during excitation, the current will increase after the switches are turned off. The increase of current after turn off angle is affected by the negative back EMF and the amount of stored energy.

Figure 2-12 illustrates the effect of the turn on angle placed before and after the alignment position. A low back EMF is observed for the turn on angle placed after the alignment position. The current directly reduces to zero after the turn off angle. When the turn on angle is placed along the increasing inductance profile, the current will peak after the turn off angle depending on the amount of stored energy and back EMF [86]. The optimal values of the firing angles will provide the highest amount of power generated.

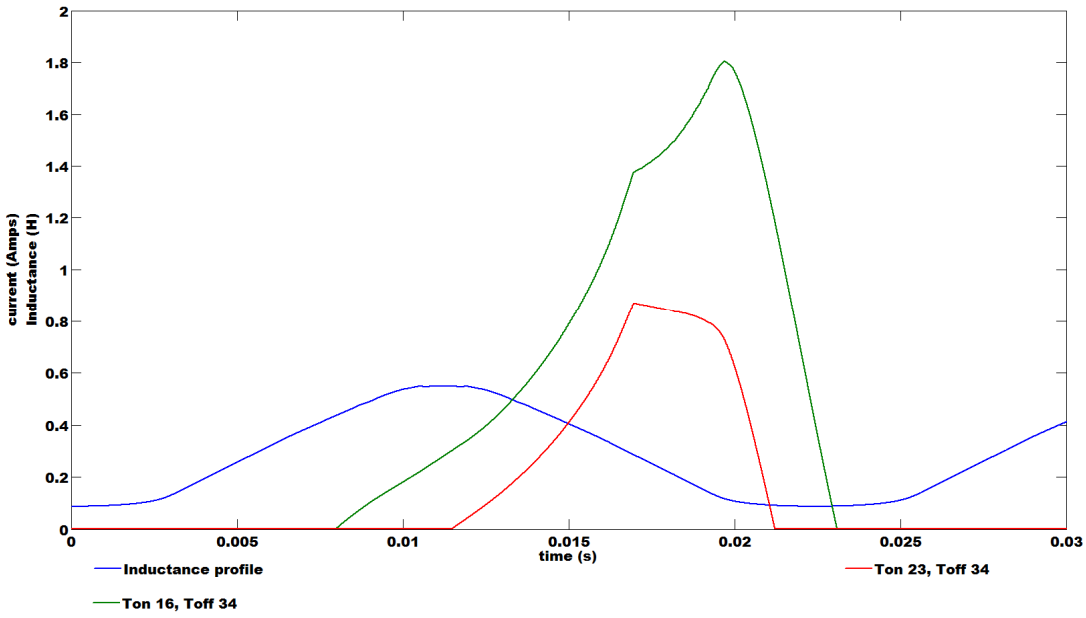

Figure 2-12: The effect of placement of turn on angle along the inductance profile at speed of 35rad/s and voltage of 50V

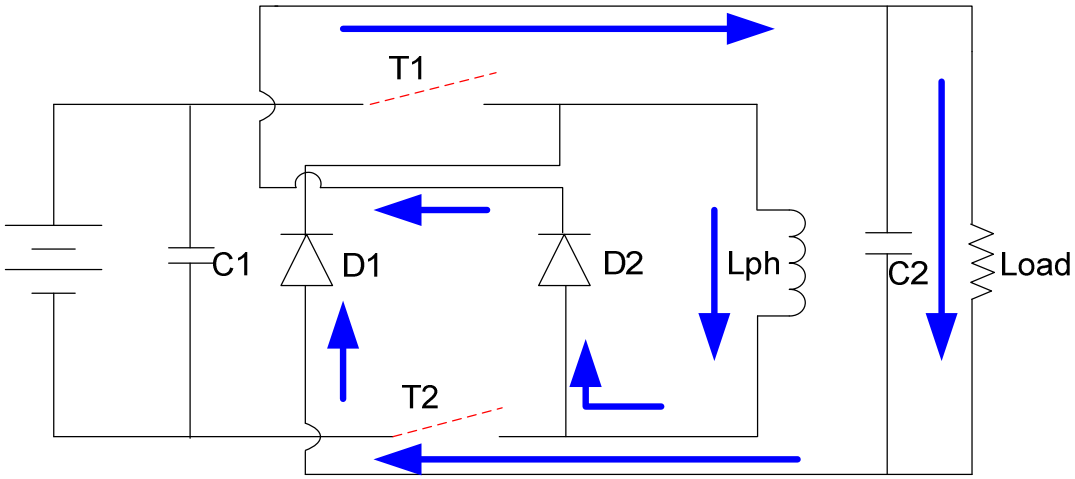

Figure 2-13: A separate excitation circuit for the switched reluctance generator

2.8 Excitation Method

The SRG requires an external supply such as a permanent magnet [87] or a battery to create the magnetic field, which can make it either be self or separately excited. The former has a simple circuit as both the excitation and generation shares the same bus line. The latter is commonly used under fault tolerant application since it has separate lines for the excitation and the generation of power [8, 66] as depicted in Figure 2-13. Due to this feature, the separate excitation circuit can be controlled independently [15]. The circuit is normally employed for applications which requires high safety features such as for aircraft starter/generator applications [66]. A well explanation on the self and separate excitation has been given in [40]. In this thesis, the self-excitation circuit will be used.

2.9 Average Power Calculation

The average output power P_{ave} of the switched reluctance generator is calculated based on the average voltage, V_{ave} and the average line current, I_{ave} of the power converter as follows:

$$P_{ave} = V_{ave} I_{ave} \tag{2.12}$$

The calculation for the average voltage and current is made based on the instantaneous values of the voltage, v and current, i across the phase winding as follows:

$$I_{ave} = \frac{1}{T}\int_0^T i.dt \tag{2.13}$$

where T is the period of one cycle of the phase current and i is the phase current of the winding. The multiplication of the instantaneous voltage and current yields power and energy can be calculated as shown below:

$$Energy = \int_0^T vi.dt \tag{2.14}$$

The energy on the other hand is power multiply by time T; hence, the average electric power of the SRG can be obtained by adding the power of each phase during one electric cycle as follows.

$$P_{ave} = \frac{1}{T}\sum_{j=1}^{m}\int_0^T v_j i_j dt = \frac{m}{T}\int_0^T v_j i_j dt \tag{2.15}$$

Where m is the number of phases, T is the conduction period of one phase, v_j and i_j is the instantaneous voltage and current of phase j. Based on the conversion of energy in subsection 2.4, the operation of the SRG involves two stages; excitation and generation. Therefore, the calculation of power can be made according to the operating cycle of the machine. Assuming that each phase of the SRG is independent of each other, the excitation and generation stage can be separated for calculation purposes as shown in Figure 2-14 for single pulse mode operation and Figure 2-15 for the current chopping

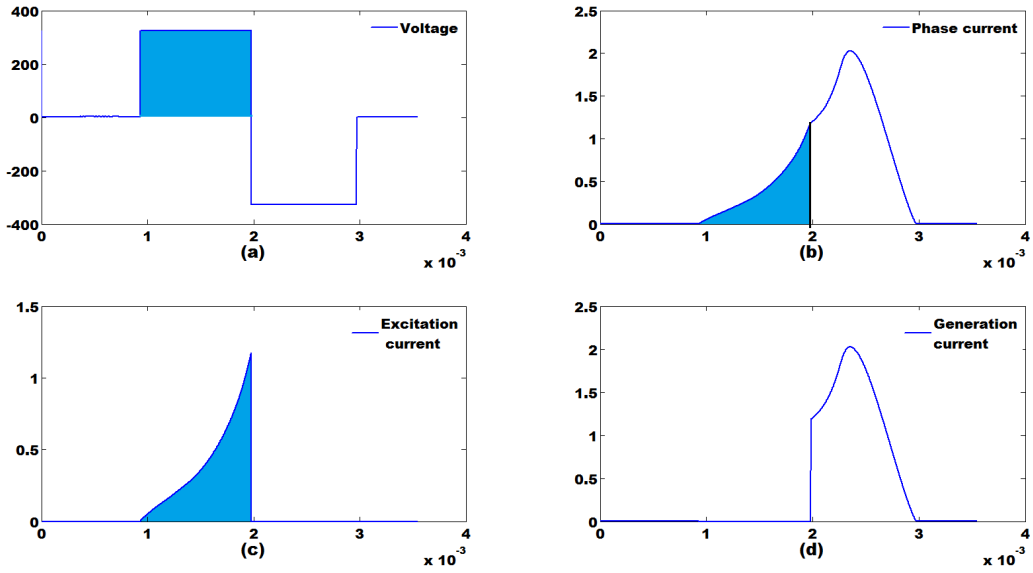

Figure 2-14: Graph of (a) terminal voltage (V) against time(s) (b) Phase current (A) against time(s) (c) Excitation current (A) against time(s) and (d) Generation current (A) against time(s) for one cycle of operation

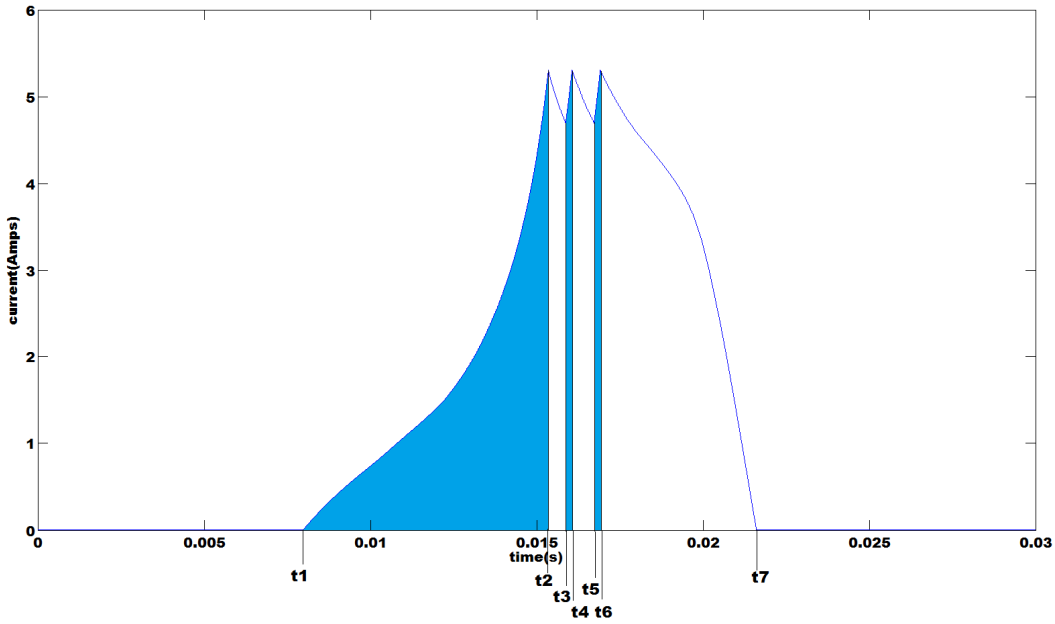

Figure 2-15: The phase current under current chopping mode operation

mode operation. The excitation power is obtained by multiplying the excitation current with the corresponding excitation voltage. For the current chopping mode operation, the excitation is calculated at each time the switches are closed. The excitation period occurs during time period t2-t1, t4-t3 and also t6-t5 whereas time t3-t2, t5-t4 and t7-t6 are the generating period. According to equation (2.15), the excitation and the generated power can be calculated as follows:

$$P_{exc} = \frac{1}{T}\int_0^T v_{exc} i_{exc} dt \tag{2.16}$$

and

$$P_{gen} = \frac{1}{T}\int_0^T v_{gen} i_{gen} dt \tag{2.17}$$

Where v_{exc}, $i_{exc,}$ is the instantaneous excitation voltage and current whereas v_{gen}, i_{gen} is the instantaneous generation voltage and current and T is the period of one current cycle. The performance of the machine can be measured in terms of the percentage of generated power P_{gen} by the following equation:

$$\%P_{gen} = \frac{v_{gen} i_{gen}}{v_{gen} i_{gen} + v_{exc} i_{exc}} \times 100 \tag{2.18}$$

The calculations shown above emphasize on the electrical components of the machine and exclude its losses. The total average output power of the SRG drive is the difference between the mechanical input power and the total losses in the system. The losses in the SRG include several components such as the semiconductor losses, $P_{semicon}$, copper losses P_{cu}, iron losses P_{iron}, mechanical losses, P_{mech} and other losses, P_{stray} such as friction and windage losses [88].

$$P_{loss} = P_{semicon} + P_{cu} + P_{iron} + P_{mech} + P_{stray} \tag{2.19}$$

The semiconductor losses comprises of the switching and conduction losses across the switches and diodes. The copper losses, P_{cu} is associated with the winding losses due to the phase current and winding resistance [89], whereas iron losses are composed of hysteresis and eddy current losses. It is highly nonlinear due to the asymmetrical flux linkage in the iron core. Because of this, the calculations of the iron losses are mainly based on estimation [90, 91]. The copper losses on the other hand can simply be calculated as:

$$P_{cu} = m.I_{rms}^2 R \tag{2.20}$$

Where m is the number of phases, I_{rms} is the root mean square (rms) phase current and R is the phase resistance.

2.10 Conclusions

This chapter covers the fundamental principle of the SRG including the machine structure, the operating principle, the converter used for SRG and also the operating modes available. The characteristics of the generating operation describe the conversion of energy from the mechanical to electrical energy. The characteristic also illustrates the development of the mathematical model based on the voltage across the phase winding. The converter operation focuses on how it can be controlled to allow for the energy conversion process. Based on the converter operation, two operating modes are discussed; current chopping and single pulse mode. The calculation to determine the performance of the machine in terms of the percentage of power generated is proposed according to the two operating modes.

CHAPTER 3

MODELLING OF ELECTROMAGNETIC PROCESSES

The electromagnetic characteristic is crucial for the development of a simulation platform for the machine. Therefore, this chapter outlines the methods to determine the nonlinear electromagnetic characteristics of the Switched Reluctance Machine (SRM). As stated in Chapter 2, the magnetic characteristic is based on the flow of flux due to the current in the winding and changes at each of the rotor position. The magnetic characteristic of the machine embodies its behaviour and is used for modelling or design of the controller. It is established based on the mathematical model of the machine, which is represented by the voltage across the phase winding. The model comprises of the electrical and the mechanical components. The electrical component is shown by the equation below:

$$V = Ri + \frac{d\lambda(i,\theta)}{dt} \tag{3.1}$$

The mechanical equation on the other hand is governed by the movement equation:

$$T_e = J\frac{d\omega}{dt} + B\omega + T_L \tag{3.2}$$

Where, V is the terminal voltage applied to the phase winding, i is the phase current, λ *is* the flux linkage of the phase coil, which is a function of both current and rotor position θ, T_e is the total torque for the machine, J is the total inertia of the rotor, B is the friction coefficient of the rotor, ω is the angular velocity of rotor and T_L is the load torque.

Since the flux linkage is a function of the phase current and the rotor position, equation (3.1) can further be expanded as follows:

$$V = Ri + L\frac{di}{dt} + \omega\frac{d\lambda}{d\theta} \tag{3.3}$$

Or

$$V = Ri + L\frac{di}{dt} + \omega i\frac{dL}{d\theta} \tag{3.4}$$

where L and R represents the phase inductance and resistance. The mathematical model of the SR machine can then be developed based on how one interprets its voltage across the phase winding; either using the inductance profile or the flux linkage profile.

According to equation (3.1) and (3.2), the magnetic characteristics that form the mathematical model of the machine include the flux linkage, inductance and also torque. They are normally pre-calculated before modelling. The pre-calculation of the magnetic characteristics can be obtained either by the finite element method (FEM), an experiment or by analytical calculation. It is the crucial point in order to optimize the design or to evaluate the machine performance. There are three methods to represent the machine in simulation for modelling:

1. Simulation using analytical method
2. Simulation using soft computing method
3. Simulation using finite element method (FEM)

The first two methods require initial data from either the FEM or experiment. The finite element method on the other hand requires the data to be validated from experiment due to the manufacturing process and the assumptions made.

The analytical model can be expressed in terms of inductance or flux linkage based model [92]. Due to the periodic nature of the inductance and the flux linkage, its variation can be represented by limited fourier series terms [93, 94]. The selected number of terms is based on the harmonic level [95]. Higher number of terms gives better precision but the calculation becomes complex. The variation of both the inductance and the flux linkage with current can be expressed by means of a polynomial [92]or an arc tangent functions [93, 94]. The geometrical dimensions of the machine can also be used to represent the machine analytically [96-98]. This method however requires exact details of the machine geometry. The analytical method involves iterative process to determine the required characteristics. It proves to reduce computation time and memory space. However, it requires accurate mathematical relation between the non-linear parameters of flux linkage and inductance with the current and rotor position. The coefficients of the function are determined based on curve fitting procedure. Also the mathematical function becomes complex as mutual coupling and flux leakage effects are included. The main advantage however is the inclusion of the phase winding end effects which increase the accuracy of the model. This method is suitable to be realized for optimization in real time simulation.

The second approach is based on the soft computing method such as fuzzy logic (FL)[99, 100], least square algorithm with orthogonal polynomial and artificial neural network (ANN)[101]. The soft computing strategies are dependent on the data set obtained from either experiment or FEM. They employ a supervised learning and training method hence the accuracy and the initial number of data set is of importance [102]. Unlike the analytical method, the soft computing strategies are suitable for both the online or offline parameter identification. The main disadvantage is that the settings of the model and network parameters require the experience and knowledge of the designer.

The FEM approach is achieved with the help of the available analysis packages such as ANSYS, FLUX 2D or COMSOL. Different from the previous methods, it only requires the geometry of the machine which can be obtained from the manufacturer. In most cases, the 2D analysis provides sufficient accuracy to model the performance of the machine. The determination of the flux linkage data is performed under different rotor positions between the aligned and unaligned rotor positions for varying excitation current conditions. The FE method allows direct coupling to other software such as MATLAB, but is not suitable for optimization purpose due to the high simulation time. The pre-calculated data gives better simulation time and is the most accurate method for analysis. The finite element method (FEM) has been well established and is widely used in the design process for electrical machines due to its ability to compute magnetic vector potential on structures with complex geometry having non-linear machine characteristics [103]. The ability of the finite element to solve such problems suits well with the SRM which have non-linear characteristics due to its double salient pole structure. Therefore, it was decided that the FEM is the best method to adopt for this study. The calculations leading to the development of the magnetic characteristics for the machine are reported in the following subsections.

The descriptions of the machines under study are highlighted under Section 3.1. Section 3.2 describes the numerical analysis and the related equations using FEM. In section 3.3, the calculations to determine the static characteristics of the machine are explained in details. Finally, section 3.4 describes the experiment to validate the procedures and results using the FEM.

3.1 Description of Machine

The fundamental step in FEM is to specify the geometrical description of the machine, which is available from the manufacturer data sheet. In this study, four machines are analysed including the existing 12/8 machine. As for the other three machines, their stator and rotor geometry structure is made to replicate the existing 12/8 machine whilst the number of rotor poles changes. The following describe the parameters of the machine in detail:

- Machine 1: The existing 12/8 machine which has been used as a motor for the wood lathe application will be the base machine model for this study.
- Machine 2: A 12/16 machine with dimensions obtained from the manufacturer's data sheet. The machine was selected to study the impact of having higher number of rotor poles.
- Machine 3: A 12/16 machine having exactly the same dimension as the 12/8 machine but the dimension of the width of rotor poles were halved.
- Machine 4: A 12/4 machine with the same dimension as the 12/8 machine but the width of the rotor poles were doubled.

The study involves the change on the number of rotor poles as it does not have any windings, thus it is the easiest part to manufacture and can reduce the time and costs from having to manufacture the complete machine. The geometrical structure and dimensions of the 12/8 machine is depicted in Figure 3-1 whilst the detailed dimensions of the machines are listed in Table 3-1. The structures of the other machines are illustrated in Appendix B.

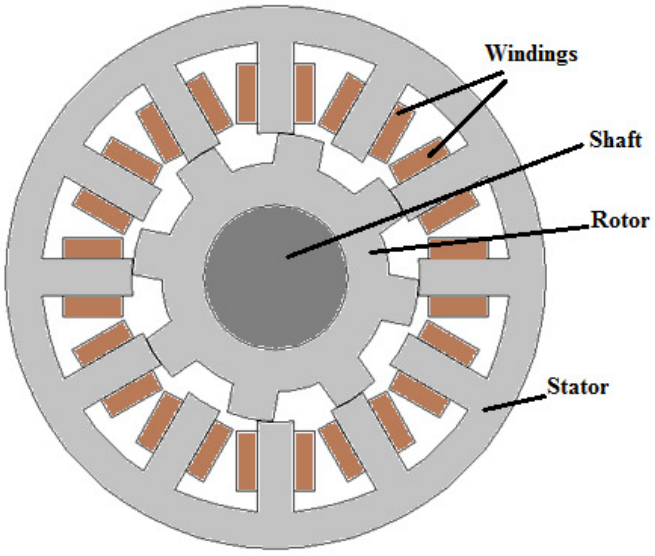

(a)

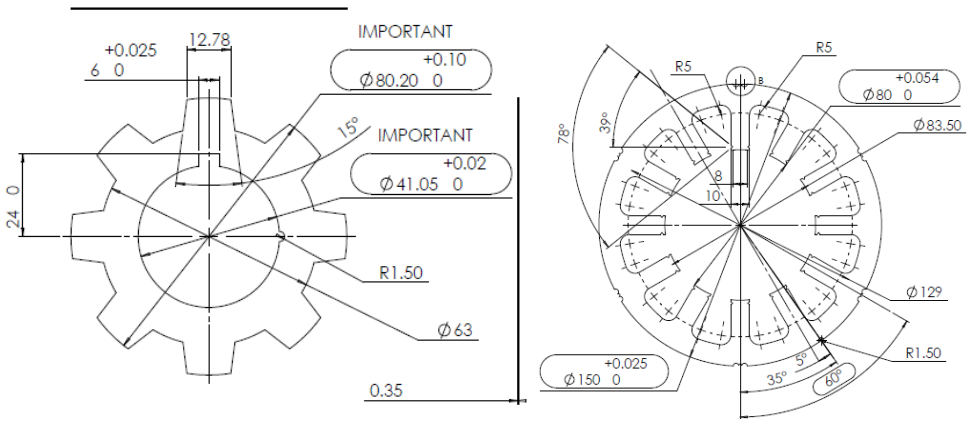

Figure 3-1: The (a) complete structure and (b) dimensions of the 12/8 switched reluctance machine

Table 3-1: Dimensions of the SR machine

PARAMETER	DIMENSIONS			
	Machine 1	**Machine 2**	**Machine 3**	**Machine 4**
Stator outer diameter S_{od}	150mm	150mm	150mm	150mm
Stator inner diameter S_{id}	130mm	130mm	130mm	130mm
Diameter of stator pole (tooth to tooth)	80mm	79.6mm	80mm	80mm
Shaft diameter d_{shaft}	41.05mm	41mm	41.05mm	41.05mm
Rotor outer diameter R_{od}	79.3mm	79mm	79.3mm	79.3mm
Rotor inner diameter R_{id}	63.05mm	69mm	63.05mm	63.05mm
Width of stator tooth S_{tw}	10mm	6mm	10mm	10mm
Width of rotor tooth R_{tw}	12.78mm	7mm	6.39mm	25.26mm
Air gap g	0.35mm	0.3mm	0.35mm	0.35mm
Stack length L	0.12m	0.12m	0.12m	0.12m
Diameter of copper wire Cu_d	0.73mm	0.73mm	0.73mm	0.73mm
Number of turns per pole N	180	180	180	180

3.2 Analysis of Electromagnetic Fields using Finite Element Method

3.2.1 Fundamental of Electromagnetic Fields

The magnetic vector potential, $\vec{A}$ computed by the FE method can be processed to obtain the field distribution, torque and flux linkage [104]. These magnetic fields are governed by the following Maxwell's equations represented in four differential forms:

A. Gauss's Law for electricity-

$$\nabla.\vec{D} = \rho \tag{3.5}$$

Where $\vec{D}$ is the electric flux density vector or displacement vector and ρ the electric charge density:

B. Gauss's Law for magnetism-

$$\nabla.\vec{B} = 0 \tag{3.6}$$

Where $\vec{B}$ is the magnetic flux density vector

C. Ampere's Law-

$$\nabla\times\vec{H} = \vec{J} + \frac{\partial\vec{D}}{\partial t} \tag{3.7}$$

where $\vec{H}$ is the magnetic field intensity vector and $\vec{J}$ the total current density vector.

D. Faraday's Law-

$$\nabla\times\vec{E} = -\frac{\partial\vec{B}}{\partial t} \tag{3.8}$$

where $\vec{E}$ is the electric field intensity vector. The equations above are supported by their relative constitutive relations which takes the assumptions that the machine used are isotropic:

$$\vec{D} = \varepsilon\vec{E} \tag{3.9}$$

$$\vec{B} = \mu\vec{H} = \mu_0\mu_r\vec{H} \tag{3.10}$$

where μ_0 and μ_r is the magnetic permeability and relative permeability.

3.2.2 Application of Maxwell's Equation to 2D Case

The 2D analysis was chosen for this study because the machine can be analysed in a plane. Furthermore, the results from the 2D analysis have been demonstrated to be efficient in providing performance evaluation provided that the axial effects are not

relevant [105]. It is easier to generate and requires less computation time as compared to the 3D model. The common applications using the 3D model includes hot spots, thermal analysis [106, 107] and also structural analysis. Due to the complexity of the 3D model and long computation time, a 2D model is used for this research work to obtain the magnetic parameters and static characteristics. End-effects can be corrected by introducing an inductance without considerable loss of accuracy [108]. The following assumptions were made for 2D modelling analysis:

- The winding is subjected to the direct current excitation source hence there is no eddy current effects.
- The magnetic field is confined within the machine. Anything outside the machine boundary is treated as zero potential.
- Magnetic material is isotropic.
- The direction of electromagnetic field is only along x and y axis. This means the axial direction of the shaft is neglected (z direction).
- The current density within the conductors is uniform.

The formulation of the problems is made in terms of the electric scalar potential V and the magnetic vector potential $\vec{A}$. The Maxwell Ampere's law for the quasi-static system gives:

$$\nabla \times \vec{H} = \sigma\left(\vec{E} + \mathrm{v} \times \vec{B}\right) + \frac{\partial \vec{D}}{\partial t} + \vec{J^e} \tag{3.11}$$

$$\vec{E} = -\nabla \mathrm{V} - \frac{\partial \vec{A}}{\partial t} \tag{3.12}$$

$$\vec{B} = \nabla \times \vec{A} \tag{3.13}$$

where, σ = the electric conductivity.

v = the velocity of the conductor.

$\vec{J^e}$ = the external current density.

$\vec{A}$ = the magnetic vector potential.

V = the electric scalar potential.

By substituting equations (3.10), (3.12) and (3.13) into (3.11) yields:

$$\sigma \frac{\partial \vec{A}}{\partial t} + \nabla \times (\mu_0^{-1} \mu_r^{-1} \nabla \times \vec{A}) + \sigma \nabla \mathrm{V} - \sigma \mathrm{v} \times (\nabla \times \vec{A}) = \vec{J^e} \tag{3.14}$$

When there is no variation in the z direction, the electric field is parallel to the z axis hence, ∇V is the potential difference over distance d and can be written as $-\Delta V / d$. In the magnetostatic case the first term of Equation (3.14) is dropped and rewritten as:

$$\nabla \times (\mu_0^{-1} \mu_r^{-1} \nabla \times \vec{A}) - \sigma v \times (\nabla \times \vec{A}) = \sigma \frac{\Delta V}{d} + \overrightarrow{J^e} \tag{3.15}$$

Here, $\overrightarrow{J^e}$ is the externally applied field and v is the velocity of the conductor which is zero in this case. The magnetic vector potential is expressed in terms of the magnetic flux density and electric field intensity as depicted in equation 3.12 and 3.13.

3.2.3 Finite Element Analysis (FEA) Software

The FE method uses the triangle elements to form the geometry of the structure, forming a grid called mesh. The size of the elements will change according to each region in the structure. The mesh grid around the air gap is fine and coarser as it gets away from the air gap. The FEA can be achieved by three principle steps namely:

- Pre-processing
- Analysis
- Post-processing

3.2.3.1 Pre-processing

Once the machine dimensions have been defined, each elements of the machine must be linked to its corresponding materials. The stator and rotor subdomains were set with the material magnetization curve of soft iron. The windings were set as copper with a unitary relative permeability. The shaft was made of aluminium also with a unitary permeability. The empty spaces between the subdomains were set as air. The current density was specified according to the respective stator pole windings. It must establish a correct direction and magnitude of the magnetic field. The machine model is then subdivided into a mesh of non-overlapping triangular elements. The size of the mesh was selected to be fine in the air gap region and coarser as it moves away from the air gap.

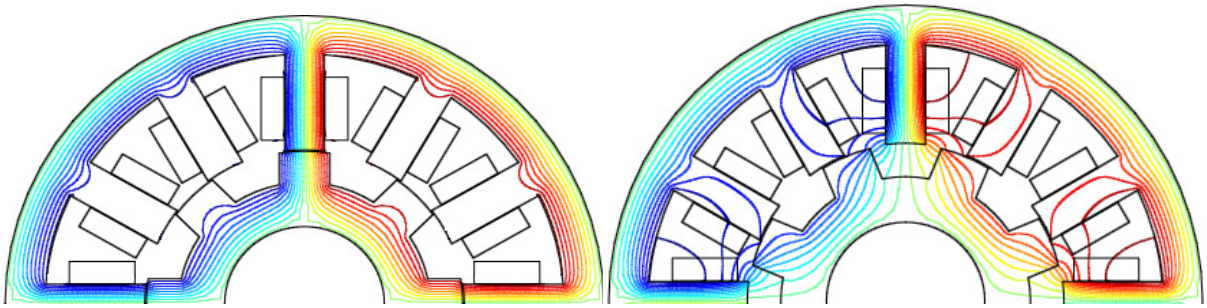

Figure 3-2: Flux distribution in the (a) aligned position and (b) unaligned position

3.2.3.2 Analysis

The analysis process includes the definition of each of the machine structures. It also involves selection of the solver for the model. The FEM solves the partial differential equation by means of algebraic equations using a specific numerical technique. The parametric solver with static analysis type provides reading for the various currents in the phase winding at each rotor position.

3.2.3.3 Post-processing

The simulation was performed under static conditions to determine the magnetic potential vector distribution along the machine. The solution leads to the calculation of the magnetic flux in each phase. The magnetic flux obtained at the aligned and unaligned rotor positions is shown in Figure 3-2. The B-H curve for the rotor and stator material is from soft iron material which gives a close match to the flux linkage characteristic of the machine.

3.2.4 Calculation of Static Magnetization Curves using FEA

The magnetization curve of the machine serves as a basis to calculate the parameters such as i-curve, co-energy and also torque. The combination of these characteristics will form the mathematical model of the SR machine.

The magnetic flux, λ through a surface can be defined as follows [109]:

$$\lambda = \oint_s \vec{B}.d\vec{S} = \oint_s (\nabla \times \vec{A}).d\vec{S} \tag{3.16}$$

where B is the magnetic flux density and A is the magnetic potential. This results in Stoke's theorem which states that the open surface S is bounded by the contour C.

$$\lambda = \oint_S (\nabla \times \vec{A}).d\vec{S} = \oint_C \vec{A}.d\vec{l} \tag{3.17}$$

In the x-y plane, the flux linkage through one winding turn can be evaluated by the difference of the magnetic vector potential between the two points multiplied by the depth of the object [103]. The total flux linkage is calculated by summation of the flux contributed by each coil [109]. These summations can be formulated by using the subdomain integration over the coil areas $F_1$and F_2 as depicted in Figure 3-3.

$$\lambda = \frac{nl}{F_1}\int_{F_1} \vec{A}_1.dF_1 - \frac{nl}{F_2}\int_{F_2} \vec{A}_2.dF_2 \tag{3.18}$$

Where l is the stack length or depth in the z direction and n is the number of turns per phase. Since the movement of the rotor pole from the aligned to the unaligned position correspond to half of the inductance profile, the readings of the flux linkage is taken between the range 0^0 to 22.5^0 in 0.5^0 increments for the 12/8 machine. The subsequent sections will discuss the calculations of other machine parameters such as torque, co-energy and also i-curve.

3.2.5 Calculation of the Static Torque Curves using FEA

Torque represents the mechanical section for the machine. The calculation is based on the electromagnetic force acting on an enclosed volume of a nonlinear magnetic system. There are several methods to calculate torque according to the theory of electromagnetism such as:

- Maxwell stress method
- Coulomb Virtual work method
- Global Virtual work Method

The first two methods are based on the calculation of the individual finite element components and rely on the computed flux density in the air gap. Thus, both are sensitive to mesh discretization and integration contour location [110-112]. Therefore, the Global Virtual work method is preferred and well suited for FE, generally because

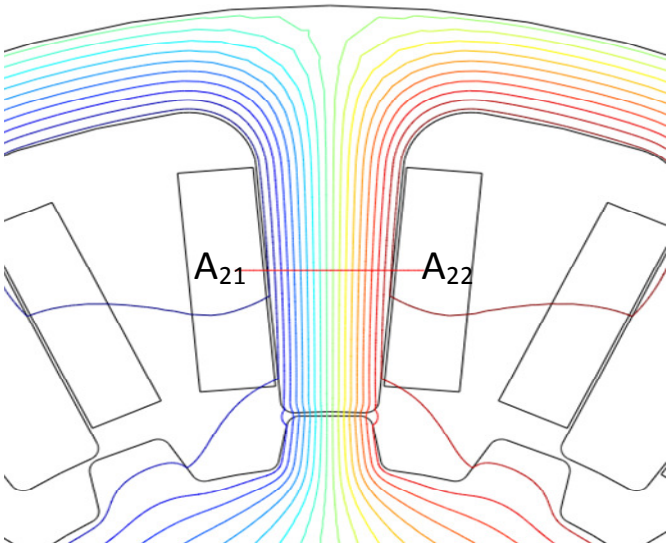

Figure 3-3: Calculation of flux linkage using FEA

it does not depend on errors caused by meshing as compared to the former methods.

The torque is derived based on the derivative of co energy, W_c with respect to the rotor position θ at constant current i or using the derivative of magnetic energy W_m with respect to the rotor position at constant flux linkage λ.

$$T_e = -\frac{\partial W_m}{\partial \theta}\bigg|_{\lambda=constant} = \frac{\partial W_c}{\partial \theta}\bigg|_{i=constant} \tag{3.19}$$

The calculations of the magnetic energy or co-energy are based on the magnetization curve of flux linkage versus current.

3.2.6 Calculation of i-curve

The current curve is developed to form a matrix corresponding to the function of current i as a function of flux linkage λ and rotor position θ, $i = f(\lambda, \theta)$. The initial data for this procedure is obtained using the magnetization curve. Both elements of the magnetization curve must be extended to its maximum value (maximum flux) to avoid the undefined elements for the i-curve. This can be achieved by extrapolation and addition of extra point without changing the initial shape of the curve. Then the i-curve can be plotted for any selected current to its corresponding flux linkage for each rotor position as depicted in Figure 3-4. Using this method, the flux linkage can be expressed as a product of two functions: current and rotor position. The i-curve data is

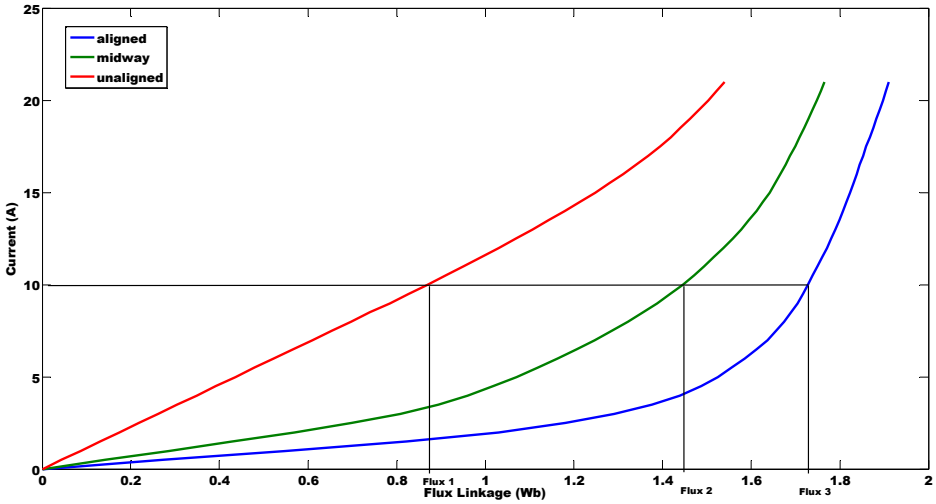

Figure 3-4: Calculation of i-curve from magnetization curve

represented as a look-up table in SIMULINK having flux and rotor position as the input.

3.2.7 Calculation of Co-energy

The co-energy, W_c is calculated by integration of the flux linkage, λ at each of the rotor position between its selected current, i values [113, 114].

$$dW_c = \int_0^i \lambda di \tag{3.20}$$

The integration is repeated for all the rotor positions and currents to obtain the graph of co-energy as a function of current and position. The calculation is performed by summation of the area under the graph using Simpson's 1/3 rule. The method uses a parabolic interpolant passing through three adjacent nodes. It approximates the integration of equation (3.20) as a trapezoidal function.

$$W_c = \left[f(i_1) + 4f\left(\frac{i_1 + i_3}{2}\right) + f(i_3) \right] \frac{h}{3} \tag{3.21}$$

The area under the magnetization curve is divided into even panels of width h indicated in Figure 3-5.The mathematical formula as in equation (3.21) can expressed using MATLAB/SIMULINK as in Figure 3-6 and Figure 3-7.The process is repeated for each rotor position giving the co-energy profile illustrated in Figure 3-8. The slope of the ramp and time of simulation can be set to match the maximum current of magnetization curve.

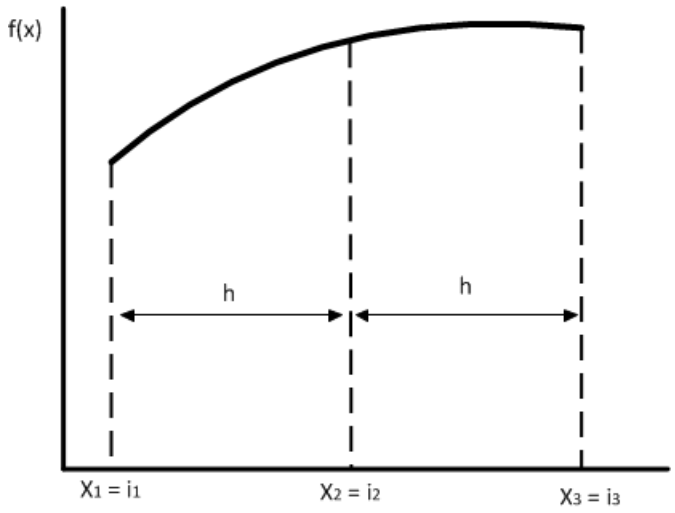

Figure 3-5: Simpson's 1/3 rule applied to magnetization curve

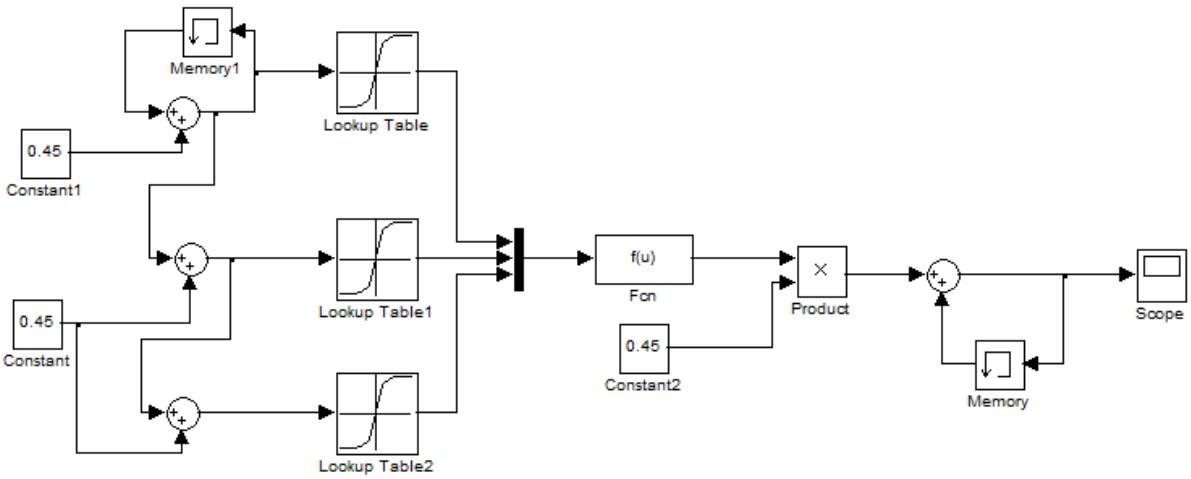

Figure 3-6: Representation of Simpson's 1/3 rule in MATLAB/SIMULINK

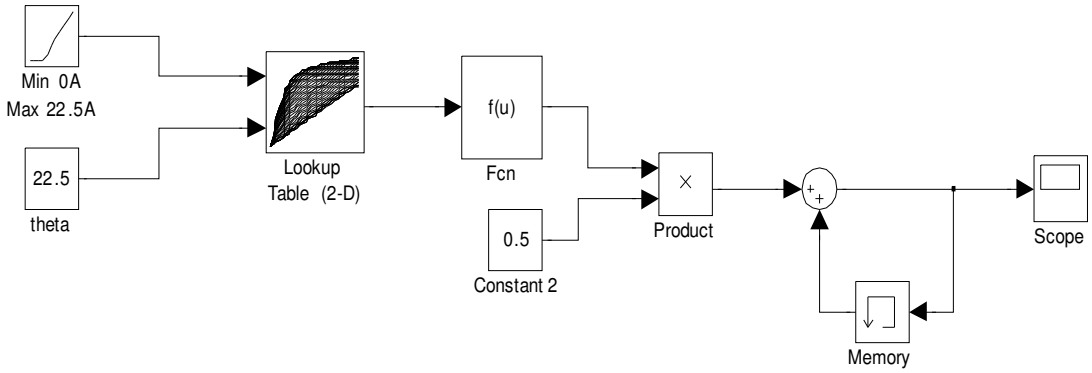

Figure 3-7: Calculation performed in MATLAB/SIMULINK to determine co-energy from magnetization curve using 1/3 Simpson's rule

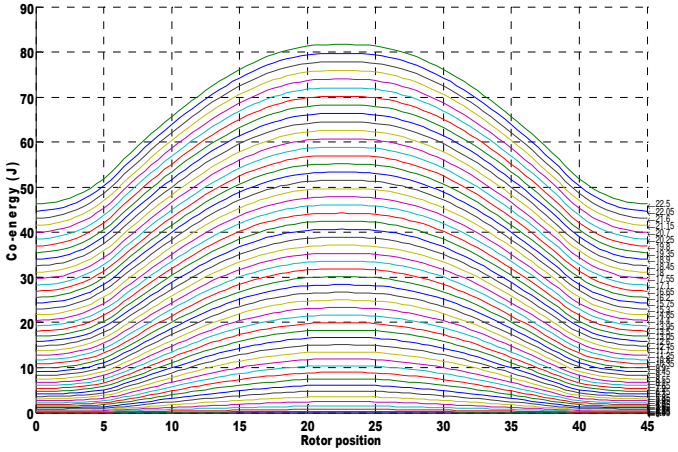

Figure 3-8: Profile of co-energy versus rotor position at various current

3.2.8 Verification of Co-energy Curve

In order to verify the process of determining the co-energy curves, derivative of co-energy with current can be used to obtain the flux linkage curve.

$$\lambda = \frac{dW_c}{di} \tag{3.22}$$

3.2.9 Calculation of Static Torque from Co-energy

Torque is obtained from the derivate of co-energy with respect to its rotor position. Similar to the calculation of the co-energy, torque can be derived using equation (3.19). It is represented in MATLAB/SIMULINK as depicted in Figure 3-9. The co-energy profile is extended to cover both the positive and negative torque region ranging from 0^0 to 45^0. The ramp is set to reach the maximum rotor position in the co-energy profile. The torque profile calculated at various phase current is illustrated in Figure 3-10.

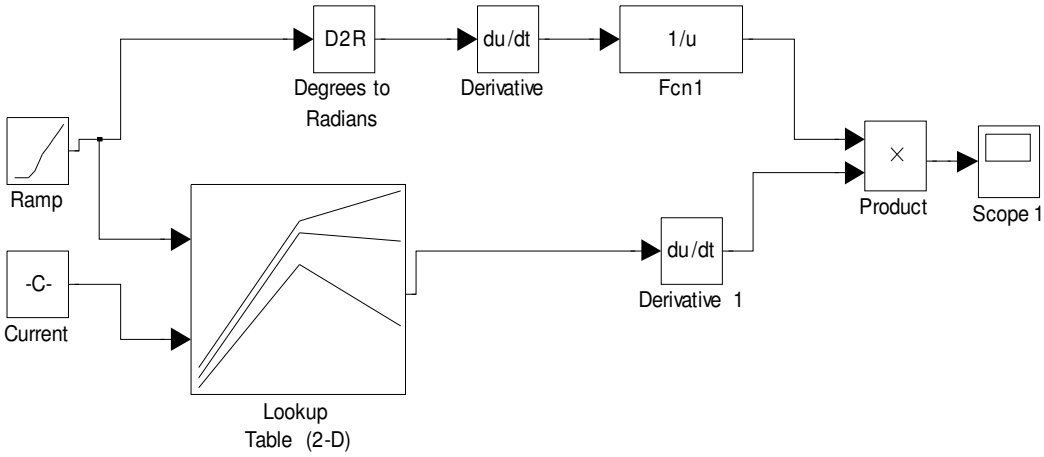

Figure 3-9: Calculation performed in MATLAB/SIMULINK to determine torque from co-energy

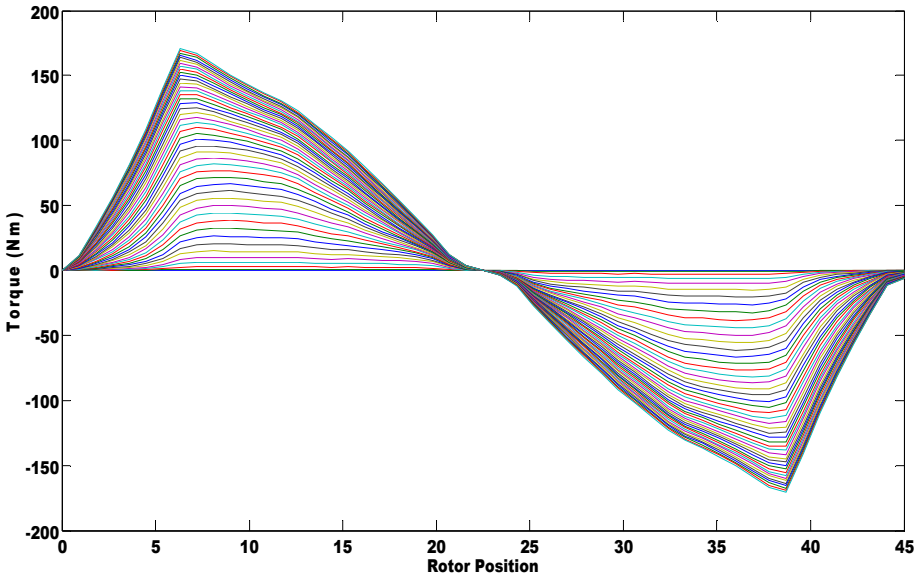

Figure 3-10: Profile of torque versus rotor position at various current

3.3 Verification of Electromagnetic Process

Although the FE method is widely used to obtain machine characteristics, its procedure and results need to be verified. The verification can be achieved by an experiment to determine the static characteristics of the machine. Similar to the FE procedure, the rotor position is changed between the aligned and unaligned position. The readings for the voltage and the currents are recorded at each rotor positions. This chapter provide details on the experiment using the DC test method that was conducted to determine the magnetization curve of the machine. Although there are various experimental procedures available such as the AC method and inductance method, the techniques will not be explained here since our objective was to verify the procedures using the FE method.

3.4 SRG Experimental Setup

The main components of the experimental circuit setup are shown in Figure 3-11. The DC test method [113, 115] was employed for our study due to its simplicity and easy access to the equipment required. It consists of:

- 6 x 12V dc battery
- 1 x 4001 Pulse Generator1 x Tektronix TPS 2014 Digital Storage Oscilloscope (DSO)
- 1 x IGBT
- 1 x Diode
- 1 x Fuse rated at 10A
- 1 phase of SR machine winding

The method is used to obtain measurement of the voltage V and phase current i to determine the flux linkage, λ by rearranging equation (3.1) as shown below:

$$\lambda = \int_0^t (V - Ri)dt \tag{3.23}$$

where R in the equation refers to the phase winding resistance. A voltage pulse was applied to the phase winding and the required parameters such as the voltage and current are recorded. The DSO was used to register and store the relevant measurement signals. In addition, the pulse was injected into the circuit by a pulse

generator. The copper resistance for each phase winding was measured by a simple relation of Ohms law, voltage over current, which yields:

Resistance of phase A, R1 = 9.85ohms

Resistance of phase B, R2=10.13ohms

Resistance of phase C, R3=9.96ohms

The calculation of the resistance was verified with a voltmeter, giving a similar result. The flux linkage measurements were taken on one machine winding and the other phases are assumed equal. The aligned position is determined by applying a current on one of the windings. The rotor rotated freely and aligned itself towards the excited phase. The rotor was locked at the required position using a rotor key. The measurements were taken at three rotor positions: aligned, midway and unaligned. One end of the winding was connected to the IGBT whereas the other end of the winding was connected to the switch. The diode was placed across the winding to divert the phase current after closing the switch. It provides a path for the stored energy after the phase winding is disconnected from the supply. The set-up of the arrangement is shown graphically in Figure 3-12. Since a DC voltage was applied, the current applied to the winding is constant, hence the effect of iron losses are eliminated because the magnetic field cannot change with time [116].

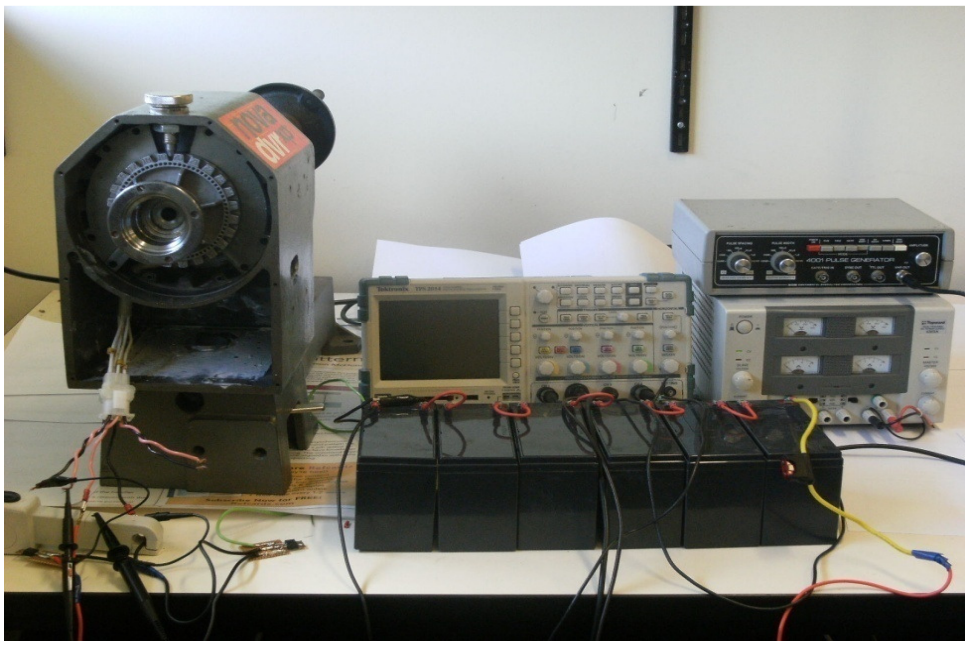

Figure 3-11: An experimental set up to measure the flux linkage of the machine

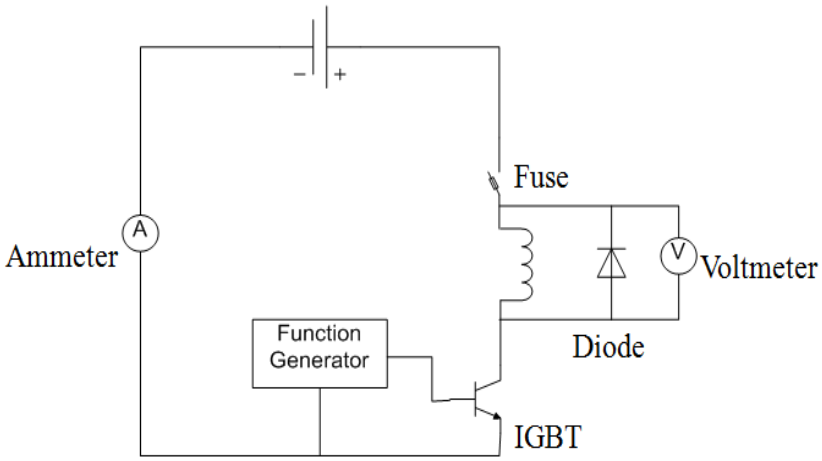

Figure 3-12: Circuit diagram of the experiment

The width of the pulse to be injected was determined based on the saturation of current at the aligned rotor position. The voltage pulse is turned off when the current no longer rises as captured in Figure 3-13. The steady state current is achieved at 7.3A at a voltage level of 76V. The slope of the current is steeper at the unaligned position, suggesting a low inductance value.

3.4.1 Calculation of Flux from Experiment

The current profiles at three different rotor positions are depicted in Figure 3-14. Due to the steady increase in the phase current at the unaligned position, the integral can

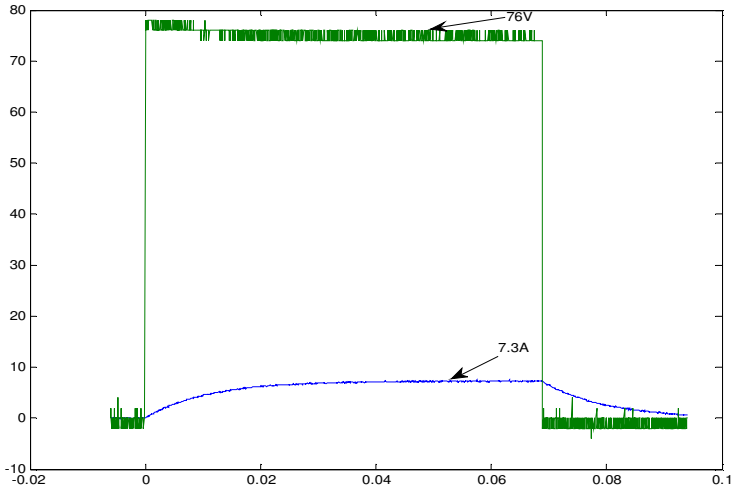

Figure 3-13: Graph of the voltage pulse (V) and current (A) against time(s) of one phase winding

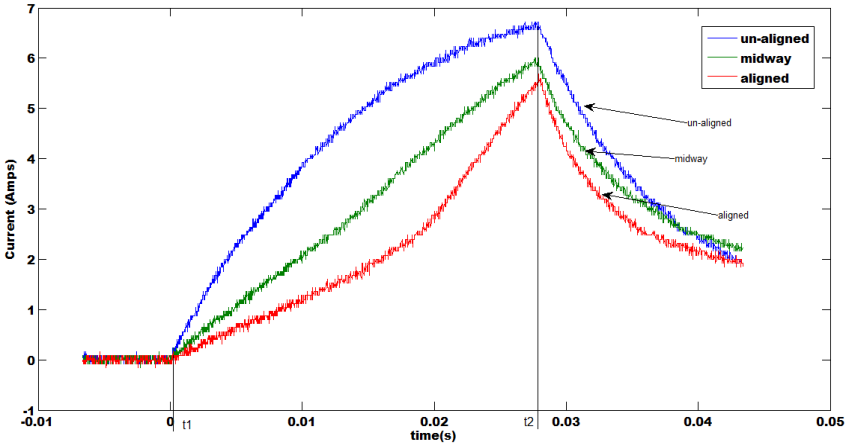

Figure 3-14: The phase current at three different rotor position

be estimated by approximating the curve as a straight line. The result agrees with the flux linkage curve obtained using COMSOL. However, the same method of approximation could not be used for the aligned position due to a mild dip at time 0.0208s. Hence, the graph can no longer be assumed linear. An accurate estimate of the integral can be obtained using the trapezoidal rule where the curve is split into a number of even segments shown below:

$$I = h_1 \frac{f(x_0)+f(x_1)}{2} + h_2 \frac{f(x_1)+f(x_2)}{2} + \ldots\ldots + h_n \frac{f(x_{n-1})+f(x_n)}{2} \qquad (3.24)$$

Where h is the width segment of the curve. The calculation at the aligned position is shown below and illustrated in Figure 3-15. The area under the curve is separated into two segments A and B. A better accuracy can be achieved using higher number of segments as shown by the following equations:

$$\lambda_A = (V - \frac{1}{2} f(i_1)R).h_1 \qquad (3.25)$$

$$\lambda_B = [V - \frac{1}{2}(f(i_1)+f(i_2))R].h_2 \qquad (3.26)$$

Where V is the terminal voltage, R the phase resistance, $h_1=t_1-t_0$ and $h_2=t_2-t_1$. The total flux λ_{total} for the aligned position will be the sum of flux in sections A and B.

$$\lambda_{total} = \lambda_A + \lambda_B \qquad (3.27)$$

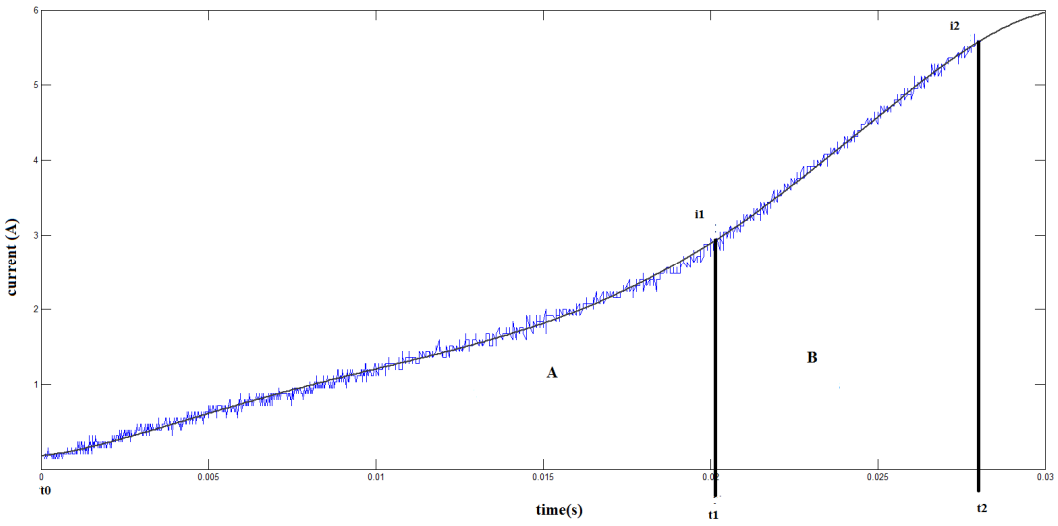

Figure 3-15: The graph showing the calculation performed for the aligned position

The same method is used for the un-aligned and midway current profile. The results obtained using the trapezoidal calculations are in good agreement with the results obtained from FEM as depicted in Figure 3-16 .

The small discrepancies in the results between the FE method and the experiment may be due to the following reasons:

- There was no information from the manufacturer regarding the B-H curve for the material hence soft iron was chosen because of its common use in the SR machine.
- The length of the air gap in FE model may not be the same as actual machine due to manufacturing errors.

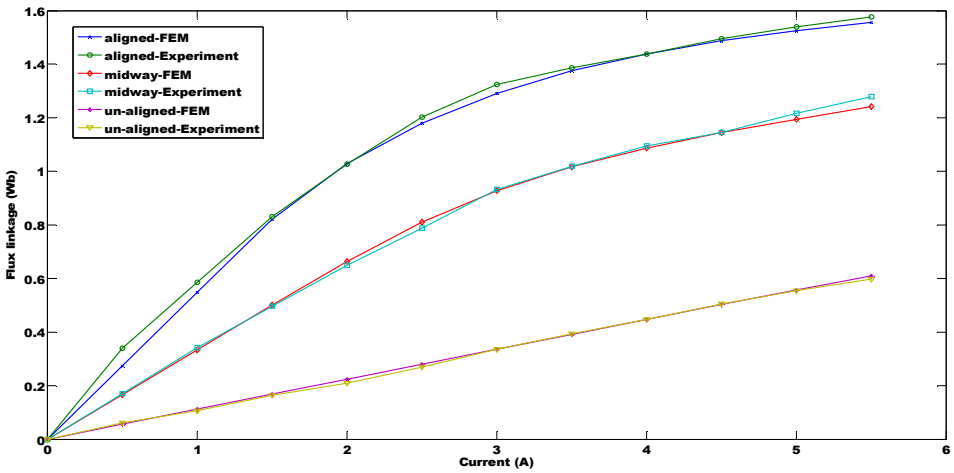

Figure 3-16: A comparison of the magnetization curve obtained using FEM and experiment

Nevertheless, the results obtained from both the experiment and FEM does not differ much. Hence, the choice of soft iron obtained from COMSOL was used throughout the study. The goodness of fit method has been used to analyse the discrepancies between the values of flux linkage obtained from experiment and FEM. These values are compared using the Kolmogorov-Smirnov (KS) test method in MATLAB. The KS test did not show any significant differences between the results. It was within the 95% confidence interval level. Therefore, the procedure used to determine flux linkage using FEM was verified. This FE method was used to determine the magnetic characteristics of other machines as well as depicted in Appendix C.

3.5 Conclusions

The magnetic characteristics of the SR machine which include the flux linkage, inductance and torque are important to predict and analyse its performance. These characteristics can be determined by various methods such as experiment, numerical and also analytical method. Obtaining the magnetic characteristics from experiment gives an accurate model for the machine. However, the time and costs involved outweigh its advantages. Furthermore, numerical method such as FE is able to provide the same result as an experiment. It requires machine dimension and high computer speed which can easily be obtained. The analytical approach does not require any field analysis hence it gives the most time efficient method. However, it requires initial data from either FEM or experiment in order to construct the mathematical equations. Also it represents coarse simplifications of reality. The difficulty in the calculation occurs when the rotor and the stator pole starts to overlap. Amongst all the methods discussed, FE proves to replicate the real machine at a reduced time and costs. Based on the FE method the 12/4 machine provides the largest magnetization curve.

CHAPTER 4

MODELLING OF SWITCHED RELUCTANCE GENERATOR

The principle of operation of the SR machine is based on a series of pulsed excitation. This results in pulsed current waveforms which increase from and decrease to zero before excitation of the next phase. Due to its operation nature, it is not easy to describe the dynamic behaviour of the SR machine in a set of equations as found in other electrical machines.

The behaviour of the machine can be analysed either by experiment or through a simulation model. The latter is selected as it is the most practical way to analyse and predict the performance of the machine. The relevant performance parameters such as the flux linkage, phase current, voltage, rotor speed, rotor position and torque can easily be analysed by performing the required changes on the simulation model, as opposed to the experimental setup. The simulation model also allows the parameter variation to be thoroughly examined, thus minimising cost and effort from having to develop the prototype machine.

This chapter introduce the mathematical description and various modelling techniques which can be applied to develop the SR generator system. The development includes a single phase and linear SR machine and how it is modified to incorporate a non-linear machine characteristic with different number of phases. It also highlights the modelling technique and simulation package chosen based on the objective.

4.1 Modelling Techniques for SR Generator

There are a few resources available on the development of the simulation model for the SR drive. The modelling approach is based on how the magnetic characteristics of the machine are being represented and how it is used within the phase voltage equation. It can be classified as the flux linkage approach, inductance based approach and also the phase current approach. It can be developed either as a linear or non-linear model. Figure 4-1 illustrates the classification of the modelling techniques

available. The analytical method can be represented by a set of equations from either the flux linkage or inductance profile whereas the look up table (LUT) method uses the magnetic characteristic obtained from either the FEM or experiment to solve the phase voltage equation.

Simulation of the SR machine is well documented, however the existing publications focused on analysing the behaviour of the machine [117, 118] and also targets a specific application such as the electric vehicle [119, 120], starter generator system [121] and its use for low voltage application [122].

Although the operating principle for the SR machine differs between motoring and generating function, the base to develop the simulation model is similar. The difference however is on the magnetic characteristics where the range of operation for generating is during the decreasing slope of the inductance profile. There was not much development of a comprehensive simulation model for the SR generator drive as compared to its motoring counterpart. An attempt has been made to evaluate the performance of the machine in generating mode by testing various parameters such as the firing angles, voltage and speed [123, 124]. The research however was limited to constant output power analysis [14, 46]. Furthermore, the studies were confined to high speed operating range. There was no attempt to characterize the elements of the drive such as the machine structure and the optimal control variables with the machine performance.

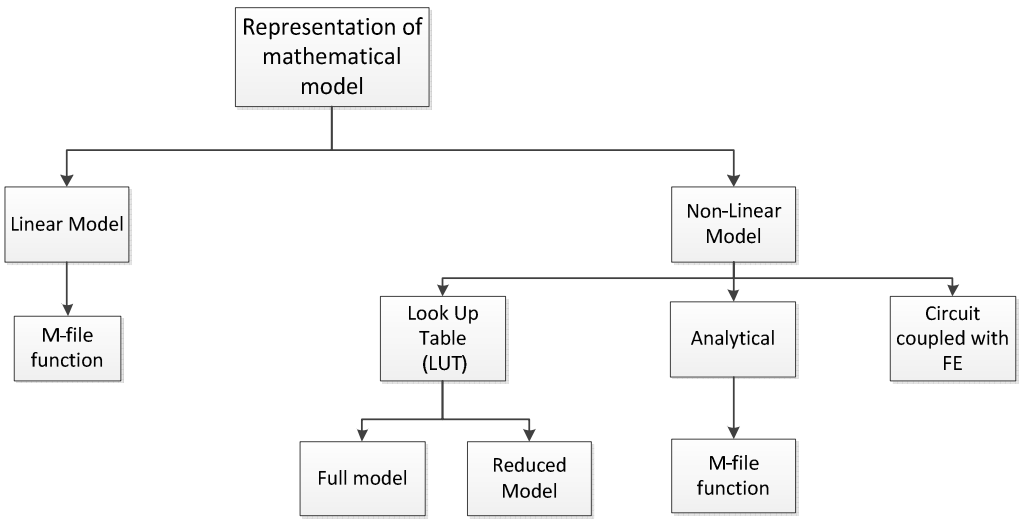

Figure 4-1: Classification of various methods to represent the mathematical model of the SRG

In general, the simulation model for the SR machine was developed to allow thorough understanding of the behaviour and performance of the machine. It focused on the development of a specific system component such as the control, the SR machine and also the converter. The modelling area lacks a platform which allows characterisation on the performance of the machine. The following sections will discuss the modelling techniques available for the SR generator which motivates the development of our modelling platform.

4.1.1 Linear Model

A linear simulation model based on the linear inductance profile was first developed to analyse the behaviour of the machine [125] shown in Appendix D. The initial result verifies the operation of the model and was used as a platform for the non-linear model. The linear method assumes a linear inductance profile with a minimum value, L_{min} and a maximum value L_{max} calculated using the flux linkage λ equation below:

$$\lambda(i,\theta) = L(\theta) * i \tag{4.1}$$

The model involves integration of the Power System Blockset (PSB) module with the SIMULINK module using the source to signal blocks: voltage block and current controlled source block. The number of phases for the machine is increased by using additional phase winding blocks. The method did not incorporate the non-linear behaviour of the materials hence the magnetic characteristics does not match the actual data. It is useful to understand the basic characteristics of the machine, but not suitable to measure or to predict its performance [12]. Therefore, the non-linear characteristics of the machine are incorporated by employing the B-H curve for the magnetic material and the magnetic characteristics obtained from the experiment.

4.1.2 Look Up Table (LUT) Model

The LUT approach can be grouped as a reduced model and full model based on how the partial derivatives of equation (2.8) are solved. The equation (2.8) determine the phase current from the flux linkage magnetization curve, thus requiring the use of only one electrical LUT; *i*-curve. It requires two input parameters; the rotor position and the flux linkage which is obtained from equation (3.23). Using the chain rule, equation (2.8) can be rearranged to obtain the phase current as follows:

$$\frac{di_j}{dt} = \frac{1}{\frac{d\lambda(i_j,\theta)}{di}}(V_j - R_j i_j - \omega\frac{d\lambda(i_j,\theta)}{d\theta}) \tag{4.2}$$

And

$$\frac{di_j}{dt} = \frac{1}{L_j}(V_j - R_j i_j - i_j\frac{dL_j(i_j,\theta)}{d\theta}\omega) \tag{4.3}$$

The above equations are grouped under the full model category. Both equations (4.2) and (4.3) involve solving the partial derivative which may accumulate errors.

The mechanical section is determined from equation (3.2) and is represented as a torque LUT which is calculated based on the derivative of the co-energy. This provides the instantaneous torque for one phase whereas the summation of the instantaneous torque for each phase will provide the total torque for the machine. The input parameters to the torque LUT are the current and also rotor position. It performs interpolation and extrapolation between the stored data based on the input parameters.

This method assumes that each phase of the windings is symmetrical hence the LUT can be prepared using the measurement from one of the windings. The assumption is valid since the induced voltages on the adjacent phases are small as depicted in Figure 4-2 where the highest voltage recorded is 14V. The advantage of this modelling method is the reduced computation time by employing the SIMULINK blocks.

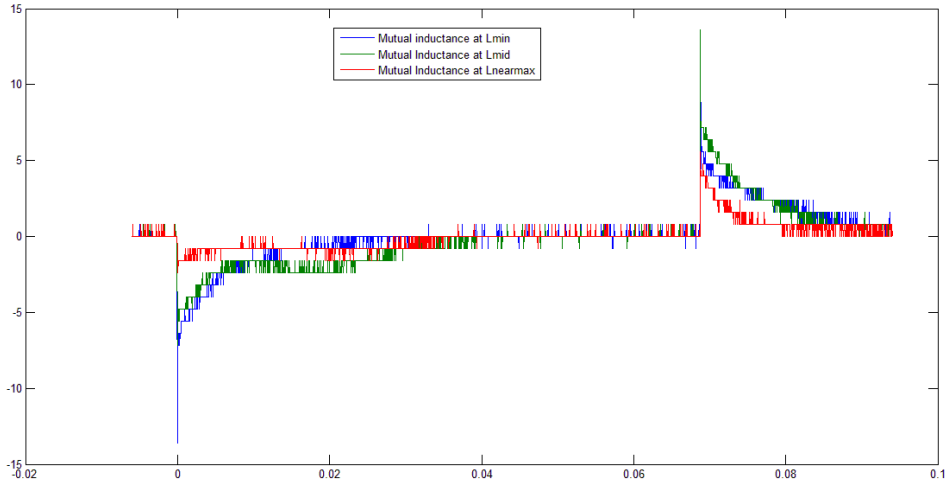

Figure 4-2: Graph of induced voltages (V) against time(s) on adjacent phases for the aligned, midway and unaligned rotor position

4.1.3 Inductance and Flux Linkage Based Method

As explained previously in Chapter 3, the inductance and flux linkage based model represents the inductance and the flux linkage using the Fourier Series (FS) terms. The coefficients of the FS terms are determined using a polynomial function. The approach normally considers three positions for the FS term namely the aligned, midway and unaligned position determined from either the FEM or experiment. These equations can be programmed in SIMULINK using the MATLAB function block [126, 127]. Due to the selected numbers of rotor position, these will result in estimation errors since the flux path differs from one position to the other.

4.1.4 Circuit Coupled with FE method

The method involves coupling of the electromagnetic field computation with circuit simulation. There are not many resources available on the coupling between two different software packages due to the longer simulation time required. Using this method, time coordination is important to synchronize the operation of the machine with the external circuit. The purpose of this method is mainly used to study the dynamic behaviour of the machine [128, 129] and also the effect of machine under fault condition [130]. The studies did not involve any work on optimizing the performance of the machine.

4.2 Selection of Modelling Techniques

The aim of the discussion above was to evaluate the available modelling techniques to be used for our model. The selected technique is based on the following criteria:

- Has the ability to make changes on the parameters
- Capable to add number of phases and to model different SRM topologies
- Easy to model

Based on the above criteria and previous discussions on modelling of the electromagnetic process, the most suitable method to represent the SRG drive in terms of a simulation platform is by using the phase current LUT approach. As reported earlier, the current curve was determined from the magnetization curve of known

rotor position and flux linkage. It does not involve any calculations hence avoiding the partial derivative errors [131]. The method also allows the calculation of torque and co-energy from the magnetization curve. The only drawback of this technique is the use of LUT which involves the use of high memory requirement. Nevertheless, the rate of growth of computer technology has increased over the years and is expected to keep on rising. Therefore, it is easy to have access to a high end computer. This will no longer be an issue for the LUT approach where the benefits will outweigh its disadvantages.

The MATLAB/SIMULINK was selected as the software to be used for the dynamic modelling of the SR generator drive. It integrates both the circuit oriented and signal oriented approach in one simulation platform that is required to build the system [117]. It also provides a convenient graphical user interface (GUI) to link and edit the function blocks thus allowing the modelling of the differential equations in a flexible modelling environment. Each of the machine components is built and tested individually before it is integrated as a complete system. The platform is developed under the following assumptions:

- Mutual coupling is neglected due to the low induced current in the non-conducting phase.
- All phases are assumed symmetrical.
- The phases are singly excited.

4.3 Construction of the Switched Reluctance Generator Drive

Unlike the other machines such as the induction machine and the permanent magnet machine which has two sets of equations for each of the rotor and stator, the SR machine only requires solving equations on the stator poles. A generalized SR generator model consists of both the electrical and mechanical section. Based on the existing linear model platform developed earlier [125], the non-linear characteristics of the machine can easily be introduced according to the modelling approach of the magnetic characteristics discussed in Chapter 3

.

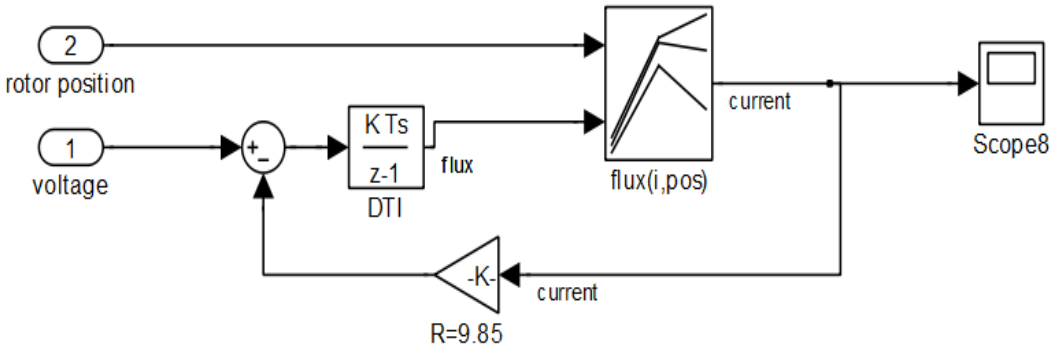

Figure 4-3: Electrical model of an SR machine in SIMULINK

The model of the SR generator system is developed in stages according to its subdomain such as: electrical subdomain, mechanical subdomain, rotor position, control and also converter subdomain.

4.3.1 Electrical Subdomain of the SRG

The electrical subdomain of the machine is implemented using the LUT method as depicted in Figure 4-3 by solving the equation (3.23). The LUT block for the *i*-curve replaces the linear calculation function block in the linear model [125]. The phase current is the output obtained from the flux linkage magnetization curve.

4.3.2 Mechanical Subdomain of the SRG

Figure 4-4 shows the implementation of the mechanical model in SIMULINK where the input to the model is the rotor position and phase current obtained from the electrical model. The output of the mechanical model is the speed of the rotor. One of the limitations of the linear model is the exclusion of the dynamic effect of the machine. Since the torque output from the LUT block represents the instantaneous torque for one phase, a summation block is added to determine the total torque for the machine.

The mechanical parameters such as the inertia and coefficient of friction for the machine have to be determined by measurement since no data was supplied by the

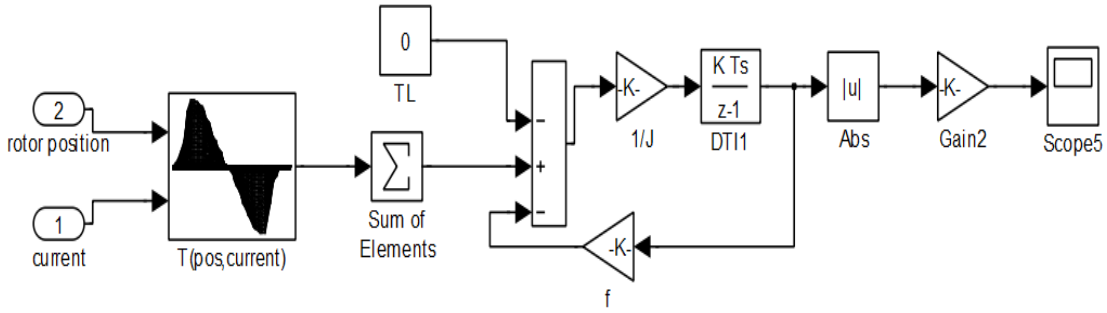

Figure 4-4: Mechanical model of a SR machine in SIMULINK

manufacturer. The calculation for the inertia of the rotor is made based on the direct drive load for a hollow cylinder [132] as shown below:

$$J = \frac{m(D_1^2 + D_2^2)}{2}[kg.m^2] \tag{4.4}$$

Where D_1 and D_2 are the external and internal diameter of the machine whereas m is the weight of the rotor. The inertia of the rotor gives 0.00216kg.m^2. To simulate the effect of a prime mover on the generator, the load inertia can be added to the inertia of the rotor.

4.3.3 Converter Subdomain of the SRG

The asymmetric half bridge converter (AHBC) was used for this study due to its flexibility to operate during the low, medium and high speed range as highlighted in subsection 2.6. It was constructed using two IGBTs and two diodes as shown in Figure 4-5. The converter acts as a switching device to control the phase current in the winding.

As illustrated in Figure 4-5, the input to the subdomain is the signal obtained from the controller and the output is the voltage across the phase winding. The converter sub domain receives DC source from the battery which is connected in parallel to all the branches. Normally this circuit arrangement is characterized as the self excitation converter circuit.

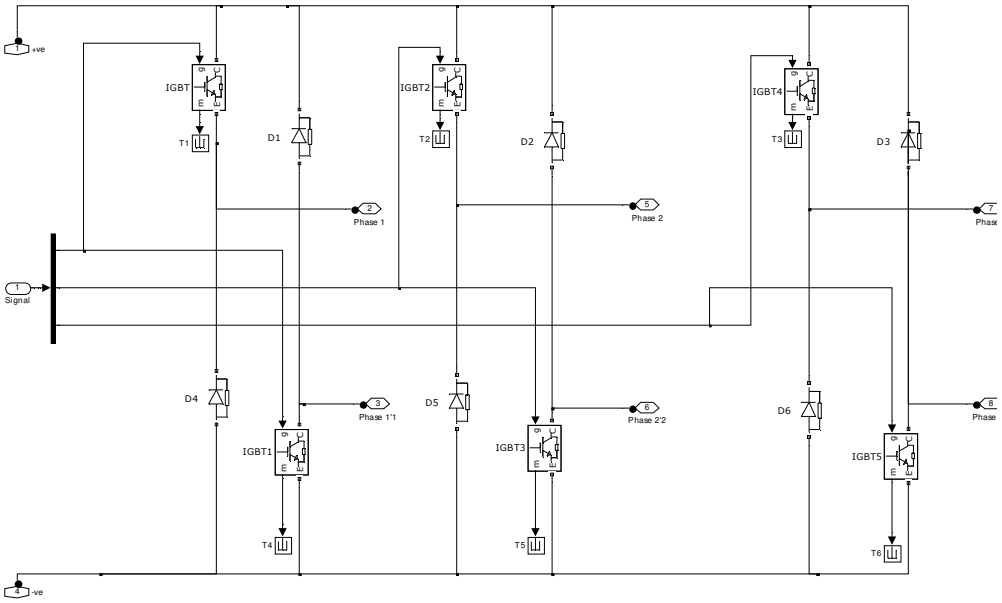

Figure 4-5: The Asymmetric Half Bridge Converter (AHBC) model for the system

4.3.4 Rotor Position Subdomain of the SRG

The overall function of the block is to provide the rotor position based on the input speed as shown in Figure 4-6. The subdomain of the block calculates the displacement between each phase according to the difference between the rotor angle and the stator angle. Since the modelling approach is based on the single phase excitation [124, 133, 134], the number of phases can be added based on the number of strokes provided that the phases are symmetrical as shown by the following equation:

$$\theta_{stroke} = \frac{360}{m * N_r} \tag{4.5}$$

Where m is the number of phase and N_r is the number of rotor poles. The following table shows the number of strokes for the different types of machines used:

Table 4-1: Table showing the stroke angles of the SRM

Machine type	**12/8**	**12/4**	**12/16**
Stroke angle	15^0	30^0	7.5^0

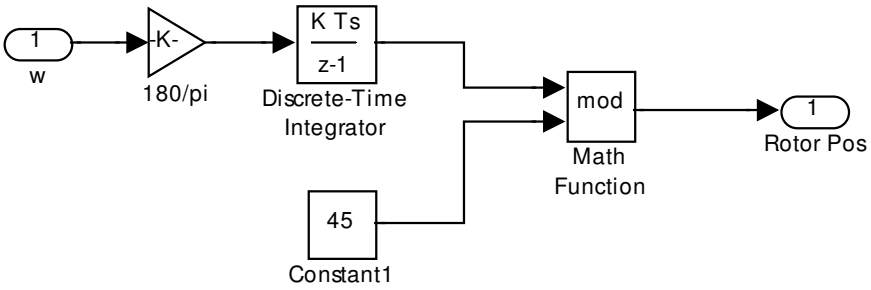

Figure 4-6: The subdomain to calculate the rotor position

4.3.5 Controller Subdomain of the SRG

The hysteresis current control is employed to take into account the low, medium and high speed range. The function of the switch block as in Figure 4-7 is to ensure the turn on and turn off angle is compared with the signal from the rotor position to develop the reference pulse for the current. The hysteresis block sets the upper and lower bound limit to regulate the current within the specified band. The band is set in terms of percentage of the phase current.

At a higher speed range, the phase current depends on the firing angles as opposed to the hysteresis current controller which only works at lower speed range. The overall SRG drive is integrated in the MATLAB/SIMULINK environment as depicted in Figure 4-8. It can be seen that any adjustment to the model can easily be made without having to perform major changes. This allows thorough analysis to be made on the optimal performance of the machine.

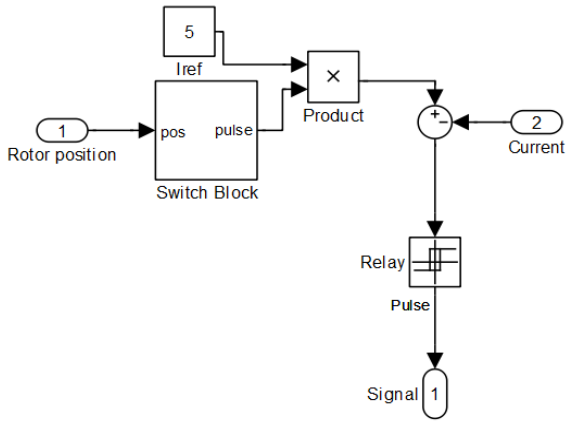

Figure 4-7: The controller subdomain for the SRG system

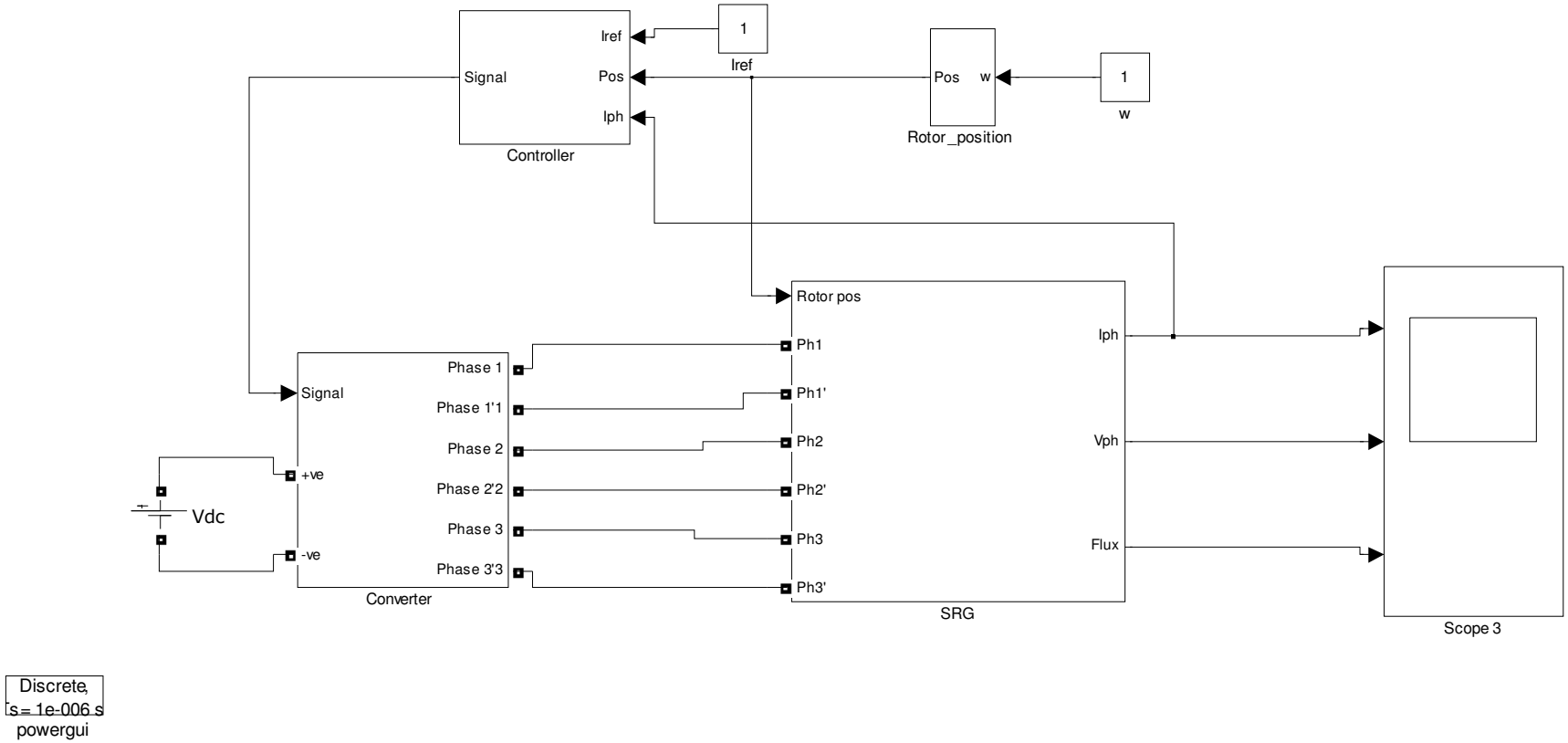

Figure 4-8: The integrated system of the switched reluctance generator

4.4 Verification of Simulation Results

The verification of the simulation results is made in terms of the existing fundamental theory of the machine. To illustrate the operation of the SRG system, a simulation study on the phase current is performed. Figure 4-9 shows the variation of phase current with the variable control parameters such as; the turn on and turn off angle, voltage and the phase resistance. The change in turn on and turn off angle as depicted in Figure 4-9(a) and (d) reflects the change of phase current accordingly. When the turn on angle is advanced in the motoring region, energy is stored to further increase the phase current after turn off angle. As the turn on angle is placed near to the aligned position, phase current is reduced. Also if the turn off angle is extended near to the unaligned region in the decreasing inductance profile, the current will extend into the excitation region of the next phase before returning to zero. With a fixed firing angle, the variation of phase current with the phase resistance is small as shown in Figure 4-9(b). The variation of the phase current with a change in the parameters has been demonstrated and it shows that the simulation results are in good agreement with the theoretical analysis.

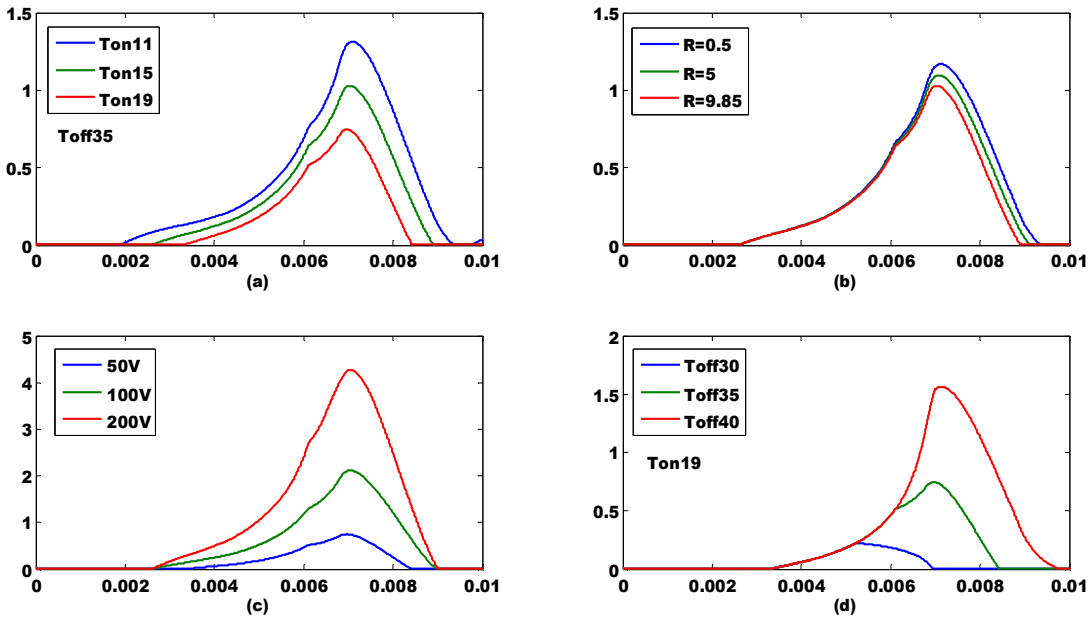

Figure 4-9: Graph of variation of phase current (A) against time (s) with (a) turn on angle (b) phase resistance (c) voltage and (d) turn off angle

4.5 Component Selection for the Simulation Platform

The effect of various machine parameters are analysed in this initial simulation. The aim is to select the parameters for the machine and evaluate its effect on the performance of the machine. Although the inertia for the machine has been estimated in sub-section 4.3.2, the numbers are varied to add in the load effect. The machine parameters chosen for the simulation studies are shown in Table 4-2.

Table 4-2: The simulation parameters for the 12/8 machine

Parameter	Values
Resistance, R	9.85Ω/phase
Inertia, J	0.00216/0.0035/0.0065/0.0085kg.m^2
Coefficient of friction, β	0.008/0.004/0.02
Ton	20^0
Toff	35^0
Voltage, V	230 V

4.5.1 Effect of the Rotor Inertia on Speed

As mentioned earlier, the rotor inertia includes the inertia of the rotor itself together with the load. The coefficient of friction relates to the friction between the rotor and the shaft. Therefore, the effect of both the inertia and the coefficient of friction was varied to study its impact on the angular velocity of the rotor. This enables us to select the suitable values for the rotor. Three values of the rotor inertia and coefficient of friction have been analysed. As expected, the lower inertia value will result in a faster rate of acceleration. This will shorten the initial start-up time for the machine as compared to rotor with higher inertia value. The acceleration rate of the speed curve of the machine depends on the selected values of the inertia [123] as shown in Figure 4-10(a). The coefficient of friction determines the steady state value of speed as in Figure 4-10(b). Therefore, to simulate the effect of a prime mover, the values of the inertia and coefficient of friction can be changed according to the required speed level [123].

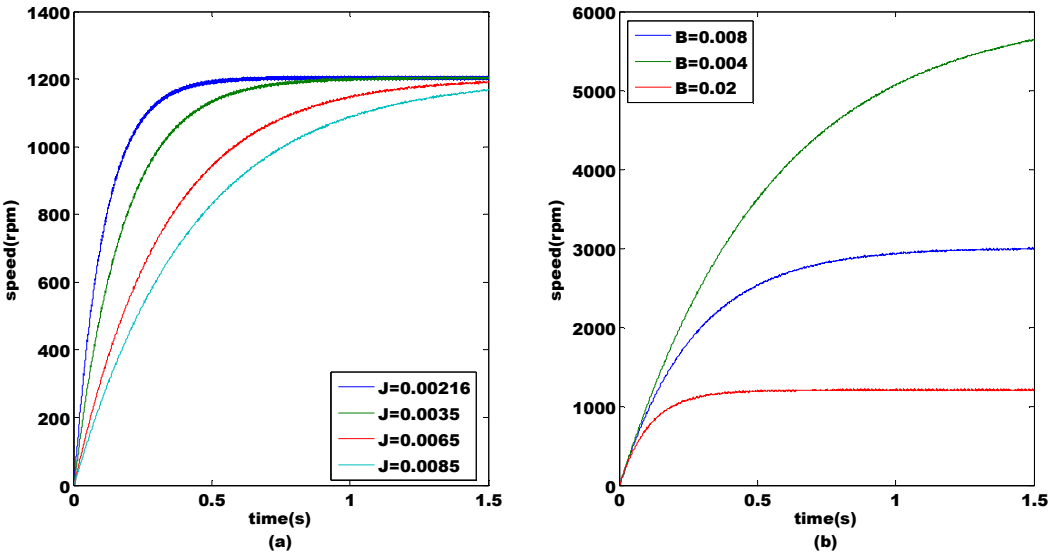

Figure 4-10: The variation of speed with (a) inertia and (b) coefficient of friction

4.5.2 Comparison of Excitation Method

The classical connection for the excitation circuit is shown in Figure 4-5. Both the excitation and generation stage share the same bus line. According to [40], by sharing the same bus line any perturbation that causes an increase in the bus voltage will affect the phase current. This in turn will cause instability as further increase in the generated current increases the generated voltage further.

The instability problem was resolved by using a separate excitation bus for the generator as shown in Figure 4-11. The phase current will freewheel through the diodes and the load until the current decreases to zero. Thus, the time for the current to reduce to zero is determined by the resistive component. If the value of the resistor is small, the generation current in the main bus is reduced as depicted in Figure 4-12. The separately excited circuit would be an advantage in the event of a fault as it will not disrupt the other healthy phases. Since this study relates to optimizing the generated power of the machine, the self-excited circuit was sufficient to perform the required calculation.

4.5.3 Effect of Soft Chopping and Hard Chopping

Hysteresis current controller was employed for this study due to its ability to perform well under the low, medium and high speed range [135]. During low speed, the

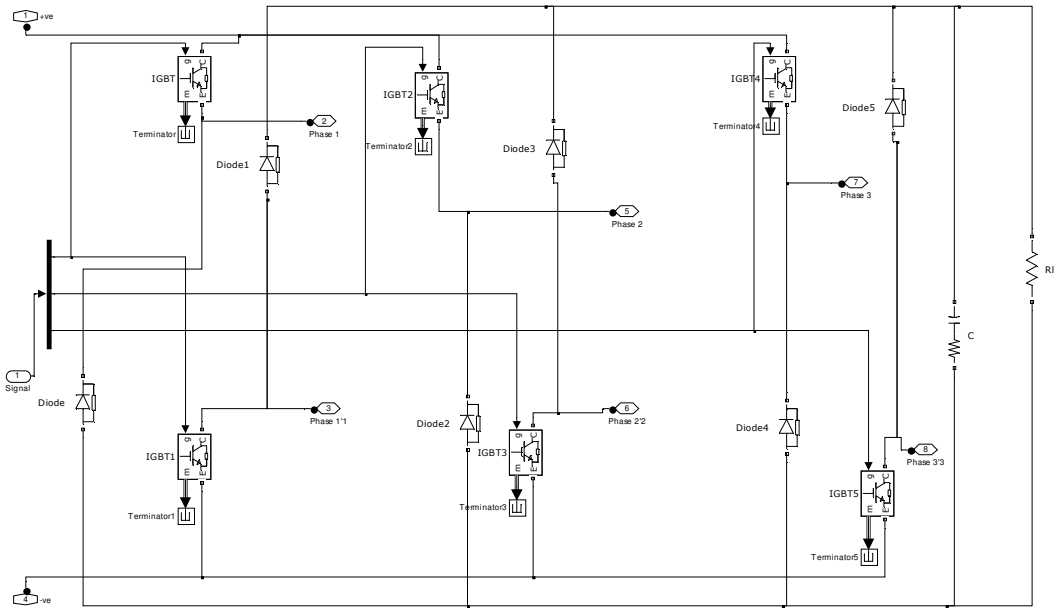

Figure 4-11: Separately excited circuit for SRG

phase current is regulated under a specified band limit which is achieved either by hard chopping or soft chopping technique. The hard chopping technique involves the switching operation of both the IGBTs whereas in soft chopping only one IGBT is working during the commutation period whilst the other remain on until turn off angle is reached.

The hysteresis current control method is widely used for the motoring operation since it is able to provide a constant current to the load. However the hard chopping technique results in high switching frequency. The soft switching technique was used

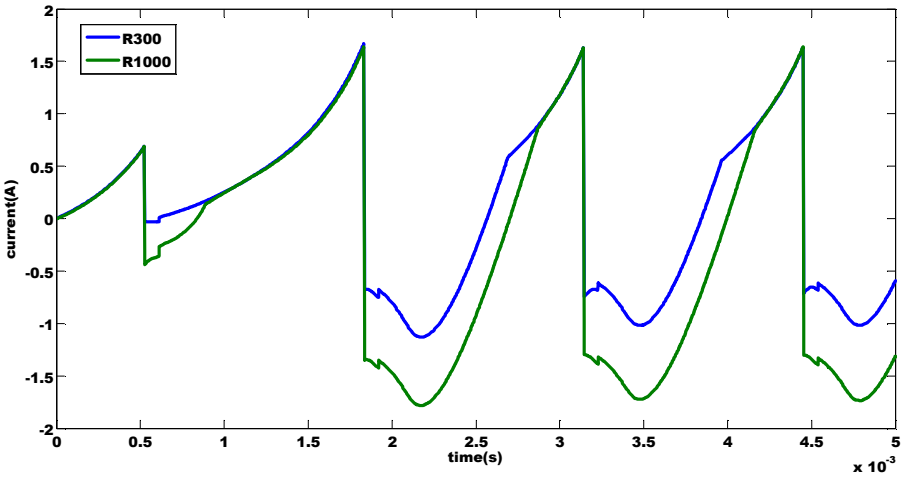

Figure 4-12: Comparison of current profile for the separate bus line with different values of load resistor.

to avoid the switching losses however it was observed not suitable to be used for generating operation. The technique involves one of the switches turned on until the turn off angle whereas the other switch will operate according to the relay setting. When the second switch is in the off position, the voltage will be zero and the current will circulate through the diode and winding. The circulation of current through the winding results in the energy being dissipated. The technique is suitable for the motoring operation, which requires the generated energy to be able to supply the load. Therefore, the hard chopping method was selected in this study.

4.6 Conclusions

This chapter highlights the various modelling techniques based on solving the phase voltage equation. The LUT approach was employed in this study based on its advantages highlighted earlier. The selection of the components for the model has also been clearly defined. Based on the previous literatures, the validation between the two methods was commonly conducted based on the steady state values of the SR machine [131, 136]. It has also been proven that the result of the steady state simulation model corresponds well with the experiment. Since this study will look into different machine structure and involves changing the control variables for the machine, the same procedure will be costly and time consuming on the experiment set up. The validation of the simulation model has been made based on the fundamental theory of the SR machine. The subsequent chapters will determine the winding configuration and optimal control variables for the machine.

CHAPTER 5

INVESTIGATION INTO THE STATOR AND ROTOR CONFIGURATION

According to the magnetic theory, the poles come in pairs of North (N) and South (S). The polarity of the poles is determined based on the flow of current and path of the flux lines. Since the arrangement between the two poles and four poles per phase machine differs, the direction of the flux lines will not be the same. This in turn will affect the energy conversion curve and torque profile. The SR machine operates based on a single phase excitation having either two or four poles per phase machine. Many literatures highlight the effect of excitation with a two poles per phase machine [137-139]. Under the single phase excitation, the flux path will be affected by the arrangement of poles within the same phase. However, for a dynamic performance of the machine, there will be an instance where two phases operate simultaneously. This will change the flux path due to the flux generated by each excited phase being either in the same or opposing direction. This chapter will analyse the influence of the different winding polarity for both the single phase and two phase excitation of a three phase four poles per phase machine. Its effect on the energy conversion curve and torque profile will be analysed. The study will also be extended to a machine with a higher number and a lower number of rotor poles. By observing the factors that affects the shape of the magnetization curve, the existing machine can be optimized without altering its main dimensions.

The existing publications on the winding arrangements concentrate upon torque production rather than study the effect on how the flux path influence the power generated. A fully pitched winding makes use of the mutual inductance between phases to increase torque production as compared to the conventional machine arrangements where torque is produced due to the change of self-inductance on the stator pole [74, 140]. A double salient interior permanent magnet machine (DSIPM) employs the reluctance torque as in the mutually coupled Switched Reluctance Machine (MCSRM). Hence, it is able to achieve higher torque and low torque ripple [141]. An asymmetrical structure of the SR machine normally employs a short flux path control scheme [142] to reduce the eccentric forces and core losses in the

machine. However, the paper did not highlight on the performance of the machine. The effects of mutual flux have been compared between the machines with odd and even number of phases. A high performance applications can be obtained with an odd number of phases which produce symmetrical flux path between the phases [137]. Yet, the study was limited to machines having only two poles per phase. A detailed winding polarity with more poles per phase and their effect on the performance of the machine had not been reported.

The focus of this chapter is to investigate the different excitation pattern of a three phase four poles per phase machine. Comparison in terms of their static magnetization curves and torque profile will be conducted in order to determine the optimum excitation pattern of the SR machine to be used. The observation will cover both the motoring and generating operation of the machine. Although the choice of the winding polarity will be made based on the flux path of one phase excitation, the observation of the flux path when two phases are excited will also be observed and discussed.

The main purpose of this chapter is to optimize the machine structure by analysing the behaviour of the magnetic flux density without having to perform changes on the dimensions and structure of the existing machine, also to justify the choice of our winding polarity. The optimal winding polarity will be balanced in terms of the flux path and size of the magnetization curve.

The study is based on the existing three phase 12/8 machine, a three phase 12/16 machine and a three phase 12/4 machine having the same stator dimensions. It involves a single phase and simultaneous two phase excitation with the following winding configurations:

- single phase excitation: NSNS and NSSN
- two phase excitation: NNSSNNSS, NNSSSSNN, NSNSNSNS and NSSNNSSN

The machines will be subjected to the same number of turns and current density level. The selection of the winding arrangements has been made based on the direction and magnitude of the magnetic field along the respective stator pole.

5.1 Winding Polarity and Flux Paths Under Single Excitation

The direction of the flux path can be determined through the winding polarity and is used to design the machine. The magnetic path of the flux can be categorized as short flux loop and long flux loop. The latter design is obtained when the flux in the neighbouring poles opposes each other [137]. The former design exhibit a short and balanced magnetic circuit path hence reducing the magnetic saturation of the machine which in turn reduces the core losses [139, 142, 143]. The short flux path can be obtained when the flux produced by the adjacent phases adds together. Also, it is normally achieved by using the asymmetrical machine structure [139, 142]. However, the existing machines available in the market are the conventional 12/8 structure. Therefore, this study aims to optimise the winding polarity without affecting the structure of the machine. Based on one phase excitation, the conventional winding polarity is the NSNS [11]. However, the study was not extended to see the effect of different phase winding polarity and is limited to the excitation for one phase. The combination of the winding polarity for a three phase machine having four stator poles per phase can be designed as: NSNS, and NSSN. The NNSS configuration is similar in pattern to the NSSN configuration hence it will not be studied. The various magnetic field distribution based on the above configuration is depicted in Figure 5-1.

The NSNS pole configuration establishes a well distributed flux path under the same constant current density in the phase winding as compared to the other configuration. Also, no flux passes through the other phases of the machine. For the NSSN configuration, there will be a portion of the back iron yoke which does not have flux passing through. The intensity of the flux is concentrated along the back yoke of its path as highlighted in Figure 5-1(b). Therefore, the iron losses will not be evenly distributed along the stator yoke. Some of the flux from phase A (PhA) also passes through the other poles.

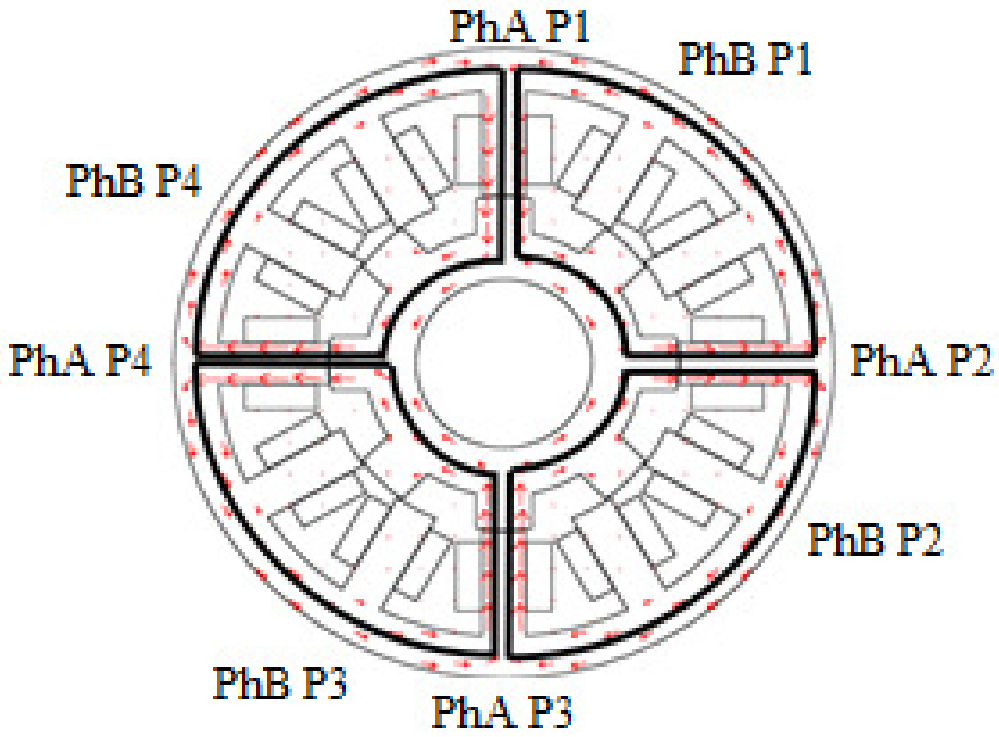

(a)

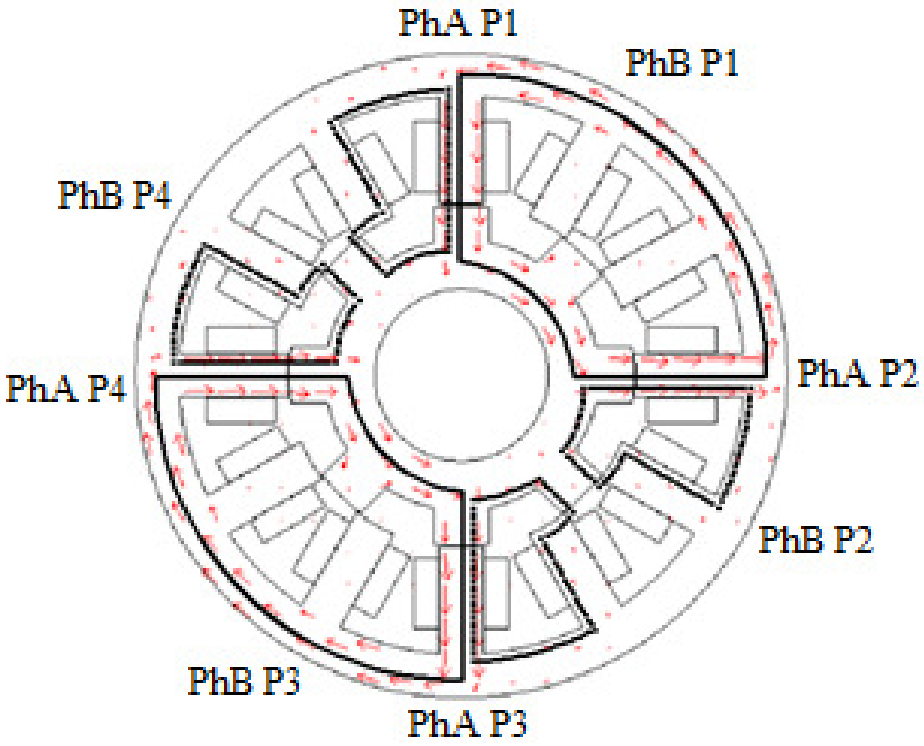

(b)

Figure 5-1: The cross sections for a 3-phase 12/8 machine and their flux directions with phase A excited at constant current (a) NSNS and (b) NSSN

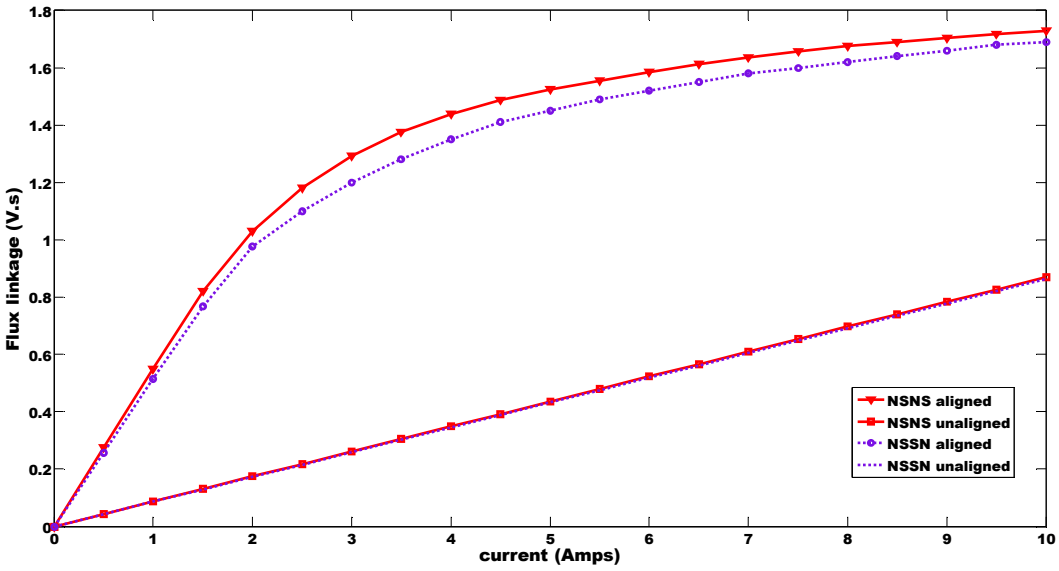

Figure 5-2: Comparison of magnetization curve for various winding polarity for a 3-phase 12/8 SR machine

Based on the observation under single pulse excitation, the NSNS configuration gives the best choice of winding polarity for a three phase four poles machine. A comparison between the flux linkage characteristics strengthens the choice of this configuration as depicted in Figure 5-2. The curve is obtained based on the flux created by the magnetomotive force (MMF) applied to the phase winding which is represented by the following equation:

$$H = \frac{Ni}{l} = \frac{MMF}{l} \tag{5.1}$$

Where H is the magnetizing intensity, N is the number of turns, l is the length of the core and i the phase current. The magnetizing intensity is directly proportional to the MMF. The applied MMF produces flux, λ which increases as current is increased. This in turn increases the magnetic flux density, B as given by:

$$\lambda = Ba \tag{5.2}$$

where a is the cross section area of the flux path. Up to a certain point, an increase in the magnetomotive force produces no change in the flux as illustrated in Figure 5-2. At this point, the material is said to be saturated. The NSSN winding configuration has the smallest area between the aligned and unaligned curve due to the flux leakage whereas the NSNS winding configuration has the largest curve. The interactions of flux between the adjacent poles contribute to the size of the magnetization curve.

The result of the magnetic flux density taken at a point in the midway of the air gap between the stator and rotor pole is shown in Figure 5-3 (a). The 0^0 marks the aligned position whereas 22.5^0 mark the unaligned position of the rotor and stator pole. The magnetic flux density is high at the aligned position because all the flux from the stator pole passes through the air gap and into the rotor pole. According to equation (5.1), the small air gap area increases the magnetic flux density. As the rotor pole moves away from the stator pole, the air gap increases hence the magnetic flux density reduces. It will again increase due to the next rotor pole approaching the alignment position at 45^0 as illustrated in Figure 5-3(a). Once the rotor is near the stator pole, flux will tend to concentrate its path into the rotor. The comparison between the torques produced by each of the winding polarity at 5A phase current for both the generating and motoring operation is illustrated in Figure 5-3(b). The equation representing the torque for one phase is shown below:

$$T_e = \frac{1}{2} i^2 \frac{dL}{d\theta} \tag{5.3}$$

Based on the observation of equation (5.3), it can be seen that the torque depends on the slope of the inductance profile, $\frac{dL}{d\theta}$. At the aligned and unaligned position, the slope is zero hence torque is also zero as shown in Figure 5-3(b) at 0^0, 22.5^0 and 45^0. The instantaneous static torque was obtained using the FEM over the rotor surface [139]. The concentration of flux linkage is higher in the NSNS configuration showing significant improvement in torque value. In addition, since the torque density is defined as maximum torque over volume of machine [29], the NSNS configuration provides higher torque density as compared to the NSSN configuration. Therefore, the NSNS configuration justifies the selection of winding polarity for this study in terms of the area of magnetization curve and torque profile. The analyses will also be extended to a simultaneous phase excitation in order to propose the best configuration for a two phase excited machine. The winding polarity will be based on the single phase excitation.

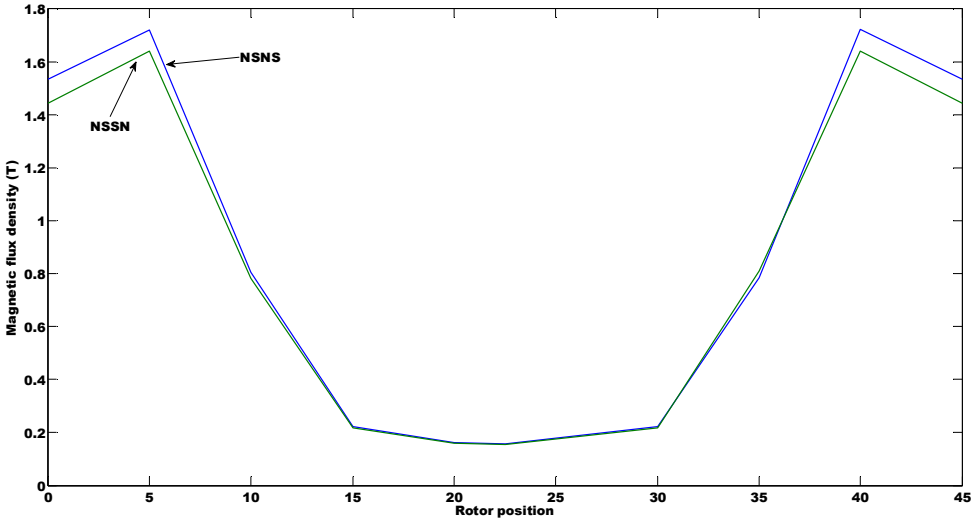

(a)

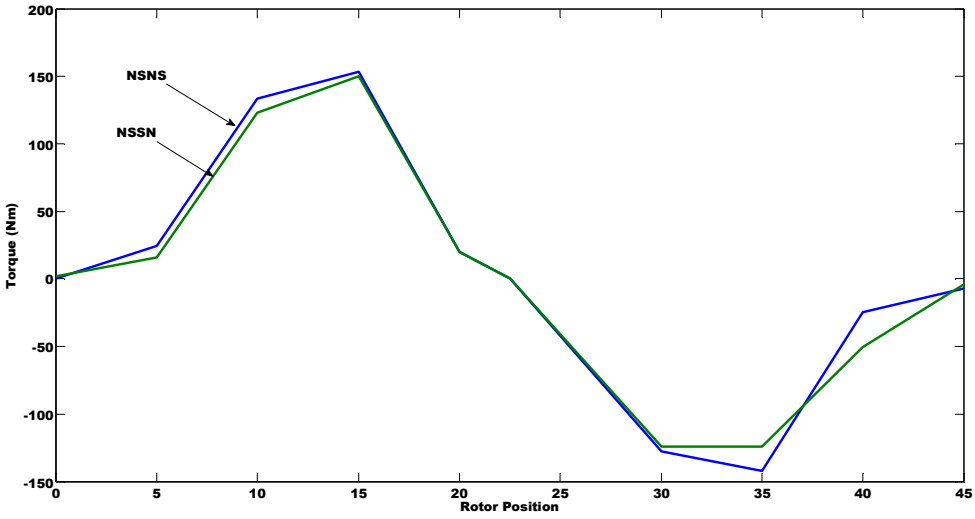

(b)

Figure 5-3: The graph of (a) magnetic flux density and (b) torque against rotor position for each winding configuration between 0^0 (aligned position) to 45^0 (unaligned position)

5.2 Calculation of Flux Linking the Adjacent Phases

As seen in the previous section, the change in the winding polarity affects the flux path. The calculation of flux linking the stator pole for the NSNS configuration is straight forward as there is no flux linking to the adjacent phases. The relationship between the phase flux linkage and the flux in each tooth can be represented as:

$$N_{phase}\begin{bmatrix}1 & 0 & 0\\ 0 & 1 & 0\\ 0 & 0 & 1\end{bmatrix}\begin{bmatrix}\phi_{tooth1}\\ \phi_{tooth2}\\ \phi_{tooth3}\end{bmatrix}=\begin{bmatrix}\lambda_{total\_ph1}\\ \lambda_{total\_ph2}\\ \lambda_{total\_ph3}\end{bmatrix} \tag{5.4}$$

Where N_{phase} is the number of turns per phase, ϕ_{tooth1} is the flux in the stator tooth for one phase and λ_{total_ph1} is the total flux linkage for one phase. However due to the flux in adjacent phases, equation (5.4) is not suitable for the NSSN configuration. The calculation will be based on the relationship developed by mutual coupling [140], when two adjacent phases conduct simultaneously.

5.3 Winding Configuration and Flux Path under Two Phase Excitation

The same winding polarity as in section 5.1 was used for the two phase excitation. An identical sequence of winding polarity was adopted for the second phase resulting in the following combination of poles under simultaneous excitation:

- NNSSNNSS
- NNSSSSNN

Other option was to arrange the phase windings so that the adjacent phase has the same sequence as the initial phase such as NSNSNSNS and NSSNNSSN. The phase configuration for possible simultaneous operation includes PhA-PhB, PhB-PhC and PhC-PhA. Therefore, the flux path when PhA and PhB conduct for the NNSSNNSS configuration is depicted in Figure 5-4(a) at a rotor angle of 15^0.The arrows mark the direction of the flux in the individual phases of the machine. The direction of the flux will depend on the polarity of the stator pole developed based from the current distribution. When phase A (PhA) and B (PhB) conducts, the flux in their neighbouring poles opposes in nature. The flux in stator pole one (P1) of PhA will be additive with the flux in stator pole four (P4) of PhB.

When PhA and PhB of the NNSSSSNN configuration is excited, the flux in P1 and P4 opposes one another and so does the flux in pole two (P2) and pole three (P3). Notably, there will be a reduction in torque due to the fluxes generated by both phases opposing each other within this region [137]. This differs from the NNSSNNSS configuration, where there is a return path in the second phase although the flux in the adjacent stator pole opposes each other as in Figure 5-4(a). Another alternative winding polarity such as the NSNSNSNS configuration can be made as depicted in Figure 5-5(a).

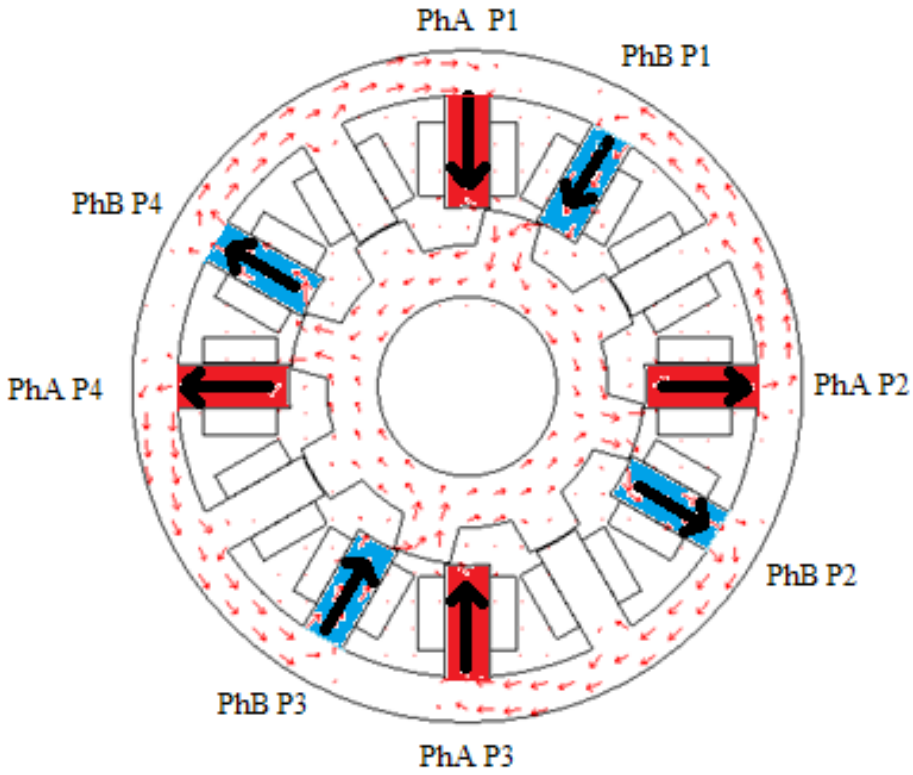

(a)

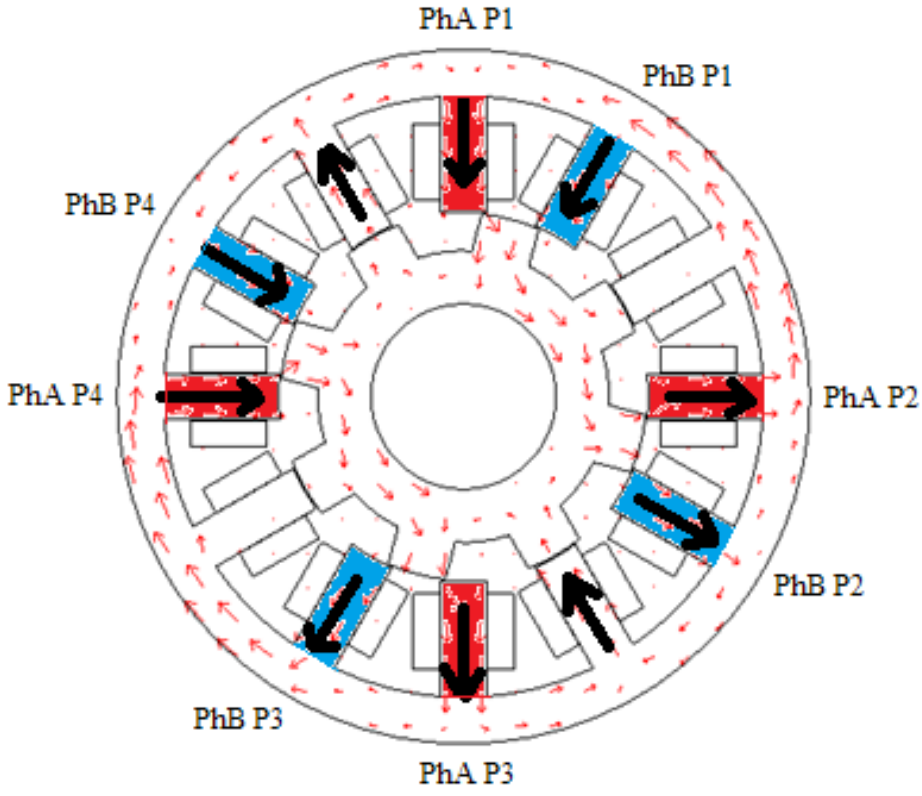

(b)

Figure 5-4: The flux path when two adjacent phases conduct simultaneously (a) NNSSNNSS (b) NNSSSSNN. The winding configuration for the second phase uses the same winding configuration as the first phase.

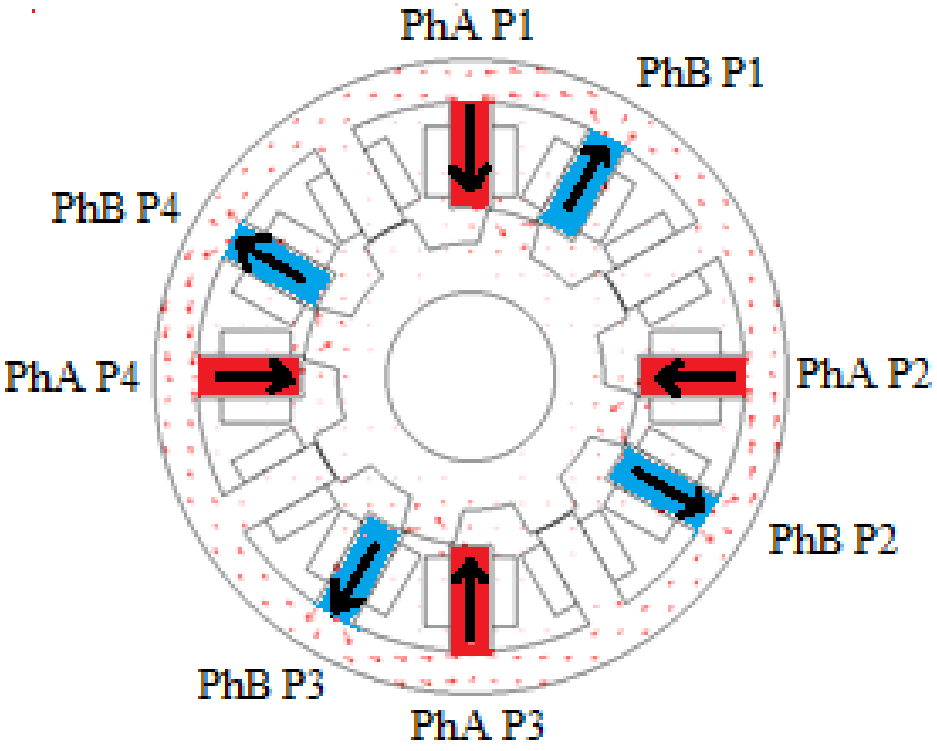

(a)

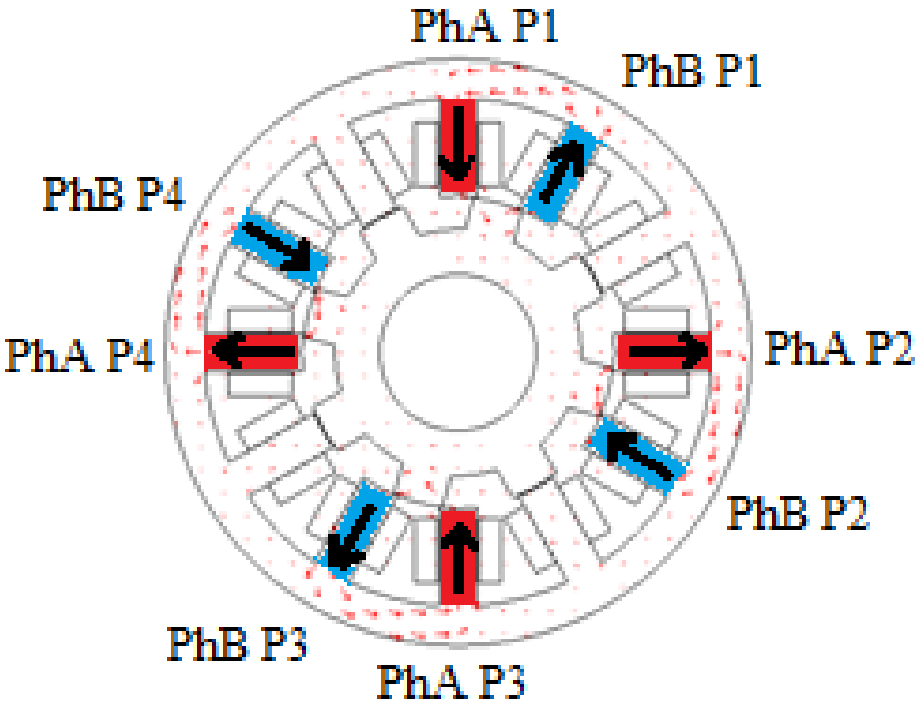

(b)

Figure 5-5 : The flux path when two adjacent phases conduct simultaneously (a) NSNSNSNS (b) NSSNNSSN. The winding configuration for the second phase uses the same sequence as the first phase.

The fluxes on the adjacent stator poles are additive with each other. The only difference with the NNSSNNSS configuration is by changing the polarity of pole 2 and 4 of Phase A and polarity of pole 1 and 3 of phase B. The last configuration consists of the NSSNNSSN pole polarity which duplicates the single phase NSSN polarity as shown in Figure 5-5(b). It has a similar arrow pattern with the NSNSNSNS configuration; however the difference is in the polarity of pole 2 and 4. The change causes the flux in the neighbouring poles such as pole 1 of phase B and pole 2 of phase A to oppose each other.

The flux path for the simultaneous excitation can be grouped as in Figure 5-6 and Figure 5-7. Each winding configurations provides their own unique flux path. Although the main flux path for the NSNSNSNS and NSSNNSSN configuration are similar in pattern as shown in Figure 5-7(a) and (b), the change in pole polarity creates a difference in the magnetic flux distribution. The NSSNNSSN configuration has higher back iron saturation between the excited phases as compared to the NSNSNSNS configuration. Even though the winding configuration has been changed, it can be concluded that all the designs produce symmetric flux path. The outcome supports the previous findings where an odd number of phases produces symmetric flux path [137]. Nevertheless, the optimal winding polarity has yet to be defined.

The simultaneous excitation creates interaction of flux between the adjacent phases normally termed mutual coupling. The mutual coupling aids to increase or decrease the net torque depending on the winding polarity. It can be said that the NNSSSSNN configuration has the weakest mutual coupling between the phases due to the long flux path. Therefore, it has the smallest torque between the other configurations as depicted in Figure 5-8. It can be seen that the NSSNNSSN, NNSSNNSS and NSNSNSNS gives better torque profile during simultaneous excitation. These configurations can be grouped under the short flux path having four groups of main flux. An optimum pole configuration can be determined by analysing the distribution and change of flux path and also the torque profile.

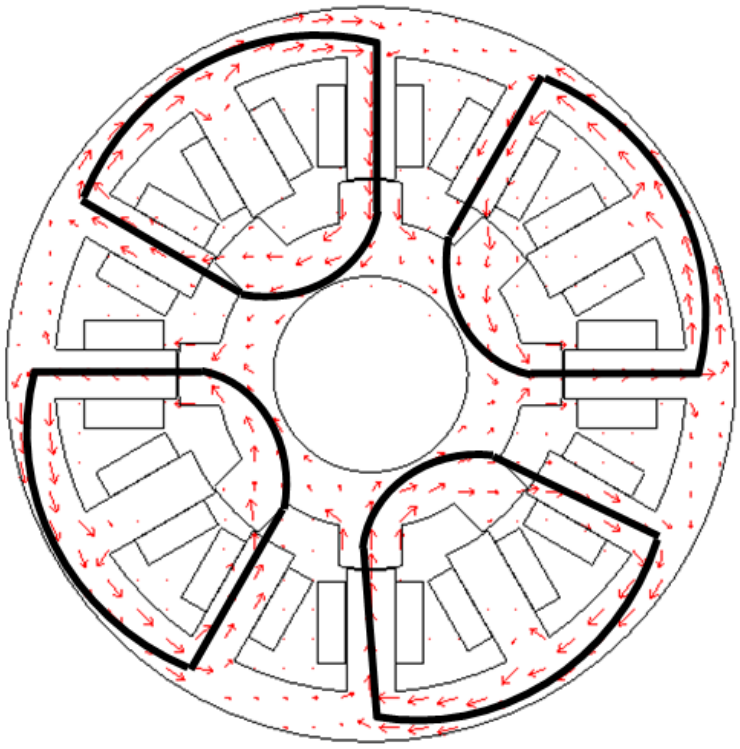

(a)

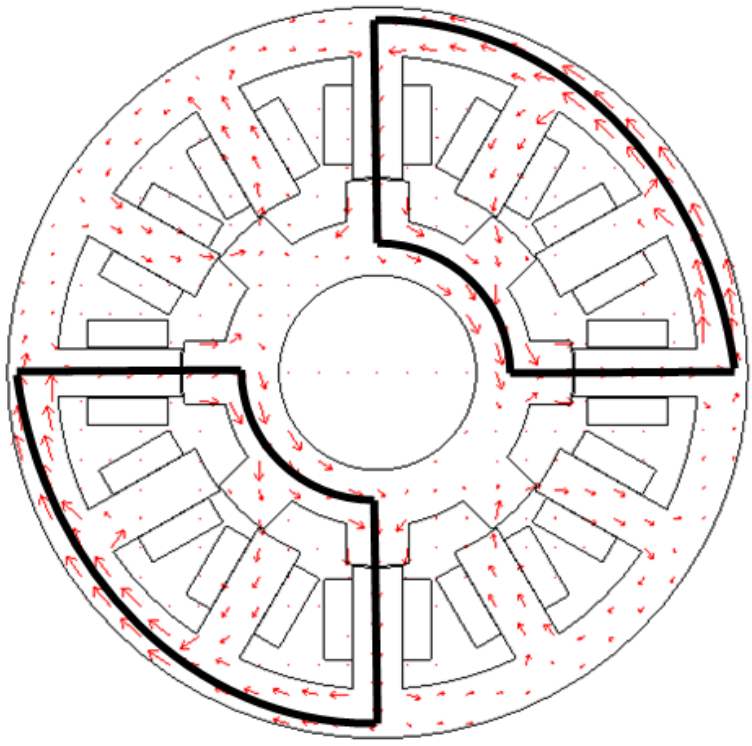

(b)

Figure 5-6: Main flux path for the (a) NNSSNNSS and (b) NNSSSSNN configuration

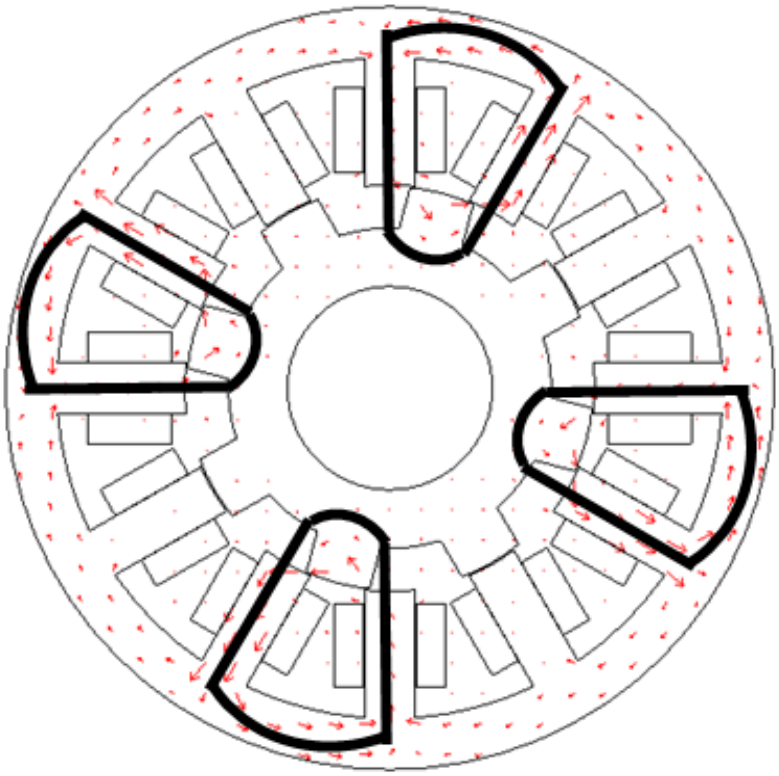

(a)

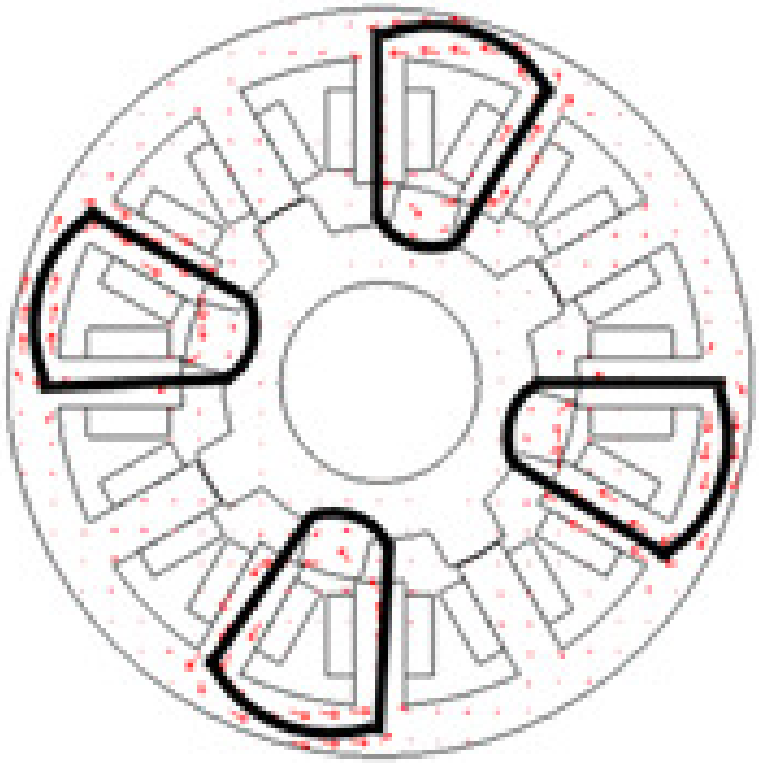

(b)

Figure 5-7: Main flux path for the (a) NSNSNSNS and (b) NSSNNSSN configuration

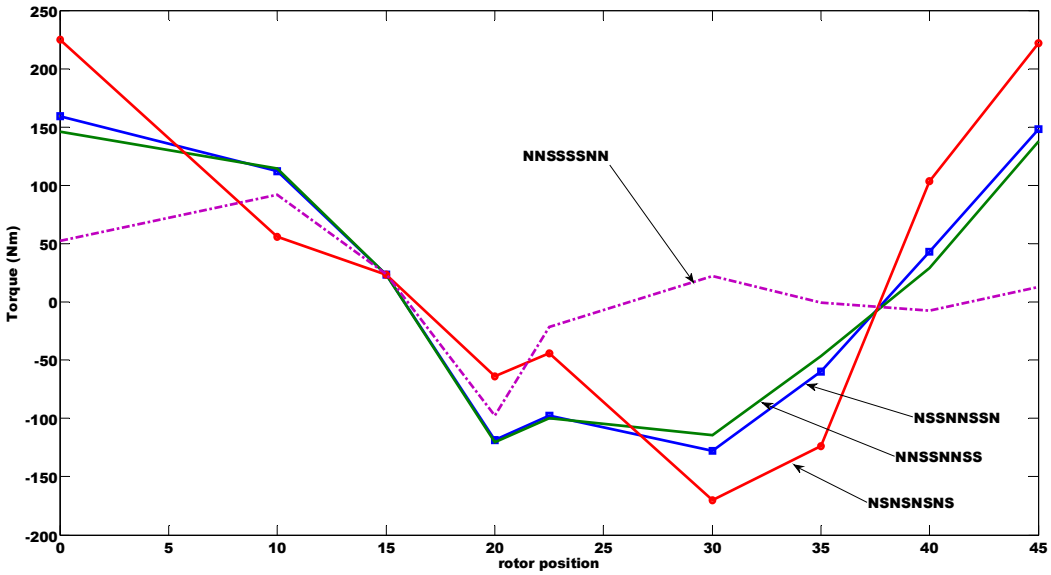

Figure 5-8: Comparison of torque under the two phase excitation for all winding configurations

5.4 Comparison of Magnetic Flux Density Distribution

The magnetic flux density can be determined by the magnetic flux lines which travel in the same direction. The low and high flux intensity is represented by the distance between the flux lines. The high concentration of flux lines represents a high saturation level in the machine. The following sections will compare the intensity of the flux between the single phase and two phase excitation for machines with different pole polarity and different number of rotor poles; 12/8, 12/16 and 12/4 machine.

5.4.1 Single Phase and Two Phase Excitation for the 12/8 Machine

The same current density level was applied to the single phase and the simultaneous excitation resulting in the magnetic flux density concentration shown in Figure 5-9 for the single phase excitation and Figure 5-10 and Figure 5-11 for the simultaneous excitation. It can be seen that the NSNS, NNSSNNSS and NSNSNSNS shows a well distributed flux density, thus avoiding the concentration of flux in a particular machine segment. A comparison between the simultaneous NNSSNNSS and NSNSNSNS configuration reveals that it originates from the single phase NSNS configuration. This shows that even though this study will be based on the NSNS configuration, the result will also reflect an optimum performance for the simultaneous operation.

As for the NSSNNSSN configuration in Figure 5-11(b), the intensity is higher in the stator yoke section of the excited poles. The result of this study indicates that the saturation effect is enhanced under the simultaneous phase excitation. Higher saturation is observed when the flux path is not evenly distributed as depicted in Figure 5-9(b), Figure 5-10(b) and also Figure 5-11(b). This may result in the machine having a hot spot area, thus reaching the thermal limit of the machine [144]. The value of the magnetic flux taken at the midpoint of the excited pole of phase A and B, the unexcited pole of phase C, and also stator yoke between the excited phases is illustrated in Figure 5-12. The value is in accordance with the earlier explanation where it can be seen that the flux value for the NNSSNNSS configuration is similar in the main machine segments due to well distributed flux. The high value of flux can be seen in the stator yoke between its excited phases for the NNSSSSNN configuration. As mentioned earlier, the main flux path for the NSNSNSNS and NSSNNSSN are similar, however, their magnetic flux distribution differs due to the polarity of the poles as depicted in Figure 5-11(a) and (b). The flux is mainly distributed around the stator yoke for the NSNSNSNS configuration whereas, for the NSSNNSSN configuration, the flux is concentrated in the segment between the excited phases. This will impose a certain limit on the number of turns for the machine to avoid high saturation of the machine segments.

It can be concluded that the winding arrangement does not produce equally distributed magnetic flux density during simultaneous phase conduction due to the direction of mutual and self-flux. The NNSSNNSS configuration clearly has a symmetrical flux density distribution under the two phase excitation. This will provide a balance in the iron losses which can be calculated based on the flux waveforms in the stator pole and yoke [88, 145, 146]. The NSNSNSNS and NSSNNSSN configuration has shorter flux path as compared to the other two configurations. However, due to the flux distribution, the NSNSNSNS configuration results in lower magnetic flux density and saturation as shown in Figure 5-12. This in turn, will reduce the core losses due to the reduction in active steel volume [72, 139].

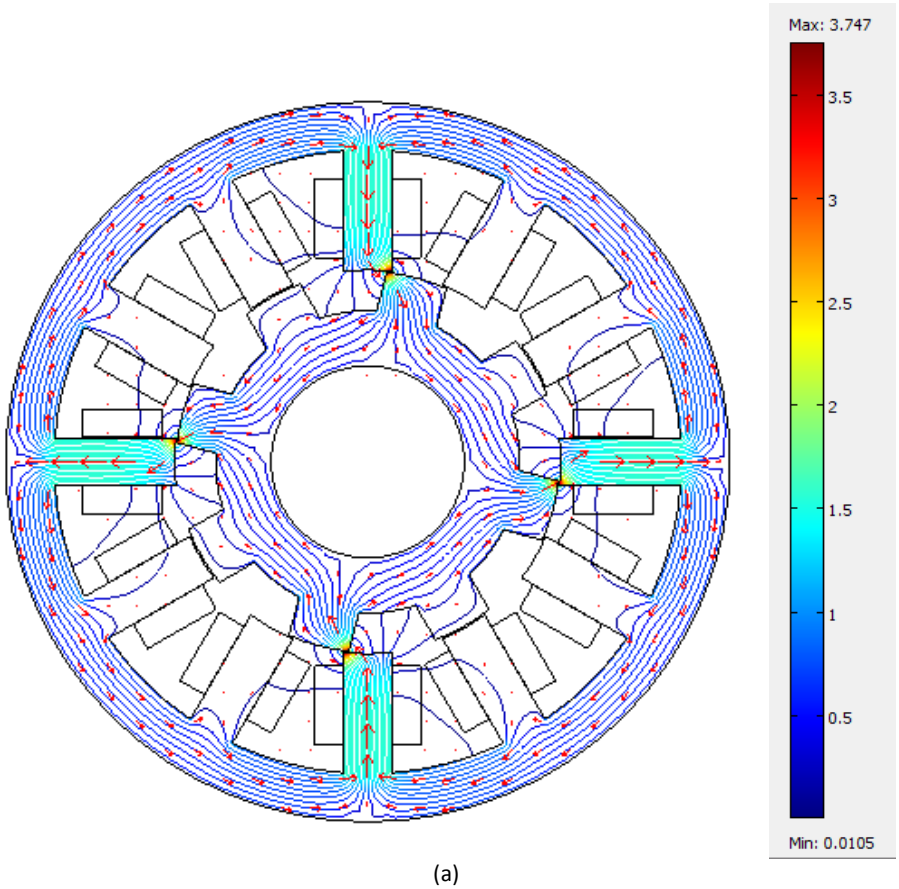

(a)

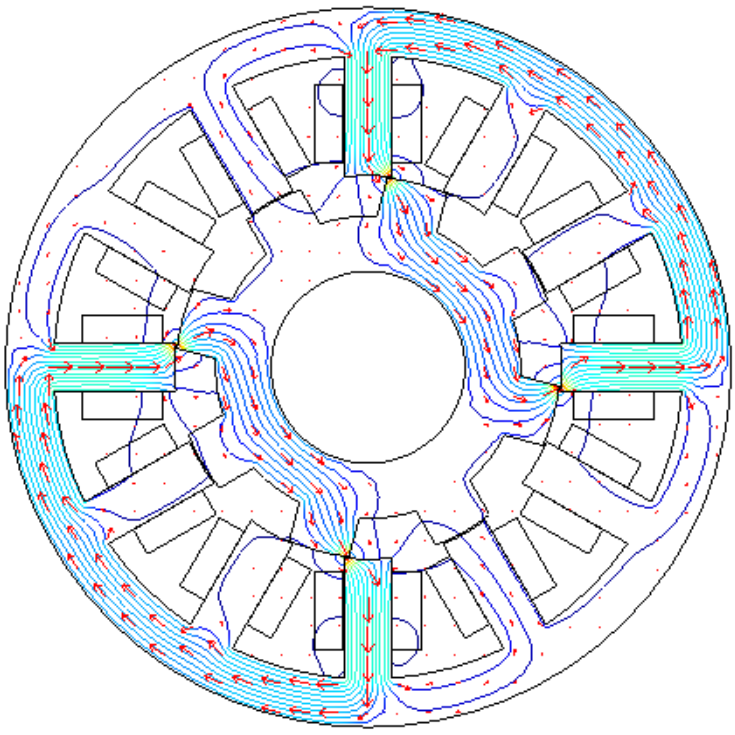

(b)

Figure 5-9: The cross sections of a 3-phase 12/8 machine and their magnetic flux distribution (Tesla) with phase A excited at constant current for configuration (a) NSNS and (b) NSSN

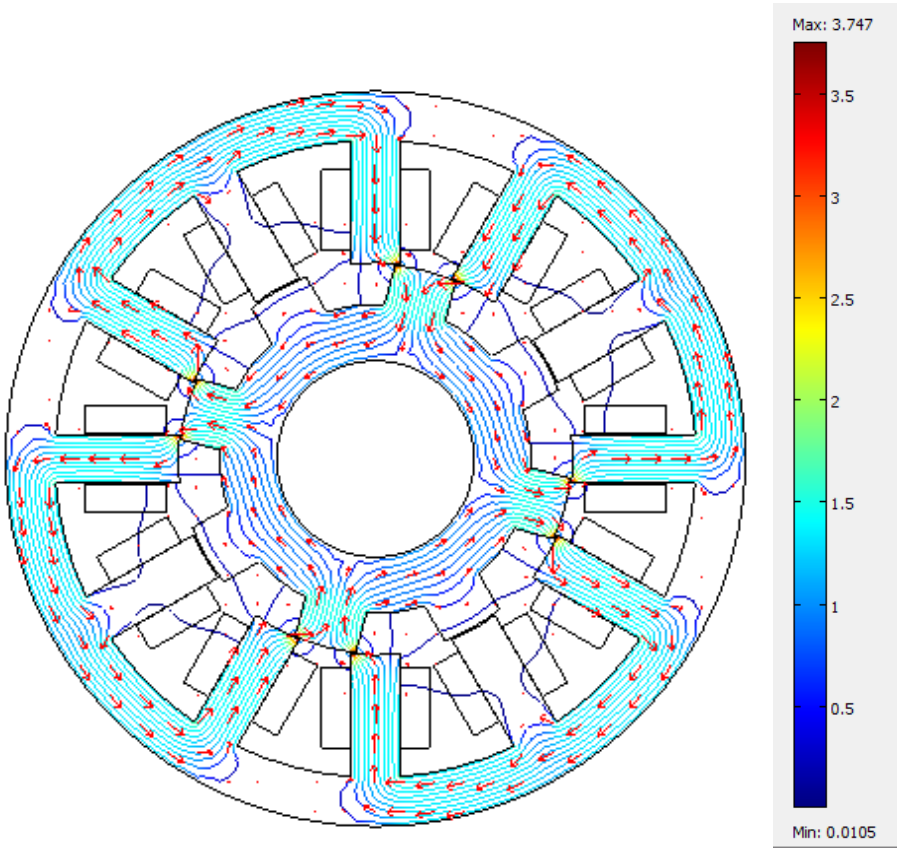

(a)

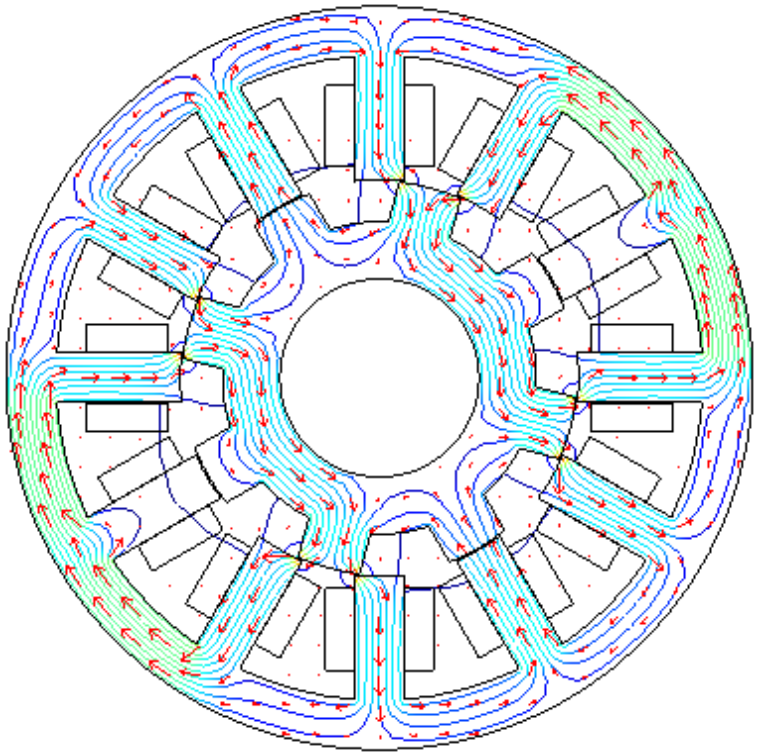

(b)

Figure 5-10: The cross sections of a 3-phase 12/8 machine and their magnetic flux distribution (Tesla) with simultaneous excitation of Phase A and B at constant current level for configuration (a) NNSSNNSS and (b) NNSSSSNN

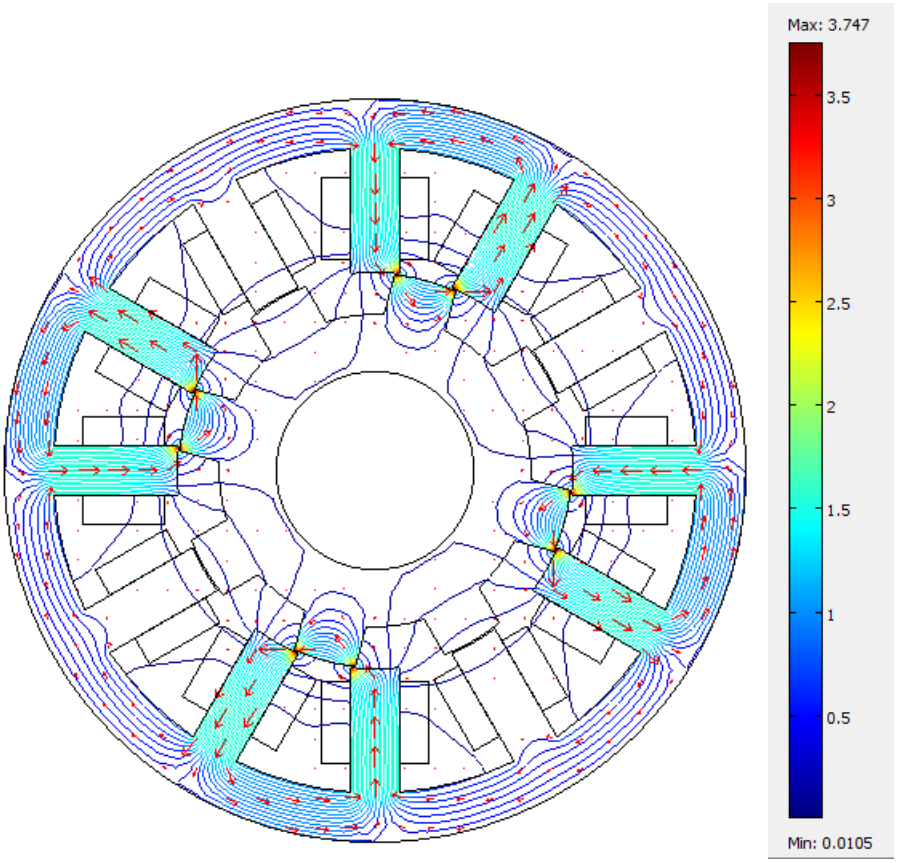

(a)

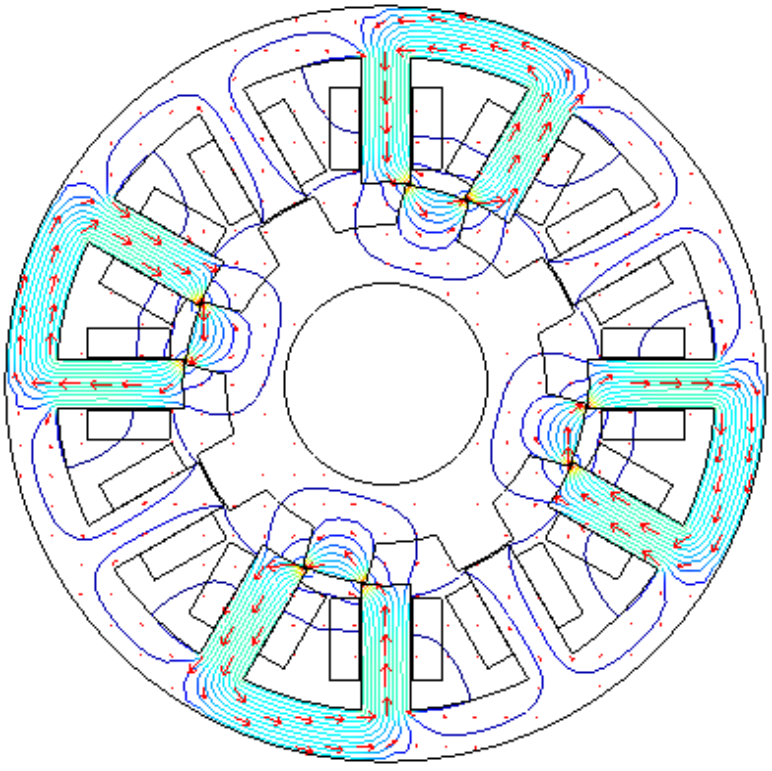

(b)

Figure 5-11: The cross sections of a 3-phase 12/8 machine and their magnetic flux distribution (Tesla) with simultaneous excitation of Phase A and B at constant current level for configuration (a) NSNSNSNS and (b) NSSNNSSN

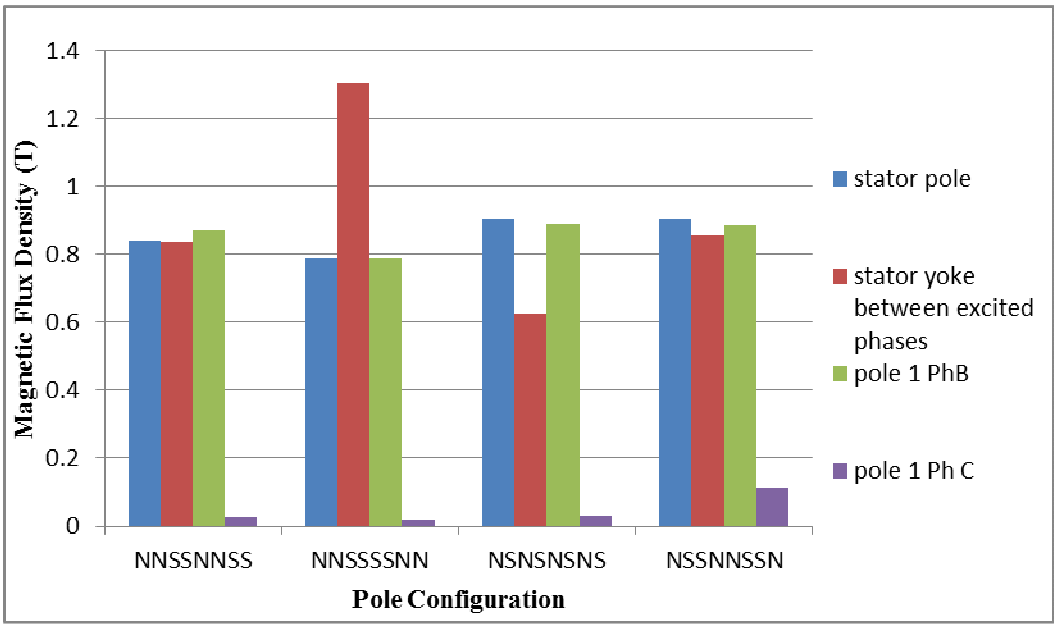

Figure 5-12: The magnetic flux density in Tesla taken at the mid-point of each machine segment for a 3 phase 12/8 machine at rotor position of 15^0

5.4.2 Comparison of Simultaneous Excitation Between the 12/8, 12/4 and 12/16 Machine

The number of rotor poles for the 12/8 machine were halved and doubled to analyse the effect of having a lower and higher number of rotor poles on the machine performance. The geometrical rotor arc satisfies the geometrical limit for the lower and higher number of rotor poles machine having a fixed outer rotor diameter as explained in [70]. Most research states that a high number of rotor poles improve the torque profile. A novel pole design formula was developed to accommodate the machine with a high number of rotor poles [70]. The aim was to improve the torque profile and focused on the geometrical parameters of both the stator and rotor poles for traction applications. Not much has been said about the lower number of rotor poles machine. In this study, the impact of a lower and higher number of rotor poles on the machine performance for wind energy application will be observed. Therefore, the intensity of the flux on the existing 12/16 machine and the new 12/4 configuration machine having the same number of turns and current density level as the 12/8 machine were analysed.

With the number of rotor poles doubled, the return paths for the flux through the rotor poles have been reduced. Therefore, it can be seen that the rotor poles in Figure 5-13(b) are subjected to higher flux intensity. Also, it can be seen that for the 12/8 machine, when phase A (PhA) is at the aligned position, the second phase B (PhB) is approaching the alignment position. This is not the case for the 12/16 machine where PhB is still in the decreasing inductance region whilst PhA is aligned with the stator pole.

When the numbers of rotor poles are halved, the width of the rotor poles doubles as illustrated in Appendix B. It has the lowest flux intensity during the aligned position under the NSNSNSNS configuration and very minimal flux leakage on the unexcited phase. However, for the other types of pole polarity, the flux density level in other parts of the machine segment for the 12/4 machine are quite high as shown in Appendix E. The width of the rotor pole determines the saturation level of flux in a particular machine segment. Although the lower number of rotor poles has larger magnetization curve, the core losses in a particular machine segments may be high. Hence, there will be a limit on the number of turns to be used to avoid over saturating the machine segments.

The 12/16 machine produces smaller degree of continuous overlap as compared to the 12/4 and the 12/8 machine. This is one of the reasons for a smoother torque profile produced by the higher number of poles machine. Also, all the machine satisfies the minimum condition of the overlapping inductance profile to avoid the self-starting problem [70]. The condition of the overlapping inductance profile will occur when the aligned inductance of PhA overlaps with the unaligned inductance of PhB.

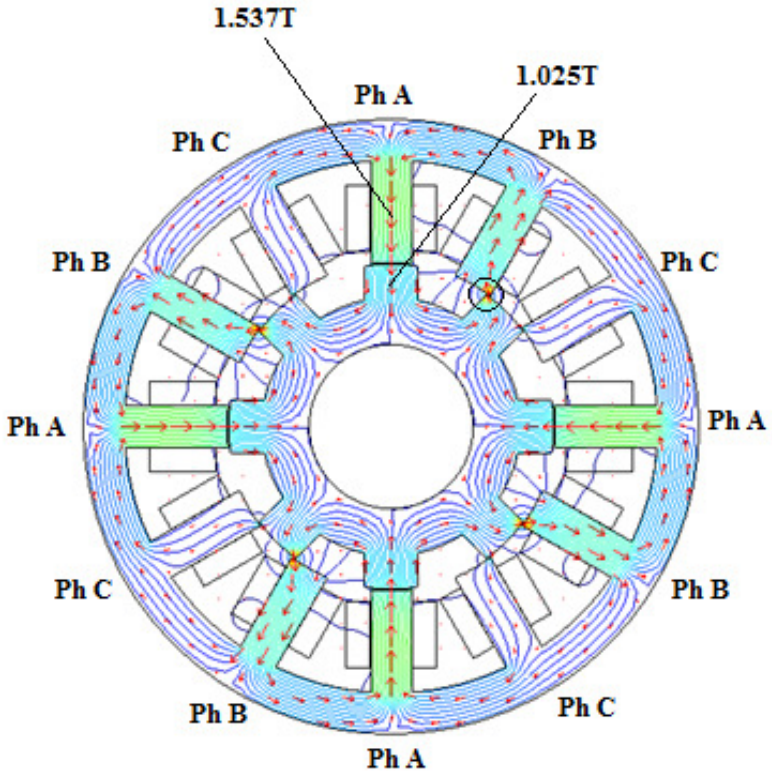

(a)

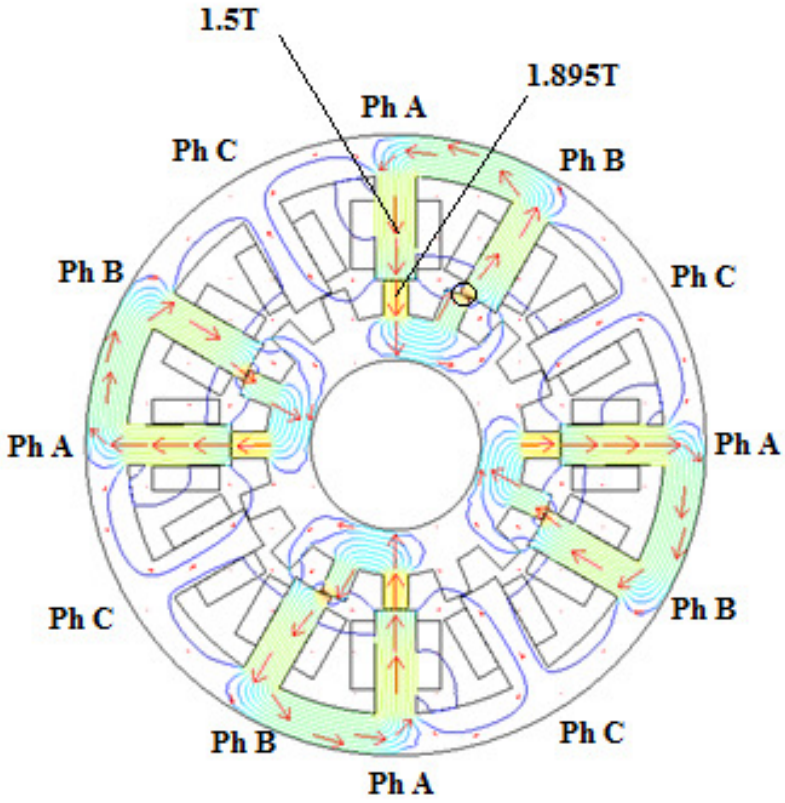

(b)

Figure 5-13: Comparison of the magnetic flux distribution between a (a) 12/8 and (b) 12/16 machine at aligned 0deg position.

5.5 Conclusions

This chapter gives an overview of the entire possible winding polarity for a four poles per phase machine subjected to a single and two phase excitation. The possible winding polarity for single phase and simultaneous excitation is as follows: NSNS and NSSN, NNSSNNSS, NNSSSSNN, NSNSNSNS and NSSNNSSN.

The study indicates that a symmetrical flux path can be accomplished when only one phase is excited. However, for a dynamic operation there will be at least two phases conducting at any one time. The flux linkages on each excited phase will influence the flux in the adjacent phases. It will either attract or distort the flux based on the polarity of the adjacent poles. The path of these fluxes will determine the level of saturation in the machine.

Under single phase excitation, the two winding configurations; NSNS and NSSN do not show any level of saturation. The best configuration in terms of the largest energy conversion loop is the NSNS configuration. Also, it is more superior in terms of having the least flux leakage. This is one of the reasons for the large energy conversion area as compared to the other configurations, making it the best choice for this study.

During simultaneous excitation, a high level of flux intensity was observed in the stator pole and yoke caused by the polarity of the poles. By taking the average flux between the four segments, the NSNSNSNS and NNSSNNSS winding configuration have the lowest level of flux intensity. Both of the configurations also show higher torque profile. The similarities between these configurations are that they provide short flux path and well balanced flux distribution. They are also formed based on the single phase NSNS configuration.

The machine with a higher number of poles will produce smoother torque profile due to continuous overlap of the rotor poles with the stator poles of its adjacent phase. However, the magnetic flux density is concentrated in the rotor poles due to the flux passing from larger stator pole area to a narrower area thus increasing the core losses.

Furthermore, the number of turns has to be reduced to incorporate the high saturation effect.

The findings suggest that the winding polarity can be selected to optimise the performance of a machine in terms of torque, losses or power generation. The torque can be analysed in terms of torque profile whereas the losses can be determined based on the machine which produce the lowest magnetic flux density within the machine segment. The configuration which provides large energy curve will produce high generation of power. The best configuration can be summarized based on the three parameters as follows:

Table 5-1: Table on summary of the best winding configurations for the SRM

Parameters	**Machine structure**	**Winding configuration**
Losses	12/8	NSNS NSNSNSNS
	12/4	NNSSNNSS
Torque	12/8	NSNS NSNSNSNS
Power generation	12/4	NSNS

Based on this investigation, the NSNS configuration has been selected for the development of the SRG modelling platform. It forms the basis for design considerations that aid to optimise the performance of the machine. This configuration will be tested for the 3-phase 12/8, 12/16 and 12/4 SR machine.

CHAPTER 6

CHARACTERIZATION OF THE OPTIMAL PARAMETERS FOR MAXIMUM OUTPUT POWER

By definition, the electric generators are devices which convert mechanical energy into electrical energy. The mechanical energy can be in the form of wind, fuel, water or nuclear energy. Within the generator, electricity is generated based on the phenomenon of electromagnetic induction. Unlike the conventional machine, the only windings on the SR machine are concentrated around the stator poles. Therefore, when the windings are energized, the stator pole behaves as an electromagnet creating a magnetic field around it. The movement of the rotor poles will cut through the magnetic field, varying the reluctance of the flux path. Thus, the machine is highly nonlinear as both its flux linkage and inductance varies as a function of the rotor position and current. The SR machine will store the electric energy in the form of magnetic field energy in the air gap during the first excitation stage, and it will be released together with the mechanical energy during the second generation stage. Therefore, the optimal performance of the machine can be determined according to its generation and excitation stage during each operating cycle.

In this chapter, the control variables that affects both the excitation and generation stage will be identified and analysed based on the voltages across the phase windings. The variable which provides the highest percentage of generated power over the excitation power is grouped as the optimal variables. Since the machine is highly nonlinear, it is not easy to determine its optimal variables. It will also be difficult to determine the polynomials relating the variables with the output power. The heuristic method is employed to obtain an accurate profile of the variables affecting the output power for each of the machines stated in Chapter 3, sub section 3.1. The geometrical structure of the stator remains the same whereas the numbers of rotor poles are varied. The rotor poles are easier to be changed and manufactured as it does not have any magnets or windings.

6.1 Determination of the Control Variables Affecting the Output Power

The phase current during the excitation and generation stages depends on the slope of the inductance, $\frac{dL}{d\theta}$, amplitude of terminal voltage, V and back EMF, $\omega i\frac{dL}{d\theta}$ as shown by the following equation:

$$\pm V = Ri + L\frac{di}{dt} + \omega i\frac{dL}{d\theta} \tag{6.1}$$

The terminal voltage will be negative during generating stage due to the freewheeling current through the diodes. Using the separation of variable method to equation (6.1), phase current, i can be written as follows:

$$i = \frac{\pm Vt}{L + (R + \omega(\pm\frac{dL}{d\theta}))t} \tag{6.2}$$

Where L is the phase inductance, R is the winding resistance, ω is the angular speed and t is the time. According to equation (6.2), the current will slowly increase depending on the voltage level and placement of the turn on angle on the inductance slope. The current will start to increase as the rotor moves away from the aligned position. It will keep on increasing as speed increases and when the back EMF is more than the terminal voltage. The current slowly extinguishes to zero as the slope of the inductance approaches the minimum value. From equation (6.2), the parameters which may increase and shape the phase current include speed, voltage, placement of firing angles and also reference current.

Generally, it can be said that the excitation stage is crucial as it needs to store as much energy as possible for the conversion of energy during the generation stage [12]. This relates to the switching on and off of the semiconductor devices and the placement of the firing angles along the inductance profile. The knowledge on the phase current is required to solve for the average output power, as stated in subsection 2.9. The high percentage of generated power will be used as the criteria to determine the performance of the machine as it implies that the excitation energy and losses are at its minimum value. The main losses in the machine include the copper and iron loss [88].

6.1.1 Copper Losses

The copper losses, P_{cu} can be expressed as:

$$P_{cu} = i_{rms}^2 R_{ph} \tag{6.3}$$

It depends on the RMS phase current, i_{rms} and resistance, R_{ph} of the winding. The RMS phase current can be calculated as:

$$i_{rms} = \sqrt{\frac{1}{T}\int_0^T I_{ph}^2 dt} \tag{6.4}$$

where T is the period for one cycle of operation and I_{ph} is the phase current.

6.1.2 Iron Losses

The iron losses occur in the magnetic material, which consists of hysteresis and eddy current loss. The latter can be reduced by laminating the core material whereas the former varies as a function of frequency of the applied field. The applied field will change the magnetic properties of the material by the magnetizing and demagnetizing process. Some of the researches to estimate the iron losses include the finite element method [145], Steinmetz equation [91] and also by using the geometry of the machine [88]. The calculation for the iron loss requires information from the manufacturer's data sheet. The iron loss becomes dominant at a very high speed operation due to the high operating frequency [147]. This is related to the fundamental frequency, f_1 of current in each phase which is equal to the rotor pole passing frequency [55] shown by the following equation:

$$f_1 = \frac{\omega}{60} \times N_r \tag{6.5}$$

Where N_r is the number of rotor poles and ω is the speed in r/min. One of the main challenges in determining the iron losses is due to the structure of the machine, which produces different flux waveforms in each segment.

Since the focus of this research is on the low and medium speed operation, only the copper losses will be included in the calculation. The following section will provide detail analysis of each of the variables from equation (6.2) and how it affects the generated power.

6.2 Analysis of the Control Variables Affecting the Generated Output Power

6.2.1 Firing Angles

Since the operation of the SRG is during the decreasing inductance slope, the placement of the turn on angle should be made along the increasing inductance region to allow the phase current to build up. The turn off angle on the other hand can be placed anywhere before the poles starts to separate, which is before the minimum inductance region. The peak current for the generating operation occurs after both the firing angles are turned off depending on the back EMF and speed. Therefore, there is a possibility of the firing angles yielding the same output power [20]. Hence, the optimal firing angles are selected in terms of the highest percentage of generated power. Some possible factors which may affect the selection of optimal firing angles are stated below:

- If the turn on angle is placed too low in the motoring region, the machine will develop positive torque, decreasing the efficiency of the generating operation.
- If the turn on angle is placed along the decreasing inductance profile, the dwell angle will reduce, resulting in a non-overlapping current profile.
- As for the turn off angle, it cannot be placed too near the minimum inductance region as this will result in the generating current tailing off into the excitation stage of the next phase. The current will increase continuously instead of returning to zero during each cycle [148, 149].

Based on the factors above, the optimal firing angles have to be determined heuristically to avoid any overlapping parameters. The range of the firing angles to be determined is narrowed according to the conditions above by starting from the mid motoring region and into the decreasing inductance region. For each turn on angle, the range of turn off angle for the 12/8 machine will be from 25^0 to 40^0. By doing this, the range of the firing angles on the inductance profile will be covered. As mentioned earlier, the angles which give the highest percentage of generated power is selected.

6.2.2 Terminal Voltage

The terminal voltage is the voltage across the battery which is connected directly to the converter. According to equation (6.2), an increase in the terminal voltage will increase the phase current provided that the back EMF is lower than the terminal voltage. Since the turn on angle will be along the increasing inductance profile, the initial increase in current will be slow. In certain application, a buck boost converter is added to aid in the increase of phase current [61]. This however, requires additional circuitry, increasing costs and reduces the available space within the existing circuit. As the voltage is proportional to the current, any increase in voltage will increase the current. However, a high voltage may reduce the generating current; thus, a suitable value of voltage to be used has to be determined. This can be achieved using the heuristic method. A different level of voltage is simulated for each of the turn on angle groups mentioned in subsection 6.2.1.

6.2.3 Speed

The velocity of the wind will turn the blades of the turbine hence turning the shaft, which is directly connected to the rotor. Thus, the speed of the rotor is influenced by the wind velocity. According to equation (6.2) the wind speed has a major impact on the back EMF. A low wind speed results in the back EMF being lower than the terminal voltage whereas a high wind speed increases the back EMF to be more than the terminal voltage. Even though the speed is not a controlled variable, it influences the selection of parameters such as the firing angles, voltage and number of rotor poles. Therefore, the optimal parameters will be determined at various speed ranges.

6.2.4 Phase Inductance

The phase inductance can be obtained from the magnetization curve profile according to the following equation:

$$L(i,\theta) = \frac{\lambda(i,\theta)}{i} \tag{6.6}$$

Both the inductance, L and flux linkage, λ varies as a function of current, i and rotor position, θ. The location of the firing angles on the inductance profile influences the shape of the phase current. From equation (6.6), the phase current is inversely

proportional to the inductance value, which is represented as the inductance profile curve. The inductance is also proportional to the reluctance, hence at the aligned position, inductance is maximum whilst reluctance is minimum.

6.2.5 Reference Current

During motoring operation, the closed loop current control is employed to shape the phase current. It was established that the generating operation of the machine is said to mirror the operation of the motoring mode. But, the generating excitation is made whilst the inductance is increasing hence the initial current will be low. On the contrary, the excitation for motoring operation is during the minimum inductance profile with high starting current. Due to this reason, the reference current for motoring is required for protection from the initial high current whilst for generating operation, for overcurrent protection after the switches are turned off.

6.2.6 Phase Resistance

The resistance of the phase winding is designed to minimise the copper loss, hence the value is made as low as possible. Due to this reason, most of the literatures neglect the resistive voltage drop in the calculation as it is insignificant as compared to the terminal voltage. Nevertheless, the effect of resistance is pronounced when the phase current is high.

The following section describes the procedures to determine the optimal parameters of the machine.

6.3 Iterative Search to Determine the Optimal Parameters

Each of the variables including the firing angles; turn on and turn off angle, reference current, voltage and speed is analysed in terms of the percentage of power generated. The turn off angle is varied between 25^0 to 40^0 for each group of turn on angle ranging from 10^0 to 24^0. The overall current profile is checked to ensure continuous operation of the machine at each of the turn on angle position. The analysis is illustrated graphically through a graph of percentage of power generated against each

of the selected variables whilst the other variables are made constant. For example, a graph of percentage of power generated against turn on angle will hold the turn off angle, reference current, voltage and speed constant.

6.3.1 Effects of Reference Current

Reference current was chosen as an appropriate control variable when operating in the low speed range. It is normally obtained through the voltage, speed or power regulation. To analyse its effect on the generated output power, it is made constant. The constant value of reference current is chosen based on the maximum value of current, which occurs before the saturation point (knee point) of the magnetization curve.

The values of the reference current are varied between 1A to 9A for all the machines. Figure 6-1 illustrates the effect of the reference current between 1A to 9A, and the results in Figure 6-1(a) shows the difference of percentage of power generated for various turn on angles selected before and after the alignment position. The turn off angle is kept constant at 35^0 hence for the turn on angle placed after the alignment position, which is at 22.5^0, it can be seen that the reference current has no impact on the percentage of power generated.

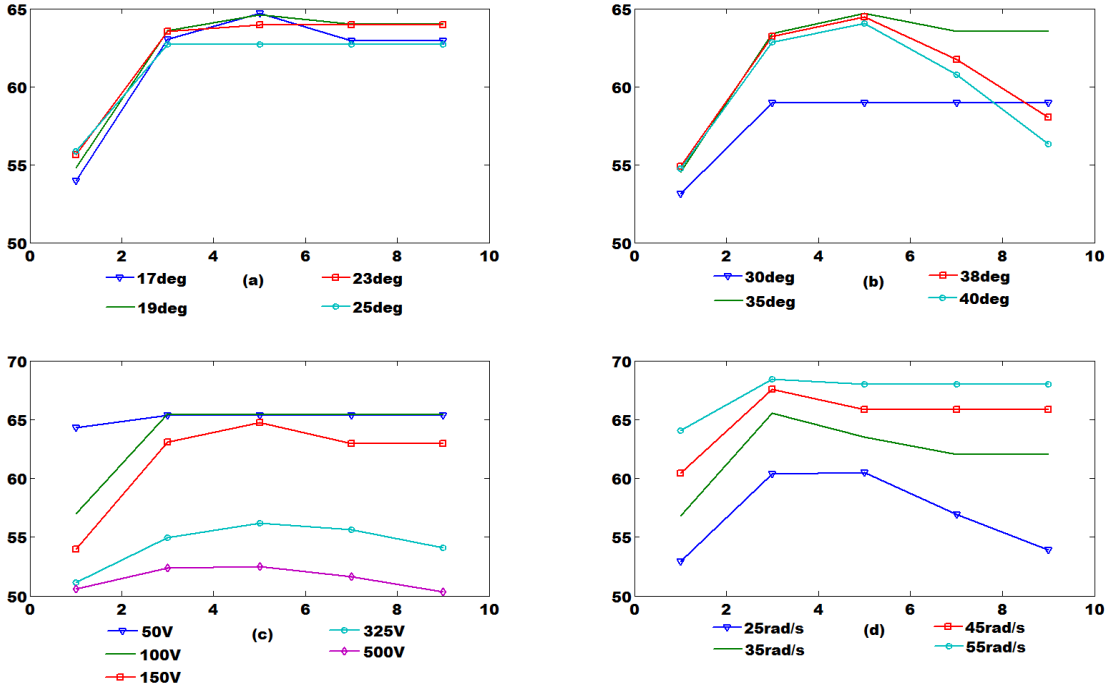

Figure 6-1: Graph of % power generated against reference current (A). Each graph shows the effect of reference current with (a) turn on angle, (b) turn off angle, (c) voltage and (d) speed

The reason for this is because the machine operates in a single pulse mode due to the fixed voltage and small difference between the turn off and turn on angle, which is termed dwell angle. When the turn on angle is placed before the alignment position, the current has time to build up. Therefore, with a suitable voltage applied, the current can reach the reference limit imposed. If the voltage is fixed whilst the reference current is increased, there will be a point when the voltage is not enough to push the current to the reference value. For turn on angle of 18^0, the turn off angle is varied between 30^0,35^0,38^0 and 40^0 as in Figure 6-1(b). The percentage of power generated increases as the turn off angle is moved further down the inductance slope. However up to a certain angle, the percentage of power generated decreases. To sum up, there is an optimal dwell angle which will provide the high percentage of power generated. At a fixed turn on angle of 17^0 and turn off angle of 35^0 the voltage level between 50V – 150V gives higher percentage of power generated as shown in Figure 6-1(c). A decrease in the percentage of power generated can be seen as the voltage is increased, allowing the current to reach its reference limit resulting in the chopping action. Figure 6-1(d) depicts an increase in the percentage of power generated as speed increases. It is observed that at a reference current of 5A, a high percentage of power generated is obtained as the firing angles, voltage and speed is varied. For this reason we chose 5A as the reference current for the 12/8 machine. The reference limit serves as an overcurrent protection as the peak value of current after the turn off angle cannot be predicted.

6.3.2 Effects of Terminal Voltage

The terminal voltage is measured across the phase winding when the switch on the converter conducts. Hence the phase current is directly proportional to the terminal voltage as in equation (6.2). An increase in the terminal voltage will also increase the phase current. Therefore, a high terminal voltage can be used to aid in the increase of phase current during the initial excitation stage, in the increasing inductance region. If the voltage is kept high during the conduction period, it will result in a faster decrease in current after turn off angle due to the higher negative voltage. Subsequently, too much voltage provides more excitation energy to enable the current to reach its reference limit, resulting in the current chopping mode. The effect of increasing the voltage on the shape of phase current at turn on angle of 18^0 is depicted in Figure 6-2.

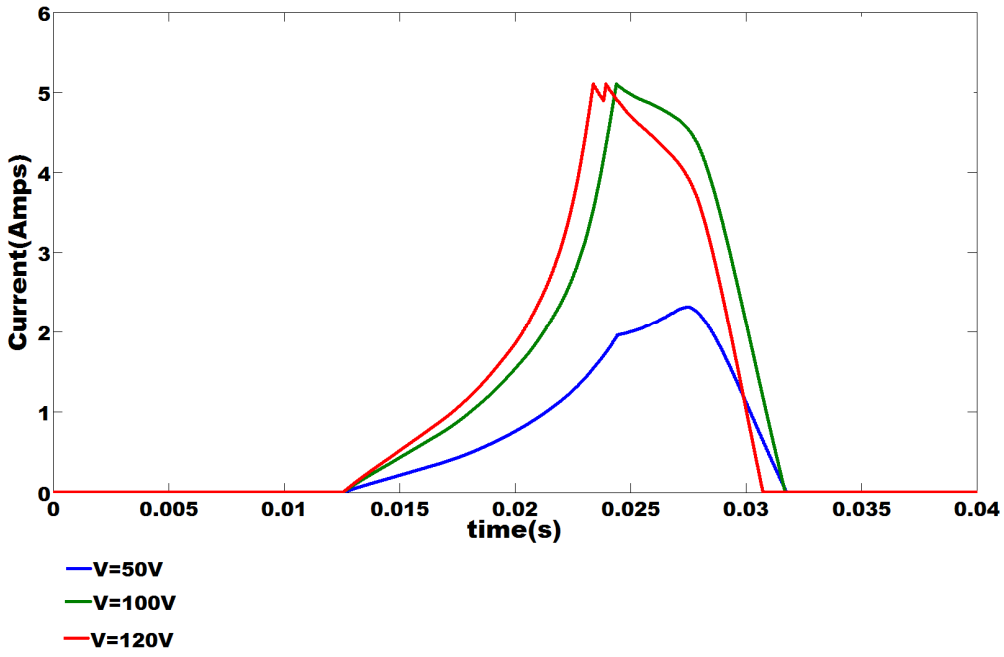

Figure 6-2: Effect of terminal voltage on the shape of phase current at turn on angle 18deg, turn off angle 35deg and speed of 25rad/s

The effect of increasing the voltage on the amount of percentage of power generated will reduce as chopping action is approached. Using the criteria highlighted in Chapter 2, the percentage of power generated for the currents in Figure 6-2 is tabulated in Table 6-1. The difference between the percentages of power generated when the voltage is increased from 100V to 120V is only 0.1%.

However, the excitation and generated power increases by at least 20%. At the point when the current starts to chop, the power generated by the machine can be increased. Any further increase in the voltage will increase the chopping frequency hence reducing the generated power. Based on this, it is clear that there is an optimal operating voltage level at each speed range especially during the low speed operation.

Table 6-1: Calculation of the percentages of power based on the excitation and generation stage of current during one cycle of operation

Voltage	Excitation power (W)	Generation power (W)	% power generated
50V	20.4	32.5	61.4%
100V	88.8	136.8	60.6%
120V	111.1	170.5	60.5%

The factors that affect the selection of optimal voltage are the firing angles and speed. It was shown that at a certain value of firing angles and voltage level, the percentage of power generated is reduced due to the current chopping mode operation. Also at different speed range, there is an optimal voltage level which provides the highest percentage of generated power.

An in-depth study on the effect of changing the terminal voltage on the power generation for SRG has not been conducted. All this while, the voltage was kept constant by employing the voltage regulation approach [14, 121]. Since an external supply is required to provide the initial excitation for the SRG, the amount of the initial voltage to increase the generation performance of the machine has to be determined. Variations of the turn on angle, turn off angle, reference current and speed with the terminal voltage is performed under the low speed range as illustrated in Figure 6-3 and medium speed range as illustrated in Figure 6-5. The low speed operating range is between 25rad/s to 55rad/s whereas the medium speed operating range is between 100rad/s to 500rad/s.

6.3.2.1 Low Speed

When the terminal voltage is increased, the time for the current to rise is reduced and the time for it to return to zero after the turn off angle is faster due to the higher negative voltage, thus reducing the generated power. Figure 6-3(a) depicts the variation of the turn on angle made before and after alignment position with the terminal voltage. The turn on angle is held constant at 35^0. For the terminal voltage below 200V at the turn on angle made prior to the alignment position, there is not much change in the percentage of power generated. However, for the turn on angle made after the alignment position, the percentage of power generated drops. It does not allow enough time for the current to build up to store the excitation energy.

The dwell angle, which is the angle between the turn off and turn on angle reduces as the voltage level is increased while the turn off angle is held constant. This in turn reduces the percentage of power generated. The machine operates in current chopping mode since the duration for the current to reach the reference limit is reduced. A large

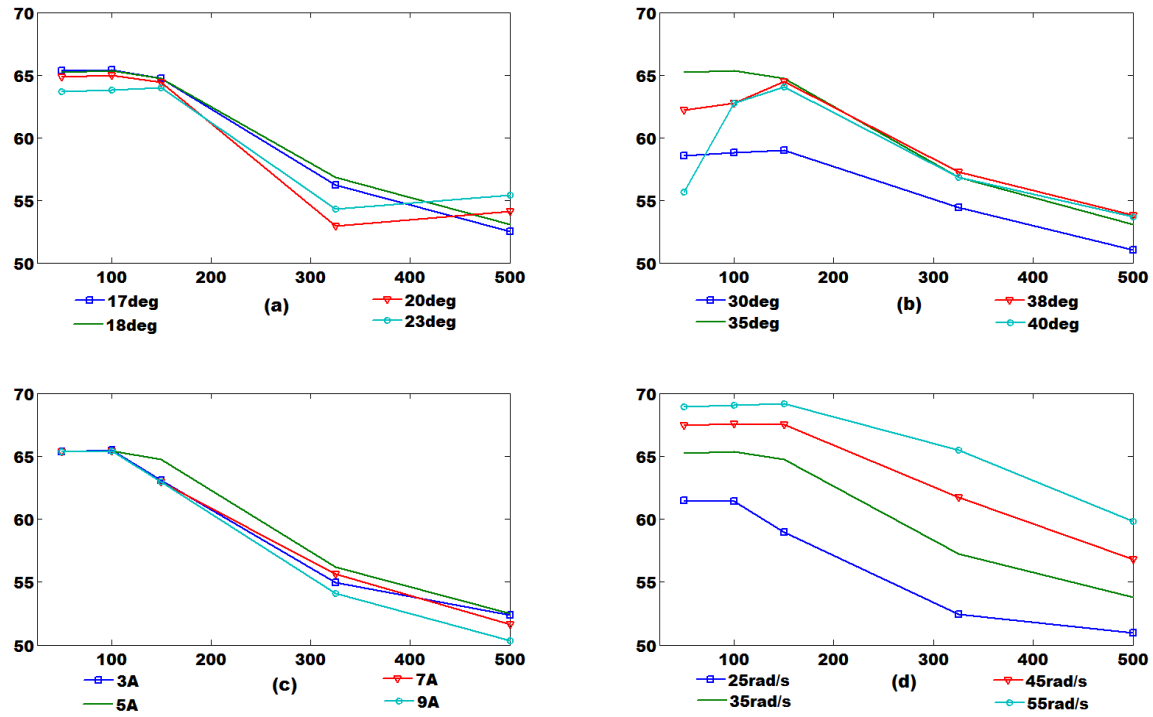

Figure 6-3: Graph of % power generated against terminal voltage (V) for the low speed range between 25rad/s to 55rad/s. Each graph shows the effect of terminal voltage with (a) turn on angle, (b) turn off angle, (c) reference current and (d) speed

turn off angle gives better percentage of power generated at turn on angle of 18^0 as in Figure 6-3(b).

However, the large turn off angle may also reduce the percentage of power generated as shown in Figure 6-4 at a voltage of 50V and turn off angle of 40^0. When the turn off angle is placed near to the minimum inductance region, the tailing current can either drop to zero or tail off into the next excitation phase, reducing the generating period of the conducting phase. In Figure 6-3(c), at a voltage of 100V and below, the percentages of generated power are similar at all the reference value. This shows that during single pulse mode, the reference value has no effect in increasing the current. And as the voltage is increased, the current has the energy to reach the reference limit thus, operating the machine in chopping mode. This is reflected by the difference in percentages as the voltage increases. The reference current is applicable under the current chopping mode operation, whilst during the single pulse mode operation; the phase current depends on the placement of firing angles along the inductance profile. The percentage of power generated reduces as the voltage level is increased for various speed ranges between 25rad/s to 55rad/s as in Figure 6-3(d). As the voltage level is increased, the percentage of power decreases. Hence, it can be said that there

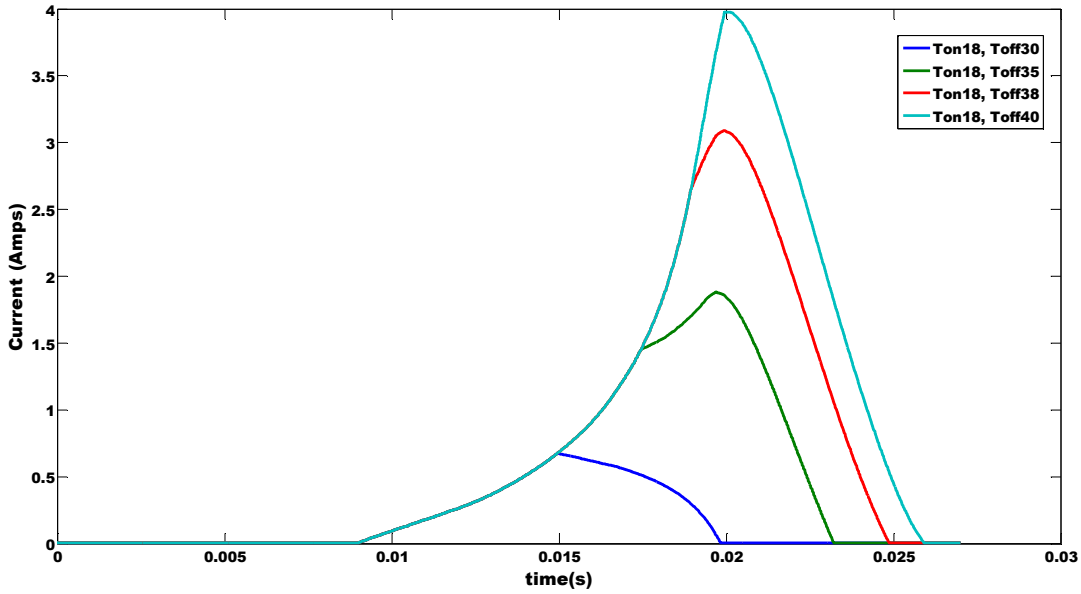

Figure 6-4: Current profile for different turn off angle while the turn on angle is constant at 18deg, at speed w=35rad/s and voltage 50V

exists an optimal voltage level which provides high performance given the right selection of variables. Also, the selection of voltage level for excitation will determine the shape of the current either in single pulse mode or current chopping.

6.3.2.2 Medium Speed

During the medium and high speed range, the machine operates in a single pulse mode when the back EMF is larger than the terminal voltage. After the turn off angle, the current will increase before it eventually decreases to zero depending on the value of the back EMF. The percentage of power generated is supposed to be high as speed increases. However, the performance also depends on the firing angles. If a fixed turn on and turn off angle is employed, the power being generated is less compared to when both the firing angles are varied. The reason being, at higher speed, the cycle period is reduced hence the time for the flux and current to rise shortens.

Table 6-2 and Table 6-3 above compares the generated power with a fixed firing angles and the ones obtained using the optimal operating angles. The percentages of power generated are higher when both the firing angles are varied.

Table 6-2: Operation of machine at fixed dwell angle

Turn on=14^0, Turn off=30^0, Dwell angle=16^0, Voltage=50V		
Speed (rad/s)	**Generated power @ 1 cycle operation (W)**	**% power generated**
100	7.03	66.6
200	3.79	68.5
300	2.61	69.2
400	2.66	72.9
500	2.82	72.5

Table 6-3: Operation of machine at optimal operating angles

Voltage=50V		
Speed (rad/s)	**Generated power @ 1 cycle operation (W)**	**% power generated**
100	16.39	73
200	9.4	75.2
300	6.49	76
400	4.96	76.4
500	4.01	76.7

The variation of the turn on and turn off angle at various levels of voltage taken at speed of 300rad/s does not show much difference in percentage of power generated as illustrated in Figure 6-5(a) and (b). However, to achieve a high percentage of power generated, the turn on angle must be placed along the midway of the increasing inductance profile, whilst the turn off angle just after the midway of the declining inductance and before reaching the minimum value. The effect of voltage at various speeds in the range of 100rad/s to 500rad/s is taken at turn on angle of 16^0 and turn off angle of 36^0 shown in Figure 6-5(c). Clearly, during the high speed range, the percentage of power generated remains constant even though the voltage level is varied.

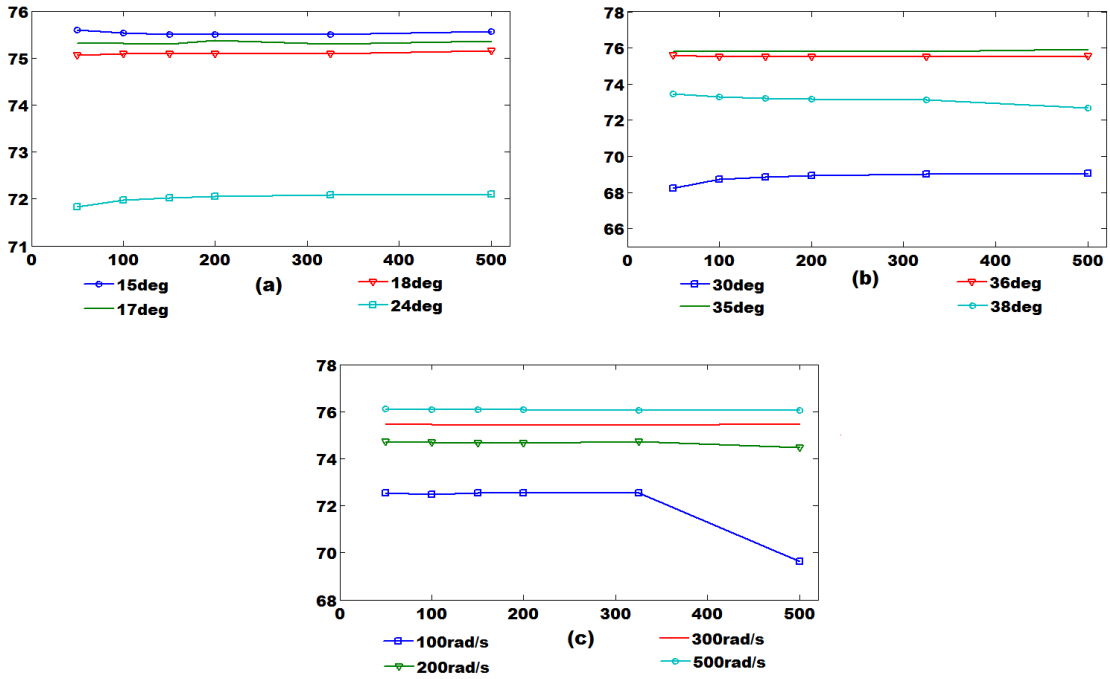

Figure 6-5: Graph of % power generated against terminal voltage (V) for high speed range between 100rad/s to 500rad/s. Each graph illustrates the effect of terminal voltage with (a) turn on angle, (b) turn off angle, and (c) speed

Comparing the low and medium speed operation, the effect of terminal voltage on the machine performance is more prominent at the lower speed range. The main reason is due to the back EMF being smaller than the terminal voltage, hence current is proportional to the voltage. When the back EMF is larger than the terminal voltage, the current no longer depends on the voltage. This is shown in Figure 6-5(c), where the percentages of generated power remains constant even though the voltage level in increased.

6.3.3 Effect of Speed

In this subsection, the effect of speed on the control variables is discussed. In theory, the higher the speed, the more energy can be captured. But not much research was conducted for the lower speed range. The current chopping control is normally employed during the low speed range. For the generating operation, the current will not increase immediately as in the motoring mode since the excitation is performed during the maximum inductance profile. As shown earlier, the current chopping mode is achieved when a high voltage level is employed. However, the high voltage level will reduce the percentage of power generated. Therefore, to maintain the high

percentage of power generated, single pulse mode operation is proposed during the low speed range as opposed to the conventional current chopping mode.

6.3.4 Effect of Firing Angle

There is a large number of papers published describing the roles of the firing angles on the generated power [148]. During the low speed operation, the initial rise of current is slow due to the high inductance value. One of the ways to aid in the fast increase of phase current is to advance the turn on angle into the decreasing inductance profile. However, when the turn on angle is placed further along the decreasing inductance profile, the dwell angle reduces. Also, the turn off angle has to be located near or along the minimum inductance region, thus reducing the generated power. The only energy being returned is the stored energy. During this time, energy will not be extracted from the prime mover due to zero torque. This section will analyse the effect of the turn on angle and turn off angle with other variables for the speed range 25rad/s to 500rad/s.

6.3.4.1 Turn on Angle

The following can be observed for variation of the turn on angle with turn off angle in Figure 6-6(a) when the SRG is subjected to a voltage level of 325V at a low speed of 35rad/s and in Figure 6-7(a) at a medium speed of 300rad/s. At a lower speed, the percentage of power generated increases as the turn on angle is placed in the decreasing inductance profile, whereas during the medium and high speed, a high percentage of power generated is obtained when the turn on angle is along the positive inductance region. Correspondingly, the optimal turn off angle for both the speed is between 30^0 to 40^0. Care must be taken to ensure that a continuous overlapping current profile is maintained to provide adequate overlap between the current with its adjacent phase. Larger turn off angle will reduce the overlap due to the longer conduction period and current being forced to return to zero at the minimum inductance region.

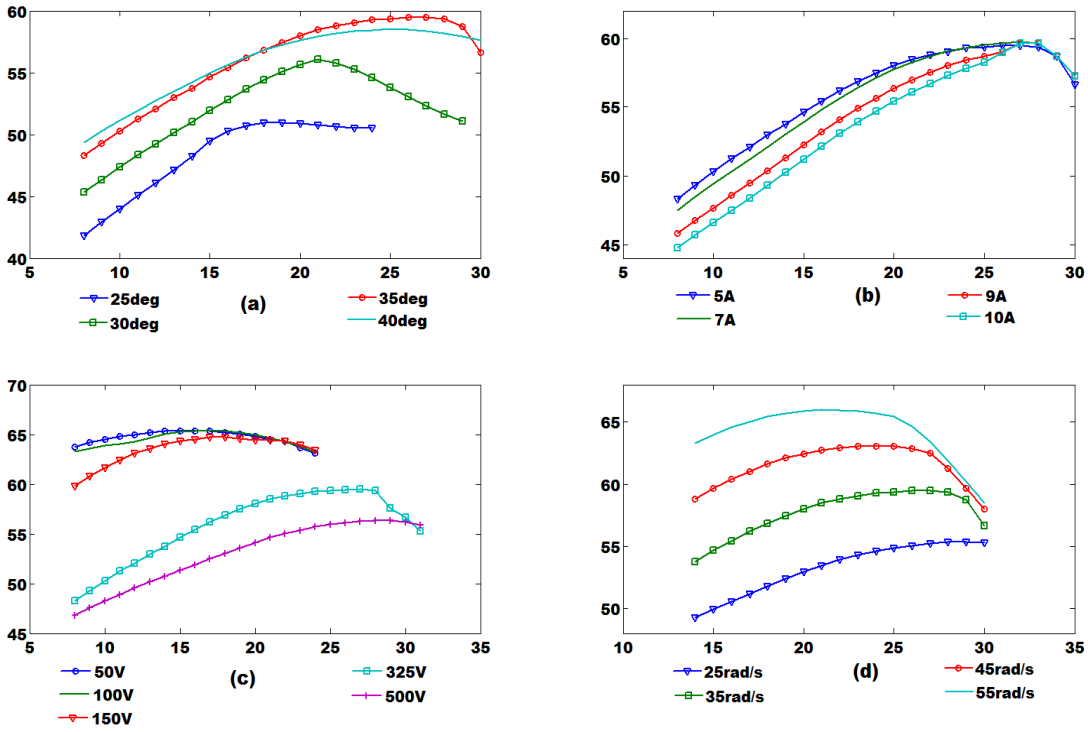

Figure 6-6: Graph of % power generated against turn on angle (degree) for low speed range between 25rad/s to 55rad/s. Each graph shows the effect of turn on angle with (a) turn off angle, (b) reference current, (c) voltage and (d) speed

Figure 6-6 (b) shows the variation of turn on angle with various reference currents. Although the percentage of power increases as the turn on angle is increased, the current profile may become discontinuous and does not overlap with the current in the adjacent phase. The reason is due to the reduced dwell angle as the turn on angle is varied while the turn off angle is fixed. The variation of the turn on angle with terminal voltage for the low and medium speed range is depicted in Figure 6-6(c) and Figure 6-7(b). The percentage of power generated does not show significant changes as the terminal voltage is varied at the higher speed range. However, for the lower speed range, the percentage of generated power decreases as the voltage is increased. The turn on angle is made prior to the alignment position for voltage level between 50V to 150V, whereas at higher voltage level, the turn on angle is made after the alignment position to achieve a high percentage of power generated. As mentioned earlier, the continuous or overlapping current profile must be maintained. At a higher speed range, the percentage of power generated decreases when the turn on angle is near the alignment position because the time for the current to rise and store the magnetic energy is reduced.

The variation of the turn on angle with speed is given in Figure 6-6(d) and Figure 6-7(c). It shows that there exists an optimal value of turn on angle at each speed range. The graph tends to converge to one value due to the constant turn off angle used. As the turn on angle moves along the decreasing inductance profile, the dwell angle reduces, therefore the percentage of power generated decreases. We can conclude that the optimal turn on angle for the low speed range is prior to or just after the alignment position whereas for the medium speed, the turn on angle has to be placed midway during the inductance profile, which is during the motoring region. The implication of having the turn on angle in the motoring region is the development of positive torque which may reduce the generating operation

6.3.4.2 Turn off Angle

Similar to the analysis on the implication of the turn on angle on various control variables, the variation of the turn off angle can also be categorized by the low and medium speed operation as depicted in Figure 6-8 and Figure 6-9. At lower speed, the variation of the turn off angle is shown in Figure 6-8(a). Even though the turn on angle is changed, the variation of the optimal turn off angle is minimal. Alternatively,

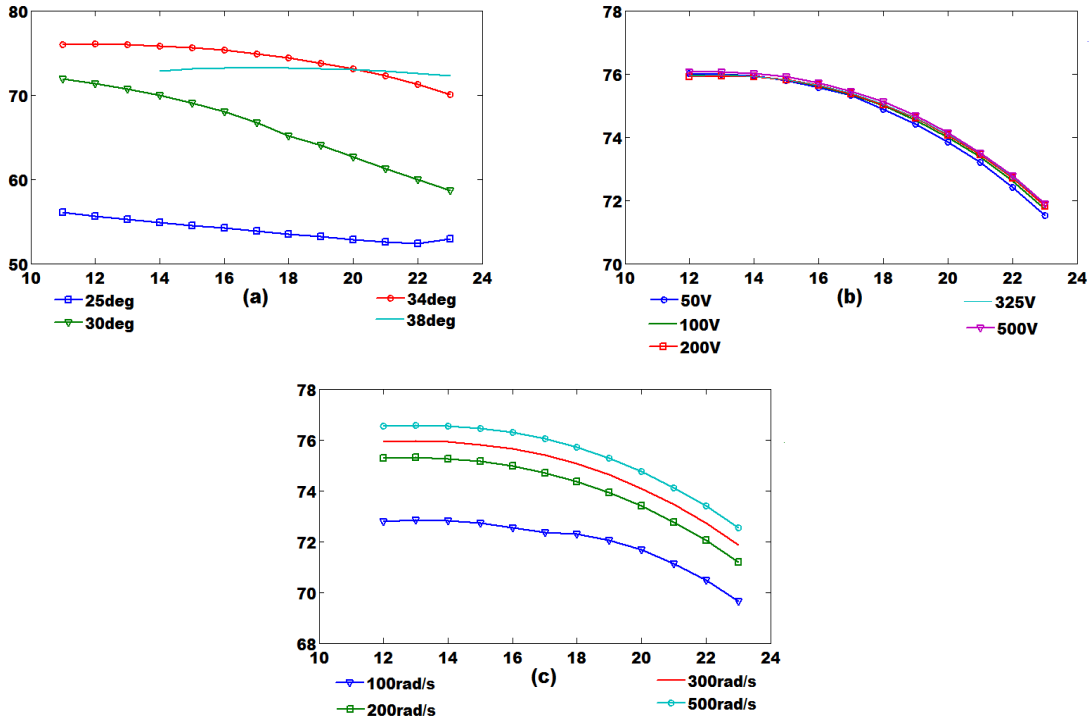

Figure 6-7: Graph of % power generated against turn on angle (degree) for medium speed range between 100rad/s to 500rad/s. Each graph illustrates the effect of turn on angle with (a) turn off angle, (b) terminal voltage, and (c) speed

during the medium speed, the optimal turn off angle shows a slight variation according to the placement of turn on angle. The placement of the turn on angle along the inductance slope for both speeds differs; after alignment position for low speed and before alignment position for medium speed. Figure 6-8(b) shows the effect of reference current at various turn off angles during the low speed operation at a voltage level of 325V and a turn on angle of 18^0. The optimal value of turn off angle differs for each reference current level because of the current chopping mode operation. During the chopping mode, the current is regulated to follow the path on the energy conversion loop. The highest power generated occurs at reference current of 5A. On the contrary, the reference current has no effect during the medium speed operation as depicted in Figure 6-9(b). When the SRG is subjected to different levels of terminal voltage as in Figure 6-8(c) and Figure 6-9(c), the optimal turn off angle at both the low and medium speed operation has similar range of values. The percentage of power generated during the medium speed does not change when the terminal voltage level is varied as compared to the lower speed range. Likewise, minimal change in percentage of power generated is seen during the medium speed range as depicted in Figure 6-9(d). On the whole, it can be observed that although various variables have

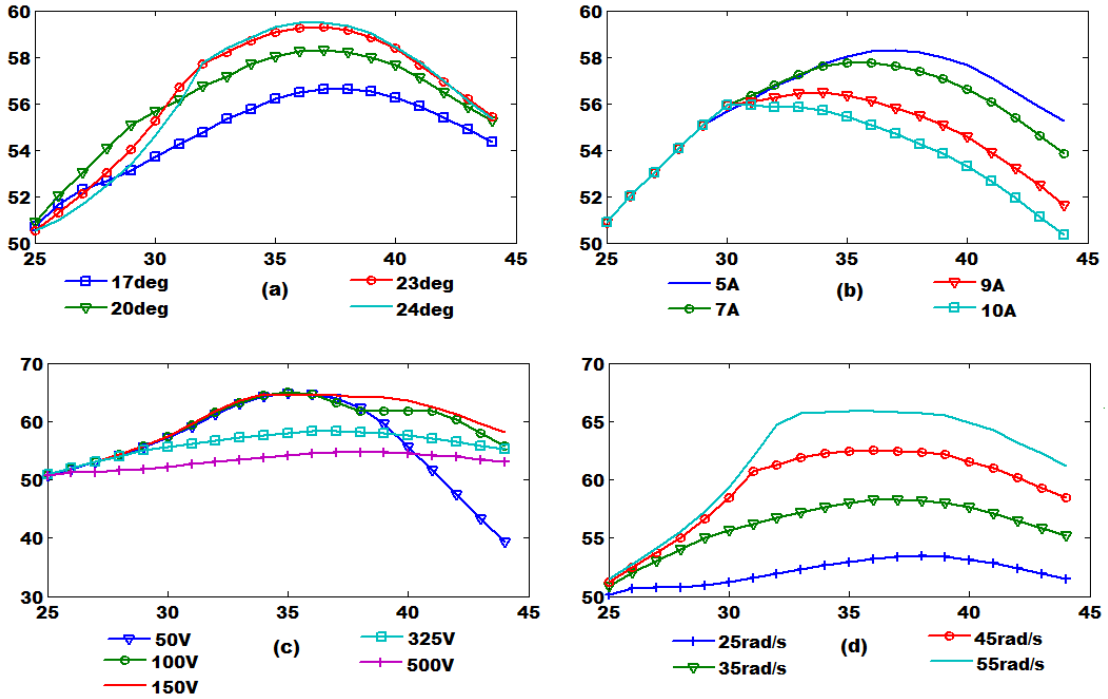

Figure 6-8: Graph of % power generated against turn off angle (degree) for the low speed range between 25rad/s to 55rad/s. Each graph shows the effect of turn off angle with (a) turn on angle, (b) reference current, (c) terminal voltage and (d) speed

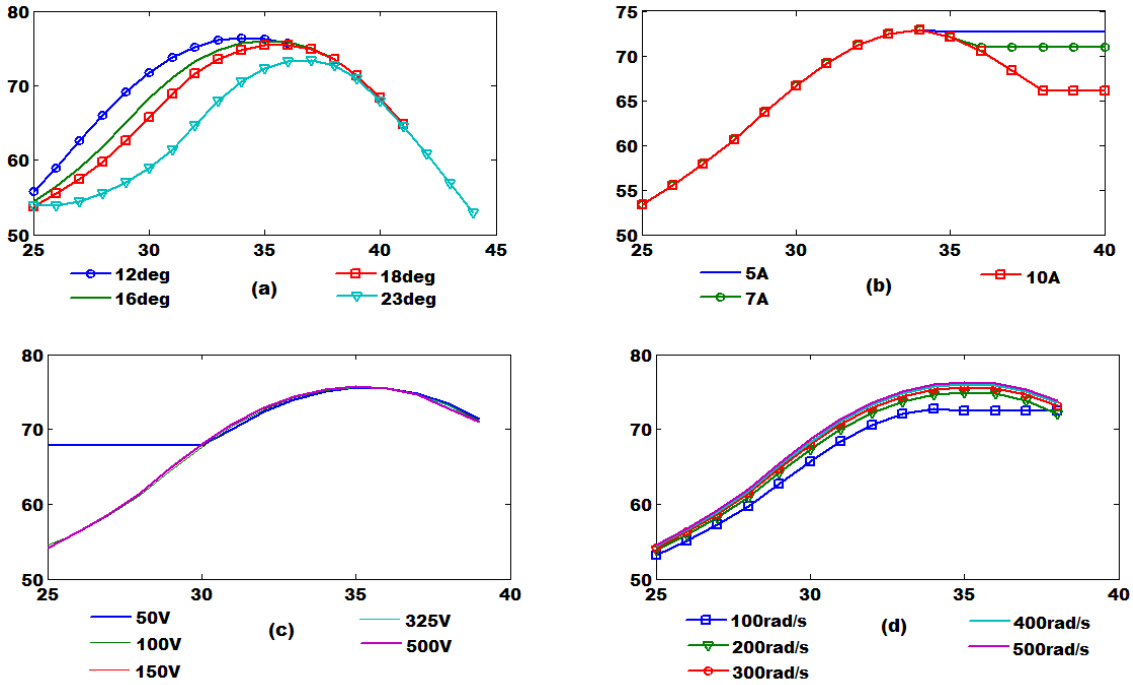

Figure 6-9:Graph of % power generated against turn off angle(degree) for the medium speed range between 100rad/s to 500rad/s. Each graph shows the effect of turn off angle with (a) turn on angle, (b) reference current, (c) terminal voltage and (d) speed

been changed, the optimal value of turn off angle remains in the same range. It can be said that turn off angle does not have considerable effects on maximizing the generated power during the low and medium speed range under the generating operation.

6.4 Conclusions

The purpose of this chapter was to investigate the variables affecting the performance of the machine. The variation of the control variables for a three phase 12/8 machine in terms of percentage of power generated has been discussed during both the low and medium speed range. Similar outcomes are obtained from the other machines but with different values of firing angles. In this context, the low and medium speed range has been defined to be in the range of 25rad/s to 100rad/s whereas the medium speed range is between 100rad/s to 500rad/s. The impact of the percentage of power generated is observed for the following variables:

- Reference current
- Terminal voltage
- Firing angles – turn on and turn off angle
- Speed

The observations are categorized according to the low and medium speed range.

6.4.1 Low speed

Since the excitation is made along the increasing inductance profile, the current chopping mode is achieved when a high voltage is employed. However, the percentage of the generated power obtained during the current chopping mode is less than 60%. Although the amount of power generated is higher, the losses due to chopping are also high. Therefore, it was suggested to employ the single pulse mode operation during the low speed range as opposed to the current chopping mode. As long as the back EMF is maintained lower than the terminal voltage, the phase current can be controlled. Thus the control variables during the low speed range are the voltage level and firing angles.

6.4.2 Medium Speed

During the medium speed operation, the most influential control variables which affect the percentage of power generated are the firing angles. The terminal voltage and speed does not have much impact on the generated power as compared to the lower speed range. This is because the back EMF dominates at higher speed hence the shape of current depends on the location of the firing angles on the inductance profile. Also at higher speed, the time required to build the magnetic flux reduces, therefore the placement of the turn on angle has to be made in the motoring region to enable the current and flux to rise. However, if the turn on angle is placed too low in the motoring region; this will result in positive torque. Also, it may store enough energy for the generating current to tail off into the next excitation phase, resulting in current not returning to zero, a condition which only occurs during the medium and high speed range. Therefore, we can categorize the medium and high speed operation into two categories:

- Zero returning current cycle or non-continuous conduction mode
- Non-zero returning current cycle or continuous conduction mode

The continuous conduction mode has been studied under the motoring operation [148], however no research details the implication of the method during the generating operation. Therefore, the following chapter analyzes the continuous

conduction mode during the generating operation and summarizes the findings of Chapter 6.

CHAPTER 7

DISCUSSIONS OF RESULTS

This chapter summarizes the findings of the research in Chapter 6 and highlight the limitations in determining the optimal control variables. It will be presented in two parts: low and medium speed range. An in depth analysis has been made based on the phase voltage equation. The results of this study indicate that the generated power strongly depends on the placement of the firing angles along the inductance profile. The findings seem to be consistent with other researches which focus on optimizing the firing angles as the control variable. However, the research is limited to high speed operation [42-44]. Only [46] have reported on optimizing the firing angles during current controlled operation. The value of current is regulated to the desired value according to the load requirement. Nevertheless, it did not evaluate the impact of other variables such as reference current and voltage to generate power at various speed ranges. Also, the limitations and issues regarding the selection of the optimal control variables have not been treated in much detail. Based on the studies presented in Chapter 6, the current chopping mode reduces the percentages of power generated; hence it is found not to be suitable for the generating operation. Therefore, the single pulse mode is proposed during the low speed range as opposed to the current chopping mode. The procedures to determine the optimal control variables are conducted the same way as for the medium and high speed operation.

As mentioned in Chapter 6, it is difficult to find relations of the generated power with the control variables due to the non-linear behaviour of the machine. Therefore, a heuristic method is applied to each control variables. The range of the voltage selected for this study varies from 50V to 500V. Each of the voltages is subjected to the low speed ranging from 25rad/s to 100rad/s and medium speed ranging from 100rad/s to 500rad/s. Within each voltage and speed range, the turn on angle is made to cover the position before and after the alignment of poles, whereas the turn off angle covers the decreasing inductance slope in 1^0 increments.

The optimal control variables are determined in terms of the highest percentage of power generated for each machine under study. A polynomial relating the optimal control variables for each machine is proposed. The related applications of the machine are proposed based on the performance of the machine.

7.1 Limitations and Effects of Control Variables on the Generated Power

There are several factors that must be considered during the selection of the optimal control variables such as the position of the firing angles on the inductance profile and voltage level. A small dwell angle will produce a discontinuous operation of the machine because the current does not overlap with the current in the adjacent phase. Also, if the dwell angle is too large, the generating current may not return to zero and coincide with the excitation current of the adjacent phase. The selection of the voltage level is employed to avoid the current chopping mode during the low speed operation. The following sections describe the conditions in detail.

7.1.1 Overlapping and Non-Overlapping of Phase Current

In this context, the overlapping refers to the overlap between the current of adjacent phases. Since the current in the winding starts and returns to zero during each current

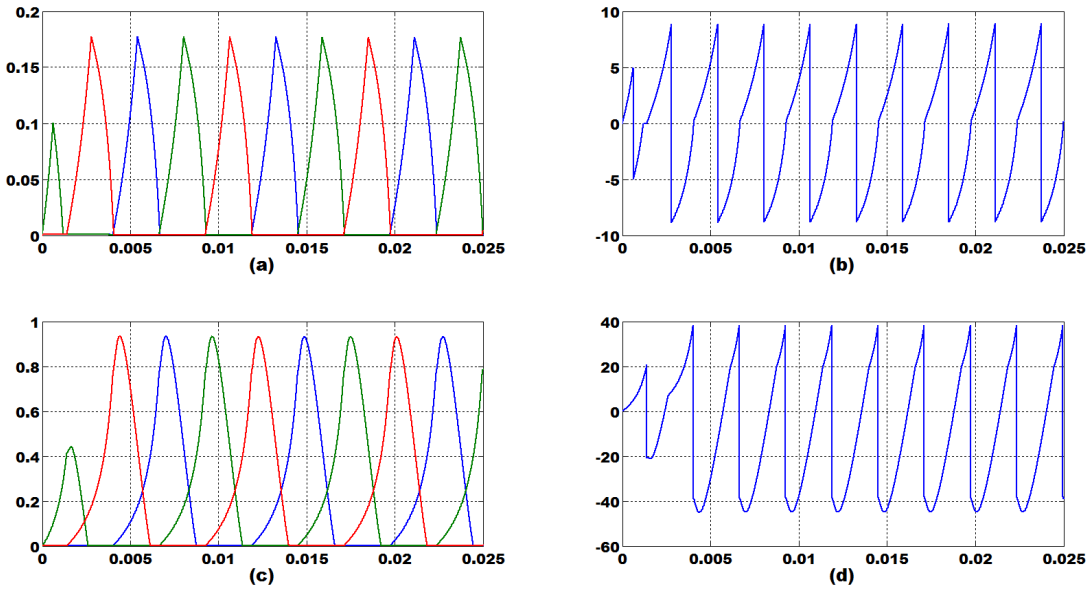

Figure 7-1: Graph of phase current (A) and current profile (A) against time (s) for (a) non-overlap of phase current (b) non-overlap phase current profile (c) overlap of phase current and (d) overlapping phase current profile

cycle, a smooth operation of the machine is achieved by adequate overlap between the phase currents as depicted in Figure 7-1 (c) and (d). The non-overlapping condition may occur if the dwell angle is small and the voltage level is high as illustrated in Figure 7-1 (a) and (b). The optimal firing angles selected in terms of the highest percentage of the power generated has good balance between the phase current profile and the total amount of the generated power.

7.1.2 Continuous and Non-Continuous Current Profile

The continuous conduction of current can only be achieved during the medium and high speed operation by increasing the dwell angle slightly greater than half of the rotor pole pitch. Since the commutation is prolonged, the generating current of the outgoing phase is directly connected to the excitation stage of the incoming phase. This action results in an offset of current, thus increasing the peak value of current. A slight change in the turn off angle produces significant change in the phase current. The transition from the non-continuous to the continuous conduction mode is illustrated in Figure 7-2. The continuous conduction is achieved by moving the turn off angle just 1^0 from the optimal value. It shows that the continuous conduction mode

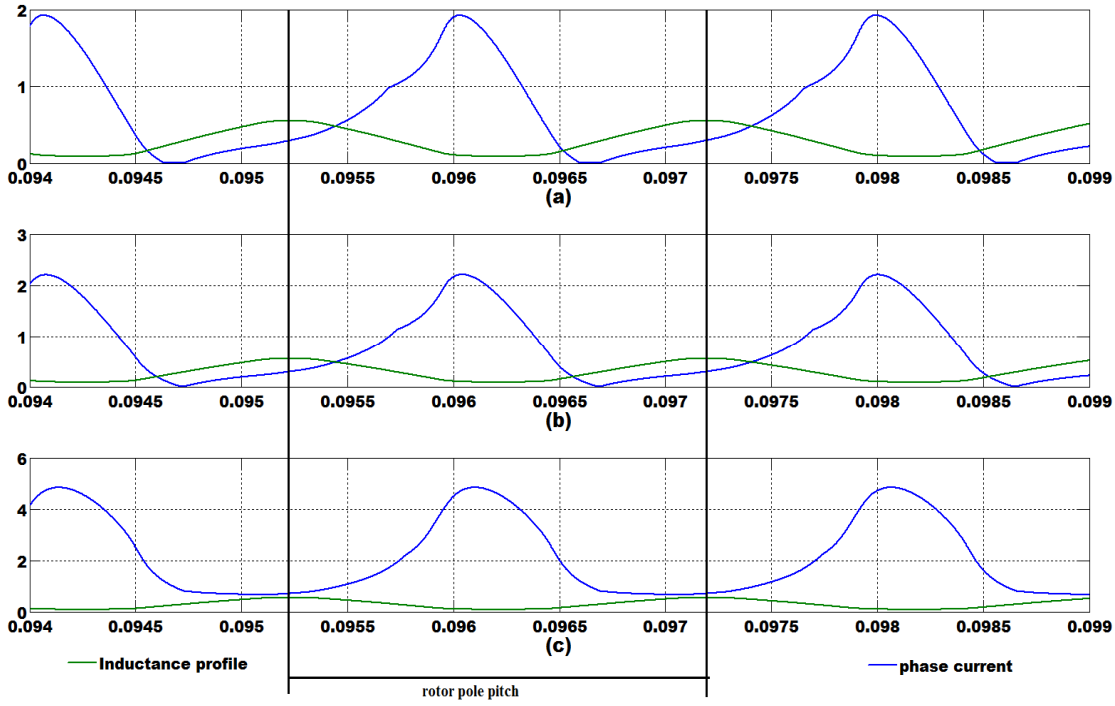

Figure 7-2: Graph of phase current (A) against time (s). The transition of phase current by changing the turn off angle in 1^0 increment (a) turn off angle 33^0 (b) turn off angle 34^0 and (c) turn off angle 35^0 at 325V and 400rad/s

is sensitive to the change of turn off angle. Since a higher current is obtained, the approach can be applied to applications which require continuous constant power and high torque, for example heavy vehicles. To enable the continuous conduction mode under generating operation, the placement of the turn on angle has to be made according to the following positions:

- in the motoring region to provide an adequate energy for the generating stage to tail off into the next excitation stage.
- near the minimum inductance region, just before the start of overlapping between the stator and rotor pole

Both of the above conditions extend the dwell angle more than half of the rotor pole pitch angle. The result of extending the dwell angle causes the steady state current to increase more than the limit of the reference current. This in turn will increase the copper losses of the winding. Although the continuous conduction mode increases the amount of the generated power, the excitation power is also increased due to the longer excitation time.

The implication of extending the conduction period is more beneficial to the motoring operation because the positive torque region is well utilized, covering half of the inductance profile. In contrast to the generating operation, the dwell period that is required to initiate the continuous conduction mode has to cover both the motoring and generating regions. This reduces the generating period due to the generating current tailing off into the excitation stage of the next phase instead of returning to zero. Figure 7-3 shows the comparison of peak current and generated power between the continuous conduction and non-continuous conduction mode. The generated power drops as speed increases during the non-continuous conduction mode. This is due to the rapid increase of back EMF, to a point it is more than the terminal voltage. As a consequence, the time for the flux to increase reduces, thus the phase current is naturally limited [148, 150]. On the other hand, the continuous conduction mode provides a higher constant current throughout the operating speed range.

The factors such as the current regulator [151], voltage level and the duration of dwell angle causes the steady state phase current to increase within the continuous conduction mode. Because of the increase in phase current, the optimal values of

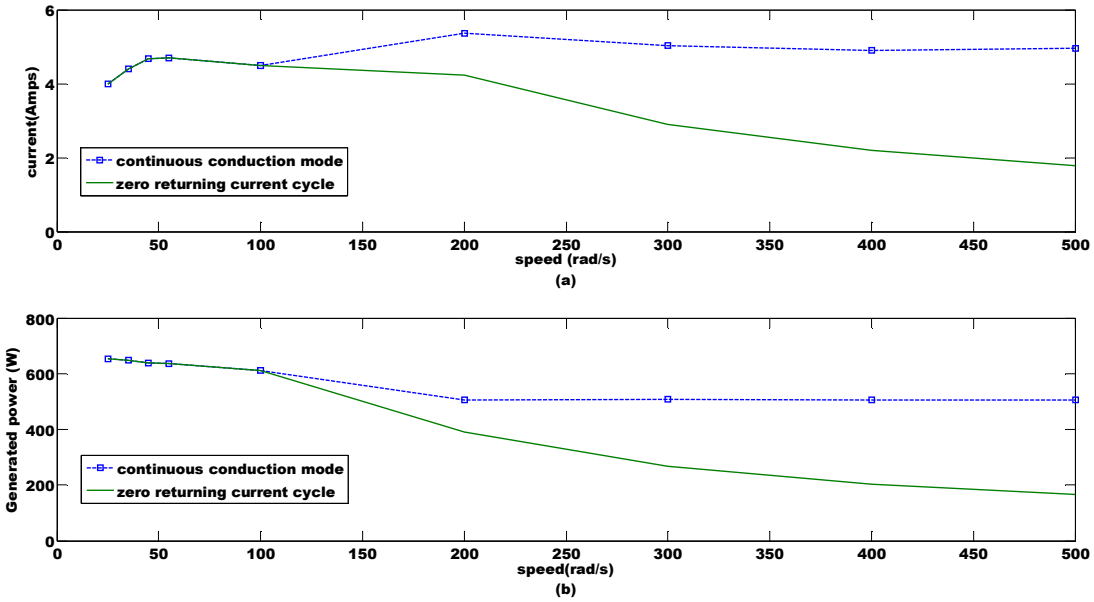

Figure 7-3: The graph of current (a) and generated power (b) versus speed to compare the performance of continuous conduction mode and the conventional non-continuous conduction mode current cycle

firing angles during the continuous conduction mode has to be selected for currents below 5A. This result in a constant amount of power generated over the operating speed range as depicted in Figure 7-3(b). By placing a limit on the peak current, the continuous conduction approach has similar behavior to the current chopping mode where the power is held at constant value by following a set of reference value [151]. Even though the loss in excitation energy is high due to the long conduction period, the overall power being generated increases. This continuous conduction mode is suitable for operations which require a constant power at high speed range. One major drawback of this approach which has been overlooked, is the high ripple produced on the DC link current profile as depicted in Figure 7-4. Although the generated current is increased, the current profile is not smooth.

Overall, it can be concluded that the method is suitable for both the motoring and generating operation as it can continuously hold the power constant over a wide speed range. It can be used in applications which require a constant generation of power, (i.e. the grid connection). Instead of the conventional maximum power point tracking (MPPT) method which operates the machine according to the optimal peak power at each speed range, the continuous conduction mode can be used as an alternative method. It does not require any changes in the control method since the dwell angle can be controlled. However, the peak value of phase current must be limited.

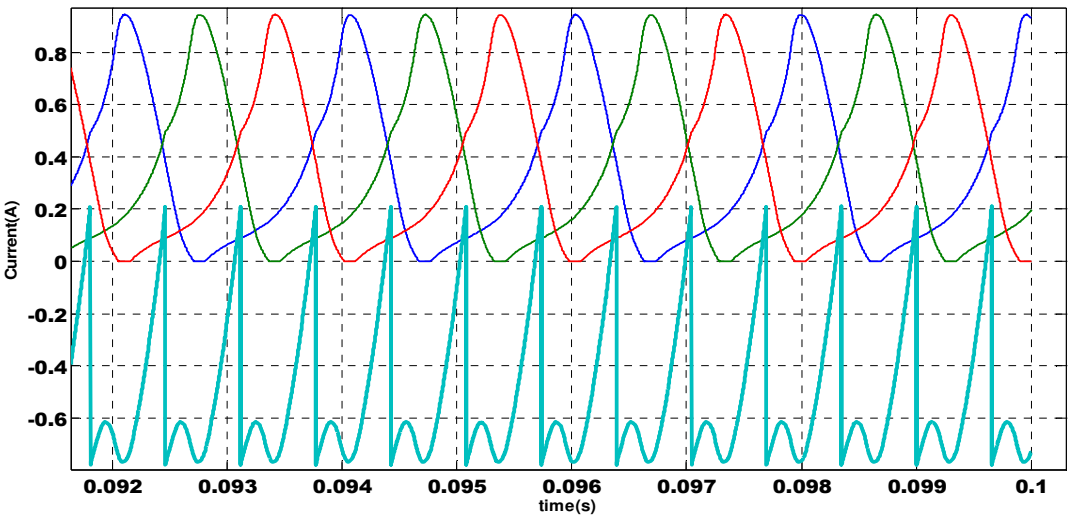

(a)

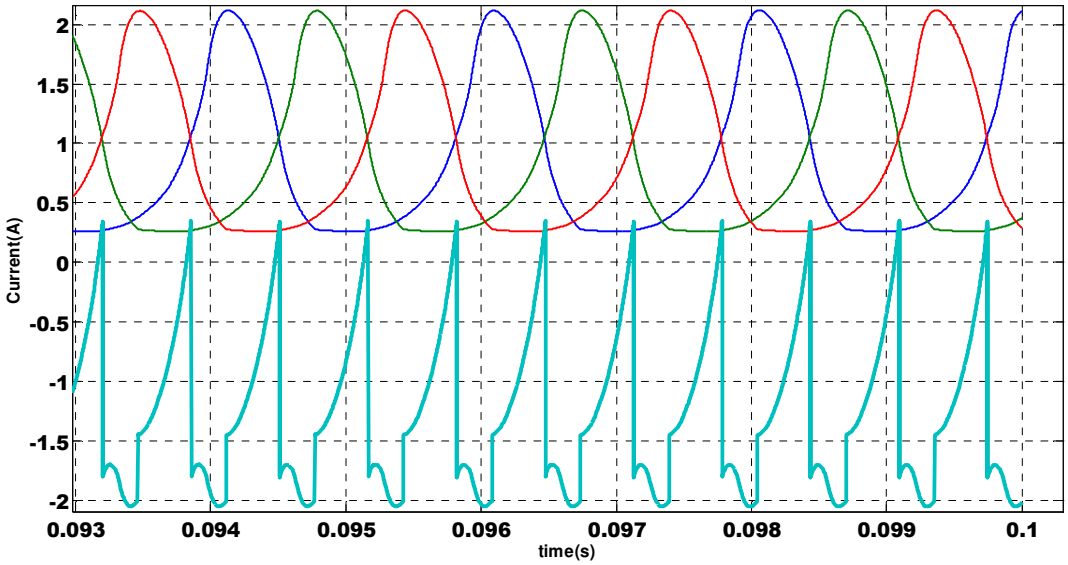

(b)

Figure 7-4: Comparison between (a) non-continuous current profile and (b) continuous current profile taken at speed 400rad/s, voltage level 100V, turn off angle34deg and turn off angle 36deg

Comparison of the percentages of power generated between the two approaches; non-continuous conduction and continuous conduction mode in Figure 7-5 shows a slight difference in percentage of power generated. Although the percentages are higher in the non-continuous conduction mode, the amount of the generated power is lower as compared to the continuous conduction mode. Also, the overall current profile for the continuous conduction mode contains more noise due to the overlap of all the three phase currents.

Generally, it can be summarized that during the generating operation, the continuous conduction approach increases the amount of generated energy without compromising

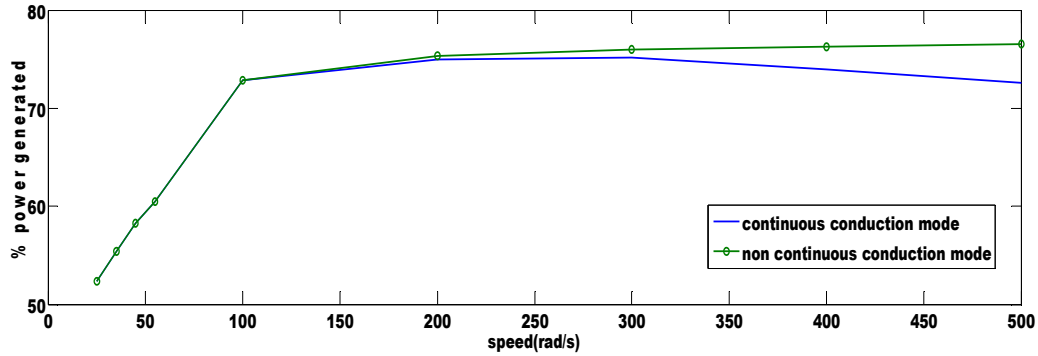

Figure 7-5: Graph showing comparison of performance between the continuous conduction mode and non-continuous conduction mode in terms of percentage of power generated versus speed at V=325

on the percentages of generated power. However, the increase in the amount of generated power has to be compromised with the increase in both the copper and iron losses. Also, another disadvantage of employing the continuous conduction mode is the requirement to limit the peak phase current as it will increase with speed and dwell angle. Once the optimal control variables at each speed and voltage level have been obtained and its limitations have been identified, the function relating the optimal variables with the percentage of power generated can be developed.

7.2 Development of Function Relating the Optimal Parameters

In Chapter 6, the optimal control variables for a three phase 12/8 machine have been identified based on the heuristic method. The method covers the low and medium speed range at various voltage levels whereas the turn on angle covering both the position before and after alignment position and turn off angle covering the angles in the negative inductance slope in increments of 1^0. The findings are similar for all the machines whereby during the low speed range, the use of a high voltage level will cause the percentage of generated power to reduce. In addition, during the medium speed range, the change in the voltage level does not affect the percentage of generated power as depicted in Figure 7-6.

Based on the observation, the machine with lower number of rotor poles gives the highest percentages of generated power. This is associated with the rotor angle, inductance profile and magnetization curve of that machine being larger than the machines with a higher number of rotor poles. The drawback of having a low number

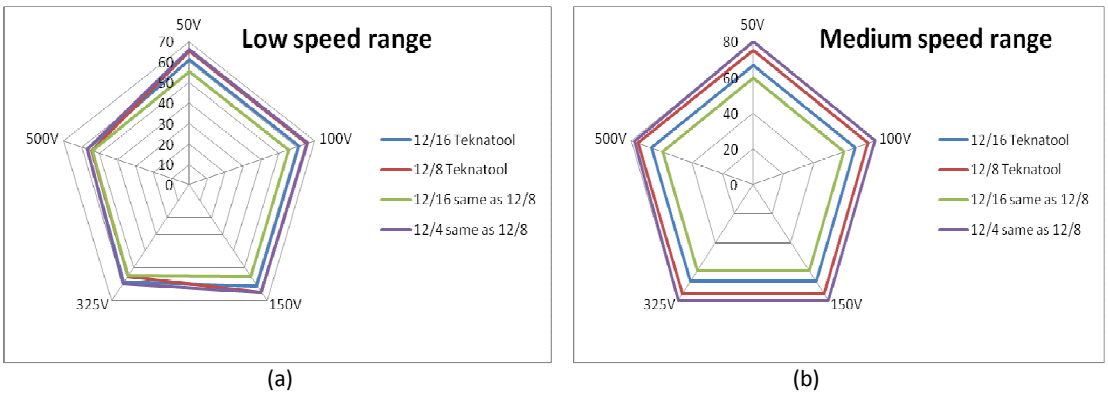

(a) (b)

Figure 7-6: Simulation result of the graph of percentage of power generated against voltage for all the machines at (a) low speed range at 35rad/s and (b) medium/high speed range at 200rad/s

of rotor poles is the high current and torque ripple. Thus, it may not be suitable for motoring application but suitable to generate energy such as for wind energy applications.

During the low speed operation, the shape of the phase current as well as the power generation is affected by the terminal voltage and the firing angles, whereas at a medium and higher speed operation only the firing angles affects the power generation. The common variables between the two speed ranges is the firing angles as illustrated in Figure 7-7. Therefore, the percentage of power generated $\%P_{gen}$ can be characterized as a function of firing angle, θ and speed, ω at different voltage level as shown by the following equation:

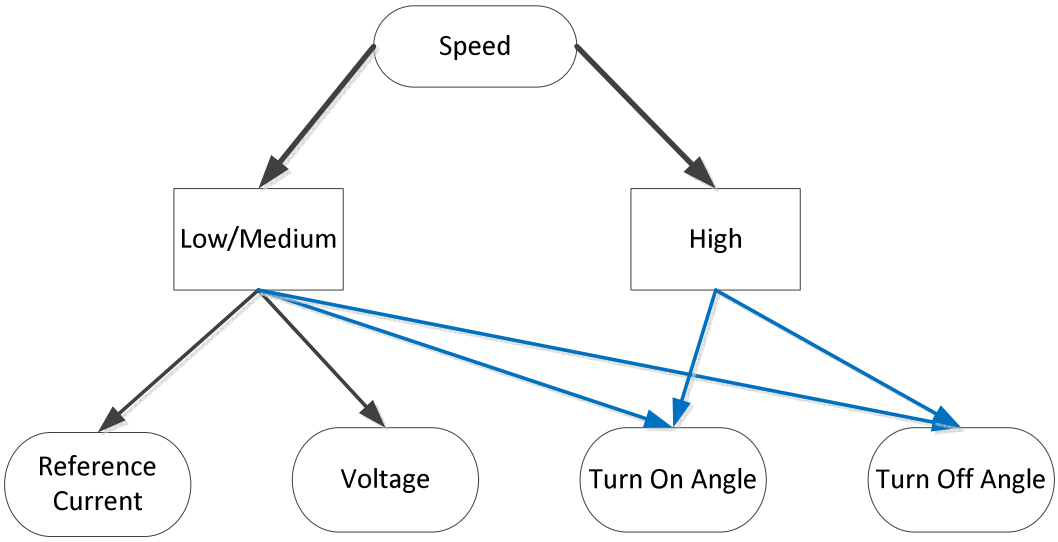

Figure 7-7: Illustration of the control variables affecting the generated power for both the low and high speed operation

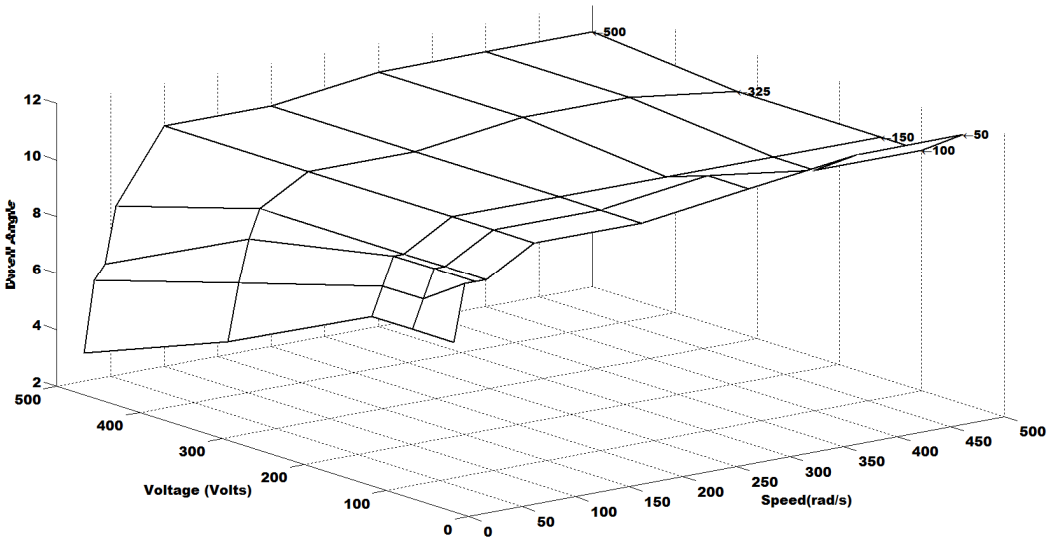

Figure 7-8: Graph of dwell angle versus speed and voltage for a three phase 12/16 machine having the same stator structure as the 12/8 machine

$$\%P_{gen}\Big|_{V=cons} = f(\theta, \omega) \tag{6.7}$$

Given that the voltage level does not affect the percentage of the power generated during the medium speed range, the selection of voltage can be made in terms of the amount of generated power.

Also, since the change in the optimal turn off angle during the low and medium speed is small and falls within the same optimal range, it can be made constant. Subsequently, the optimal dwell angle θ_d can be determined according to the difference between the turn off angle θ_{off} and turn on angle θ_{on} as shown below:

$$\theta_d = \theta_{off} - \theta_{on} \tag{6.8}$$

As a result, a controller model of dwell angle can be defined as a function of speed. The regression method is used to determine the relation between the optimal control variables. The following figures illustrate the optimal dwell angle versus speed for the four machines under study. Figure 7-9, Figure 7-8, Figure 7-10 and Figure 7-11 show the graph of dwell angle versus speed at each voltage level between 50V to 500V.

All the graphs confirm the similar results obtained during the medium speed range, where the dwell angle is almost constant. The change of dwell angle is more prominent at the lower speed range. The reason being, at the medium and higher

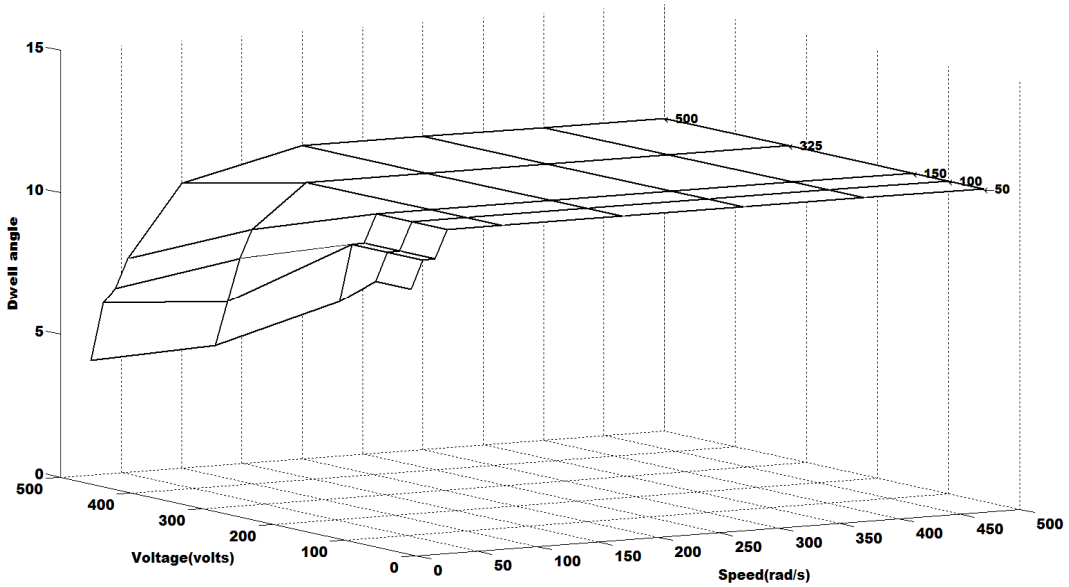

Figure 7-9: Graph of dwell angle versus speed and voltage for a three phase 12/16 machine

speed range the voltage level does not have an effect on the percentages of generated power and phase current due to the back EMF. At lower speed, the shape of phase current depends on the speed and voltage level. For this reason, the voltage is used to characterize the optimal variables during various speed ranges. At lower speed, the voltage is characterized to maximize the percentage of generated power by operating the machine in single pulse mode. Meanwhile, the voltage at medium speed is used to categorize the performance in terms of the amount of power generated or torque ripple or noise ratio. Table 7-1 categorizes the voltage according to the lower speed range

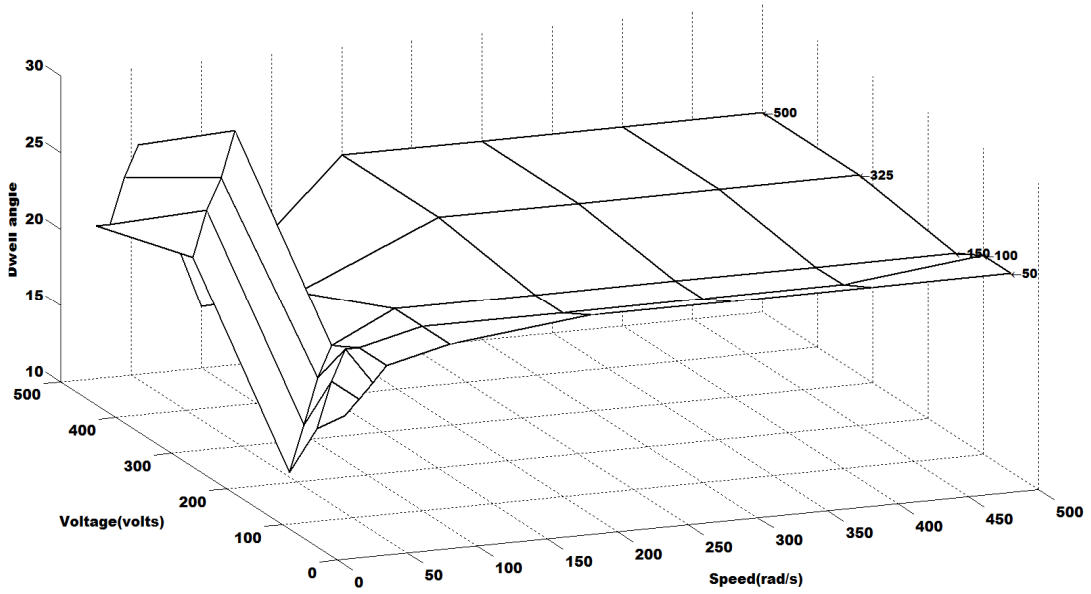

Figure 7-10: Graph of dwell angle versus speed and voltage for the existing three phase 12/8 machine

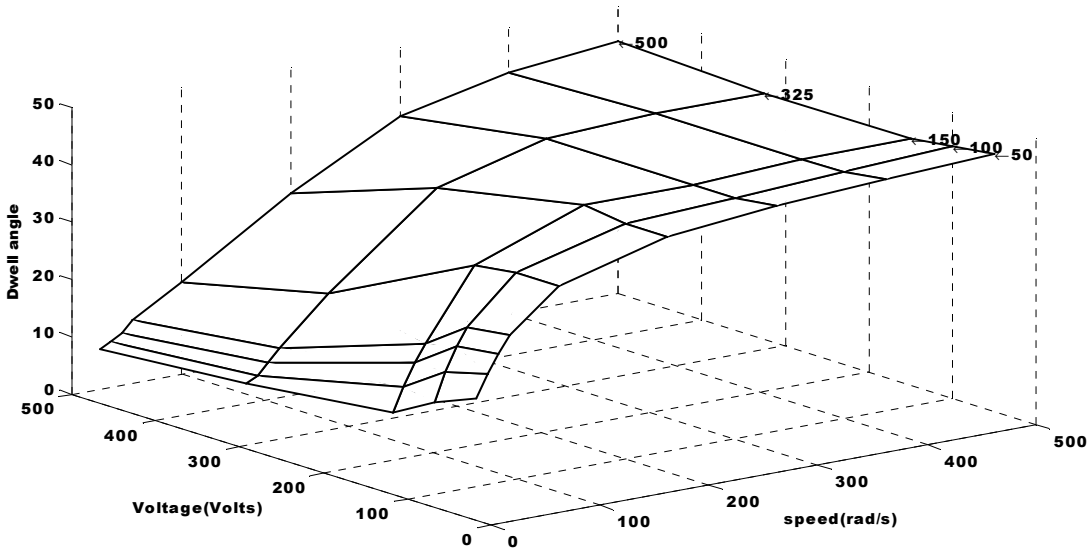

Figure 7-11: Graph of dwell angle versus speed and voltage for a three phase 12/4 machine having the same structure as the 12/8 machine

for each of the machine whereas Table 7-2 compiles the characterization of voltage level in the medium speed range according to the current profile as illustrated in Appendix F.

Once the voltage has been characterized, the related function can be developed according to the speed range. Figure 7-12 depicts the percentages of power generated versus voltage level for all the four machines operating at their optimal angles for two speed ranges.

It is observed that the change in the voltage level for all the machine under study is prominent during the low speed range as compared to the medium speed where the percentages of power generated is almost constant as the voltage level is increased.

Table 7-1: Characterization of voltage at low speed range between 25rad/s to 100rad/s

Machine	Speed range	Voltage level
Machine 1: 12/8	w<=35rad/s	100V
	35rad/s<w<100rad/s	150V
Machine 2: 12/16	w<=35rad/s	100V
	35rad/s<w<100rad/s	150V
Machine 3: 12/16 same stator structure with 12/8	w<=25rad/s	100V
	25rad/s<w<100rad/s	150V
Machine 4: 12/4 same stator structure with 12/8	w<=45rad/s	100V
	45rad/s<w<100rad/s	150V

Table 7-2: Characterization of voltage level in the speed range between 100rad/s to 500rad/s

Speed, w (rad/s)	Voltage level
100rad/s≤ w ≤ 500rad/s Low noise and low generated power	200V
100rad/s≤ w ≤ 500rad/s Low noise with moderate amount of generated power	325V
100rad/s≤ w ≤ 500rad/s High generated power at the expense of higher noise level	500V

Nevertheless, the total amount of power being generated and the torque profile differs. Compared to the lower speed, the amount of power generated during the medium speed is higher due to the frequent number of excitation. One cycle of current at 45rad/s is equivalent to 10 current cycles at 400rad/s under the same excitation voltage level as illustrated in Figure 7-13. Since the change in the optimal turn off angle is minimal for all speed range, it is made constant. Thus, the firing angles can be represented in terms of dwell angle at each speed range and voltage level.

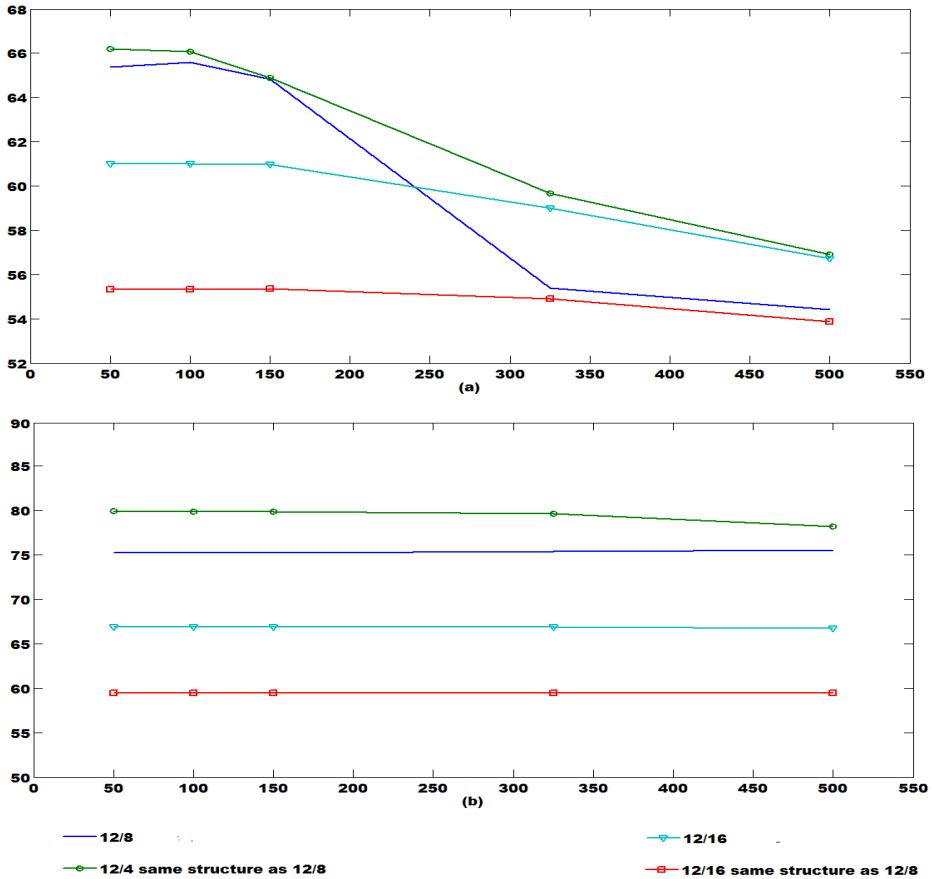

Figure 7-12: Graph of percentages of power generated versus voltage level (V). The graph shows comparison of speed for four machines at their optimal firing angles during low and medium speed (a) 35rad/s and (b) 200rad/s

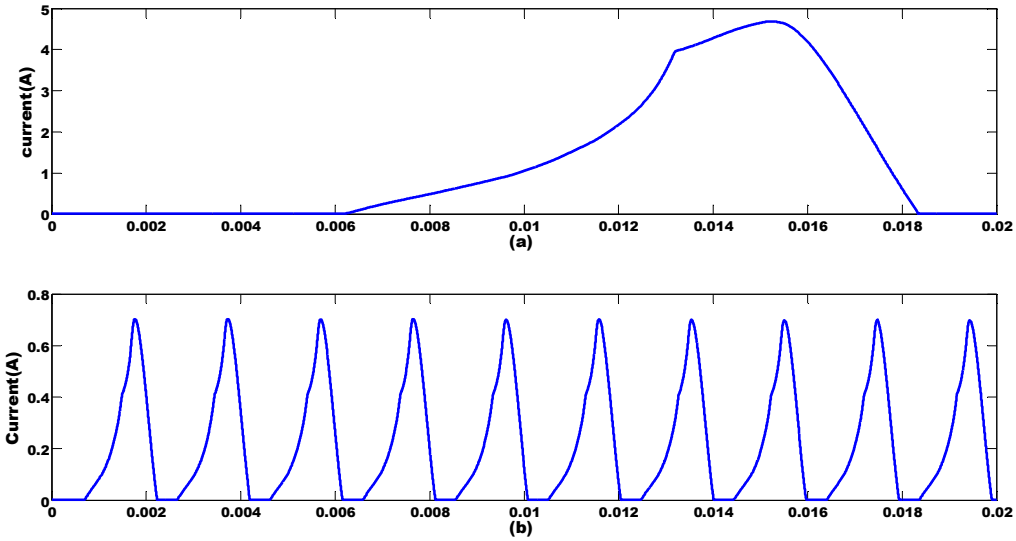

Figure 7-13: Comparison of phase current during one current cycle at low speed (a) 45rad/s and high speed (b) 400rad/s

The function of dwell angle in terms of speed at each voltage level is evaluated using the Sigmoidal Model for each of the machine. A closed loop control is established to provide the optimal dwell angle for various speed ranges. The controller allows the voltage to be selected in order to maintain the high percentage of power generated. Appendix G shows the two types of curve; the Weibull and the Ratkowsky curve which best fits the dwell angle data. The related function is developed using both the Ratkowsky and the Weibull model based on the following equation:

$$\theta_{dwell\_n} = \frac{a}{1+e^{b-c\omega}} \tag{6.9}$$

$$\theta_{dwell\_n} = a - be^{-c\omega^d} \tag{6.10}$$

Where, θ_{dwell} is the dwell angle, ω is the speed, a, b, c and d are the coefficient parameters and n is the voltage level. The functions of dwell angle in terms of speed and voltage are determined using Figure 7-9, Figure 7-8, Figure 7-10 and Figure 7-11 which represents each of the machines. For the 12/8 machine, only three levels of voltage are selected since at higher voltage the percentages of power generated is less than 60%.

7.2.1 Ratkowsky Model

The function for the 12/8 machine is represented in matrix form using the equation (6.9) as shown below:

$$\begin{bmatrix} \theta_{dwell\_50V} \\ \theta_{dwell\_100V} \\ \theta_{dwell\_150V} \end{bmatrix} = \begin{bmatrix} 22.97 \\ 22.17 \\ 22.04 \end{bmatrix} . \begin{bmatrix} \frac{1}{1+e^{M}} \end{bmatrix} \tag{6.11}$$

where $M=b\text{-}c\omega$ and n is the voltage level.

$$M = \begin{bmatrix} -0.528 \\ 1.104 \\ 1.539 \end{bmatrix} - \begin{bmatrix} 0.0306 \\ 0.0826 \\ 0.0674 \end{bmatrix} .\omega \tag{6.12}$$

The parameters for the 12/16 machines and 12/4 machine are listed in Appendix H.

7.2.2 Weibull Model

The equation relating the optimal parameters for the 12/8 machine is represented in matrix form according to equation (6.10) as follows:

$$\begin{bmatrix} \theta_{dwell\_50V} \\ \theta_{dwell\_100V} \\ \theta_{dwell\_150V} \end{bmatrix} = \begin{bmatrix} 23 \\ 22.3 \\ 22 \end{bmatrix} - \begin{bmatrix} 13.5 \\ 30599 \\ 13.5 \end{bmatrix} \exp - \begin{bmatrix} 0.09 \\ 0.24 \\ 2.36 \end{bmatrix} \omega^{d} \tag{6.13}$$

Where $d = \begin{bmatrix} 0.76 \\ 0.24 \\ 2.4 \end{bmatrix}$

The parameters for the 12/16 and 12/4 machine are listed in Appendix H.

7.3 Proposed Control Method

The implementation of the controller can be made based on the group which has been assigned to the respective voltage level and speed. The dwell angle is obtained from the polynomial function according to the speed range. The selection of voltage level also depends on the speed range. The existing simulation platform has been modified to include the voltage selector circuit as depicted in Figure 7-14.

The scheme is simple to implement since it does not include any complex circuitry. Based on the speed range, the controller will switch to its optimal voltage level that has been set. In this way, the machine can accommodate the change in wind velocity and provide the highest percentages of generated power. Figure 7-15 shows the result when a step input speed is applied. The input signal to the simulation model is represented using step input, triangular input and a combination of both which correspond well with the scheme proposed as depicted in Appendix I. The proposed scheme adjusts to the required voltage level in order to provide high percentage of generated power.

7.4 Verification Through Simulation

The results are verified by comparing the optimal dwell angle obtained via the heuristic method against the ones obtained using both the Weibull and Ratkowsky model. The difference in the results obtained are tabulated in Table 7-3 and illustrated in Figure 7-16. Both models shows slight difference as compared to the parameters

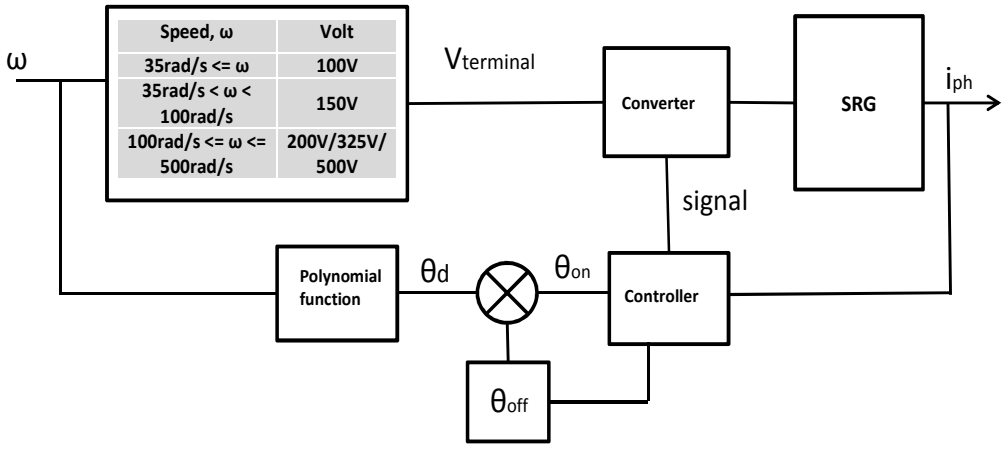

Figure 7-14: Schematic diagram of the proposed controller

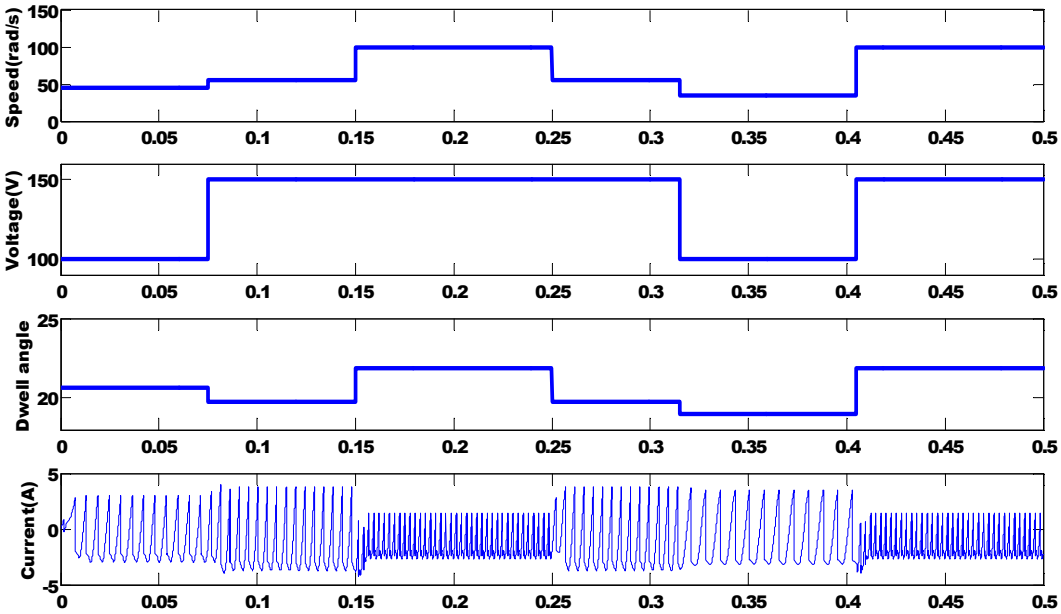

Figure 7-15:Simulation result of the proposed algorithm when a step input is applied. The speed range was tested at 45rad/s-55rad/s-100rad/s-55rad/s-35rad/s-100rad/s

obtained from the simulation model. Thus, the results were further verified using the Kolmogorov-Smirnov (KS) test method. From the test, the Ratkowsky model was selected for this study due to its higher confidence value. The model also gives stable result during the low speed range as illustrated in Appendix G and Table 7-3.

7.5 Conclusions

Each of the variables such as the reference current, terminal voltage and firing angles has an effect on the performance of the machine in terms of generated power. The selection of the optimal control variables is made in terms of the highest percentages of power generated. It provides a good balance between the excitation and generated power.

Table 7-3: Comparison of optimal dwell angle between the Weibull and Ratkowsky model with the simulation

Speed (rad/s)	Voltage (V)	Tdwell Weibull	Tdwell Ratkowsky	Tdwell Simulation
25	*100*	15.89	16.03	16
35	*100*	19.17	18.99	19
45	*100*	20.53	20.65	21
55	150	19.74	19.74	20
100	150	21.99	21.88	22

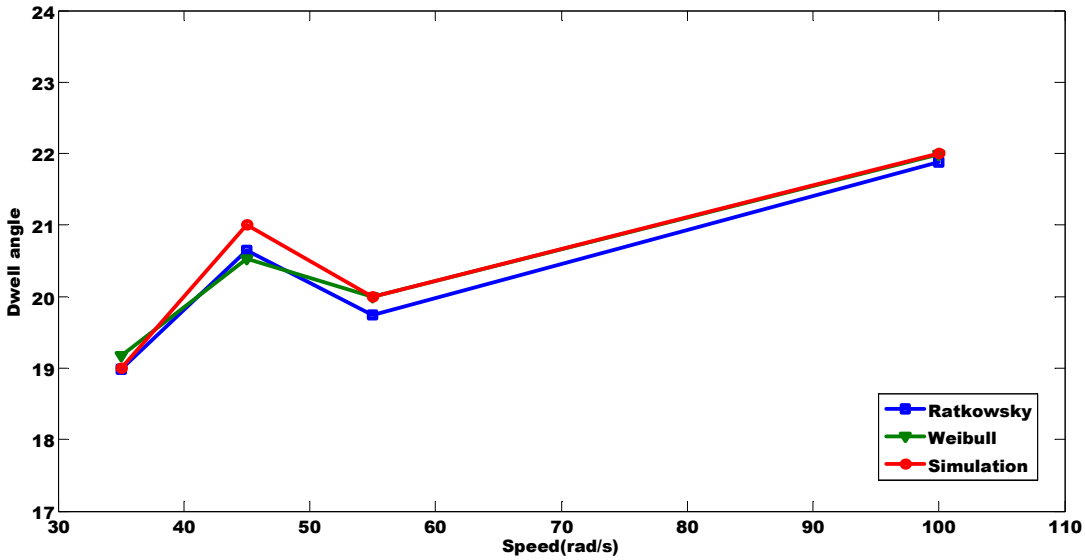

Figure 7-16: Comparison of the dwell angle obtained between the Ratkowsky model and Weibull model with the simulation result at speed of 35,45,55 and 100rad/s

The shape of the phase current is dependent on the placement of the firing angles along the inductance profile. An optimal firing angle will provide a continuous overlapping of phase current. It also avoids the generating current from tailing off into the excitation of the next phase, thus reducing the build up of a positive torque.

As for the voltage, it has been shown that during the low speed range, the use of high voltage level results in the current chopping mode and decreases the percentages of generated power. Also, there exists an optimal voltage level which provides the highest percentages of generated power. Therefore, the voltage can be grouped according to the speed range and selected to maintain the high percentage of generated power by operating the machine in single pulse mode thus avoiding the current chopping mode during the low speed range. Since the voltage level does not affect the percentage of generated power during the medium speed range, it is categorized in terms of the amount of power being generated by the machine.

The most influential parameter affecting the generated power at all speed range is the firing angles whereas the voltage level only affects the lower speed range. From the analysis, the performance of the machine is categorised in terms of the percentage of power generated for the low speed range and amount of generated power for the medium speed range. Polynomial functions for the controller based on the firing angle and speed has been proposed.

The controller is designed to operate the machine at its optimal performance based on the functions developed for each machine. This allows the machine to be selected according to the required application and tested before the development of the prototype saving costs and time.

CHAPTER 8

CONCLUSIONS AND FUTURE WORK

8.1 Conclusions

An integrated simulation platform for the SRG operating in the low and medium speed range has been developed using the MATLAB/SIMULINK software. It has been demonstrated that the optimal performance in terms of the generated power of the machine is determined based on the overall SRG system.

The structure of a three phase 12/8 machine which was previously used as a motor has been modelled using a two dimensional finite element analysis. All the possible winding configurations for the three phase four poles machine operating in the single phase and dual phase excitation has been analyzed. It has been demonstrated that the distribution of flux within the core will impact the performance of the machine in terms of generated power, torque production and losses. The NSNS polarity of the poles was proposed based on the winding configuration which produces the largest magnetization curve, whereas the NSNSNSNS and NNSSNNSS configuration was proposed for dual phase excitation. A better performance in terms of torque and losses was achieved by proper arrangement of the winding configuration.

Using the simulation platform of the SRG, the control variables affecting both the excitation and generation stage based on the voltage across the phase winding was investigated. An extensive discussion on each of the variables and how it affects the generation stage has been put forward. The optimal operating point in terms of the ratio between the generation and excitation stage for each of the control variables has been determined based on the heuristic method. The highest percentage of power generation was found to be when the SRG operates during single pulse mode as opposed to the current chopping mode during low speed.

The determination of the optimal variables poses several challenges as the machine operates based on pulsed signals. From the findings, two sets of current profiles are

identified; overlapping and non-overlapping of current during the low speed range and continuous current during medium speed operation. The non-overlapping current should be avoided as it will affect the operation of the machine by producing jerking motion. It was also shown that the continuous current mode is not suitable for the generating operation as it requires large excitation, which reduces the current in the generation stage.

The optimal control variables has been selected and characterized based on the percentages of power generated while ensuring the overlapping of current. The nonlinear regression method; Ratkowsky model was used to relate these optimal variables with the percentage of power generated. A novel control scheme was proposed to operate the machine at its high performance using the single pulse mode during the low speed range.

Based on the analysis performed on the various number of rotor poles machine, it was observed that the performance of the machine in terms of generated power relates to the magnetization curve. The change in the magnetization curve is affected by the change in winding polarity and also the number and width of rotor poles. Lower number of rotor poles provide large magnetization curve with a high inductance ratio. As the number of rotor poles increases, the inductance ratio decreases. In addition, a lower number of rotor poles have lower value of peak current thus; the volt-ampere (VA) requirement of converter circuit is reduced. The higher number of rotor poles on the other hand gives better torque profile as compared to the lower number of rotor poles machine. Therefore, a low number of rotor poles machine is suggested for application which requires high generation of power.

8.2 Future Research Work

The principal aim of this research was to integrate the overall drive system of the SRG into one single platform and analyse the performance of the machine during the low and medium speed range. The platform allows the designer to perform changes on the machine parameters without having to redesign the prototype circuit. This would save

time and costs incurred during the experimental stage. However, the comparative performance analysis of the machine was mainly based on simulations. Thus, an experimental analysis should be conducted to evaluate the effectiveness of the model. The hardware implementation of the system should include the induction motor as the prime mover, the 12/8 machine, controller, power supply used for supplying voltage sources to the controller, the converter which is composed of two MOSFETs and two normal recovery power diodes and battery set for excitation of the winding.

In this research, the simulation was limited to using the existing machine and changing the number of rotor poles and polarity of the phase winding. It can further be extended to see the effect of changing the number of phases and number of poles per phase without altering the main geometrical structure of the stator.

Furthermore, the performance of the machine is determined based on one cycle of operation. However, for a dynamic operation the current overlaps with each other, thus require further investigation that includes the calculation and effect of the overlap.

A more advanced control system ought to be designed to extend the operation of the machine in both generating and motoring operation.

Finally, the available simulation platform can be enhanced to provide a user friendly environment for the development of the machine through a graphical user interface (GUI) based application.

References:

[1] E. I. Administration, International Energy Outlook, 2011, W. U.S. DOE, DC, http://www.eia.gov/forecasts/ieo/.

[2] D. Venables, N. F. Pidgeon, K. A. Parkhill, K. L. Henwood, and P. Simmons, "Living with nuclear power: Sense of place, proximity, and risk perceptions in local host communities," *Journal of Environmental Psychology,* vol. 32, pp. 371-383, 2012.

[3] N. Kopytko and J. Perkins, "Climate change, nuclear power, and the adaptation–mitigation dilemma," *Energy Policy,* vol. 39, pp. 318-333, 2011.

[4] G. W. E. Council, Global Wind Energy Outlook, 2012, http://www.gwec.net/contact/contact-us/.

[5] WWEA, Small Wind World Report, 2012, http://www.wwindea.org/home/index.php.

[6] C. Bratiloveanu, D. Anghelus, and I. Boldea, "A comparative investigation of three PM-less MW power range wind generator topologies," in *13th International Conference on Optimization of Electrical and Electronic Equipment (OPTIM)*, Brasov, 2012, pp. 535-543.

[7] K. Ogawa, N. Yamamura, and M. Ishda, "Study for Small Size Wind Power Generating System Using Switched Reluctance Generator," in *IEEE International Conference on Industrial Technology*, Mumbai, 2006, pp. 1510-1515.

[8] M. Nassereddine, J. Rizk, and M. Nagrial, "Switched Reluctance Generator for Wind Power Applications," *Proceedings of World Academy of Science, Engineering and Technology,* vol. 31, pp. 126-130, 2008.

[9] J.-b. Hu and Y.-k. He, "Dynamic modelling and robust current control of wind-turbine driven DFIG during external AC voltage dip," *Journal of Zhejiang University - Science A,* vol. 7, pp. 1757-1764, 2006.

[10] K. T. Chau, W. L. Li, and C. H. T. Lee, "*Challenges and Opportunities of Electric Machines for Renewable Energy*," *Progress In Electromagnetics Research B,* vol. 42, pp. 45-74, 2012.

[11] H. Chen, "Electromagnetic design of switched reluctance generator," in *The Fifth International Conference on Power Electronics and Drive Systems (PEDS)*, Singapore, 2003, pp. 777-780 Vol.1.

[12] Z. Pan, Y. Jin, and H. Zhang, "Study on switched reluctance generator," *Science Journal of Zhejiang University,* vol. 5, p. 594, 2004.

[13] V. R. Bernardeli, D. A. Andrade, A. W. F. V. Silveira, L. C. Gomes, G. P. Viajante, and L. G. Cabral, "Self-excited switched reluctance generator," in *Brazilian Power Electronics Conference (COBEP)*, Praiamar, 2011, pp. 55-60.

[14] H. Chen, "Implementation of a Three-Phase Switched Reluctance Generator System for Wind Power Applications," in *14th Symposium on Electromagnetic Launch Technology*, Victoria BC, 2008, pp. 1-6.

[15] M. Ruba, C. Oprea, and L. Szabo, "Comparative study on Switched Reluctance Machine based fault-tolerant electrical drive systems," in *IEEE International Electric Machines and Drives Conference (IEMDC)* Miami, Fl, 2009, pp. 987-992.

[16] E. Echenique, J. Dixon, R. Cardenas, and R. Pena, "Sensorless Control for a Switched Reluctance Wind Generator, Based on Current Slopes and Neural Networks," *IEEE Transactions on Industrial Electronics,* vol. 56, pp. 817-825, March 2009.

[17] I. H. Al-Bahadly, "Examination of a Sensorless Rotor-Position-Measurement Method for Switched Reluctance Drive," *IEEE Transactions on Industrial Electronics,* vol. 55, pp. 288-295, 2008.

[18] H. Keunsoo, K. Rae-Young, and R. Ramu, "Position Estimation in Switched Reluctance Motor Drives Using the First Switching Harmonics Through Fourier Series," *IEEE Transactions on Industrial Electronics,* vol. 58, pp. 5352-5360, Sept. 2011.

[19] A.Arifin, I.H.Al-Bahadly, and S.C.Mukhopadhyay, "A Comprehensive Simulation Platform for Switched Reluctance Generator System," *WSEAS Transactions on Power Systems,* vol. 7, pp. 198-208, October 2012.

[20] D. A. Torrey, "Switched reluctance generators and their control," *IEEE Transactions on Industrial Electronics,* vol. 49, pp. 3-14, Feb. 2002.

[21] P. Pillay and W. Cai, "An investigation into vibration in switched reluctance motors," *IEEE Transactions on Industry Applications,* vol. 35, pp. 589-596, 1999.

[22] M. Nassereddine, J. Rizk, M. Nagrial, and A. Hellany, "Study analysis on the excitation of a switched reluctance generator for wind energy conversion," in *International Conference on Advances in Computational Tools for Engineering Applications (ACTEA)* Zouk Mosbeh, 2009, pp. 112-116.

[23] N. Radimov, N. Ben-Hail, and R. Rabinovici, "Simple model of switched-reluctance Machine based only on aligned and unaligned position data," *IEEE Transactions on Magnetics,* vol. 40, pp. 1562-1572, 2004.

[24] P. S. J. R. French, "Switched reluctance motor drives for rail traction: relative assessment," *Electric Power Applications, IEE Proceedings B [see also IEE Proceedings-Electric Power Applications],* vol. 131, pp. 209-219, 1984.

[25] B. Bilgin, A. Emadi, and M. Krishnamurthy, "Comprehensive Evaluation of the Dynamic Performance of a 6/10 SRM for Traction Application in PHEVs," *IEEE Transactions on Industrial Electronics,* vol. 60, pp. 2564-2575, April 2012.

[26] C. C. Chan, "The state of the art of electric and hybrid vehicles," *Proceedings of the IEEE,* vol. 90, pp. 247-275, 2002.

[27] M. Ehsani, K. M. Rahman, and H. A. Toliyat, "Propulsion system design of electric and hybrid vehicles," *IEEE Transactions on Industrial Electronics,* vol. 44, pp. 19-27, 1997.

[28] W. Shuanghong, Z. Qionghua, M. Zhiyuan, and Z. Libing, "Implementation of a 50-kW four-phase switched reluctance motor drive system for hybrid electric vehicle," *IEEE Transactions on Magnetics,* vol. 41, pp. 501-504, Jan. 2005.

[29] M. Takeno, A. Chiba, N. Hoshi, S. Ogasawara, M. Takemoto, and M. A. Rahman, "Test Results and Torque Improvement of the 50-kW Switched Reluctance Motor Designed for Hybrid Electric Vehicles," *IEEE Transactions on Industry Applications,* vol. 48, pp. 1327-1334, Jul-Aug 2012.

[30] A. V. Radun, "High power density switched reluctance motor drive for aerospace applications," in *Conference Record of the 1989 IEEE Industry Applications Society Annual Meeting*, San Diego, CA, USA, 1989, pp. 568-573 vol.1.

[31] C. A. Ferreira, S. R. Jones, W. S. Heglund, and W. D. Jones, "Detailed design of a 30-kW switched reluctance starter/generator system for a gas turbine engine application," *IEEE Transactions on Industry Applications,* vol. 31, pp. 553-561, May-June 1995.

[32] E. Richter and C. Ferreira, "Performance evaluation of a 250 kW switched reluctance starter generator," in *IEEE Industry Applications Conference Record* Orlando, FL, USA, 1995, pp. 434-440.

[33] S. R. MacMinn and W. D. Jones, "A very high speed switched-reluctance starter-generator for aircraft engine applications," in *Proceedings of the IEEE 1989 National Aerospace and Electronics Conference*, Dayton OH, 1989, pp. 1758-1764.

[34] S. R. MacMinn and J. W. Sember, "Control of a switched-reluctance aircraft engine starter-generator over a very wide speed range," in *Proceedings of the 24th Intersociety Energy Conversion Engineering Conference*, Washington DC, 1989, pp. 631-638.

[35] N. Schofield and S. Long, "Generator Operation of a Switched Reluctance Starter/Generator at Extended Speeds," *IEEE Transactions on Vehicular Technology,* vol. 58, pp. 48-56, Jan. 2009.

[36] A. Fleury, D. A. de Andrade, F. dos Santos e Silva, and J. L. Domingos, "Switched Reluctance Generator for complementary Wind Power Generation in Grid Connection," in *IEEE International Electric Machines & Drives Conference*, Antalya, 2007, pp. 465-470.

[37] D. A. Torrey, "Variable-reluctance generators in wind-energy systems," in *24th Annual IEEE Power Electronics Specialists Conference (PESC)*, Seattle, WA, 1993, pp. 561-567.

[38] Q. Zhang, X. Wang, X. Zhu, and D. Liu, "A small single-phase switched reluctance generator for wind power generation," in *Proceedings of the Fifth International Conference on Electrical Machines and Systems*, Shenyang China, 2001, pp. 1003-1006.

[39] R. Cardenas, W. F. Ray, and G. M. Asher, "Switched reluctance generators for wind energy applications," in *26th Annual IEEE Power Electronics Specialists Conference (PESC)*, Atlanta, GA, USA, 1995, pp. 559-564.

[40] A. Radun, "Generating with the switched reluctance motor," in *Ninth Annual Conference Proceedings of Applied Power Electronics Conference and Exposition (APEC)* Orlando, Fl, 1994, pp. 41-47.

[41] C. Yuan-Chih and L. Chang-Ming, "On the Design of Power Circuit and Control Scheme for Switched Reluctance Generator," *IEEE Transactions on Power Electronics,* vol. 23, pp. 445-454, January 2008.

[42] I. Kioskeridis and C. Mademlis, "Optimal efficiency control of switched reluctance generators," *IEEE Transactions on Power Electronics,* vol. 21, pp. 1062-1072, July 2006.

[43] P. Asadi, M. Ehsani, and B. Fahimi, "Design and control characterization of switched reluctance generator for maximum output power," in *Twenty-First Annual IEEE Applied Power Electronics Conference and Exposition* Dallas Texas, 2006, pp. 1639-1644.

[44] Y. Sozer and D. A. Torrey, "Closed loop control of excitation parameters for high speed switched-reluctance generators," *IEEE Transactions on Power Electronics,* vol. 19, pp. 355-362, March 2004.

[45] E. Mese, Y. Sozer, J. M. Kokernak, and D. A. Torrey, "Optimal excitation of a high speed switched reluctance generator," in *Fifteenth Annual IEEE Applied Power Electronics Conference and Exposition (APEC)*, New Orleans, Louisiana, 2000, pp. 362-368.

[46] C. Mademlis and I. Kioskeridis, "Optimizing Performance in Current-Controlled Switched Reluctance Generators," *IEEE Transactions on Energy Conversion,* vol. 20, pp. 556-565, September 2005.

[47] C. Yuan-Chih and L. Chang-Ming, "Development and voltage feedback control for a switched reluctance generator," in *International Conference on Electrical Machines and Systems (ICEMS)*, Seoul, 2007, pp. 392-397.

[48] X. D. Xue, K. W. E. Cheng, J. K. Lin, Z. Zhang, K. F. Luk, T. W. Ng, and N. C. Cheung, "Optimal Control Method of Motoring Operation for SRM Drives in Electric Vehicles," *IEEE Transactions on Vehicular Technology,* vol. 59, pp. 1191-1204, Mac. 2010.

[49] R. Cardenas, R. Pena, M. Perez, J. Clare, G. Asher, and P. Wheeler, "Control of a switched reluctance generator for variable-speed wind energy applications," *IEEE transactions on Energy conversion,* vol. 20, pp. 781-791, December 2005.

[50] H. Chen and Z. Shao, "Turn-on angle control for switched reluctance wind power generator system," in *The 30th Annual Conference of IEEE Industrial Electronics Society (IECON)*, Busan, Korea, 2004, pp. 2367-2370.

[51] E. Elwakil and M. Darwish, "Critical review of converter topologies for switched reluctance motor drives," *International Review of Electrical Engineering,* vol. 2, pp. 50-58, January-February 2007.

[52] E. S. L. Oliveira, A. Fleury, G. A. Fleury-Neto, and T. F. Oliveira, "Performance Comparison of an Alternative Converter for Wind Powered Switched Reluctance Generators," in *International Conference on Renewable Energies and Power Quality (ICREPQ)*, Spain, 2008.

[53] A. Takahashi, H. Goto, K. Nakamura, T. Watanabe, and O. Ichinokura, "Characteristics of 8/6 Switched Reluctance Generator Excited by Suppression Resistor Converter," *IEEE Transactions on Magnetics,* vol. 42, pp. 3458-3460, Oct. 2006.

[54] N. K. Singh, J. E. Fletcher, S. J. Finney, D. M. Grant, and B. W. Williams, "Evaluation of Sparse PWM Converter for Switched Reluctance Generator," in *International Conference on Power Electronics and Drives Systems (PEDS)*, 2005, pp. 721-725.

[55] T. J. E. Miller, "Optimal design of switched reluctance motors," *IEEE Transactions on Industrial Electronics,* vol. 49, pp. 15-27, Feb. 2002.

[56] C. Pollock and A. Michaelides, "Switched reluctance drives: a comparative evaluation," *Power Engineering Journal,* vol. 9, pp. 257-266, December 1995.

[57] M. Mueller, "Design and performance of a 20 kW, 100 rpm, switched reluctance generator for a direct drive wind energy converter," in *IEEE International Conference on Electric Machines and Drives*, San Antonio Tx, 2005, pp. 56-63.

[58] M. K. El-Nemr, M. A. Al-Khazendar, E. M. Rashad, and M. A. Hassanin, "Modeling and steady-state analysis of stand-alone switched reluctance generators," in *IEEE Power Engineering Society General Meeting*, 2003, p. 1899 Vol. 3.

[59] M. A. Mueller, "Design of low speed switched reluctance machines for wind energy converters," in *Ninth International Conference on Electrical Machines and Drives*, Canterbury UK, 1999, pp. 60-64.

[60] H. C. Lovatt and J. M. Stephenson, "Influence of number of poles per phase in switched reluctance motors," *IEE Proceedings-B Electric Power Applications,* vol. 139, pp. 307-314, July 1992.

[61] L. Zhenguo, Z. Na, K. Zhizhong, L. Dong-Hee, and A. Jin-Woo, "Modeling and simulation of a switched reluctance generator system based on variable generation voltage converter," in *31st International Telecommunications Energy Conference (INTELEC)*, Incheon, 2009, pp. 1-4.

[62] R. Karthikeyan, K. Vijayakumar, R. Arumugam, and V. Kamaraj, "Design and analysis of a switched reluctance generator for rural electrification in stand alone wind energy coversion system," in *International Conference on Power Systems (ICPS)*, Kharagpur India, 2009, pp. 1-6.

[63] S. Ning, C. Dawoon, L. Jian, and C. Yunhyun, "The Angle Control of Switched Reluctance Generator for Maximum Output Power," in *Sixth International Conference on Electromagnetic Field Problems and Applications (ICEF)*, Dalian, Liaoning, 2012, pp. 1-4.

[64] M. Qin, L. Dong, X. Huang, and X. Liao, "A rapid design method for high speed aeronautic switched reluctance generator," in *International Conference on Electric Information and Control Engineering (ICEICE)*, Wuhan, China, 2011, pp. 1937-1941.

[65] Y. C. Chang, C. H. Cheng, L. Y. Lu, and C. M. Liaw, "An experimental switched-reluctance generator based distributed power system," in *2010 XIX International Conference on Electrical Machines (ICEM)*, Rome, 2010, pp. 1-6.

[66] A. V. Radun, C. A. Ferreira, and E. Richter, "Two-channel switched reluctance starter/generator results," *IEEE Transactions on Industry Applications,* vol. 34, pp. 1026-1034, 1998.

[67] R. B. Inderka, M. Menne, and R. W. A. A. De Doncker, "Control of switched reluctance drives for electric vehicle applications," *IEEE Transactions on Industrial Electronics,* vol. 49, pp. 48-53, 2002.

[68] Y. Sozer and D. A. Torrey, "Optimal turn-off angle control in the face of automatic turn-on angle control for switched-reluctance motors," *IET Electric Power Applications,* vol. 1, pp. 395-401, 2007.

[69] P. C. Desai, M. Krishnamurthy, N. Schofield, and A. Emadi, "Novel Switched Reluctance Machine Configuration With Higher Number of Rotor Poles Than Stator Poles: Concept to Implementation," *IEEE Transactions on Industrial Electronics,* vol. 57, pp. 649-659, Feb 2010.

[70] B. Bilgin, A. Emadi, and M. Krishnamurthy, "Design Considerations for Switched Reluctance Machines With a Higher Number of Rotor Poles," *IEEE Transactions on Industrial Electronics,* vol. 59, pp. 3745-3756, 2012.

[71] E. Levi, "Multiphase Electric Machines for Variable-Speed Applications," *IEEE Transactions on Industrial Electronics,* vol. 55, pp. 1893-1909, May 2008.

[72] A. M. Michaelides and C. Pollock, "Modelling of a new winding arrangement to improve performance in the switched reluctance motor," in *Sixth International Conference on Electrical Machines and Drives*, Oxford, 1993, pp. 213-218.

[73] H. Chen and Q. Song, "Windings arrangement of a three-phase switched reluctance machine," in *IEEE International Electric Machines and Drives Conference, 2003. IEMDC'03.* . vol. 3, 2003, pp. 1665-1668 vol.3.

[74] B. C. Mecrow, "New winding configurations for doubly salient reluctance machines," *IEEE Transactions onIndustry Applications,* vol. 32, pp. 1348-1356, Nov/Dec 1996.

[75] Y. Xu and D. A. Torrey, "Study of the mutually coupled switched reluctance machine using the finite element-circuit coupled method," *IEE Proceedings -Electric Power Applications,* vol. 149, pp. 81-86, Mac 2002.

[76] C. Neagoe, A. Foggia, and R. Krishnan, "Impact of pole tapering on the electromagnetic torque of the switched reluctance motor," in *IEEE International Electric Machines and Drives Conference Record*, Milwaukee, WI, 1997.

[77] J. Corda, A. M. Tataru, P. O. Rasmussen, and E. Ritchie, "Analytical estimation of torque enhancement of the SR machine with saw-shaped (shark) pole surfaces," *IEE Proceedings - Electric Power Applications,* vol. 151, pp. 223-229, 2004.

[78] M. Sanada, S. Morimoto, Y. Takeda, and N. Matsui, "Novel rotor pole design of switched reluctance motors to reduce the acoustic noise," in *Conference Record of the 2000 IEEE Industry Applications Conference*, Rome, 2000, pp. 107-113

[79] L. Moreau, M. Machmoum, and M. Zaim, "Design of Low-Speed Slotted Switched Reluctance Machine for Wind Energy Applications," *Electric Power Components and Systems,* vol. 34, pp. 1139-1156, 2006.

[80] M. Abbasian, M. Moallem, and B. Fahimi, "Double-Stator Switched Reluctance Machines (DSSRM): Fundamentals and Magnetic Force Analysis," *IEEE Transactions on Energy Conversion,* vol. 25, pp. 589-597, 2010.

[81] T.J.E. Miller, *Electronic Control of Switched Reluctance Machines*. Oxford, U.K: Newnes, 2001.

[82] R. Krishnan, *Switched Reluctance Motor Drives: Modeling, Simulation, Analysis, Design, and Applications*: CRC Press, 2001.

[83] S. Vukosavic and V. R. Stefanovic, "SRM inverter topologies: a comparative evaluation," *Industry Applications, IEEE Transactions on,* vol. 27, pp. 1034-1047, 1991.

[84] M. Barnes and C. Pollock, "Power electronic converters for switched reluctance drives," *Power Electronics, IEEE Transactions on,* vol. 13, pp. 1100-1111, 1998.

[85] J. Faiz and R. Fazai, "Optimal Excitation Angles of a High Speed Switched Reluctance Generator by Efficiency Maximization," in *12th International Power Electronics and Motion Control Conference (EPE-PEMC)*, Portoroz, Slovenia, 2006, pp. 287-291.

[86] H. Zhao, Y. Lingzhi, P. Hanmei, and Z. Kunyan, "Research and control of SRG for variable-speed wind energy applications," in *IEEE 6th International Power Electronics and Motion Control Conference (IPEMC)*, Wuhan, 2009, pp. 2238-2243.

[87] V. Nedic and T. A. Lipo, "Experimental verification of induced voltage self-excitation of a switched reluctance generator," in *Conference Record of the 2000 IEEE Industry Applications Conference*, 2000, pp. 51-56 vol.1.

[88] V. Raulin, A. Radun, and I. Husain, "Modeling of losses in switched reluctance machines," *IEEE Transactions on Industry Applications,* vol. 40, pp. 1560-1569, Nov-Dec 2004.

[89] J. Corda and M. Olaca, "Analysis of losses in power electronic converter of SR drive," in *Fifth European Conference on Power Electronics and Applications*, Brighton UK, 1993, pp. 49-53.

[90] J. T. Charton, J. Corda, J. M. Stephenson, and S. P. Randall, "Dynamic modelling of switched reluctance machines with iron losses and phase interactions," *Electric Power Applications, IEE Proceedings -,* vol. 153, pp. 327-336, 2006.

[91] Y. Hayashi and T. J. E. Miller, "A new approach to calculating core losses in the SRM," *IEEE Transactions on Industry Applications,* vol. 31, pp. 1039-1046, Sept/Oct 1995.

[92] H. Hannoun, M. Hilairet, and C. Marchand, "Analytical modeling of switched reluctance machines including saturation," in *IEEE International Electric Machines & Drives Conference (IEMDC)*, Antalya Turkey, 2007, pp. 564-568.

[93] D. Wen and L. Deliang, "A Fast Analytical Model for an Integrated Switched Reluctance Starter/Generator," *IEEE Transactions on Energy conversion,* vol. 25, pp. 948-956, Dec 2010.

[94] H. P. Chi, R. L. Lin, and J. F. Chen, "Simplified flux-linkage model for switched-reluctance motors," *EE Proceedings -Electric Power Applications, ,* vol. 152, pp. 577-583, May 2005.

[95] S. Song and W. Liu, "A Comparative Study on Modeling Methods for Switched Reluctance Machines," *Computer and Information Science,* vol. 3, pp. 205-210, May 2010.

[96] P. Materu and R. Krishnan, "Analytical prediction of SRM inductance profile and steady-state average torque," in *Conference Record of the IEEE Industry Applications Society Annual Meeting*, Seattle, WA , USA 1990, pp. 214-223 vol.1.

[97] D. A. Torrey, X. M. Niu, and E. J. Unkauf, "Analytical modelling of variable-reluctance machine magnetisation characteristics," *IEE Proceedings Electric Power Applications,* vol. 142, pp. 14-22, Jan. 1995.

[98] A. Radun, "Analytically computing the flux linked by a switched reluctance motor phase when the stator and rotor poles overlap," *IEEE Transactions on Magnetics,* vol. 36, pp. 1996-2003, July 2000.

[99] M. Nagrial, J.Rizk, and W.Aljaism, "Dynamic Simulation of Switched Reluctance Motor Using Matlab and Fuzzy Logic," in *Proceedings of the 14th International Middle East Power Systems Conference (MEPCON'10)*, Cairo University, Egypt, 2010.

[100] C. Hao and J. J. Gu, "Implementation of the Three-Phase Switched Reluctance Machine System for Motors and Generators," *IEEE/ASME Transactions on Mechatronics,* vol. 15, pp. 421-432, June 2010.

[101] T. Lachman, T. R. Mohamad, and C. H. Fong, "Nonlinear modelling of switched reluctance motors using artificial intelligence techniques," *IEE Proceedings - Electric Power Applications,* vol. 151, pp. 53-60, 9 Jan. 2004.

[102] L. Xiao, H. Sun, Y. Zheng, Y. Dong, and F. Gao, "Non-linear modeling and dynamic simulation of 8/6 poles SRM," in *31st Chinese Control Conference (CCC)*, Hefei, 2012, pp. 4534-4538.

[103] D. Wen and L. Deliang, "Calculation of Flux Linkages of a 12/8 Dual-Channel SRM Including Mutual Coupling and Saturation: From Magnetic Circuit Model to FEM Analysis," in *IEEE Industry Applications Society Annual Meeting (IAS)*, Edmonton, Alta, 2008, pp. 1-8.

[104] G. E. Dawson, A. R. Eastham, and J. Mizia, "Switched-Reluctance Motor Torque Characteristics: Finite-Element Analysis and Test Results," *IEEE Transactions on Industry Applications,* vol. IA-23, pp. 532-537, May 1987.

[105] M. Van der Giet, C. Schlensok, B. Schmulling, and K. Hameyer, "Comparison of 2-D and 3-D Coupled Electromagnetic and Structure-Dynamic Simulation of Electrical Machines," *IEEE Transactions on Magnetics,* vol. 44, pp. 1594-1597, June 2008.

[106] S. Prabhu, V.Chandrasekar, P.Karthikeyan, N.C.Lenin, and R.Arumugam, "Vibration and Thermal Analysis of Switched Reluctance Hub Motor," *European Journal of Scientific Research,* vol. 68, pp. 12-20, 2012.

[107] K. N. Srinivas and R. Arumugam, "Analysis and characterization of switched reluctance motors: Part II. Flow, thermal, and vibration analyses," *IEEE Transactions on Magnetics,* vol. 41, pp. 1321-1332, 2005.

[108] W. Wu, B. A. Kalan, and H. C. Lovatt, "Time-stepping analysis of a switched reluctance motor by coupling electrical circuit and electromagnetic finite element methods," in *Sixth International Conference on Electrical Machines and Systems (ICEMS)*, Beijing, China, 2003, pp. 728-731.

[109] T. S. Low, H. Lin, and S. X. Chen, "Analysis and comparison of switched reluctance motors with different physical sizes, using a 2D finite element method," *IEEE Transactions on Magnetics,* vol. 31, pp. 3503-3505, Nov 1995.

[110] J. Coulomb, "A methodology for the determination of global electromechanical quantities from a finite element analysis and its application to the evaluation of magnetic forces, torques and stiffness," *IEEE Transactions on Magnetics,* vol. 19, pp. 2514-2519, Nov. 1983.

[111] J. Mizia, K. Adamiak, A. R. Eastham, and G. E. Dawson, "Finite element force calculation: comparison of methods for electric machines," *IEEE Transactions on Magnetics,* vol. 24, pp. 447-450, 1988.

[112] M. Moallem and C. M. Ong, "Predicting the torque of a switched reluctance machine from its finite element field solution," *IEEE transactions on Energy conversion,* vol. 5, pp. 733-739, Dec 1990.

[113] B. Parreira, S. Rafael, A. J. Pires, and P. J. C. Branco, "Obtaining the magnetic characteristics of an 8/6 switched reluctance machine: from FEM analysis to the experimental tests," *IEEE Transactions on Industrial Electronics,* vol. 52, pp. 1635-1643, Dec 2005.

[114] H. Zhang, J. Zhang, and R. Gao, "A Novel Method of Phase Current Compensation for Switched Reluctance Motor System Based on Finite Element," *Journal of Computers,* vol. 4, p. 1064, Oct. 2009.

[115] C. E. Carstensen, N. H. Fuengwarodsakul, and R. W. De Doncker, "Flux Linkage Determination for Correct Modeling of Switched Reluctance Machines - Dynamic Measurement versus Static Computation," in *IEEE International Electric Machines & Drives Conference (IEMDC)*, Antalya, 2007, pp. 1317-1323.

[116] L. Kaiyuan, P. O. Rasmussen, and A. E. Ritchie, "Investigation of Flux-Linkage Profile Measurement Methods for Switched-Reluctance Motors and Permanent-Magnet Motors," *IEEE Transactions on Instrumentation and Measurement,* vol. 58, pp. 3191-3198, 2009.

[117] K. F. Wong, K. W. E. Cheng, and S. L. Ho, "Simulation of Switched Reluctance Motor Based on a Combination of Circuit-oriented and Signal-oriented Approaches Using Matlab/SimPowerSystems," *Electric Power Components and Systems,* vol. 35, pp. 205-219, Feb. 2007.

[118] H. Le-Huy and P. Brunelle, "A versatile nonlinear switched reluctance motor model in Simulink using realistic and analytical magnetization characteristics," in *31st Annual Conference of IEEE Industrial Electronics Society (IECON)*, Raleigh, NC, 2005, pp. 1556-1561.

[119] S. Sadeghi, J. Milimonfared, M. Mirsalim, and M. Jalalifar, "Dynamic Modeling and Simulation of a Switched Reluctance Motor in Electric Vehicles," in *1st IEEE Conference on Industrial Electronics and Applications*, Singapore, 2006, pp. 1-6.

[120] B. Fahimi, A. Emadi, and R. B. Sepe, Jr., "A switched reluctance machine-based starter/alternator for more electric cars," *IEEE transactions on Energy conversion,* vol. 19, pp. 116-124, 2004.

[121] D. Wen and L. Deliang, "Dynamic modeling and control for a switched reluctance starter/generator system," in *International Conference on Electrical Machines and Systems (ICEMS)* Wuhan, 2008, pp. 3315-3320.

[122] N. H. Fuengwarodsakul, R. W. De Doncker, and R. B. Inderka, "Simulation model of a switched reluctance drive in 42 V application," in *The 29th Annual Conference of the IEEE Industrial Electronics Society (IECON)*, Virginia, USA, 2003, pp. 2871-2876 Vol.3.

[123] H. Le-Huy and M. Chakir, "Optimizing the performance of a switched reluctance generator by simulation," in *XIX International Conference on Electrical Machines (ICEM)*, Rome, Italy, 2010, pp. 1-6.

[124] L.-H. Hoang, "Performance study of a four-phase 8/6 switched reluctance generator using a nonlinear model based on magnetization curves," in *35th Annual Conference of IEEE Industrial Electronics (IECON)*, Porto, Portugal, 2009, pp. 3910-3915.

[125] A. Arifin and I. Al-Bahadly, "Switched Reluctance Generator for Variable Speed Wind Energy Applications," *Smart Grid and Renewable Energy,* vol. 2, pp. 27-36, Feb 2011.

[126] Zeki Omac, Hasan Kurum, and A. H. Selcuk, "Digital Current Control of Switched Reluctance Motor," *International Journal of Electrical and Power Engineering,* vol. 5, pp. 54-61, 2011 2011.

[127] K. I. Hwu, "Applying POWERSYS and SIMULINK to Modeling Switched Reluctance Motor," *Tamkang Journal of Science and Engineering,* vol. 12, pp. 429-238, 2009.

[128] K. N. Srinivas and R. Arumugam, "Finite Element Analysis Combined Circuit Simulation of Dynamic Performances of Switched Reluctance Motors," *Electric Power Components and Systems,* vol. 30, pp. 1033-1045, 2002.

[129] Y. Xu and D. A. Torrey, "Study of the mutually coupled switched reluctance machine using the finite element-circuit coupled method," *IEE Proceedings -Electric Power Applications,* vol. 149, pp. 81-86, 2002.

[130] L. Szabo and M. Ruba, "Using co-simulation in Fault Tolerant Machine Study," in *23rd European Conference on Modelling and Simulation (ECMS)* Madrid, Spain, 2009.

[131] F. Soares and P. J. Costa Branco, "Simulation of a 6/4 switched reluctance motor based on Matlab/Simulink environment," *IEEE Transactions on Aerospace and Electronic Systems,* vol. 37, pp. 989-1009, 2001.

[132] http :// www. leadshine.com / resources / motortorquecalculation.

[133] S. Shoujun and L. Weiguo, "A Novel Method for Nonlinear Modeling and Dynamic Simulation of a Four-phase Switched Reluctance Generator System Based on

MATLAB/SIMULINK," in *2nd IEEE Conference on Industrial Electronics and Applications (ICIEA)*, 2007, pp. 1509-1514.

[134] H. Le-Huy and P. Brunelle, "A versatile nonlinear switched reluctance motor model in Simulink using realistic and analytical magnetization characteristics," in *31st Annual Conference of IEEE Industrial Electronics Society (IECON)*, Raleigh, NC, 2005, p. 6.

[135] G. Ramasamy, R. V. Rajandran, and N. C. Sahoo, "Modeling of Switched Reluctance Motor Drive System using Matlab/Simulink for Performance Analysis of Current Controllers," in *International Conference on Power Electronics and Drives Systems (PEDS)*, 2005, pp. 892-897.

[136] D. B. Wicklund and D. S. Zinger, "Voltage feedback signal conditioning in switched reluctance generation systems," in *Fifteenth Annual IEEE Applied Power Electronics Conference and Exposition (APEC)*, New Orleans, LA, 2000, pp. 376-380.

[137] P. Debiprasad and V. Ramanarayanan, "Mutual Coupling and Its Effect on Steady-State Performance and Position Estimation of Even and Odd Number Phase Switched Reluctance Motor Drive," *IEEE Transactions on Magnetics,* vol. 43, pp. 3445-3456, Aug 2007.

[138] Q. Bingni, S. Jiancheng, L. Tao, and Z. Hongda, "Mutual coupling and its effect on torque waveform of even number phase switched reluctance motor," in *Proceedings of the International Conference on Electrical Machines and Systems* Wuhan, 2008, pp. 3405-3410.

[139] A. M. Michaelides and C. Pollock, "Modelling and design of switched reluctance motors with two phases simultaneously excited," *IEE Proceedings -Electric Power Applications,* vol. 143, pp. 361-370, Sept 1996.

[140] B. C. Mecrow, C. Weiner, and A. C. Clothier, "The modeling of switched reluctance machines with magnetically coupled windings," *IEEE Transactions on Industry Applications,* vol. 37, pp. 1675-1683, 2001.

[141] G. J. Li, X. Ojeda, E. Hoang, M. Gabsi, and C. Balpe, "Design of double salient interior permanent magnet machine based on mutually coupled reluctance machine for increasing the torque density and flux-weakening capability," in *IEEE International Symposium on Industrial Electronics (ISIE)*, Bari, Italy, 2010, pp. 1253-1258.

[142] K. Min-Tsun, R. Sotudeh, and D. Lee, "Switched reluctance motor based on short flux path control method," in *39th International Universities Power Engineering Conference (UPEC)*, Bristol, UK, 2004, pp. 559-562.

[143] C. S. Edrington, D. C. Kaluvagunta, J. Joddar, and B. Fahimi, "Investigation of electromagnetic force components in SRM under single and multiphase excitation," *IEEE Transactions on Industry Applications,* vol. 41, pp. 978-988, 2005.

[144] P. Pillay, Y. Liu, W. Cai, and T. Sebastian, "Multiphase operation of switched reluctance motor drives," in *Conference Record of the IEEE Thirty-Second Annual Meeting Industry Applications Conference (IAS)* New Orleans, LA, 1997, pp. 310-317 vol.1.

[145] J. Faiz, B. Ganji, C. E. Carstensen, and R. W. D. Doncker, "Loss prediction in switched reluctance motors using finite element method," *European Transactions on Electrical Power,* vol. 19, pp. 731-748, July 2009.

[146] P. N. Materu and R. Krishnan, "Estimation of switched reluctance motor losses," *IEEE Transactions on Industry Applications,* vol. 28, pp. 668-679, May/June 1992.

[147] H. Yunkai, Z. Jianguo, G. Youguang, L. Zhiwei, and H. Qiansheng, "Design and Analysis of a High-Speed Claw Pole Motor With Soft Magnetic Composite Core," *IEEE Transactions on Magnetics,* vol. 43, pp. 2492-2494, 2007.

[148] H. Hannoun, M. Hilairet, and C. Marchand, "Design of an SRM Speed Control Strategy for a Wide Range of Operating Speeds," *IEEE Transactions on Industrial Electronics,* vol. 57, pp. 2911-2921, Sept. 2010.

[149] J. S. Lawler, J. M. Bailey, J. W. McKeever, and P. J. Otaduy, "Impact of continuous conduction on the constant power speed range of the switched reluctance motor," in *IEEE International Conference on Electric Machines and Drives*, San Antonio, TX, 2005, pp. 1285-1292.

[150] M. Rekik, M. Besbes, C. Marchand, B. Multon, S. Loudot, and D. Lhotellier, "High-speed-range enhancement of switched reluctance motor with continuous mode for automotive applications," *European Transactions on Electrical Power,* vol. 18, pp. 674-693, 2008.

[151] N. A. Patil and J. S. Lawler, "Issues in the Control of the Switched Reluctance Motor During Continuous Conduction," in *39th North American Power Symposium (NAPS)*, 2007, pp. 534-540.

Appendix A: Research Output

Research Outputs:

Below are the research outputs in conjunction with the author's PhD candidacy:

Journal Publications:

1. **A. Arifin** and I. Al-Bahadly, "Switched Reluctance Generator for Variable Speed Wind Energy Applications," *Smart Grid and Renewable Energy*, Vol. 2 No. 1, pp. 27-36, February 2011.
2. **A. Arifin**, I. H. Al-Bahadly, and S. C. Mukhopadhyay, "Simulation of Switched Reluctance Generator in Low and Medium Speed Operations for Wind Energy Application," *ISRN Renewable Energy*, Vol. 2012, pp.1-13, July 2012.
3. **Arifin, Amissa**, Ibrahim Al-Bahadly, and Subhas Chandra Mukhopadhyay. "State of the Art of Switched Reluctance Generator." *Energy and Power Engineering* , Vol.4 No.6, p.p. 447-458, November 2012
4. **A. Arifin**, I. H. Al-Bahadly, and S. C. Mukhopadhyay, "A Comprehensive Simulation Platform for Switched Reluctance Generator System," *WSEAS Transactions on Power Systems,* Vol. 4 No.7, p.p.198-208, October 2012

Conference Publications:

1. **A. Arifin** and I. H. Al-Bahadly, "Switched Reluctance Generator for Wind Energy Application", in *6th Annual Energy Postgraduate Conference*, New Zealand, 26-27 November 2009.
2. **A. Arifin**, I. H. Al-Bahadly, and S. C. Mukhopadhyay, "Analysis of a 12/16 switched reluctance machine using combined circuit and field computation", in *IEEE 5th International Power Engineering and Optimization Conference (PEOCO), Shah Alam, Malaysia, 6-7 June 2011.*
3. **A. Arifin**, I. H. Al-Bahadly, and S. C. Mukhopadhyay, "Performance Analysis of a 12/8 and 12/16 Switched Reluctance Machine in Low and

Medium Speed Operations for Wind Energy Applications", in *IEEE International Conference on Power and Energy (PECON), Sabah, Malaysia, 2-5 December 2012.*

Presentations:

1. **A. Arifin,** "Switched Reluctance Generator for Wind Energy Application". PhD confirmation seminar. 13th November 2009. Massey University, Palmerston North, New Zealand.
2. **A. Arifin**. "Integrated Modelling of Switched Reluctance Generator". Electronics, Information and Communication System (*EICS*) Seminar, 9th August 2010. Massey University, New Zealand.
3. **A. Arifin**. "Analysis of Switched Reluctance Machine using Combined Circuit and Field Computation". Electronics, Information and Communication System (*EICS*) Seminar, 17th May 2011. Massey University, New Zealand.
4. **A. Arifin**. "Performance Analysis of a Switched Reluctance Machine in the Low and Medium Speed Operations for Wind Energy Applications". Electronics, Information and Communication System (*EICS*) Seminar, 22nd Nov 2012. Massey University, New Zealand.

Appendix B

Machine 2: 12/16 machine

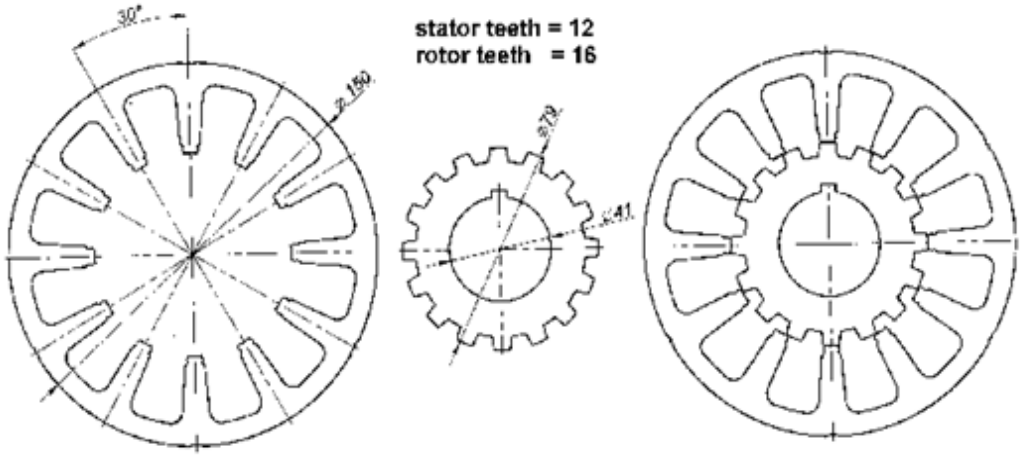

Machine 3: 12/16 machine having the same geometrical structure as the 12/8 machine

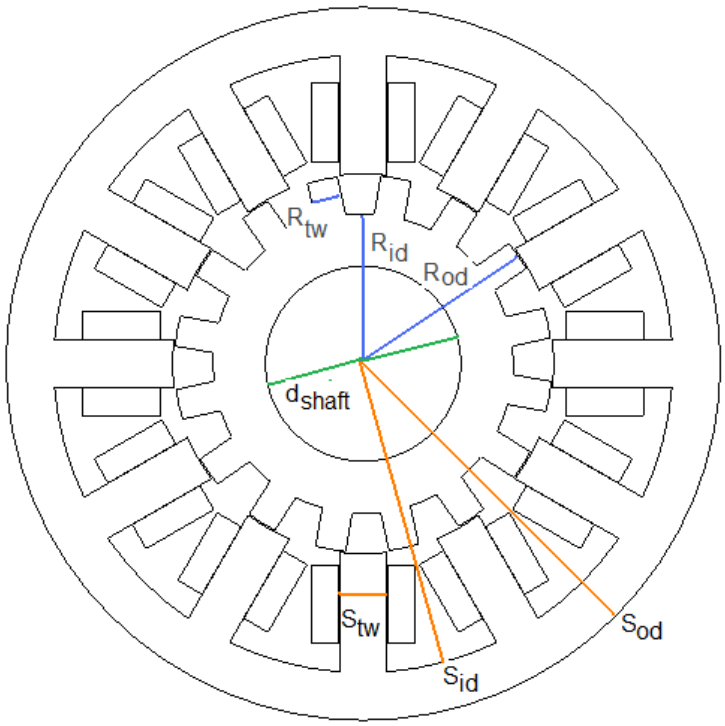

Machine 4: 12/4 machine having the same geometrical structure as the 12/8 machine

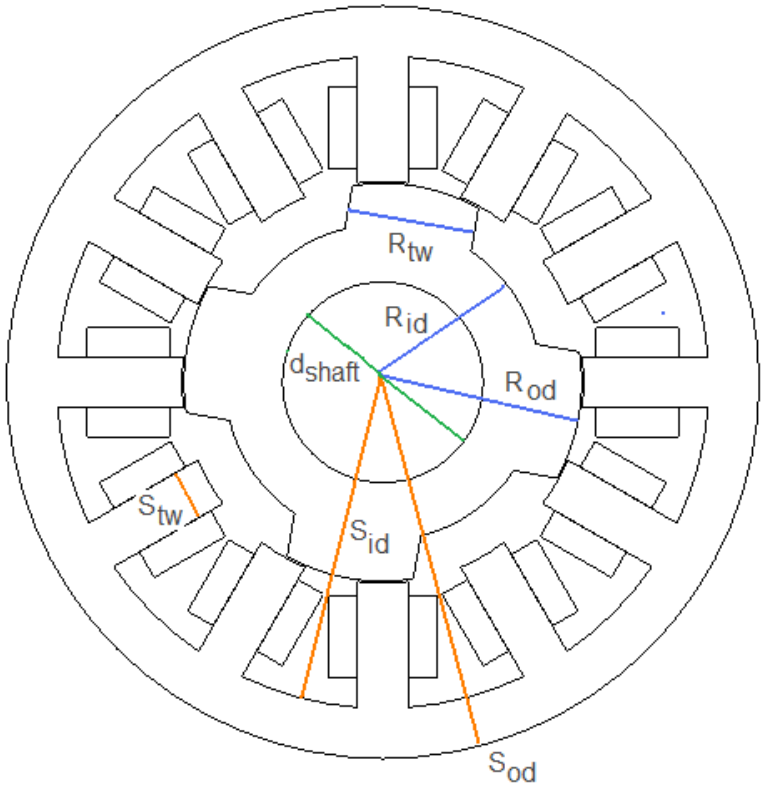

Appendix C

Inductance profile of the machines under study

Machine 1: 12/8

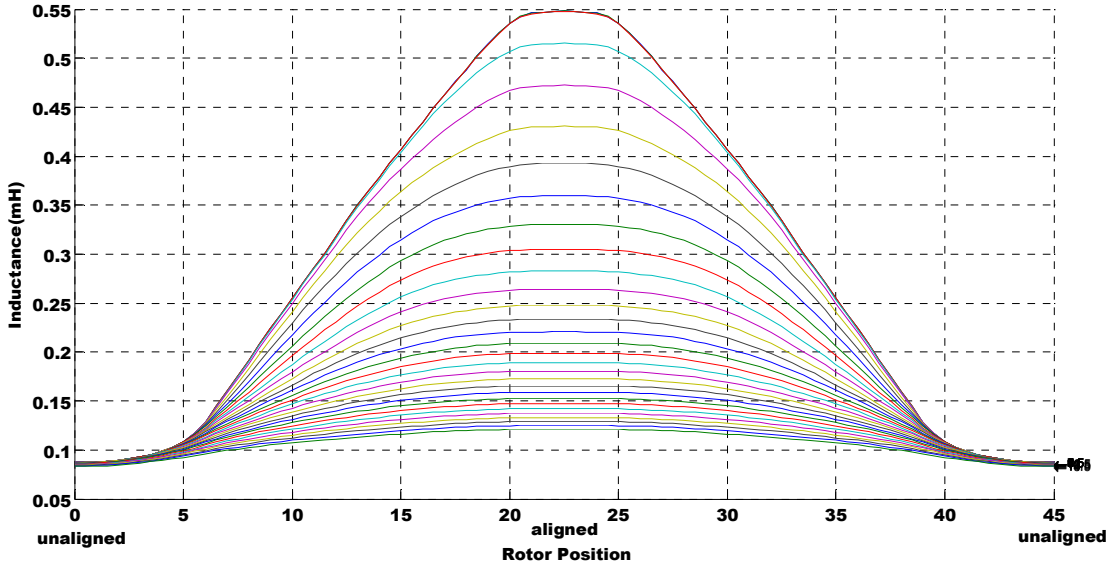

Machine 2: 12/16

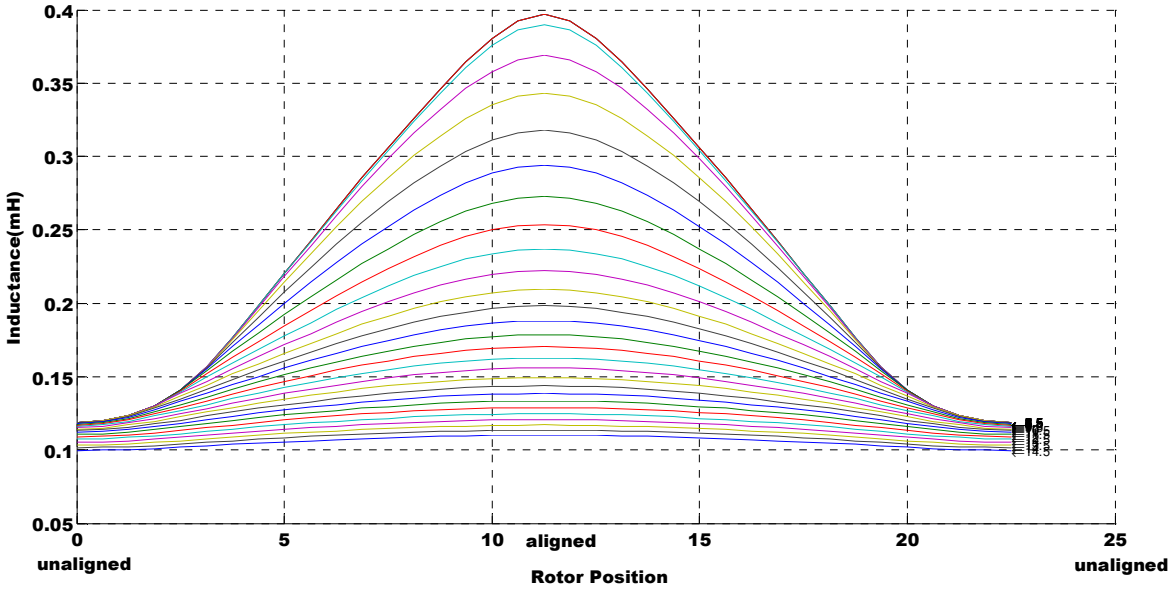

Machine 3: 12/16 with the same geometrical structure as the 12/8 machine

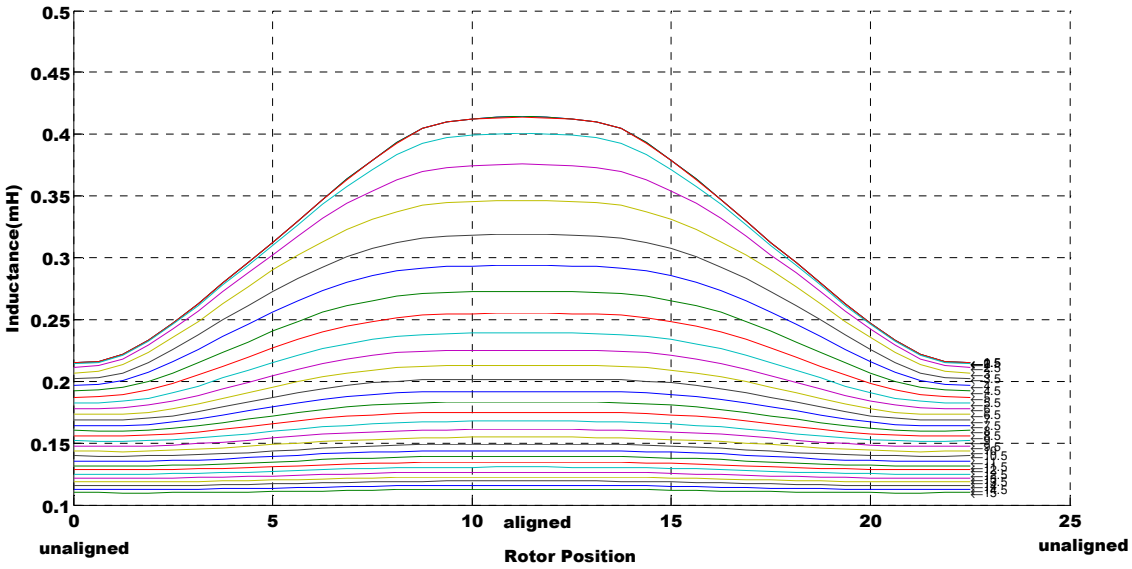

Machine 4: 12/4

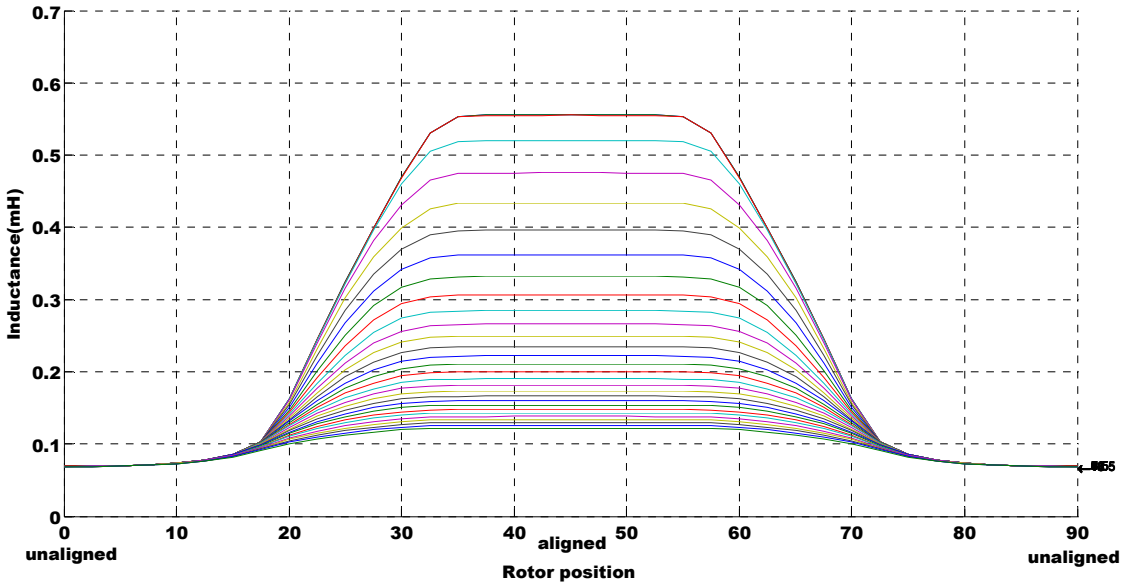

Appendix D

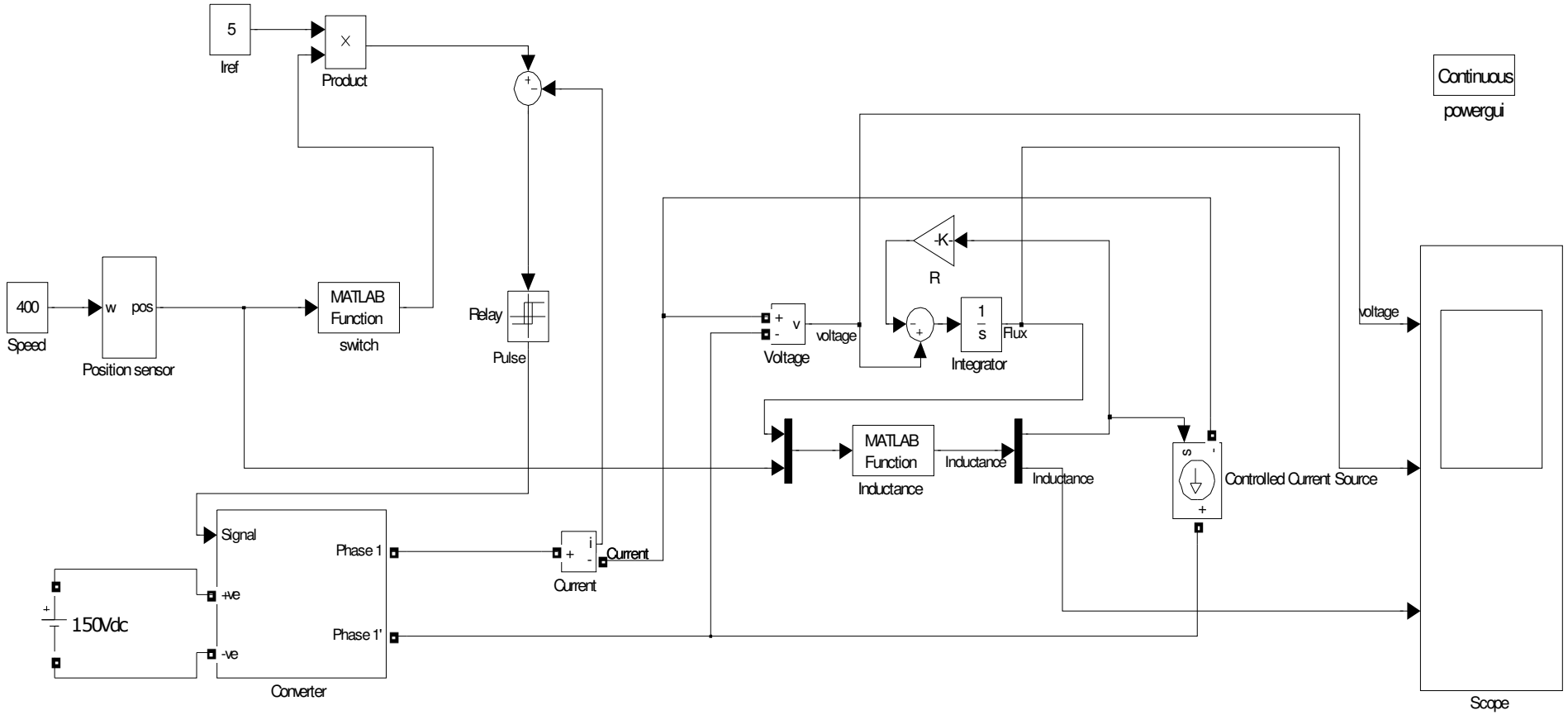
5
Iref
Product
Continuous
powergui
400
Speed
w pos
Position sensor
MATLAB Function
switch
Relay
Pulse
-K-
R
v
Voltage
voltage
1/s
Flux
Integrator
voltage
MATLAB Function
Inductance
Inductance
Inductance
Controlled Current Source
Signal
Phase 1
Phase 1'
+ve
-ve
150Vdc
Converter
i
Current
Current
Scope

Appendix E

Machine 2: Graph of magnetic flux density (T) against winding configuration for the 12/16 machine during 2 phase excitation at rotor position of 15deg

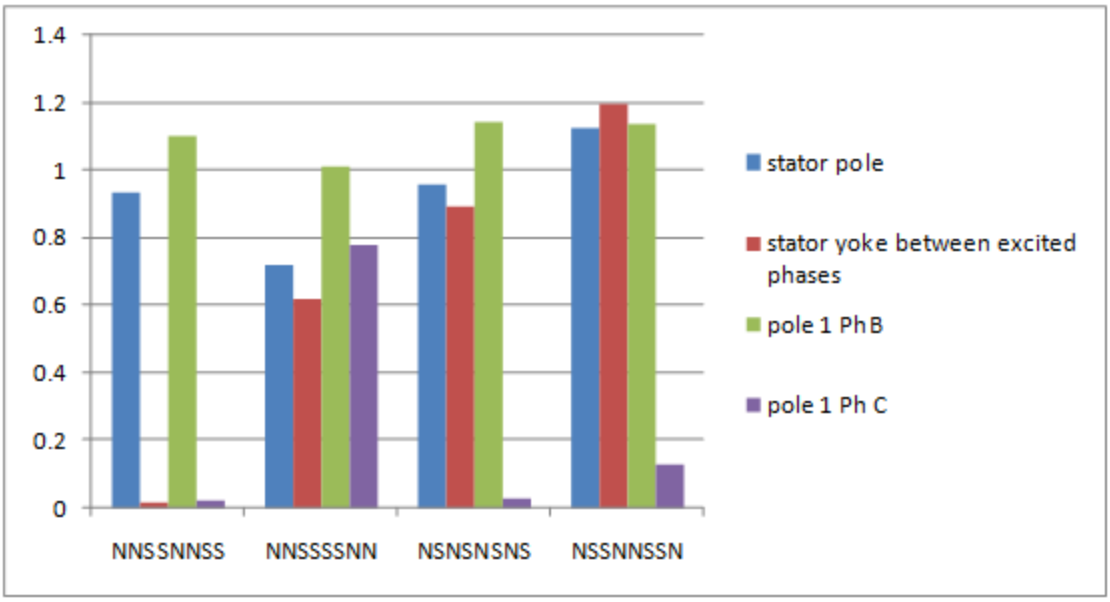

Machine 4: Graph of magnetic flux density (T) against winding configuration for the 12/4 machine during 2 phase excitation at rotor position of 15deg

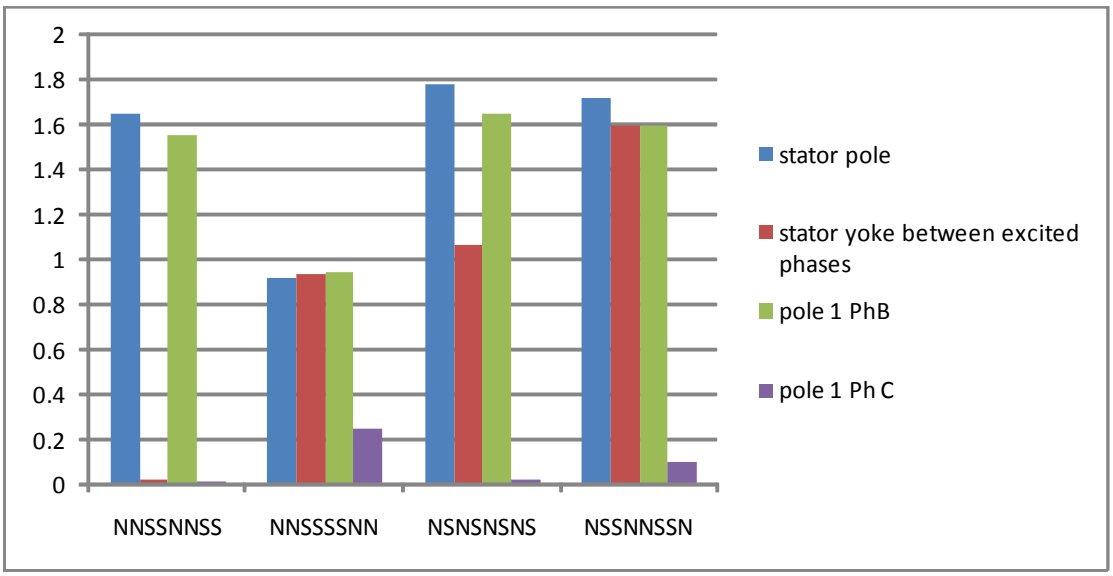

Appendix F

Current profiles for each of the machines taken during the medium speed range

Machine 1: 12/8 taken at its optimal firing angles at 200rad/s

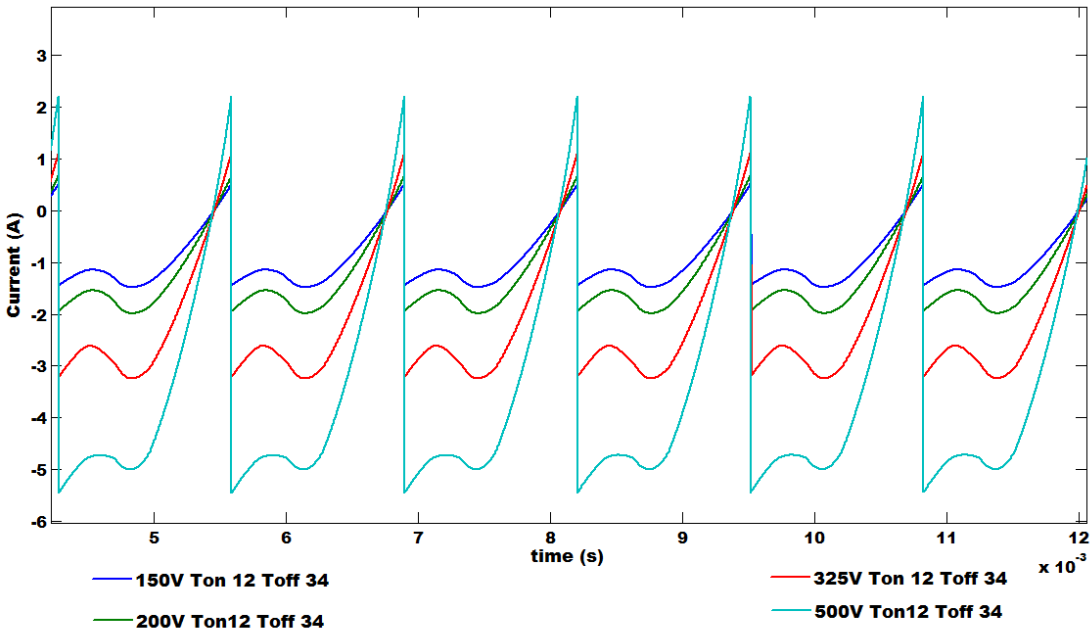

Machine 2: 12/16 taken at its optimal firing angles at 200rad/s

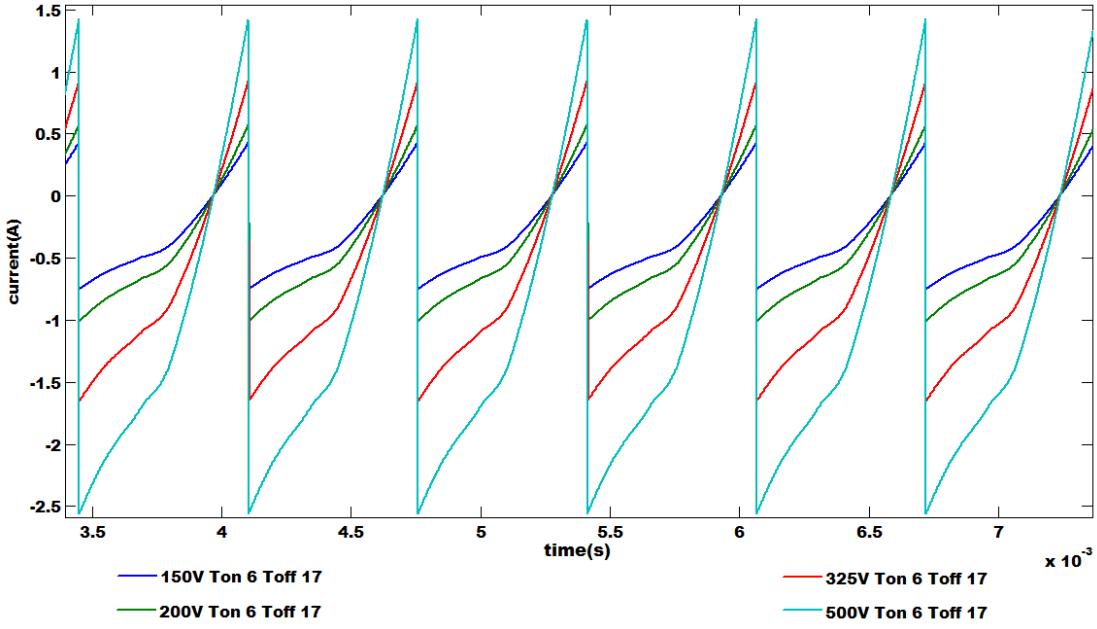

Machine 3: 12/16 having same structure as the12/8 machine taken at its optimal firing angles at 200rad/s

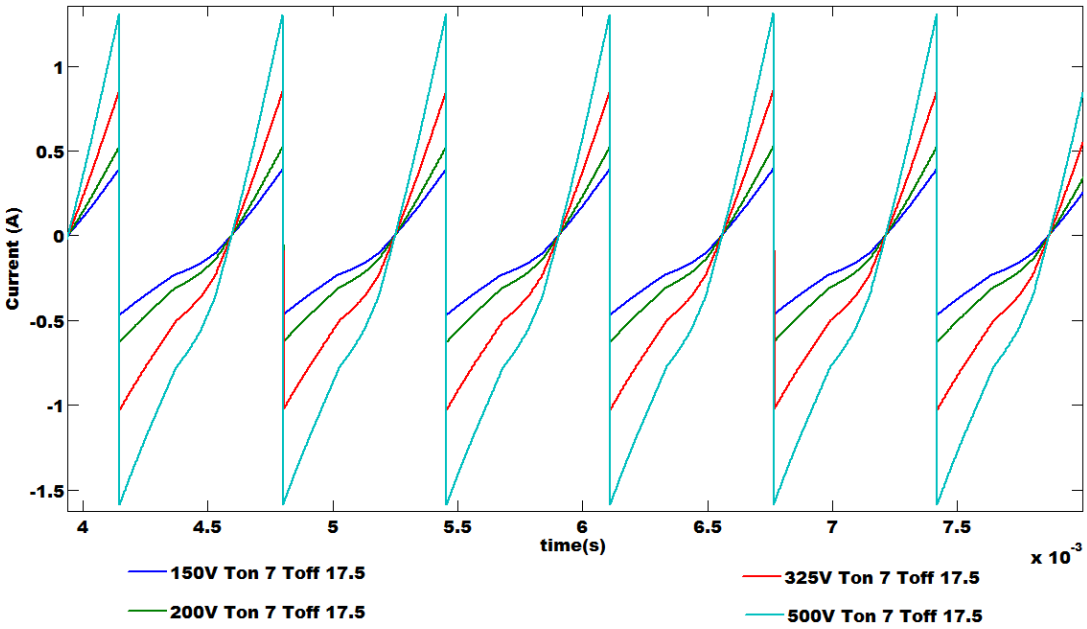

Machine 4: 12/4 machine having the same structure as the 12/8 taken at its optimal firing angles at 400rad/s

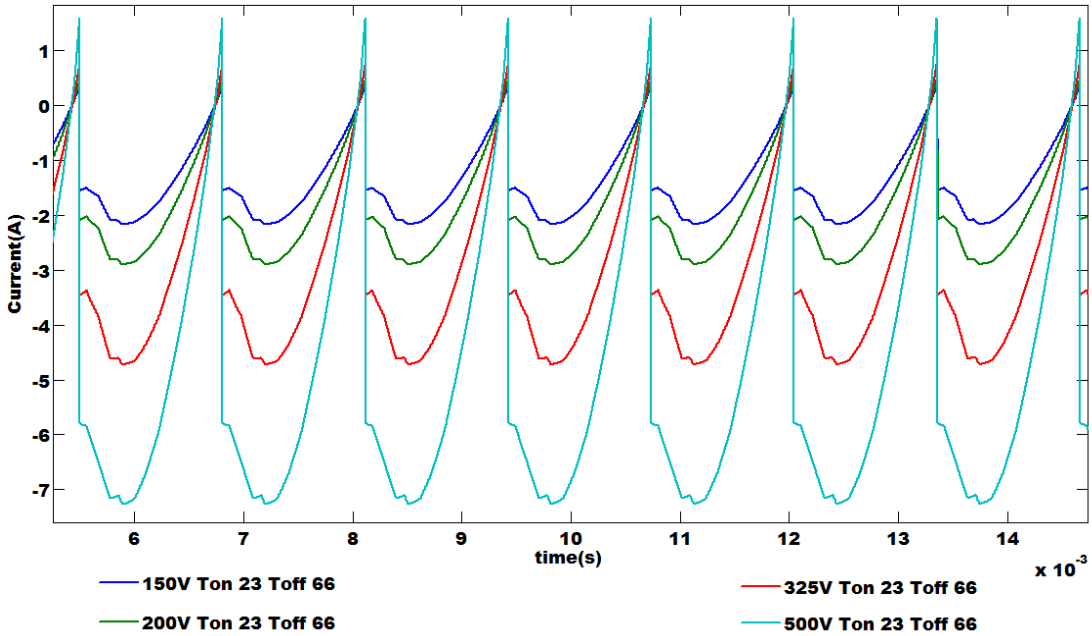

Appendix G

12/8 machine. Optimal dwell angles at 100V

Weibull

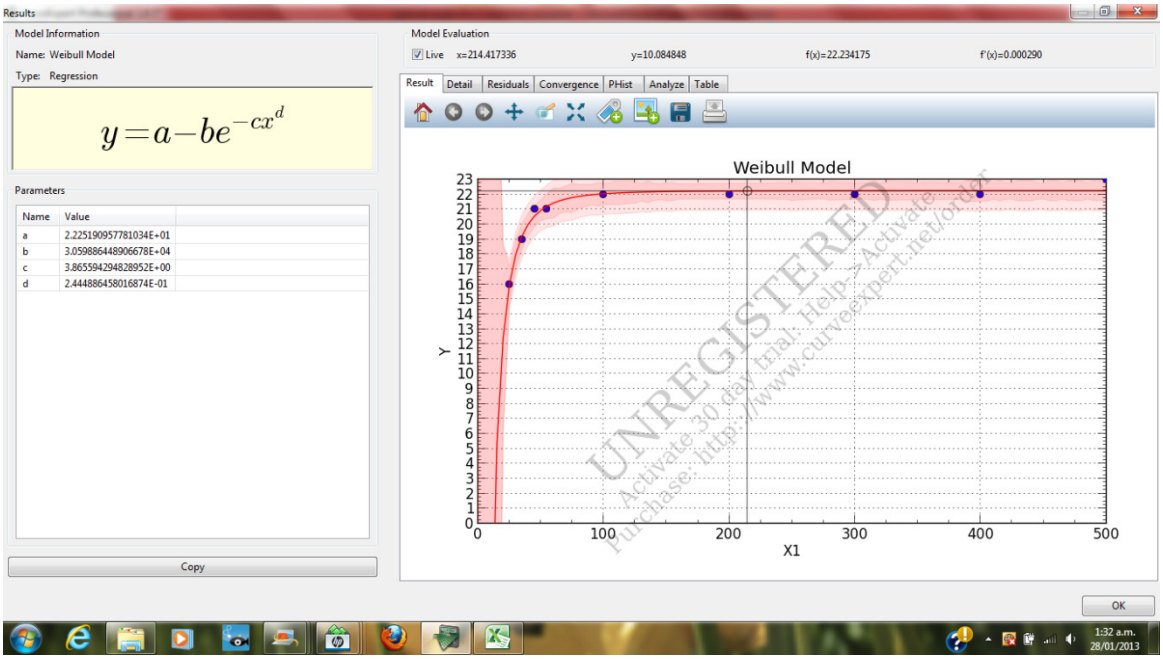

Ratkowsky

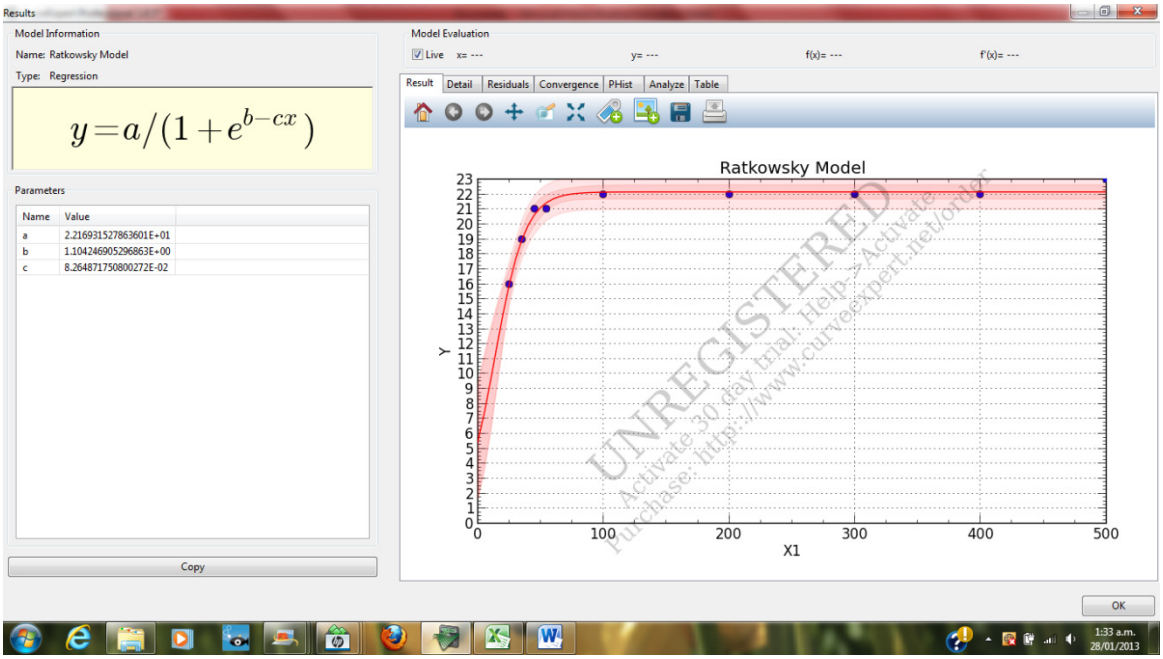

Appendix H

Ratkowsky Model

Machine 1: 12/8 machine

Voltage (V)	Coefficients		
	a	b	c
50V	23	-0.5277	0.03
100V	22.17	1.1	0.08
150V	22	1.54	0.067

Machine 2: 12/16 machine

Voltage (V)	Coefficients		
	a	b	c
50V	11.02	0.12	0.06
100V	11.02	0.12	0.06
150V	11	1.47	0.099
325V	11.02	1.56	0.06
500V	10.97	1.38	0.039

Machine 3: 12/16 machine having the same geometrical structure as the 12/8 machine

Voltage (V)	Coefficients		
	a	b	c
50V	11.06	-0.017	0.038
100V	10.6	0.366	0.05
150V	10.5	0.427	0.054
325V	10.71	1.95	0.073
500V	10.86	2.29	0.059

Machine 4: 12/4 machine having the same geometrical structure as the 12/8 machine

Voltage (V)	Coefficients		
	a	b	c
50V	43.96	0.357	0.0173
100V	42.45	1.13	0.03
150V	42.54	1.657	0.033
325V	43.07	1.77	0.018
500V	44.34	1.87	0.012

Weibull Model

Machine 1: 12/8 machine

Voltage (V)	Coefficients			
	a	b	c	d
50V	23	13.47	0.086	0.755
100V	22.25	30599	3.87	0.244
150V	22	13.52	0.00015	2.36

Machine 2: 12/16 machine

Voltage (V)	Coefficients			
	a	b	c	d
50V	11	3.02	0.0004	2.17
100V	11	3.02	0.0004	2.17
150V	11	30413.5	3.75	0.28
325V	11	7.71	0.0005	2.02
500V	11	11.63	0.016	1.08

Machine 3: 12/16 machine having the same geometrical structure as the 12/8 machine

Voltage (V)	Coefficients			
	a	b	c	d
50V	11.39	190674	8.21	0.09
100V	10.64	14.42	0.14	0.74
150V	10.51	9.19	0.045	0.996
325V	10.72	11.81	0.0073	1.43
500V	10.89	11.97	0.0042	1.44

Machine 4: 12/4 machine having the same geometrical structure as the 12/8 machine

Voltage (V)	Coefficients			
	a	b	c	d
50V	45.45	67.45	0.172	0.524
100V	43.69	74.77	0.15	0.58
150V	42.65	38.28	0.0023	1.416
325V	43.08	35.91	0.000224	1.69
500V	45.24	39.29	0.000233	1.55

Appendix I

12/8 machine

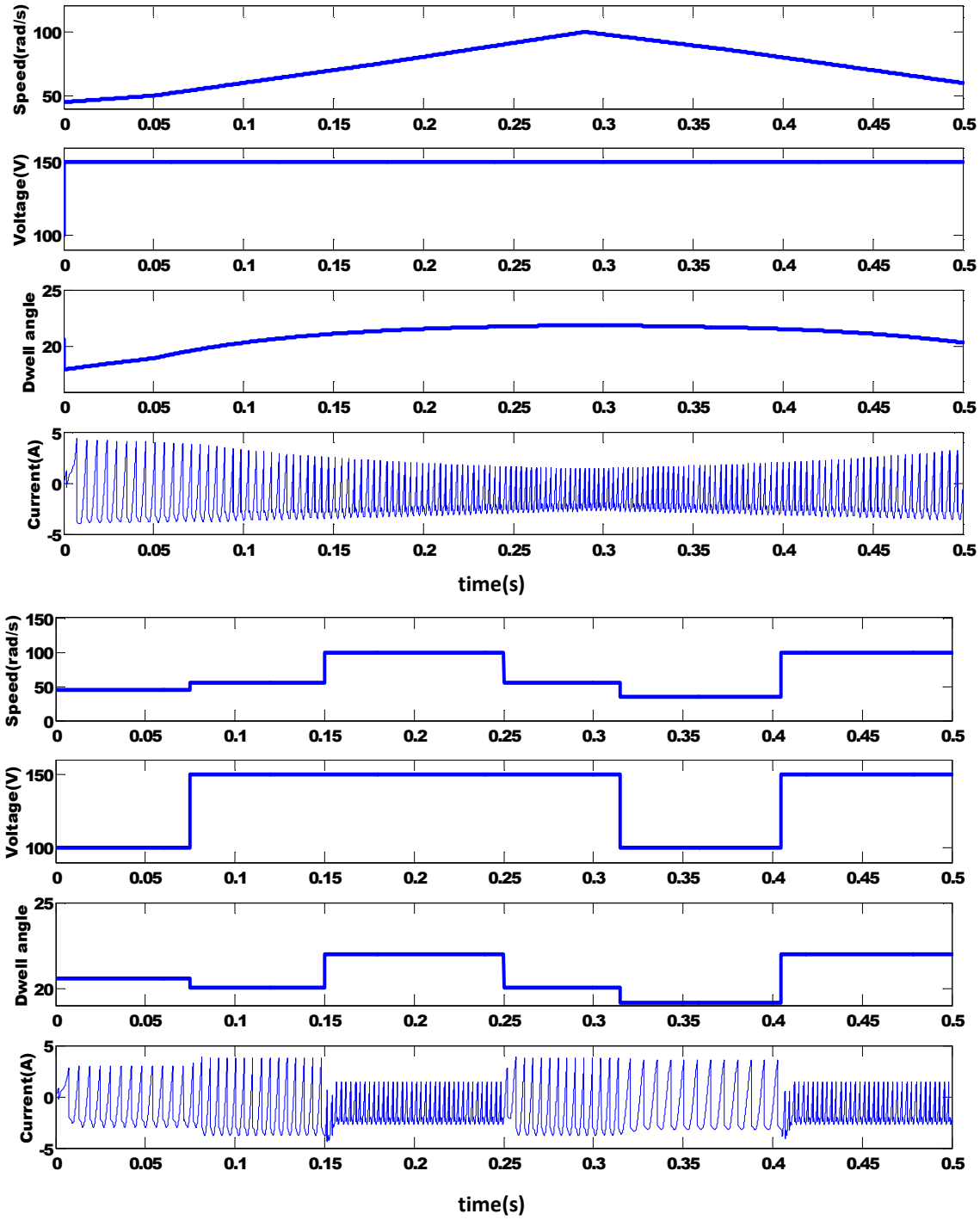

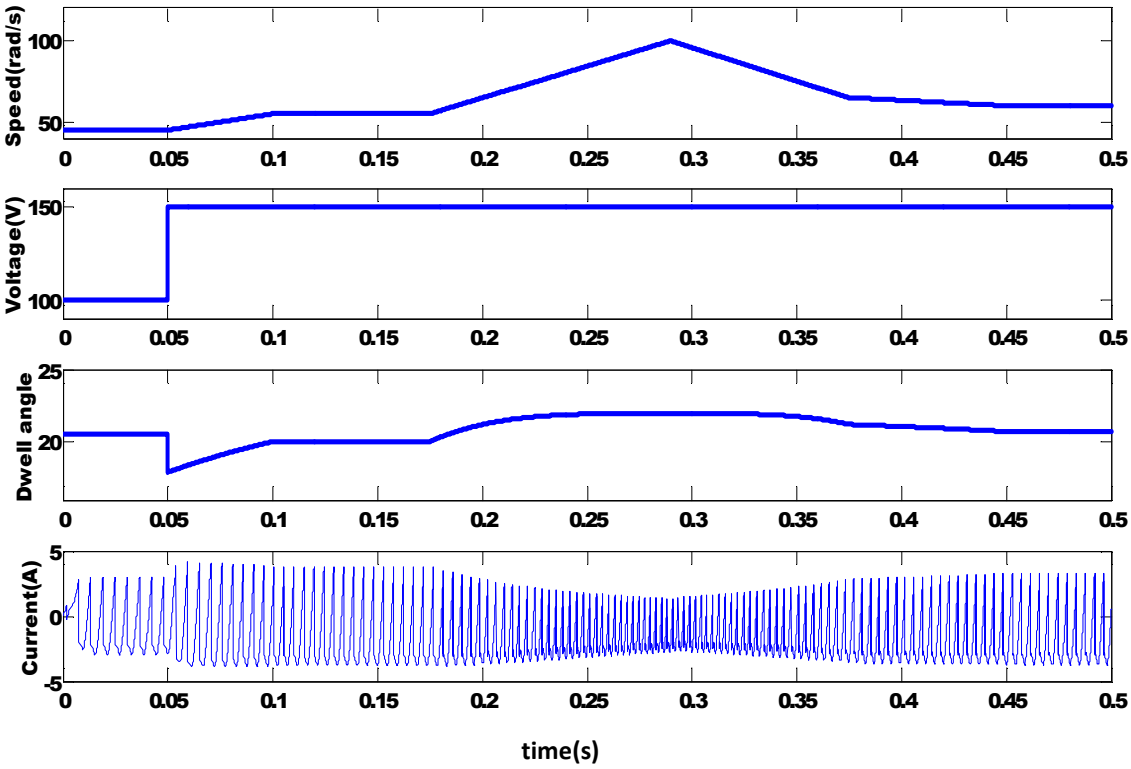
Speed(rad/s)
100
50
Voltage(V)
150
100
Dwell angle
25
20
Current(A)
5
0
-5
0
0.05
0.1
0.15
0.2
0.25
0.3
0.35
0.4
0.45
0.5
time(s)